

THESE

Présentée à

L'UNIVERSITE VIA DOMITIA (université de Perpignan)

Par Caroline LABAUNE

Pour obtenir le grade de

DOCTEUR

Spécialité : Océanologie-Géologie

**Architecture, genèse et évolution du littoral du Languedoc-Roussillon :
Impact des facteurs physiques au cours du Quaternaire terminal**

Volume II : Annexes et Publications

Soutenue le : 13 Décembre 2005

Devant la commission d'examen formée de :

Mr Serge Berné, Chercheur C3, IFREMER, Brest	Rapporteur
Mr Eric Chaumillon, Maître de conférences, Université de La Rochelle	Rapporteur
Mr Jean-Noël Proust, Professeur, Université de Rennes 1	Examinateur
Mr Paul Le Strat, Docteur, Ingénieur Brgm	Examinateur
Mr Michel Tesson, Professeur, Université de Perpignan	Directeur de thèse
Mr Bernard Gensous, Maître de conférences, Université de Perpignan	Examinateur

Tables des matières

ANNEXE I : Quelques principes et systèmes utilisés.....	i-1
I. Le principe et les outils de sismique réflexion monotrace.....	i-3
I.1. Les principes de la sismique réflexion.....	i-3
I.2. Les profils sismiques	i-4
I.3. La chaîne d'acquisition et de traitement des données	i-5
I.4. Le boomer IKB Seistec®.....	i-8
II. Le vibrocarottier petits fonds	i-9
II.1. Généralités	i-9
II.2. Composition de l'appareil.....	i-9
II.2.1. <i>La structure porteuse</i>	i-10
II.2.2. <i>La « lance »</i>	i-10
ANNEXE II : Profils sismiques, cartes isobathes et isopaques.....	i-11
I. Le Roussillon.....	i-12
I.1. Les profils sismiques et leur pointé.....	i-12
I.1.1. <i>Sismique HR</i>	i-12
I.1.2. <i>Sismique THR.....</i>	i-19
I.2. Les cartes isobathes des principales discontinuités.....	i-26
I.3. Les cartes isopaques des unités sismiques	i-30
II. La plate-forme du Rhône et son extension occidentale	i-35
II.1. Les cartes isobathes des principales discontinuités.....	i-35
II.2. Les cartes isopaques des unités sismiques	i-38
III. Le Sud-Languedoc.....	i-43
III.1. Les profils sismiques et leur pointé.....	i-43
III.2. Les cartes isobathes des principales discontinuités.....	i-49
III.3. Les cartes isopaques des unités sismiques	i-51
ANNEXE III : Description détaillée des carottages et vibrocarottages réalisés sur le secteur Roussillon.....	i-53
Mission TRANSLIT-2004.....	i-56
Mission LIPPER-2003.....	i-60
Mission LITTO-2003.....	i-67
ANNEXE IV : Présentation des résultats des analyses granulométriques.....	i-79
LK03-01.....	i-81
LK03-01b.....	i-82
LK03-03.....	i-83
LK03-04.....	i-84
03VK-01.....	i-85
03VK-02.....	i-86
03VK-03.....	i-87
03VK-04.....	i-88
03VK-05.....	i-89
03VK-06.....	i-90
03VK-07.....	i-91
Communications et Publications.....	i-93

Liste des figures

ANNEXE I : Quelques principes et systèmes utilisés.....	i-1
Figure I-1. Trajets de ondes acoustiques et appareillage d'émission et de réception sismique (modifié d'après Sweat, 1997)	i-5
Figure I-2. Impédance acoustique et coefficient de réflexion : construction de la trace sismique.....	i-4
Figure I-3. Formation des profils sismiques à partir de la compression des traces des tirs successifs.....	i-5
Figure I-4. Organisation de la chaîne d'acquisition sismique utilisée et photographie des appareils.....	i-7
Figure I-5. Photographie du boomer IKB Seistec® et de notre embarcation côtière.....	i-8
Figure I-6. Récepteur acoustique type « line-in-cone »	i-8
Figure I-7. Composition de la structure porteuse du vibrocarottier : une échelle permettant d'accéder à la « tête » de l'appareil et des jambes de force pour la stabilisation.....	i-10
Figure I-8. Les éléments constituants la « lance » du vibrocarottier.....	i-10
ANNEXE II : Profils sismiques, cartes isobathes et isopaques.....	i-11
Profil sismique HR SAL-12 (site du Roussillon, Etang de Salses-Leucate).....	i-12
Profil sismique HR ERA96-03 (site du Roussillon, secteur Sud).....	i-13
Profil sismique HR SIG95-49 (site du Roussillon, secteur Sud).....	i-14
Profil sismique HR LSPK02-05 (site du Roussillon, secteur Sud).....	i-15
Profil sismique HR SAL-14 (site du Roussillon, secteur Nord).....	i-16
Profil sismique HR ERA95-08 (site du Roussillon, secteur Nord).....	i-17
Profil sismique HR ERA95-02 (site du Roussillon, secteur Nord).....	i-18
Profil sismique THR IKB02-03 (site du Roussillon, secteur Sud).....	i-19
Profil sismique THR IKB02-43 (site du Roussillon, secteur Sud).....	i-20
Profil sismique THR IKB02-48 (site du Roussillon, secteur Sud).....	i-21
Profil sismique THR IKB02-31 (site du Roussillon, secteur Sud).....	i-22
Profil sismique THR IKB02-07 (site du Roussillon, secteur Nord).....	i-23
Profil sismique THR LAG02-06 (site du Roussillon, Etang de Salses-Leucate).....	i-24
Profil sismique THR LAG02-14 (site du Roussillon, Etang de Salses-Leucate).....	i-25
Figure 2.1. Cartes isobathes (en mètres) des discontinuités D200 (a), D300 (b) et D400 (c). Ve : 1500 m.s^{-1} et Vs : 1600 m.s^{-1} . Les zones hachurées correspondent aux zones où les discontinuités sont amalgamées avec la discontinuité supérieure.....	i-36
Figure 2.2. Cartes isobathes (en mètres) des discontinuités D500 (a), D501 (b) et D502 (c). Ve : 1500 m.s^{-1} et Vs : 1600 m.s^{-1}	i-37
Figure 2.3. Cartes isobathes (en mètres) des discontinuités D503 (a), D600 (b) et D610 (c). Ve : 1500 m.s^{-1} et Vs : 1600 m.s^{-1}	i-38
Figure 2.4. Cartes isopaques (en mètres) des unités U200 (a) et U300 (b). Vs : 1600 m.s^{-1}	i-39
Figure 2.5. Cartes isopaques (en mètres) des unités U400 (a) et U500 (b). Vs : 1600 m.s^{-1}	i-40
Figure 2.6. Cartes isopaques (en mètres) des unités U501 (a) et U502 (b). Vs : 1600 m.s^{-1}	i-41
Figure 2.7. Cartes isopaques (en mètres) des unités U503 (a) et U600 (b). Vs : 1600 m.s^{-1}	i-42
Figure 2.8. Cartes isopaques (en mètres) des unités U601 (a) et U610 (b). Vs : 1600 m.s^{-1}	i-43
Profil sismique HR SIG95-41 (site du Sud-Languedoc, secteur Sud).....	i-44
Profil sismique HR SIG95-48 (site du Sud-Languedoc, secteur Sud).....	i-45
Profil sismique HR ERA97-11 (site du Sud-Languedoc, secteur Nord).....	i-46
Profil sismique HR SIG95-08 (site du Sud-Languedoc, secteur Sud).....	i-47
Profil sismique HR ERA97-15 (site du Sud-Languedoc, secteur Nord).....	i-48
Figure 3-1. Cartes isobathes des discontinuités D1-1 (a) et D2-1 (b)	i-49
Figure 3-2. Cartes isobathes des discontinuités D2-2b (a) et D2-3 (b)	i-50
Figure 3-3. Cartes isopaques de l'unité U1 (a) correspondant aux dépôts anté post-glaciaires et du Post-Glaciaire (b)	i-51

ANNEXE III : Description détaillée des carottages et vibrocarottages réalisés sur le secteur

Roussillon.....	i-53
Figure III-1. Log lithologique de la carotte TRANSK-01.....	i-56
Figure III-2. Log lithologique de la carotte TRANSK-01bis.....	i-57
Figure III-3. Log lithologique de la carotte TRANSK-01ter.....	i-58
Figure III-4. Log lithologique de la carotte TRANSK-01quat.....	i-59
Figure III-5. Log lithologique de la carotte LK03-01.....	i-61
Figure III-6. Log lithologique de la carotte LK03-01bis.....	i-63
Figure III-7. Log lithologique de la carotte LK03-03.....	i-64
Figure III-8. Log lithologique de la carotte LK03-04.....	i-66
Figure III-9. Log lithologique et photographie de la carotte 03VK01.....	i-68
Figure III-10. Log lithologique, photographie et rayon X de la carotte 03VK02.....	i-70
Figure III-11. Log lithologique, photographie et rayon X de la carotte 03VK03.....	i-72
Figure III-12. Log lithologique, photographie et rayon X de la carotte 03VK04.....	i-74
Figure III-13. Log lithologique, photographie et rayon X de la carotte 03VK05.....	i-75
Figure III-14. Log lithologique et photographie de la carotte 03VK06.....	i-76
Figure III-15. Log lithologique et photographie de la carotte 03VK07.....	i-78

ANNEXE IV : Présentation des résultats des analyses granulométriques.....i-79

LK03-01.....	i-81
LK03-01b.....	i-82
LK03-03.....	i-83
LK03-04.....	i-84
03VK-01.....	i-85
03VK-01.....	i-86
03VK-01.....	i-87
03VK-01.....	i-88
03VK-01.....	i-89
03VK-01.....	i-90
03VK-01.....	i-91

ANNEXE I

QUELQUES PRINCIPES ET SYSTEMES UTILISES

Le principe et les outils de sismique réflexion monotrace

Les principes de la sismique réflexion

L'étude du sous-sol par les techniques de prospection sismique, sismique réflexion, a été initiée en 1920 par Mintrop. L'objectif est de pouvoir étudier les formes géométriques des différentes couches géologiques afin de comprendre les mécanismes de mise en forme. Cette technique est basée sur la propagation des ondes acoustiques à travers l'eau et les couches sédimentaires.

Impédance acoustique et coefficient de réflexion

Les caractéristiques de propagation des ondes acoustiques diffèrent en fonction des propriétés physiques et acoustiques du milieu traversé, on parle d'impédance acoustique. Celle-ci est fonction de la célérité de propagation des ondes dans le milieu considéré et de la densité de ce milieu :

$$Z = V\rho \quad \text{avec } Z : \text{impédance}$$

V : célérité en m.s⁻¹

ρ : densité

Le contraste d'impédance au niveau des interfaces des couches successives va entraîner un phénomène de transmission avec changement de l'angle d'incidence et la réflexion d'une partie des ondes émises. L'énergie réfléchie va être fonction du contraste d'impédance qui se traduit par le coefficient de réflexion (R0) :

$$R_0 = \frac{Z_2 - Z_1}{Z_2 + Z_1} \quad \text{avec } Z_1 \text{ impédance de la couche supérieure et } Z_2 \text{ de la couche inférieure.}$$

Les appareils de sismique réflexion sont donc composés d'un système émetteur qui va produire une onde acoustique et d'un récepteur qui va enregistrer les ondes réfléchies (Figure I-1), leur « signature » ou trace sismique sera fonction du coefficient de réflexion et donc du contraste d'impédance (Figure I-2).

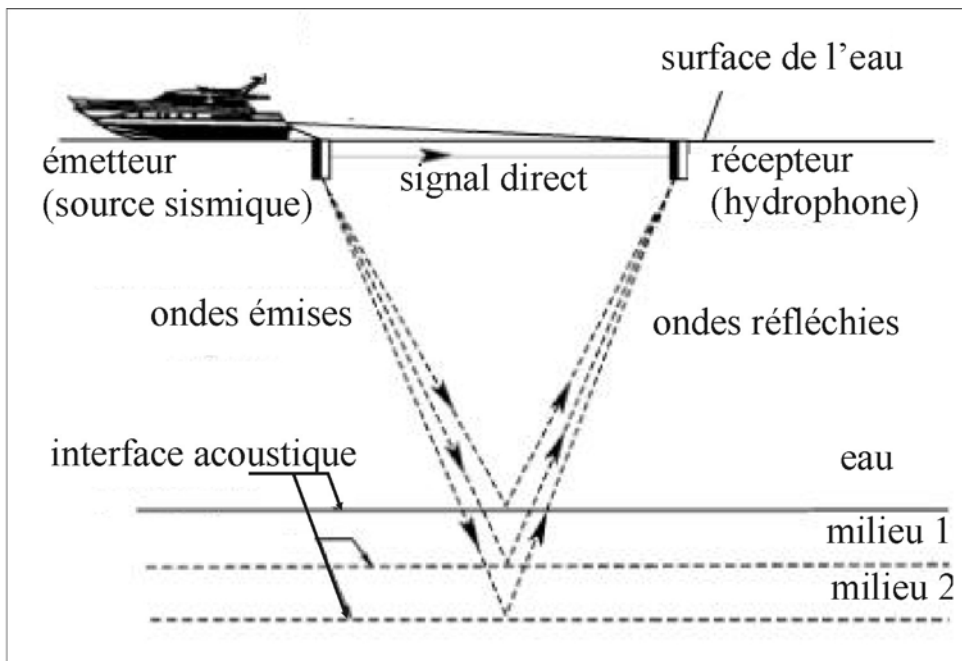


Figure I-1. Trajets de ondes acoustiques et appareillage d'émission et de réception sismique (modifié d'après Sweat, 1997)

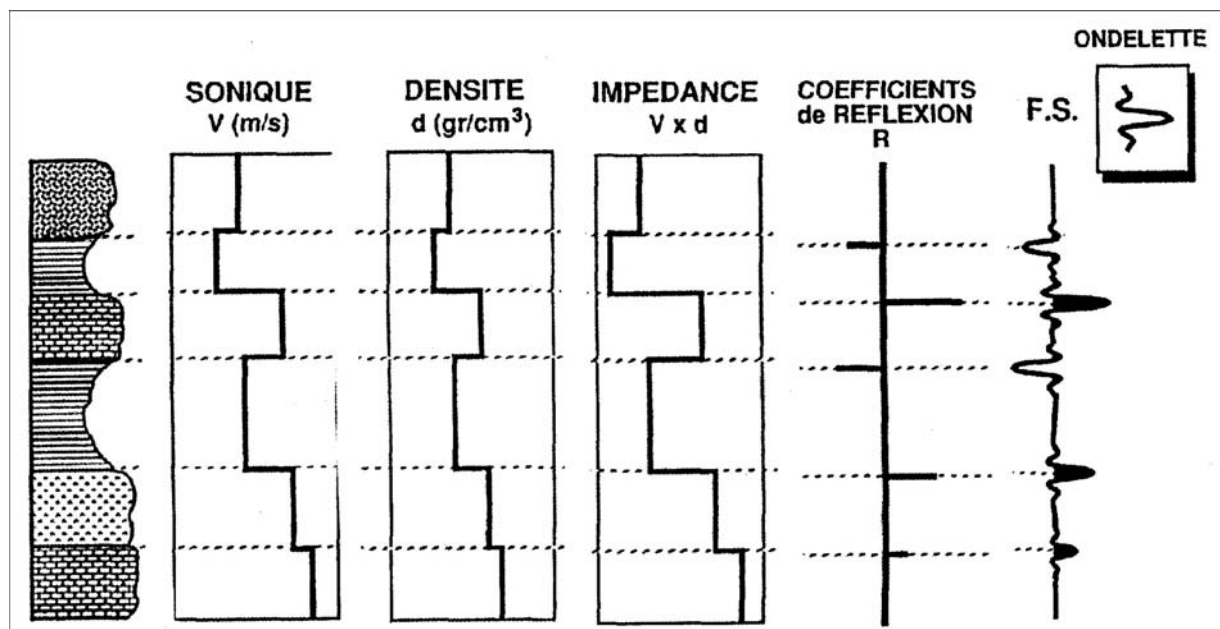


Figure I-2. Impédance acoustique et coefficient de réflexion : construction de la trace sismique

Les profils sismiques

Lors de l'émission des ondes acoustiques, qui se fait selon une cadence de tir déterminée par l'utilisateur en fonction des besoins, les ondes se propagent en tout sens. Le récepteur enregistre ainsi ce que l'on note l'onde directe, trajet entre l'émetteur et le récepteur, et des multiples, réflexions multiples de l'onde réfléchie. L'utilisation de sismique multitrace permet de s'affranchir de ces ondes parasites. Dans notre cas, nous utilisons la

sismique monotrace, la trace sismique enregistrée va donc être perturbée par les multiples qui masquent une partie du signal réel. En revanche, l'onde directe nous permet de corriger nos données en fonction de la valeur du déport (distance entre l'émetteur et le récepteur).

Les profils sismiques correspondent à la reconstruction des interfaces, appelées dans ce cas réflecteur, entre les différents milieux rencontrés par compression des traces sismiques enregistrées pour chaque tir (Figure I-3).

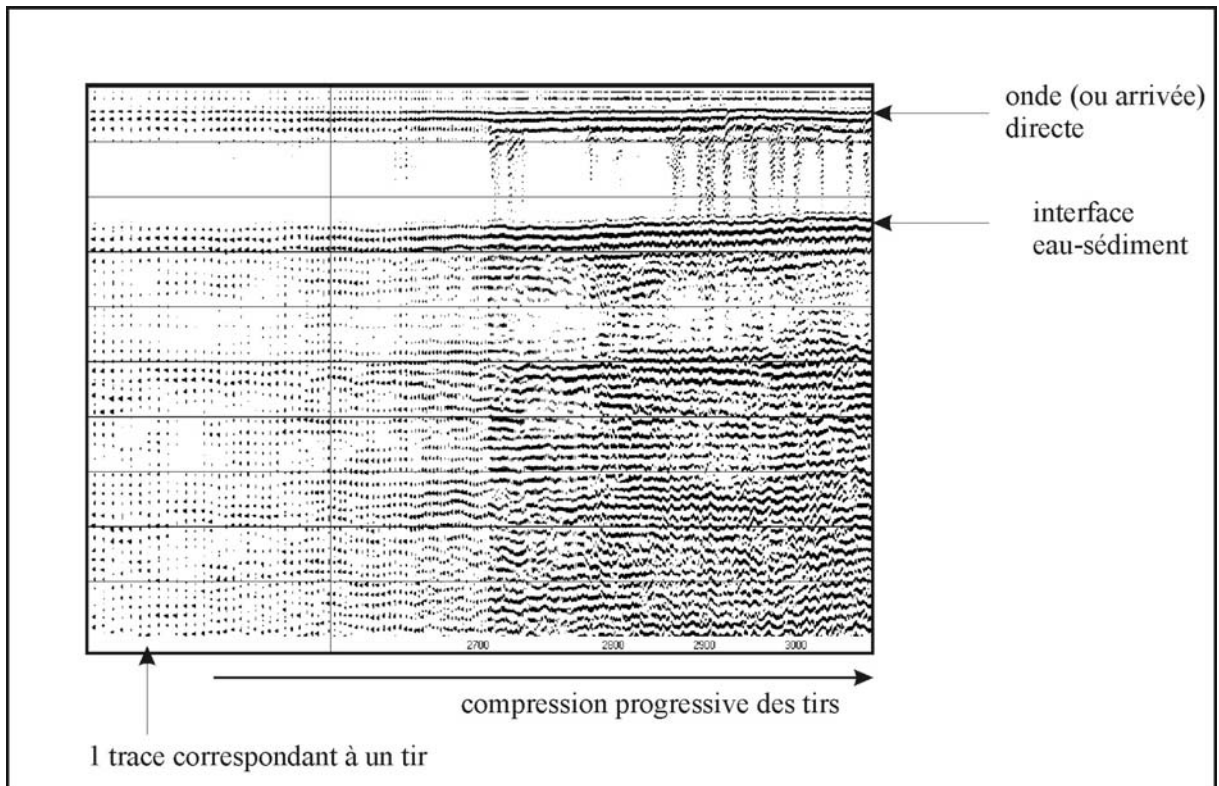


Figure I-3. Formation des profils sismiques à partir de la compression des traces des tirs successifs

La chaîne d'acquisition et de traitement des données

La chaîne d'acquisition de données (Figure I-4) comprend en plus des outils de sismique :

- un générateur modulable ou non du point de vue puissance d'émission qui alimente la source sismique (« power supply »).
- une unité centrale équipée d'un logiciel de sismique (ex : DelphSeismic) qui permet la gestion des paramètres d'émission, l'enregistrement et le traitement du signal sismique
- un système d'enregistrement des coordonnées géographiques

Dans notre cas, nous avons intégré à cette chaîne un magnétoscope afin de pouvoir amplifier le signal après réception et un oscilloscope pour le contrôle de ce signal. Le montage informatique à l'intérieur de l'embarcation est représenté sur la photo suivante.



Les outils de sismique réflexion en eux-mêmes sont composés d'une source qui crée l'onde sonore et d'un récepteur composé de plusieurs hydrophones alignés. Les sources peuvent fonctionner selon différents principes :

- les formes d'onde contrôlée : type sondeur de sédiment
- les sources explosives : type sparker
- les sources à accélération des masses d'eau : type boomer

Deux de ces systèmes ont été mis en œuvre au cours de cette étude, un sparker type mini-sparker SIG® et un boomer type IKB Seistec®. Le mini-sparker est constitué d'une électrode multibrains (ou peigne), la réception se fait au moyen d'une flûte composée de 5 ou 7 hydrophones espacés d'un mètre. Nous reviendrons sur le boomer IKB Seistec® dans le chapitre suivant.

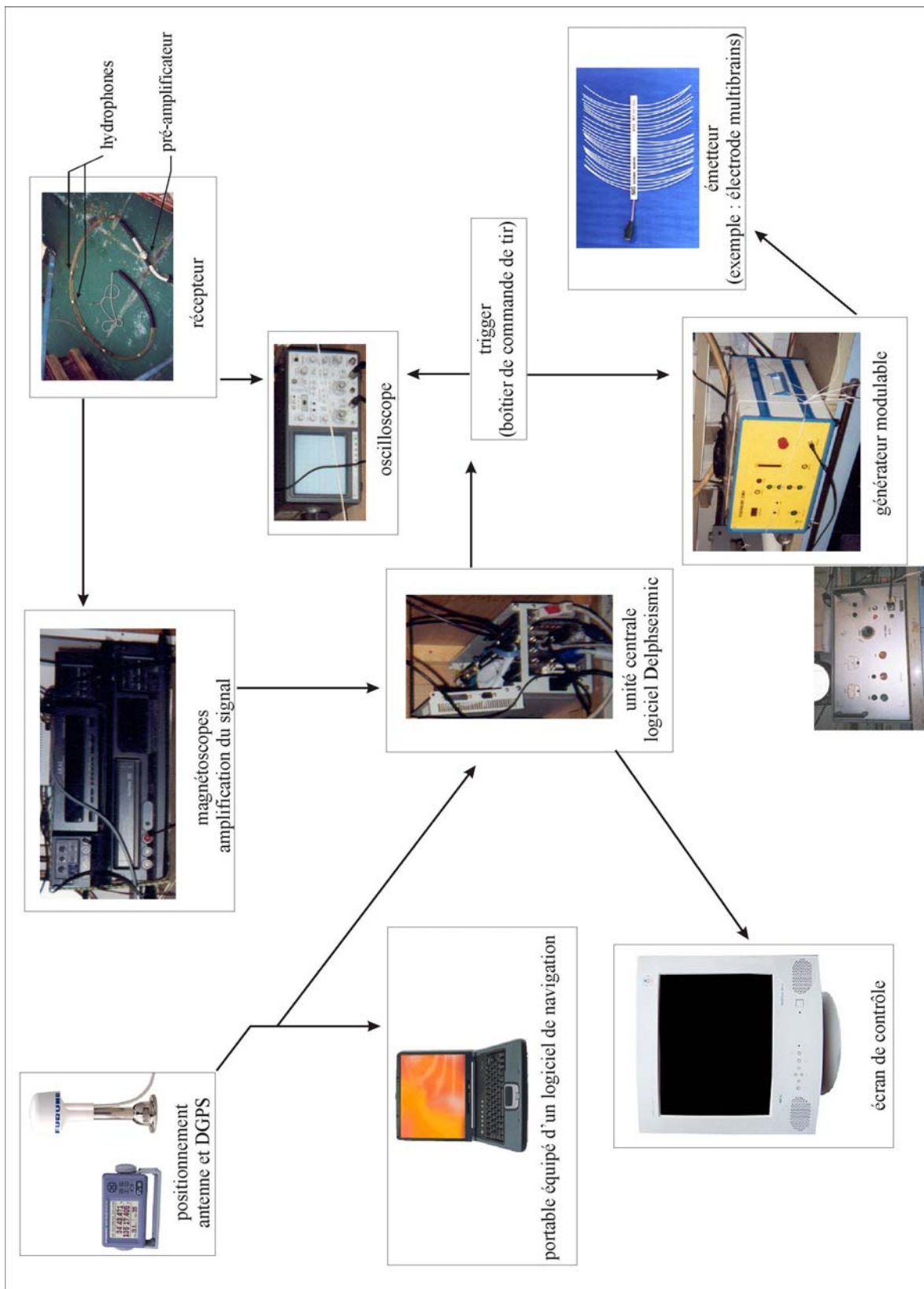


Figure I-4. Organisation de la chaîne d'acquisition sismique utilisée et photographie des appareils

Le boomer IKB Seistec®

Nous avons vu précédemment que le boomer fonctionnait selon le principe d'accélération des masses d'eau, on parle également de source électrodynamique. La production d'une onde acoustique se fait par la création d'une dépressurisation liée à la résonance d'une membrane, principe du haut-parleur.

L'une des particularités du boomer IKB vient de sa configuration, l'émetteur et le récepteur sont montés côté à côté sur un catamaran (Figure I-5). L'espace entre les deux systèmes est de 0,70 m. Le regroupement de l'ensemble émission-réception sur un catamaran à faible tirant d'eau rend l'utilisation de cette appareil beaucoup plus aisée dans les environnements de faibles profondeur d'eau.

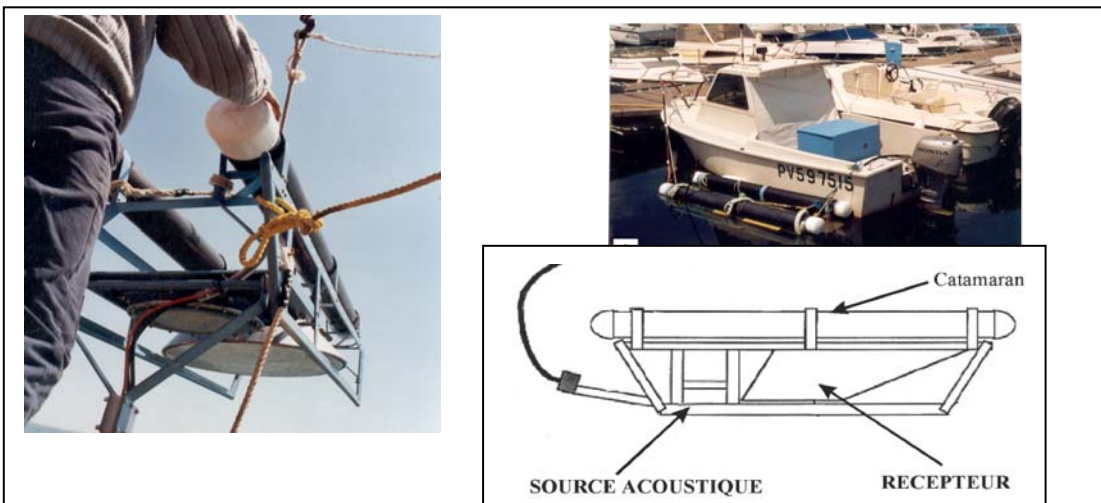


Figure I-5. Photographie du boomer IKB Seistec® et de notre embarcation côtière

Le récepteur placé sur le catamaran se présente sous forme d'un cône contenant une série de 7 hydrophones placés verticalement (Figure I-6). Ce montage appelé « line-in-cone » (Simpkin and Davis, 1993 ; Mosher et Simpkin, 1997) améliore la qualité du signal reçu. Il crée une réception directionnelle par la faible ouverture du cône et permet également une atténuation des bruits liés à l'arrivée directe et aux échos latéraux. De plus, le faible espacement entre les hydrophones entraîne une amélioration de la résolution.

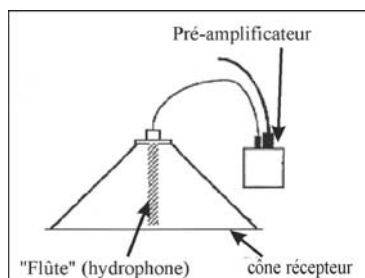


Figure I-6. Récepteur acoustique type « line-in-cone ».

Le vibrocarottier petits fonds

Généralités

Le vibrocarottier petits fonds a été créé au sein de l'UMR EPOC de l'université de Bordeaux 1 par Mr Amaury de Resseguier. Cet appareil spécialement conçu pour les travaux à terre et dans les petits fonds peut pénétrer dans une large gamme de sédiment, de la vase aux graviers, voir aux galets épars. La pénétration maximale pouvant être atteinte est de 10 m. Deux des grands avantages de cet appareil sont sa facilité de transport et de mise en œuvre. Nous avons ainsi pu le transporter à bord de notre petite embarcation côtière et effectué des carottages dans l'étang de Salses-Leucate.

Le vibrocarottier peut fonctionner selon deux modes : la vibration ou la percussion selon les types de matériaux et la résistance rencontrée. L'enfoncement par percussion étant plus lent que celui par vibration, il est essentiellement utilisé pour les matériaux les plus résistants.

Composition de l'appareil

Le vibrocarottier peut être décomposé en deux parties principales, la structure porteuse et la « lance ». Un moteur thermique à haute fréquence (12 à 15 kHz) est utilisé pour la création des percussions ou des vibrations. Le moteur thermique est relié soit à une aiguille à béton ou aiguille vibrante soit à un percuteur (type marteau piqueur). La majorité des pièces utilisées sont faite en aluminium afin d'augmenter la résistance et la transmission des vibrations mais aussi pour alléger l'appareil.

La structure porteuse

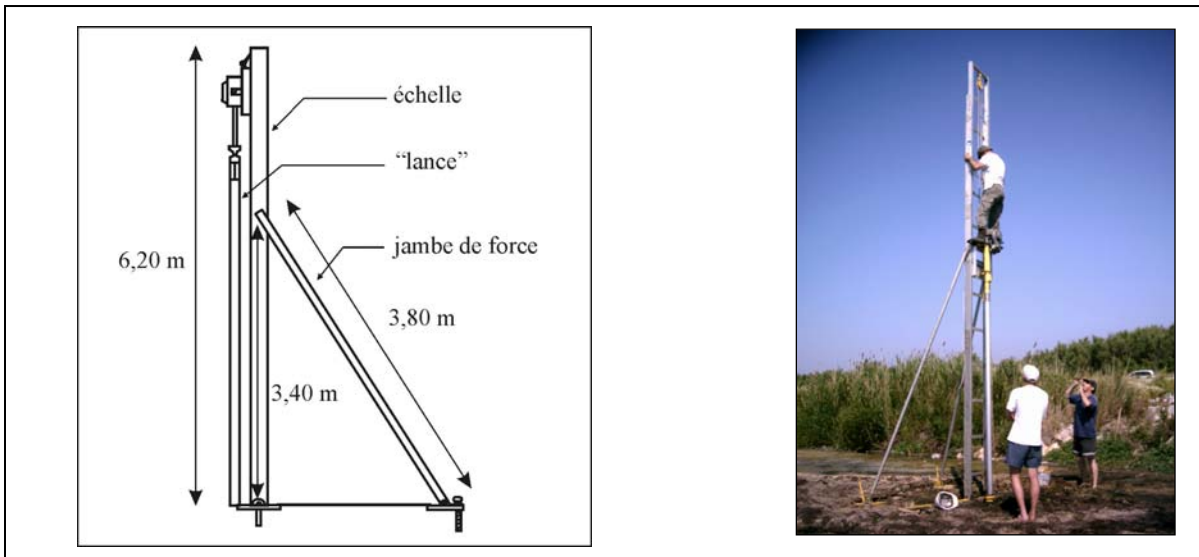


Figure I-7. Composition de la structure porteuse du vibrocarottier : une échelle permettant d'accéder à la « tête » de l'appareil et des jambes de force pour la stabilisation.

La « lance »

Elle se compose d'un assemblage de pièce permettant la fixation des tubes, aluminium ou pvc, leur pénétration et leur extraction. On notera que la tête du système est démontable et permet ainsi un échange en fonction du type d'opération à réaliser : carottage par vibration (manchon seul) ou percussion (module de frappe) ou extraction (module d'extraction).

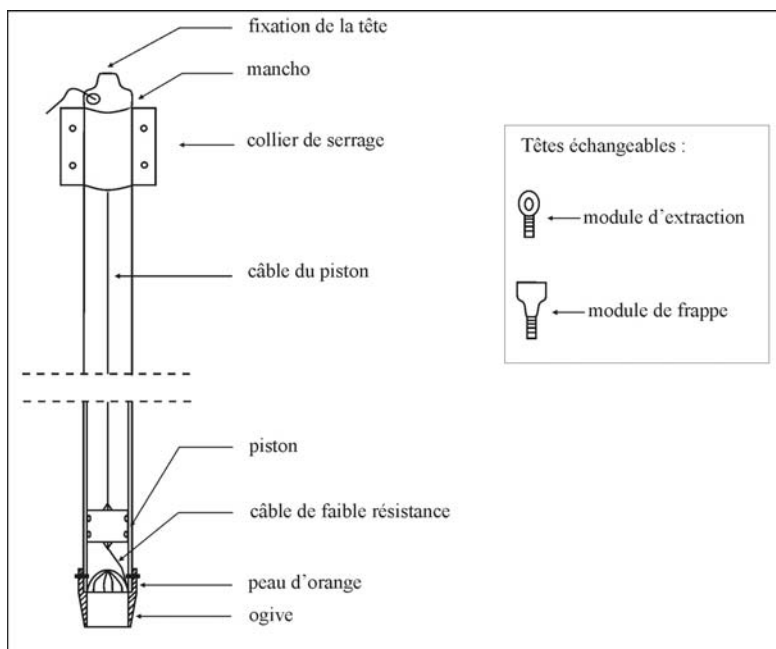


Figure I-8. Les éléments constitutants la « lance » du vibrocarottier.

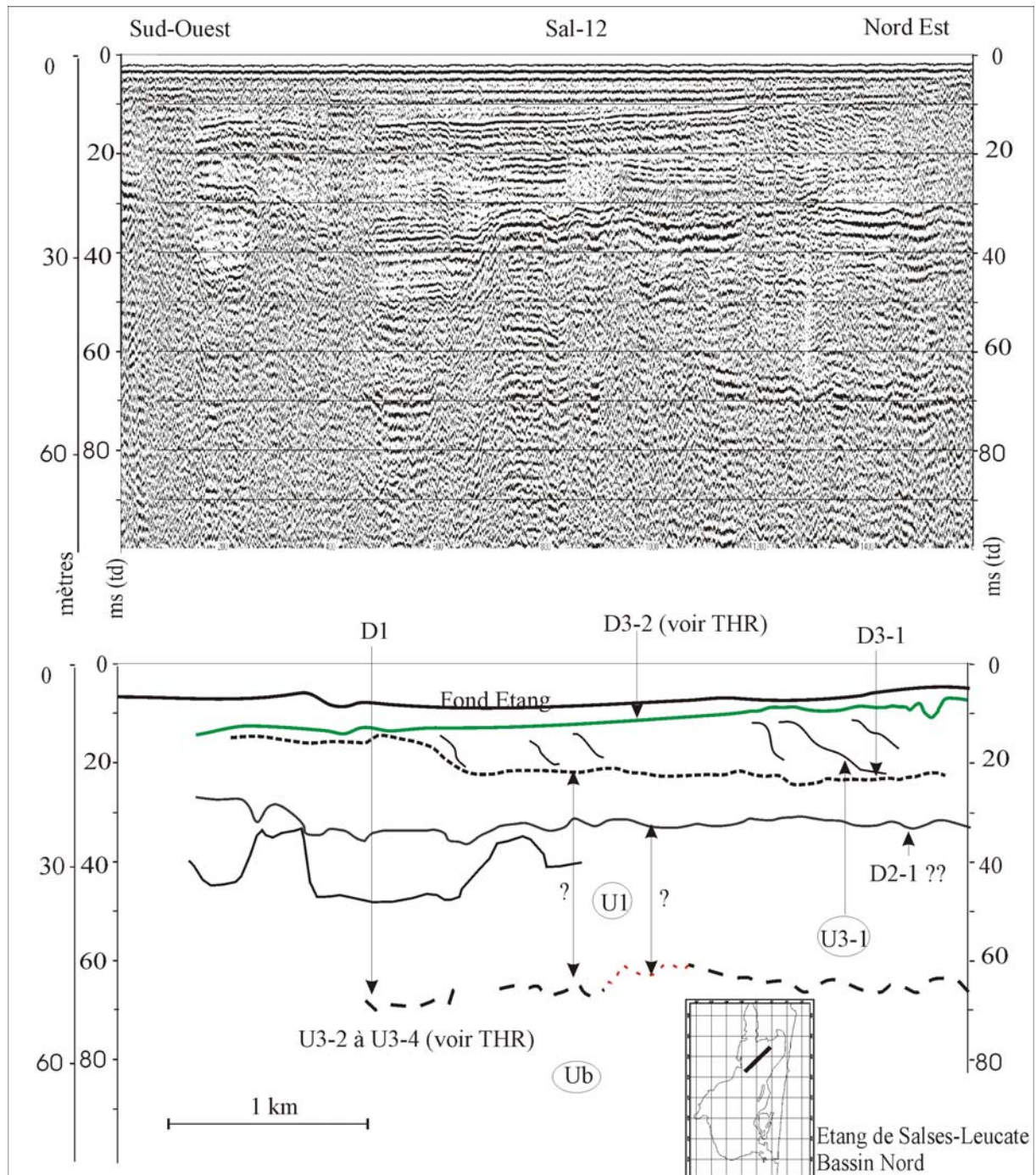
ANNEXE II

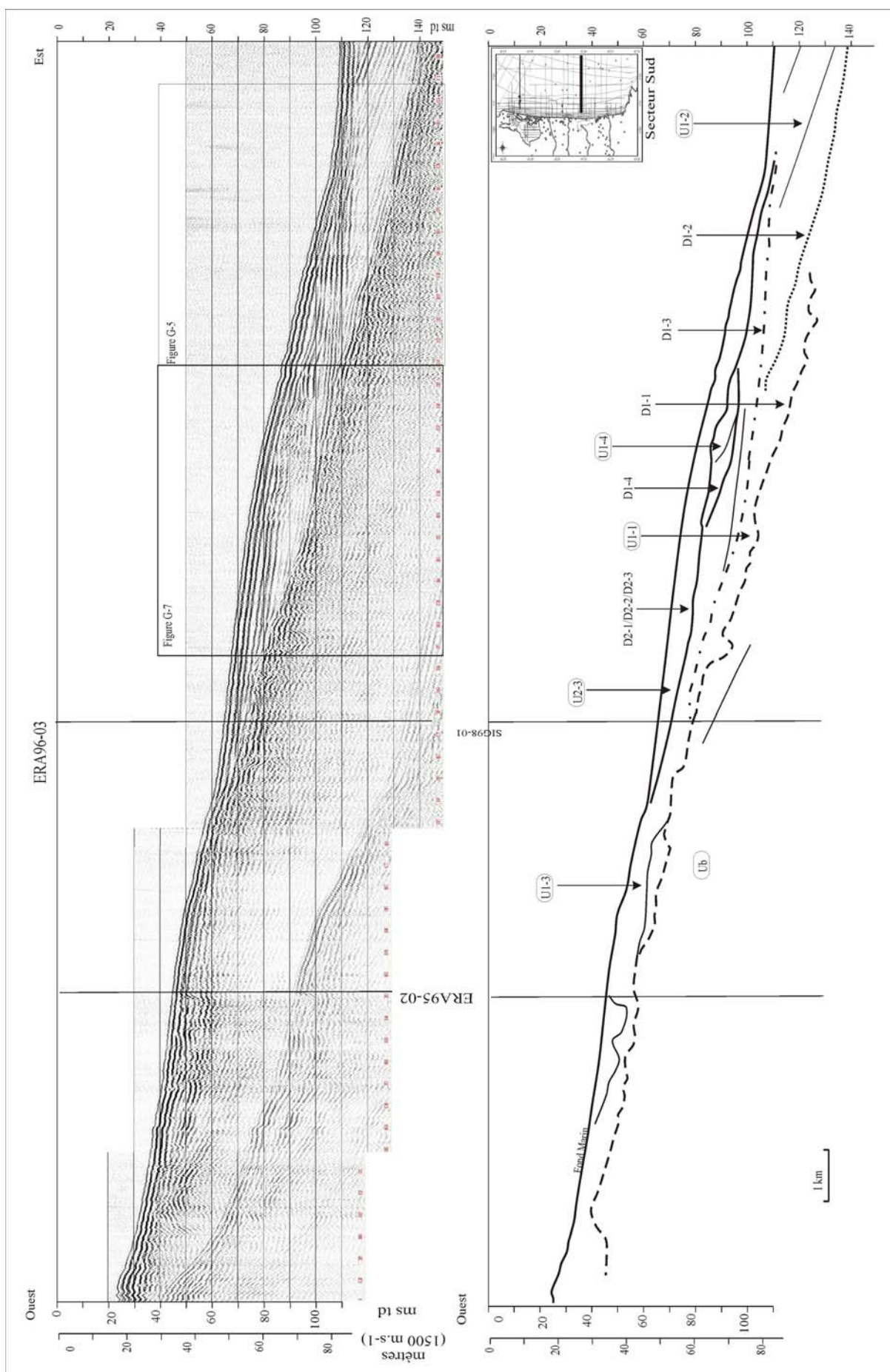
PROFILS SISMIQUES, CARTES ISOBATHES ET ISOPAQUES

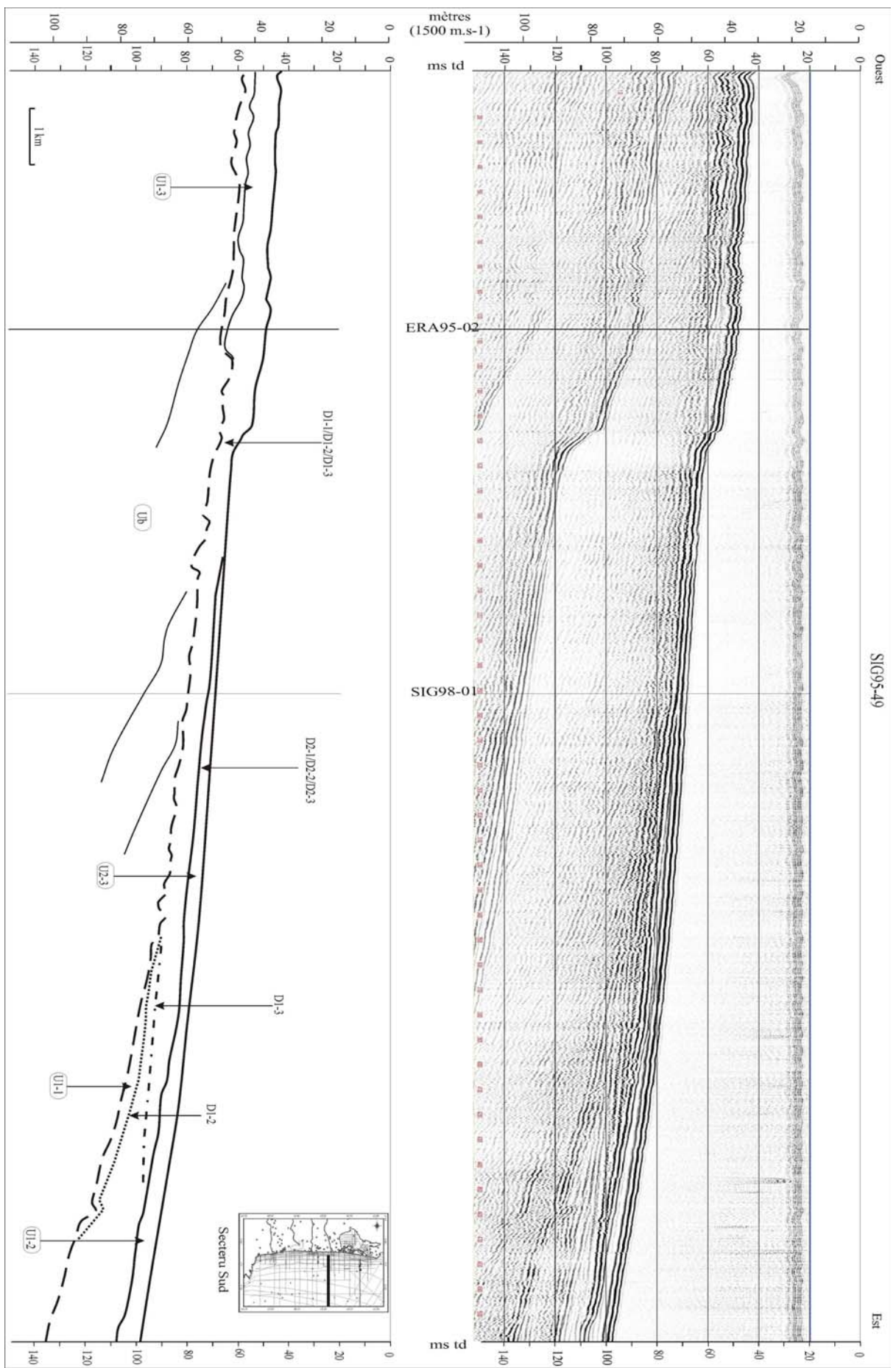
Le Roussillon

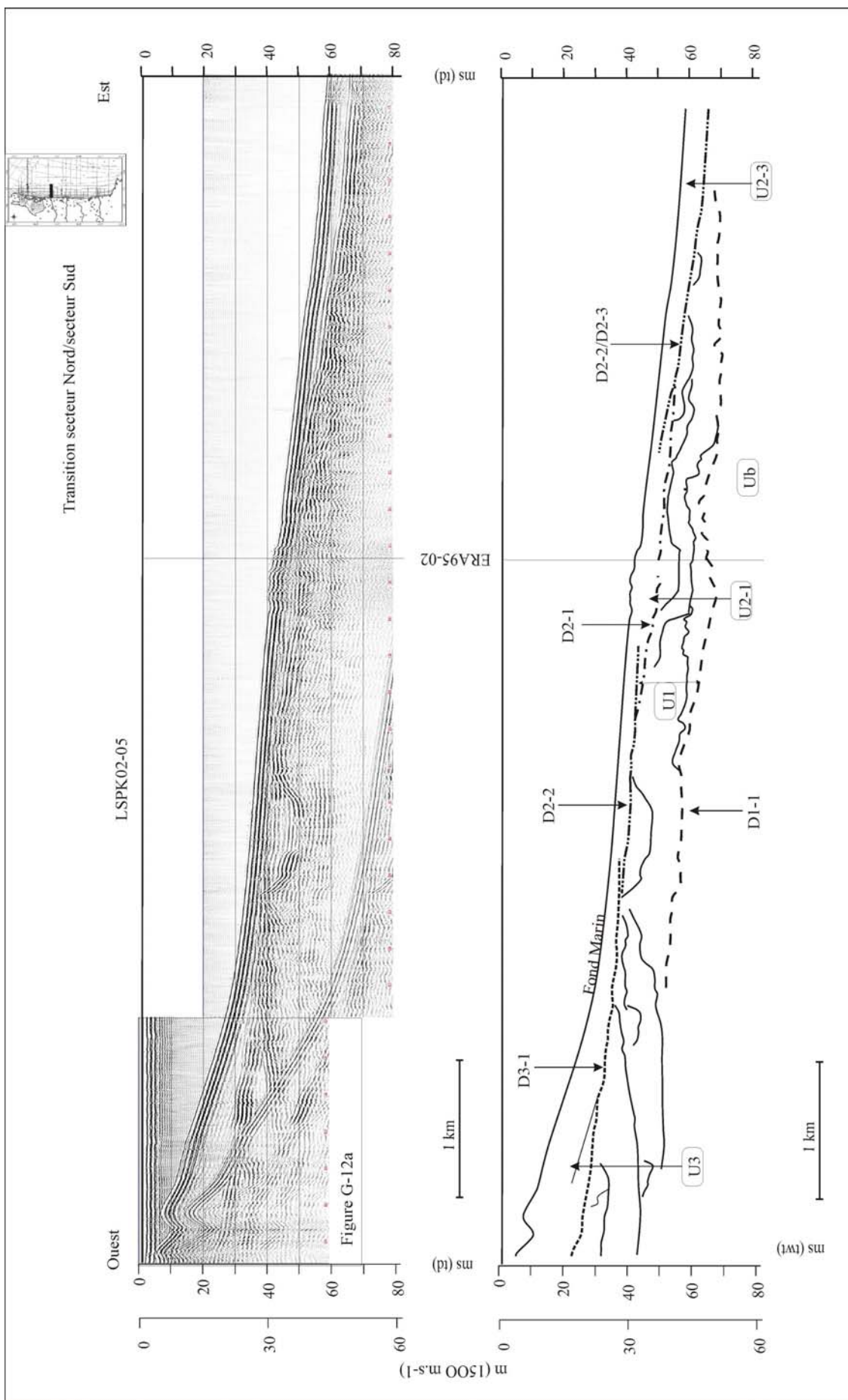
Les profils sismiques et leur pointé

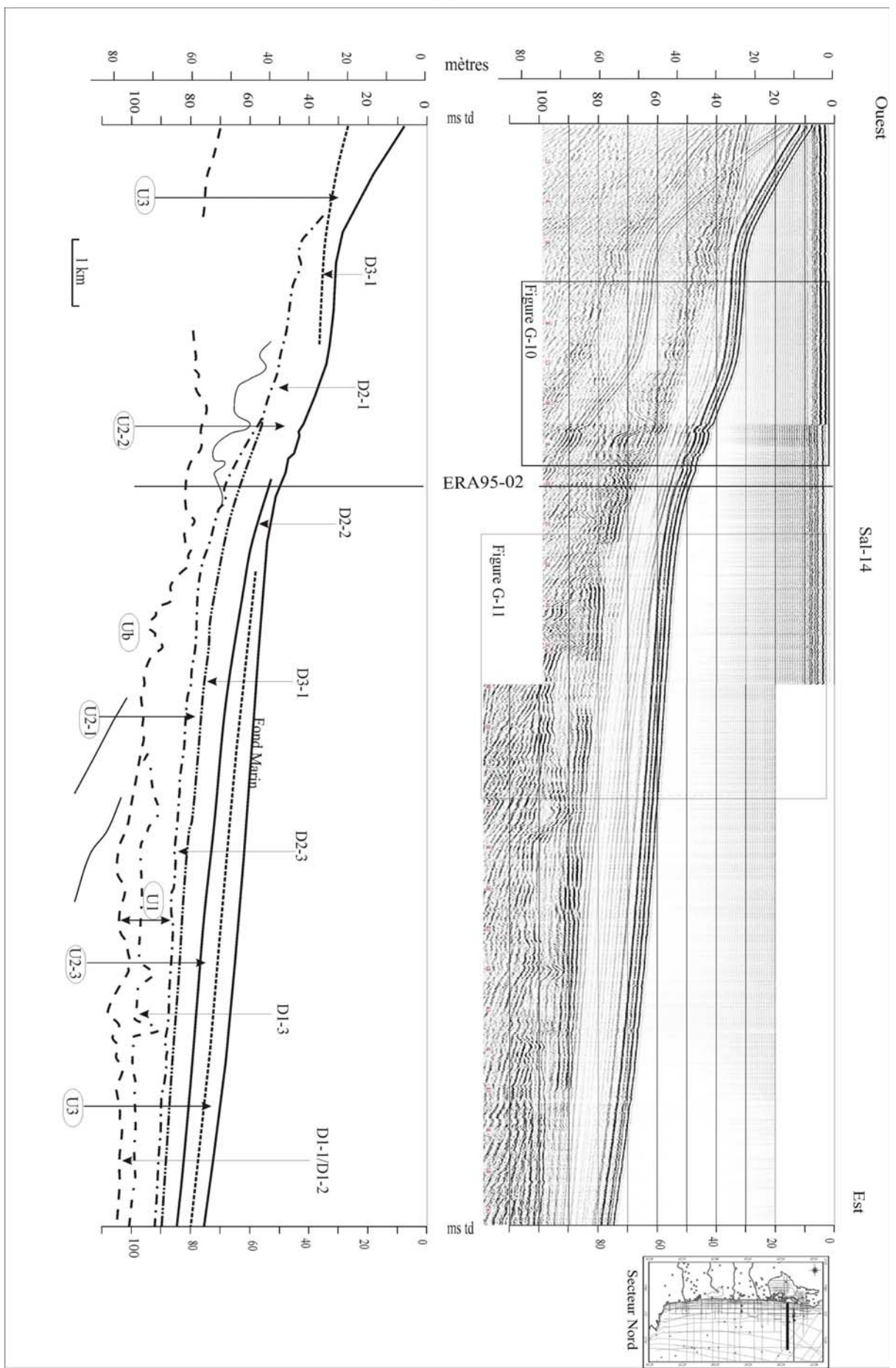
Sismique HR

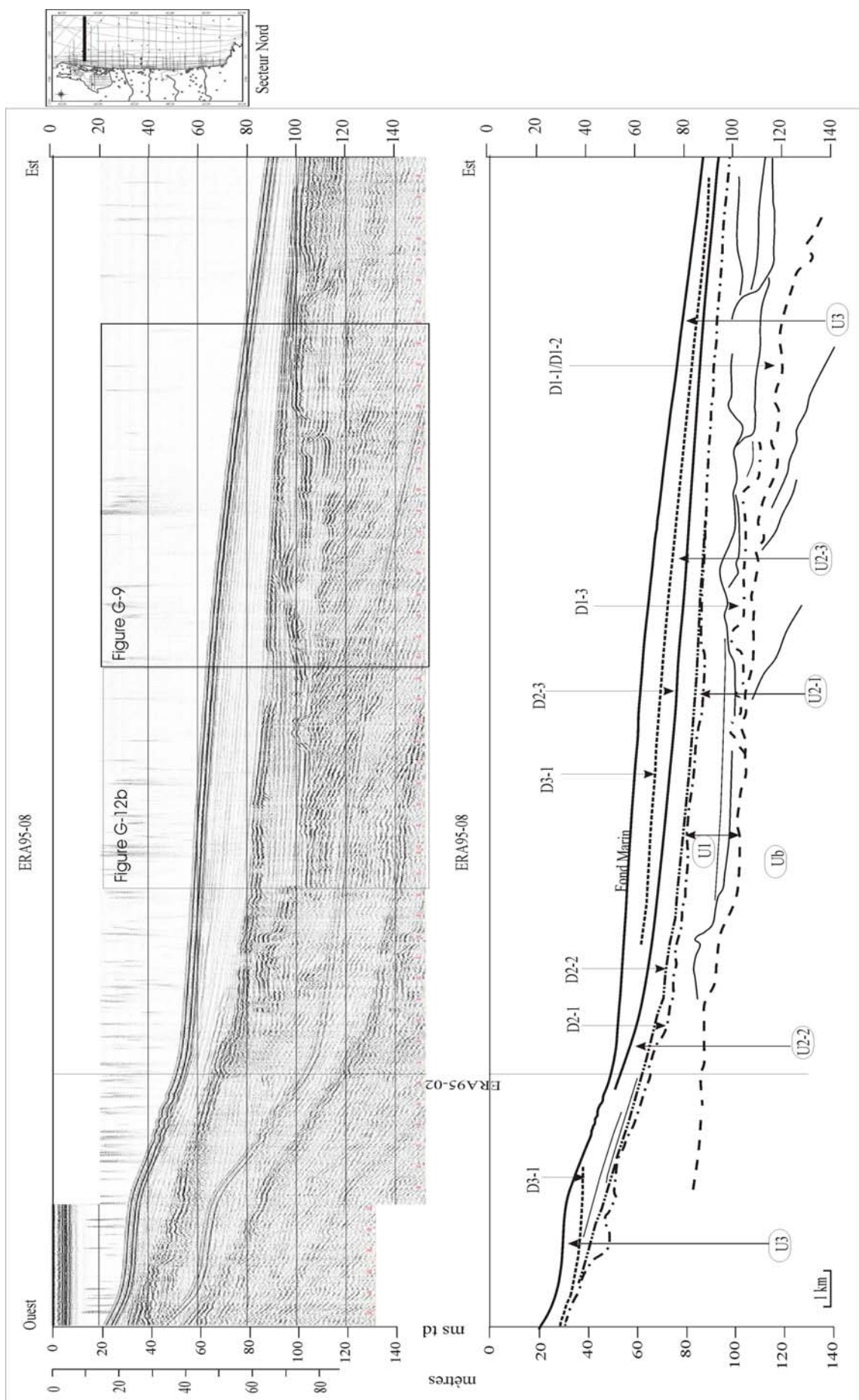


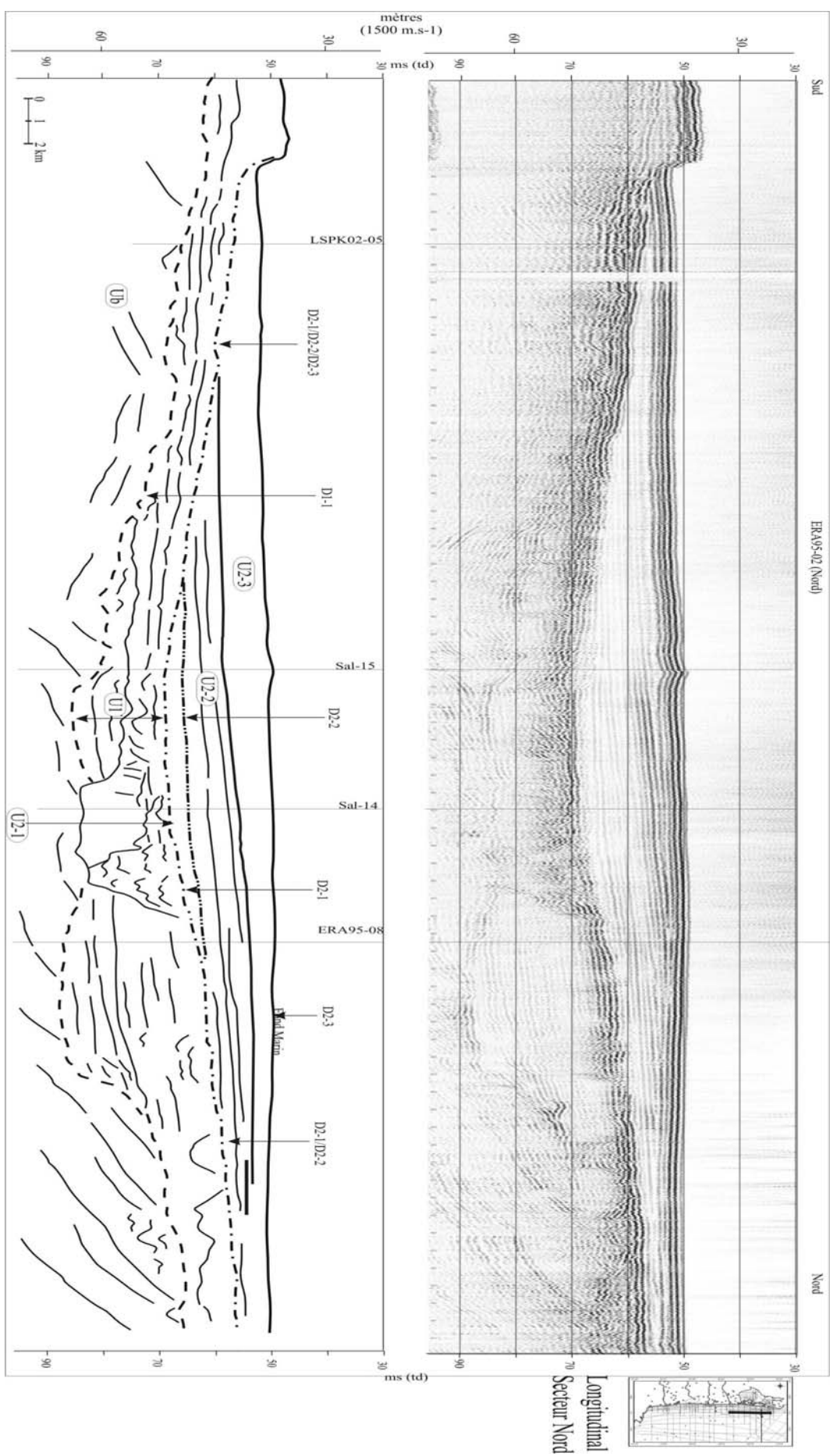




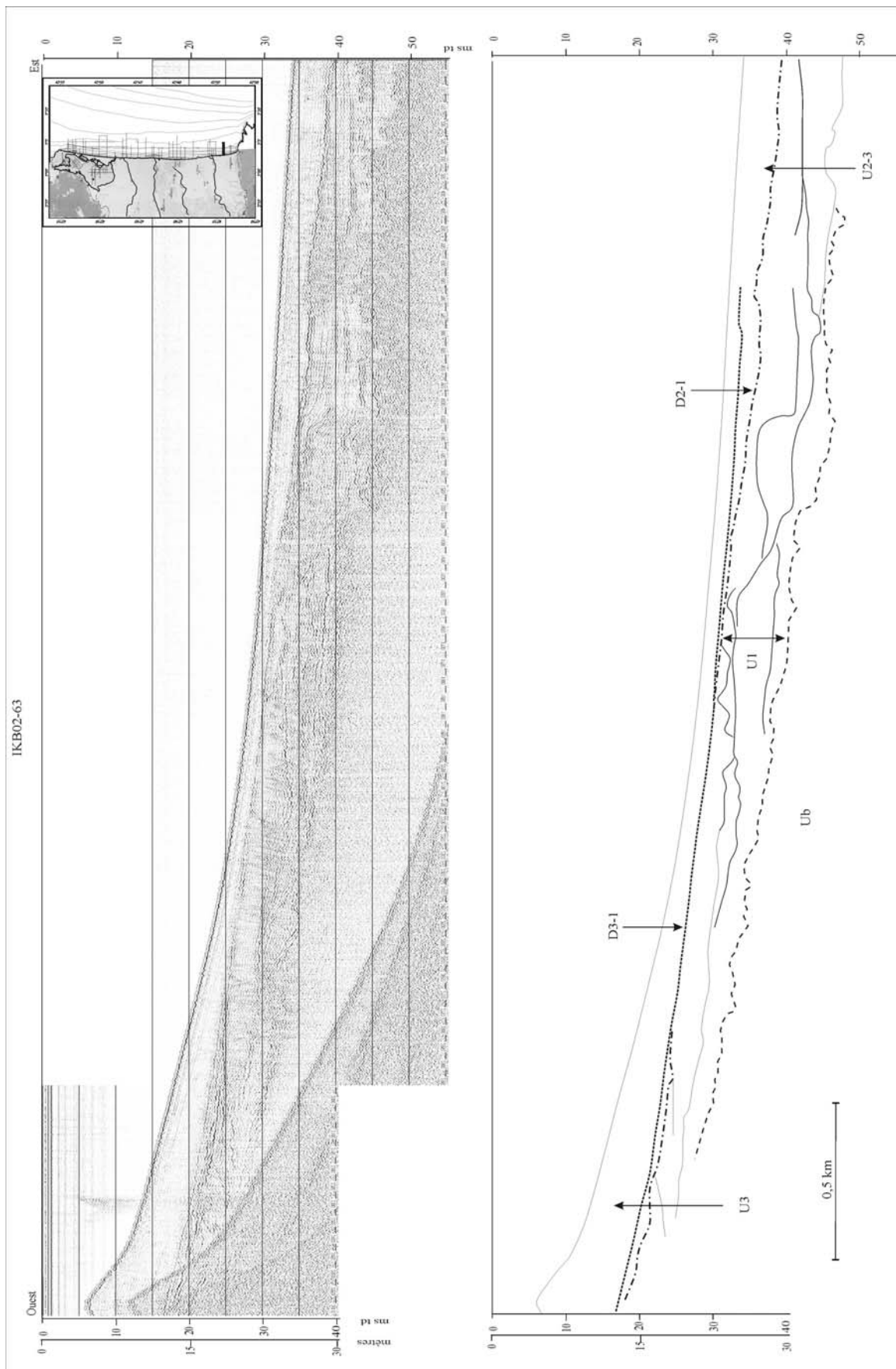


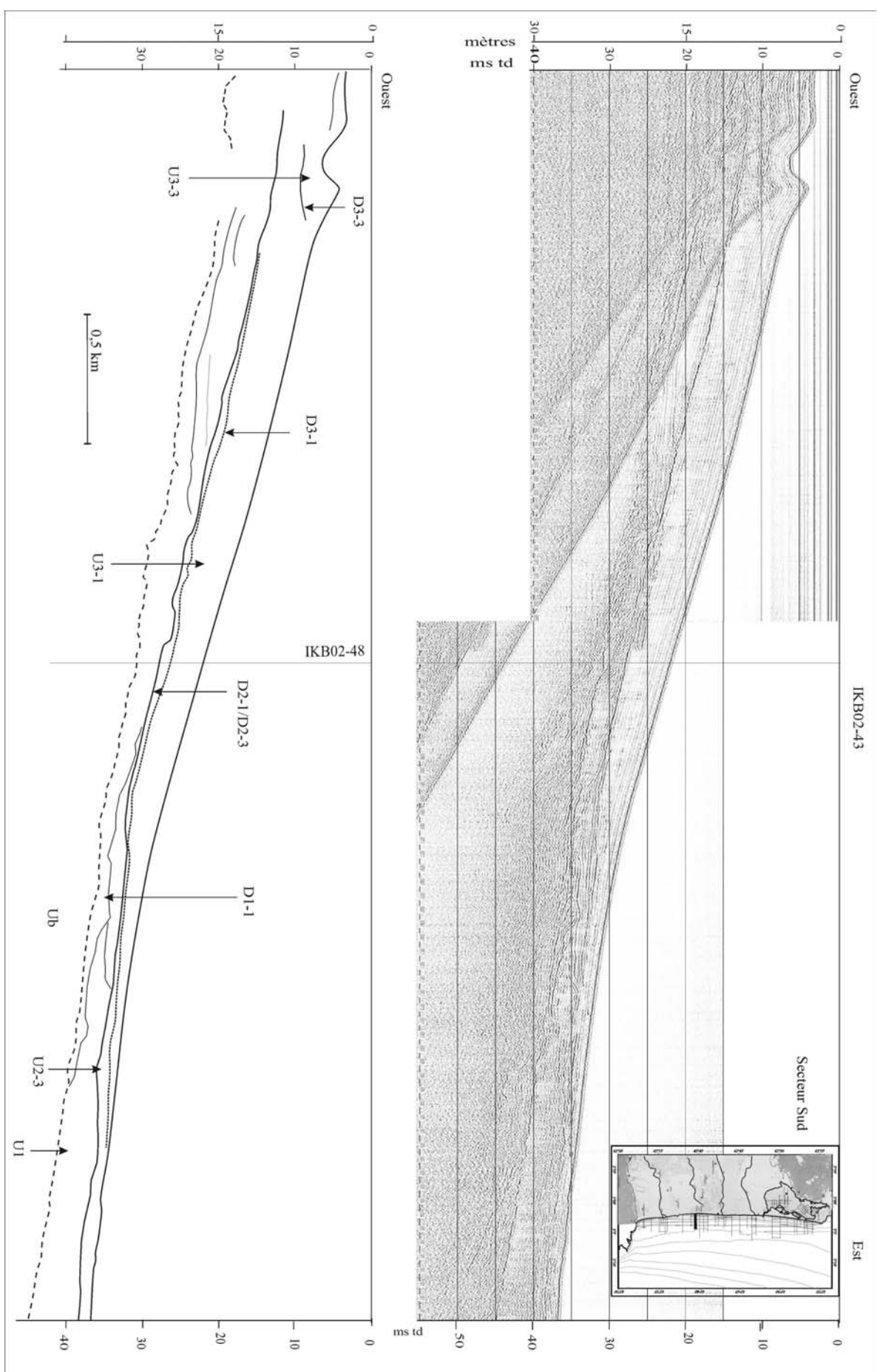


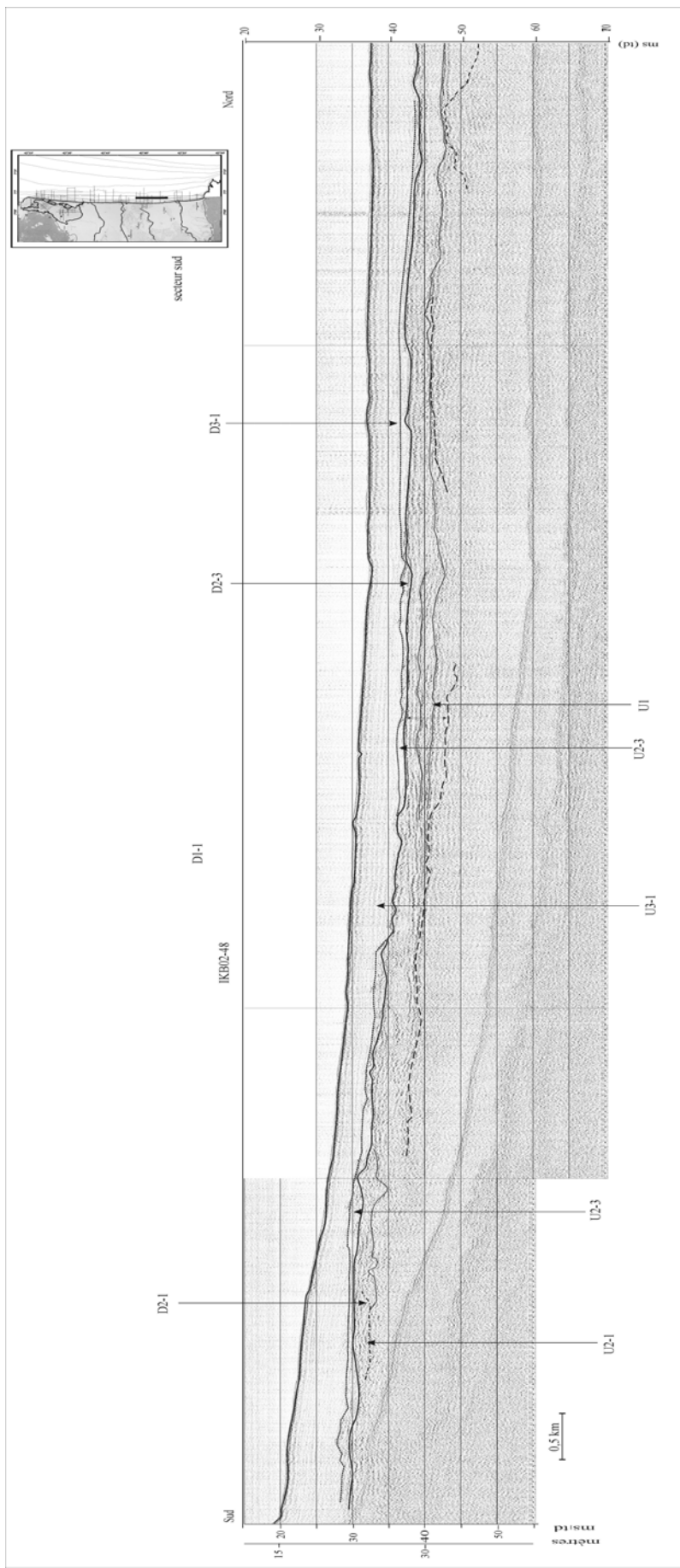


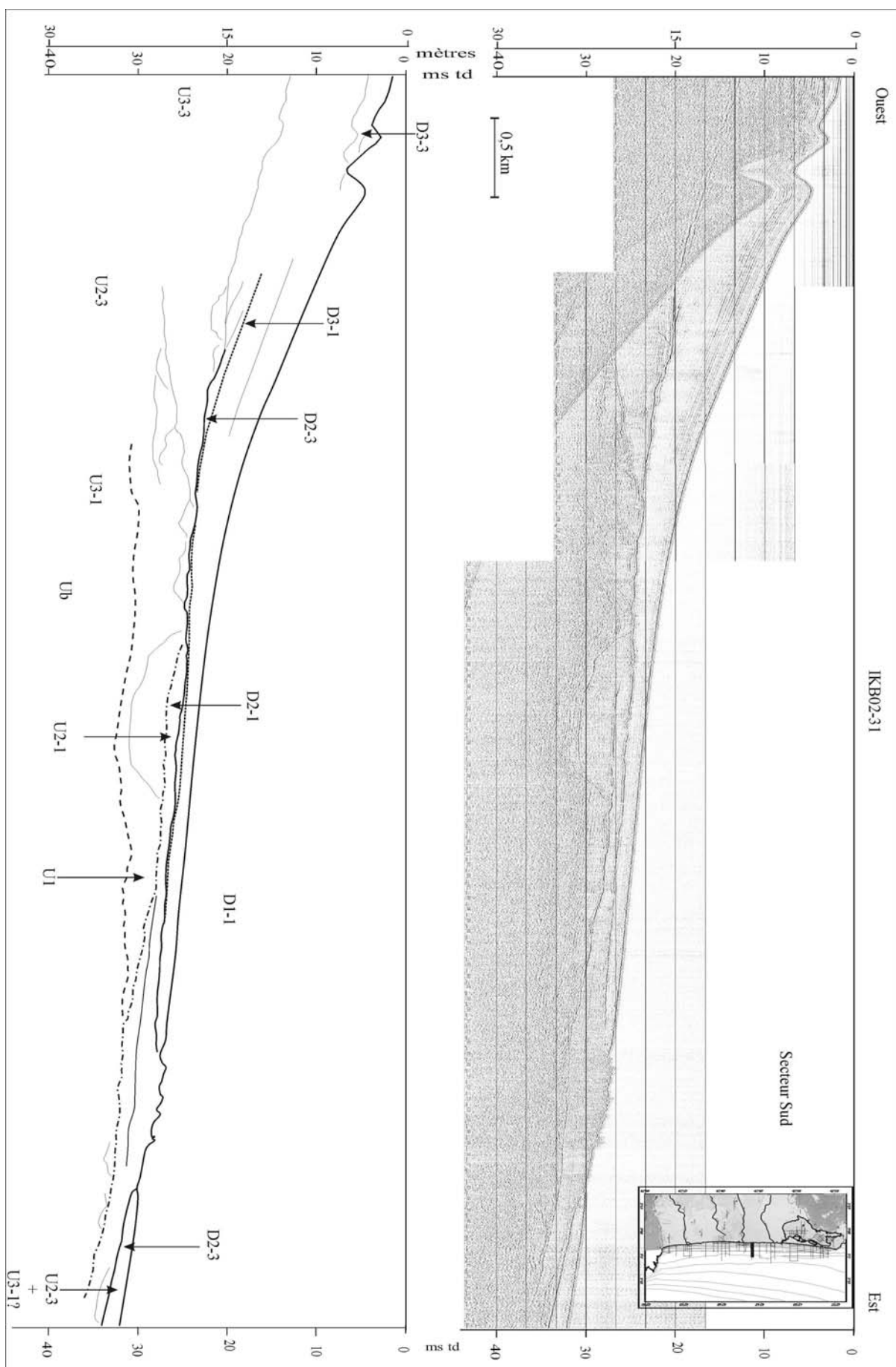


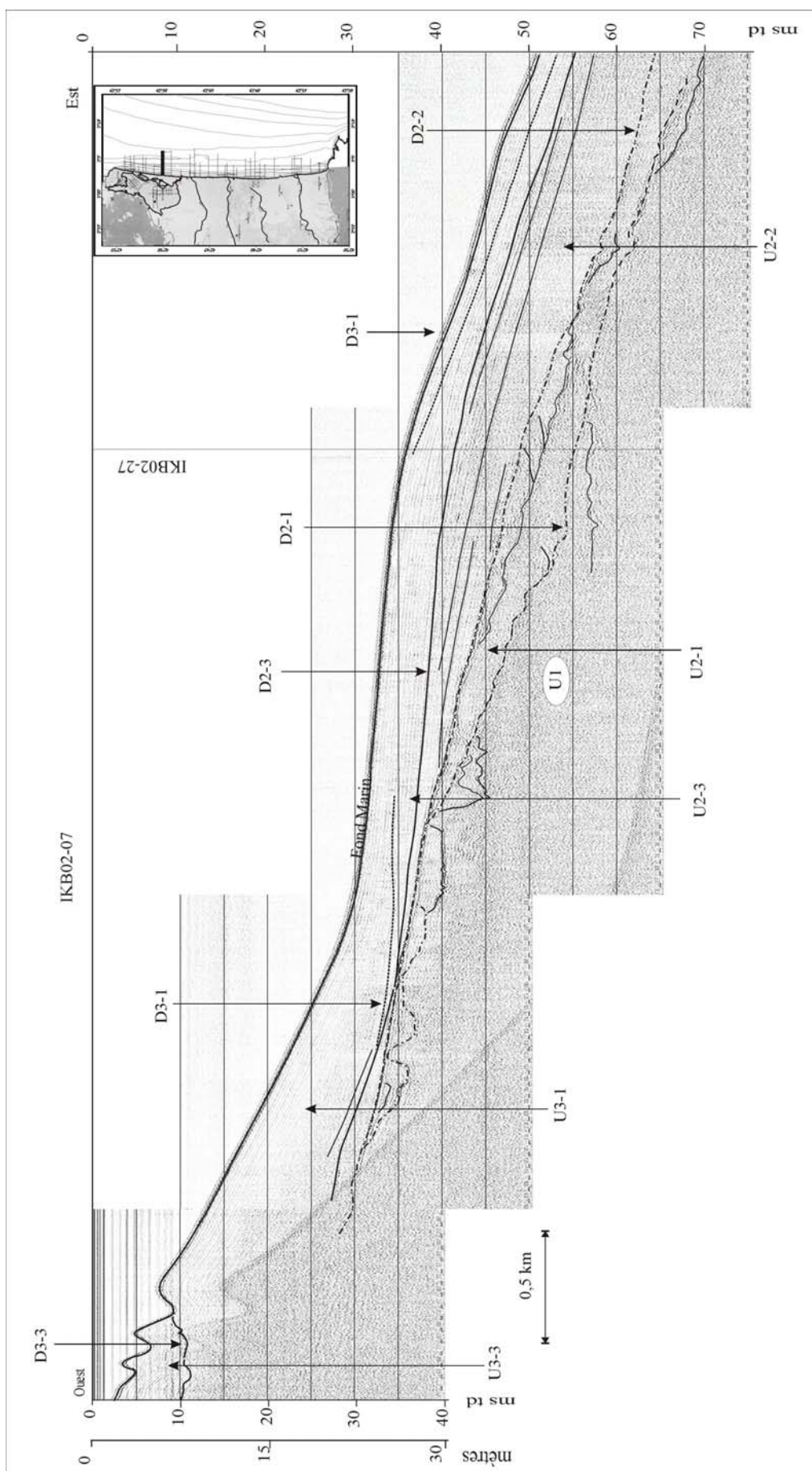
Sismique THR

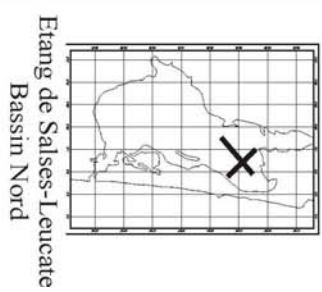
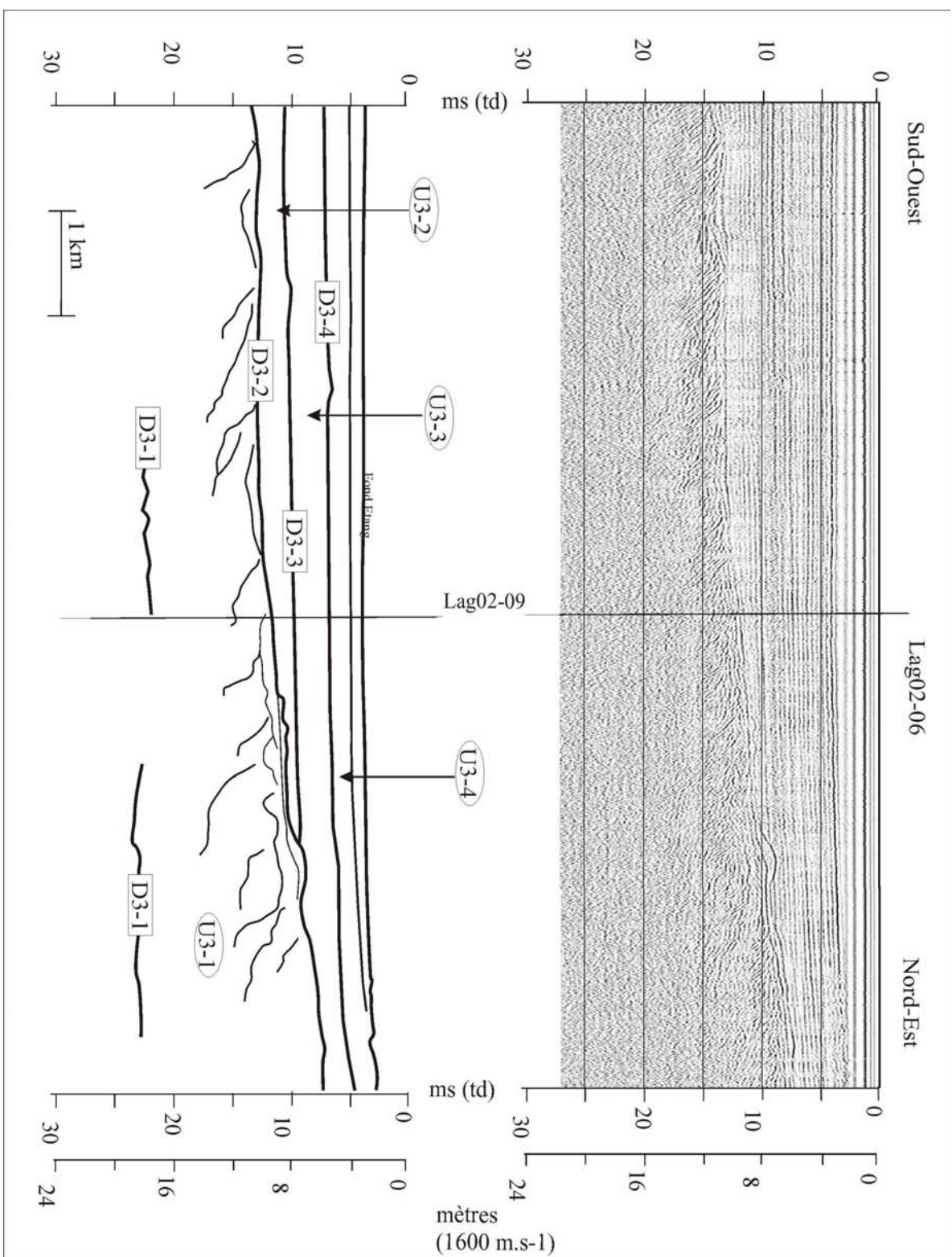


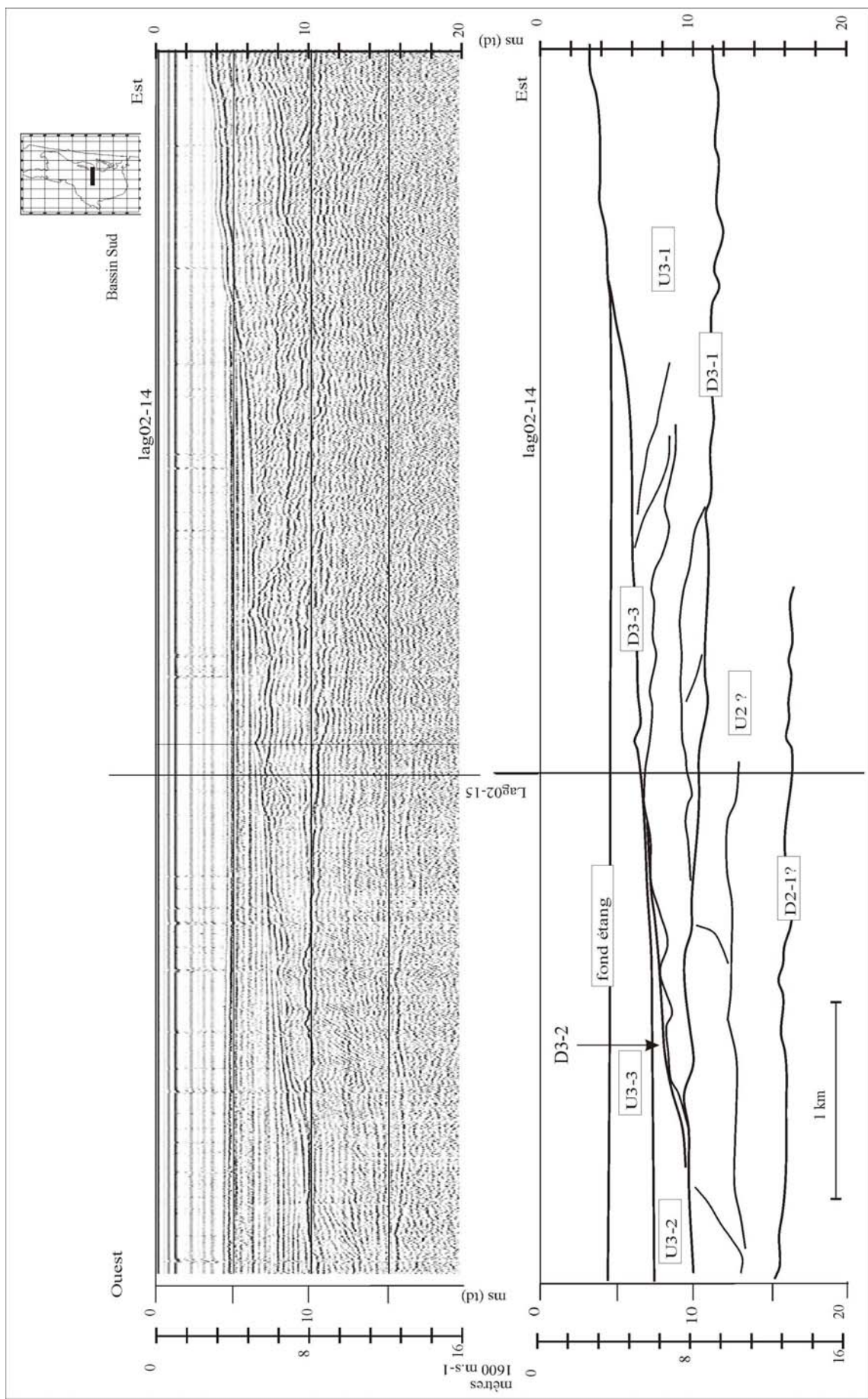












Les cartes isobathes des principales discontinuités

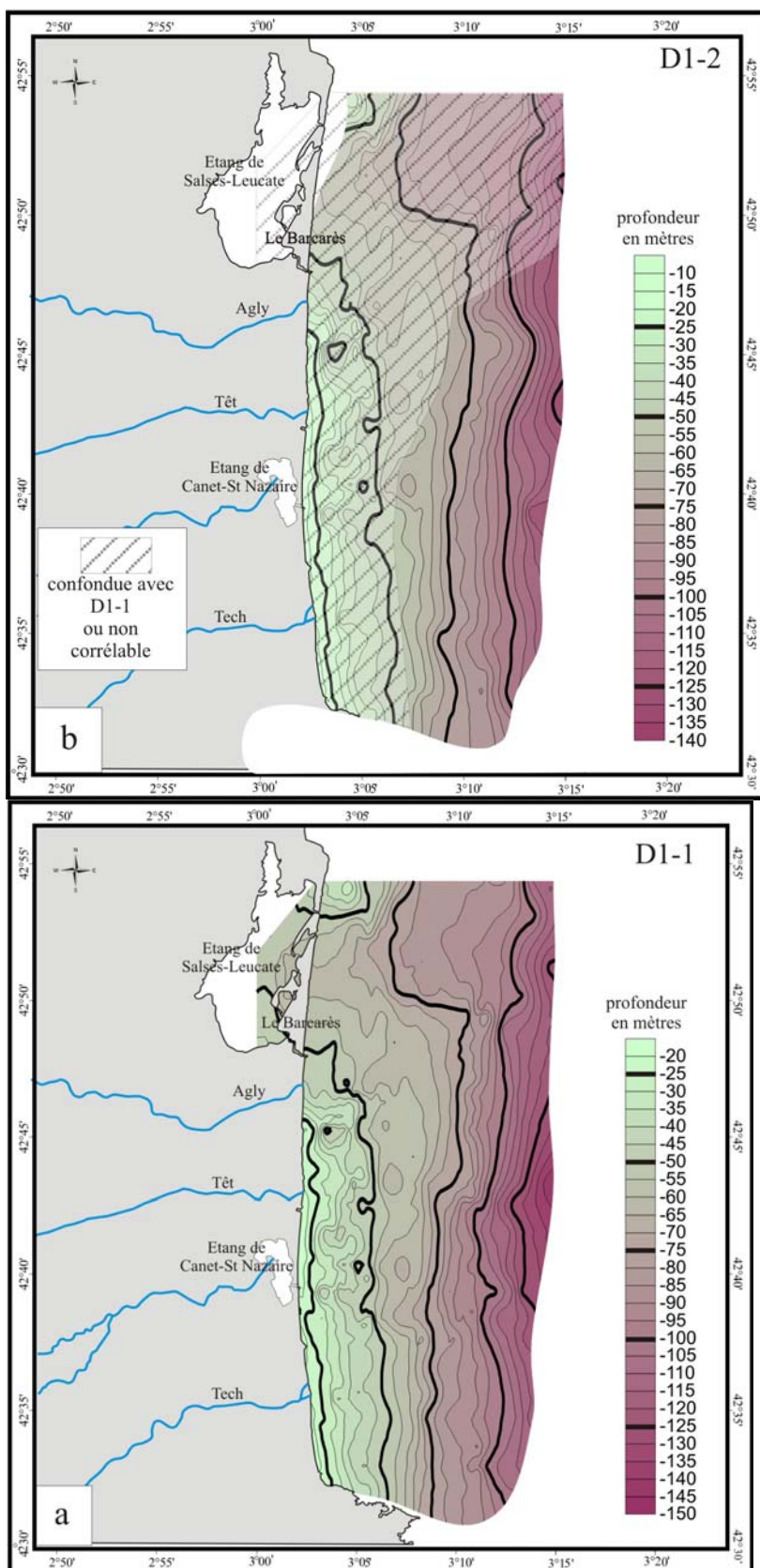


Figure 1.-1. Cartes isobathes des discontinuités D1-1 (a) et D1-2 (b).

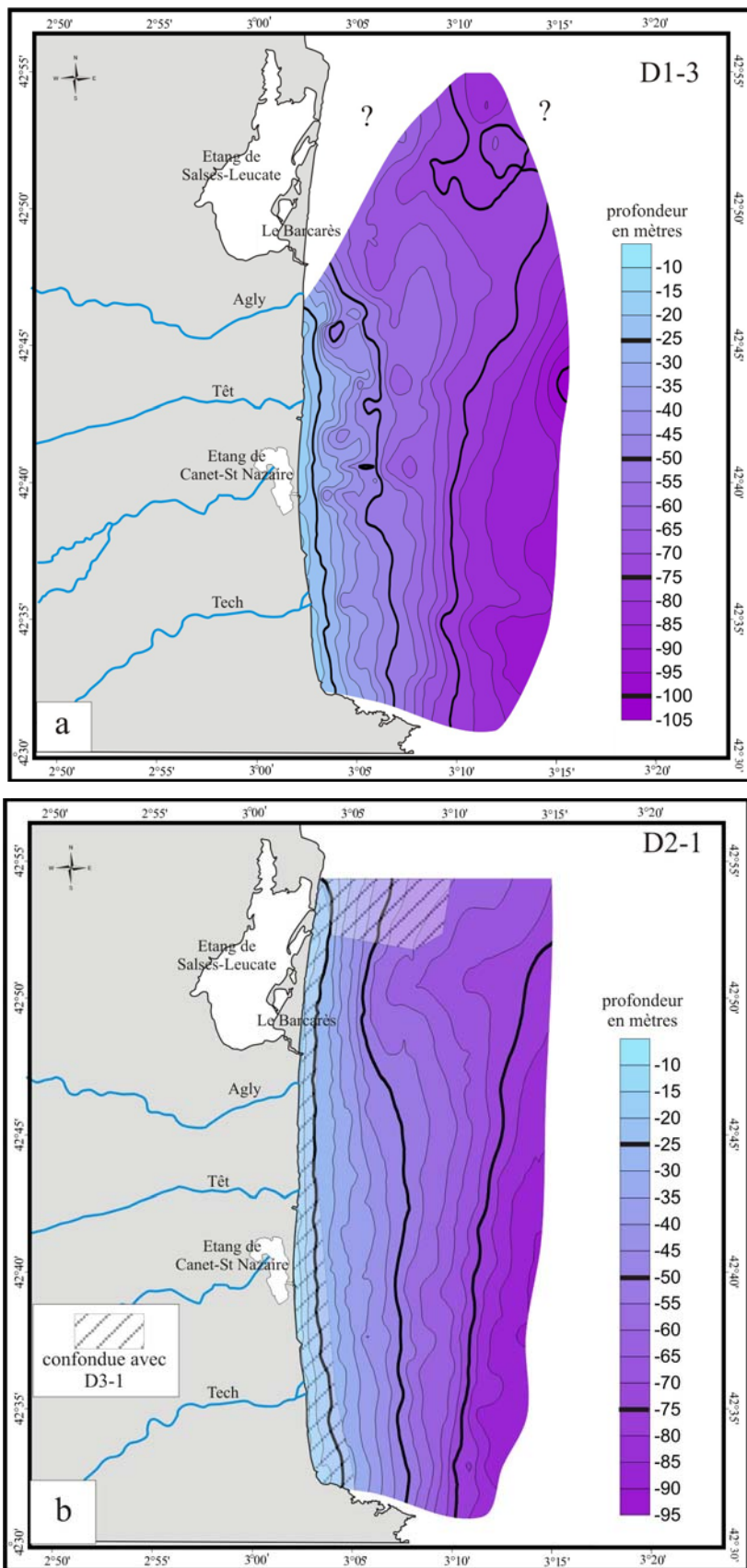


Figure 1.0-2. Cartes isobathes des discontinuités D1-3 (a) et D2-1(b).

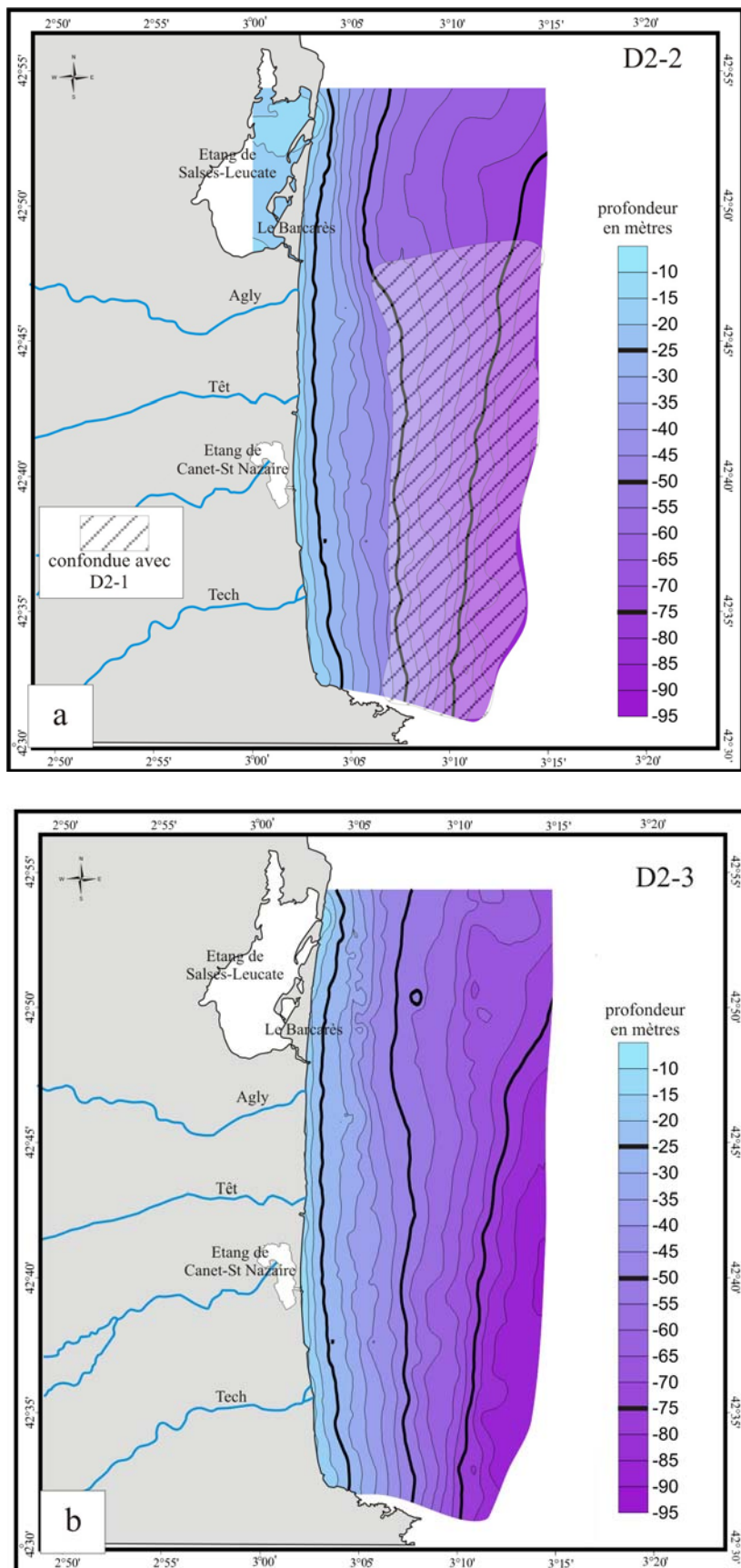


Figure 1.-3. Cartes isobathes des discontinuités D2-2 (a) et D2-3(b).

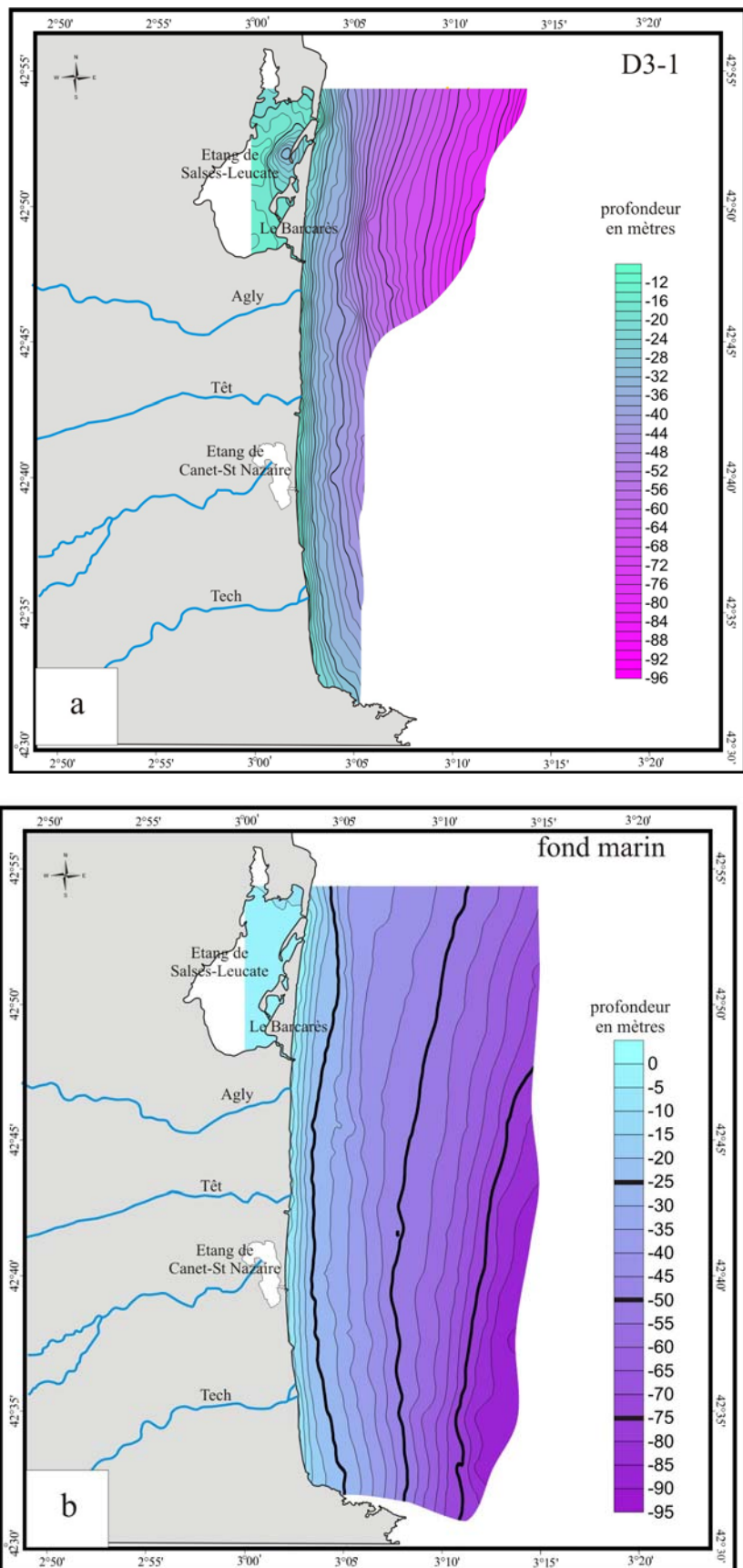


Figure 1.-4. Cartes isobathes des discontinuités D3-1 (a) et du fond marin (b).

Les cartes isopaques des unités sismiques

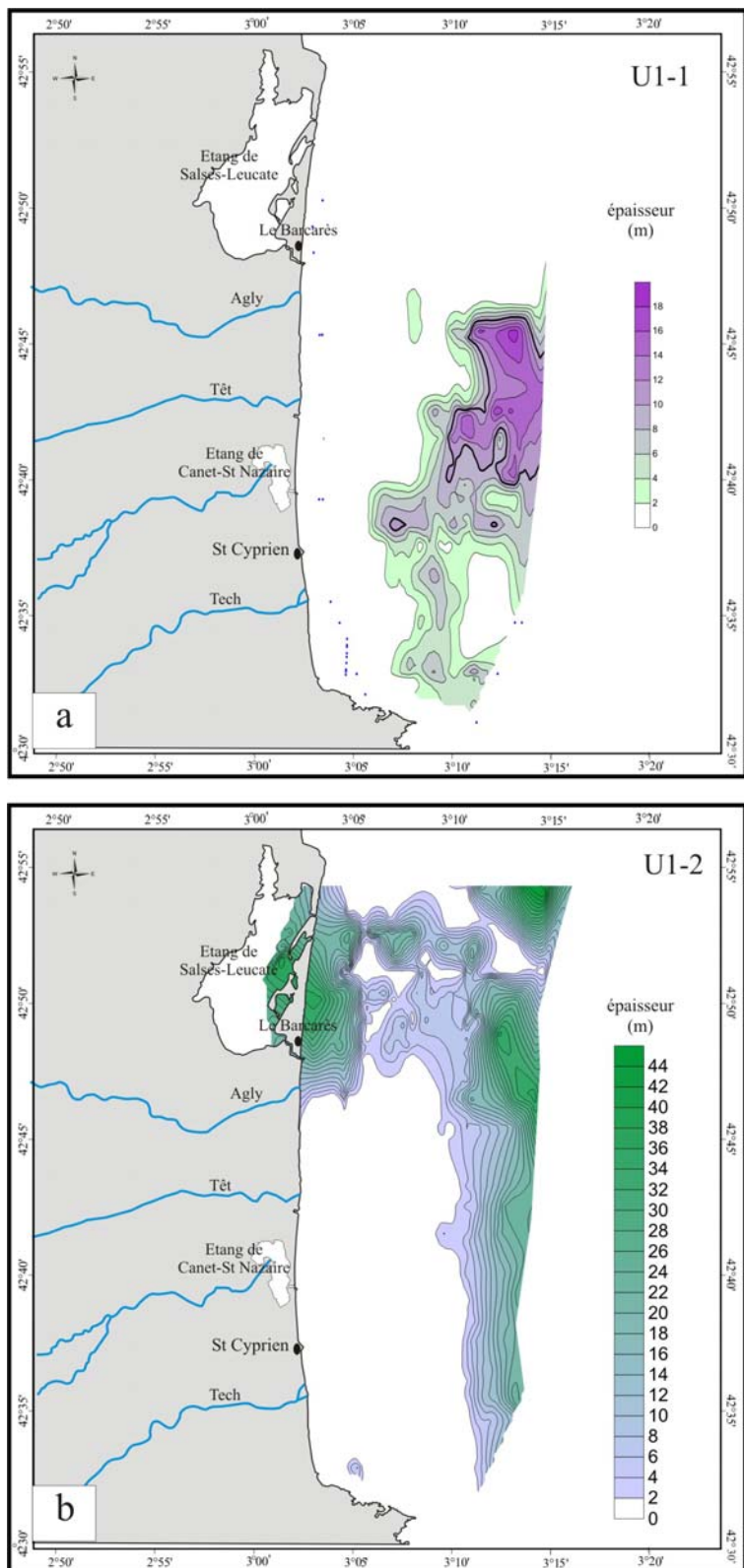


Figure 1. -5. Cartes isopaques des unités U1-1 (a) et U1-2 (b). Vs : 1750 m.s⁻¹

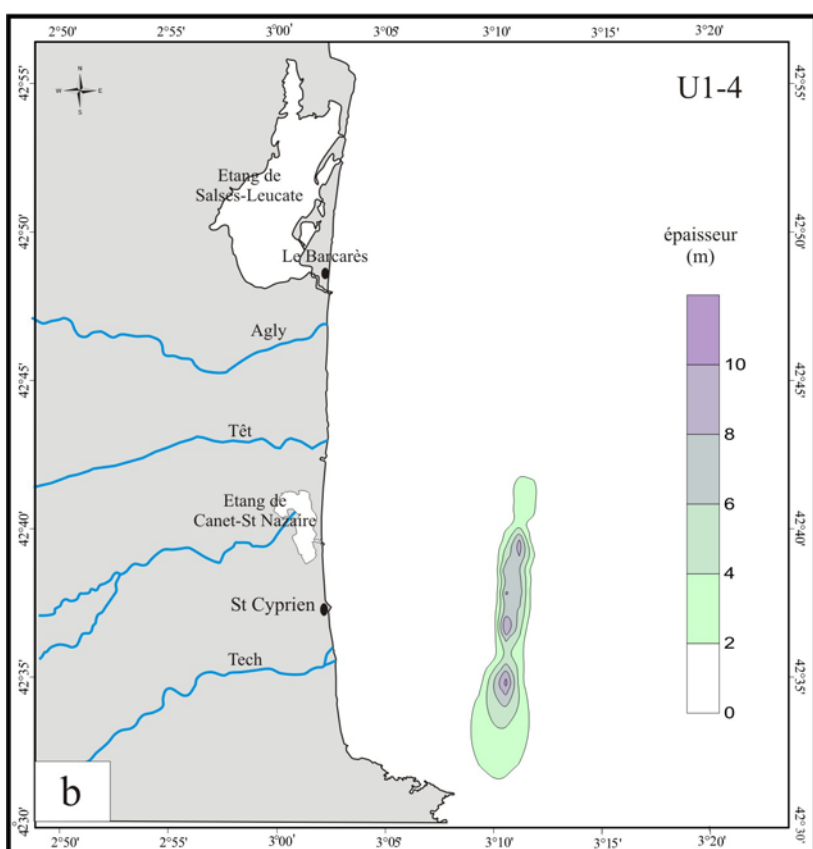
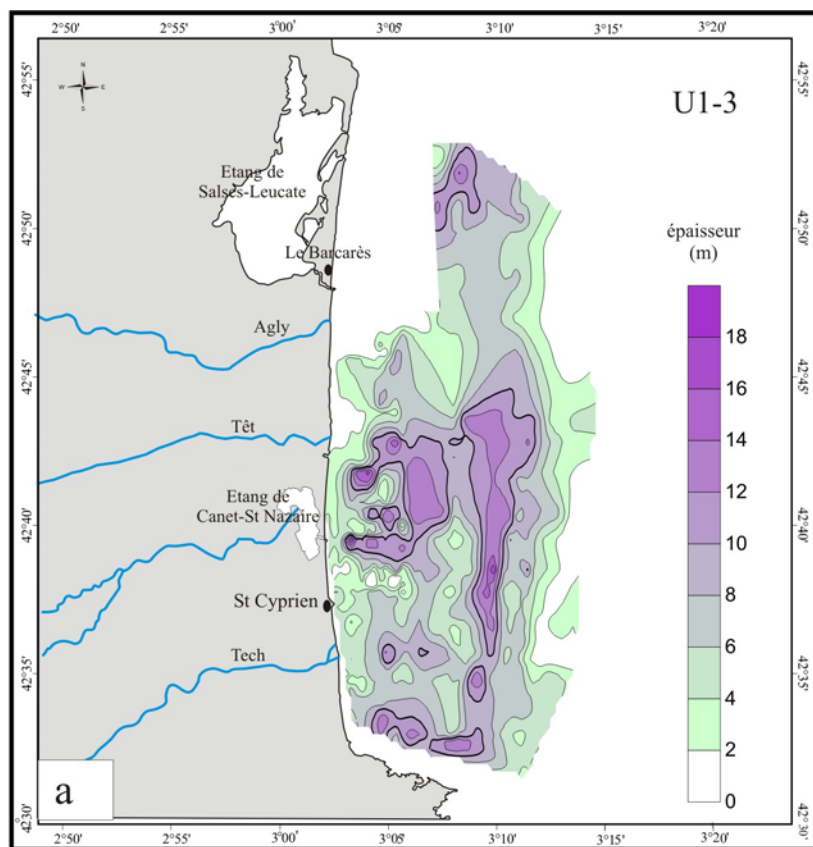


Figure 1.0-6. Cartes isopaques des unités U1-2 (a) et U1-3 (b). Vs : 1750 m.s⁻¹

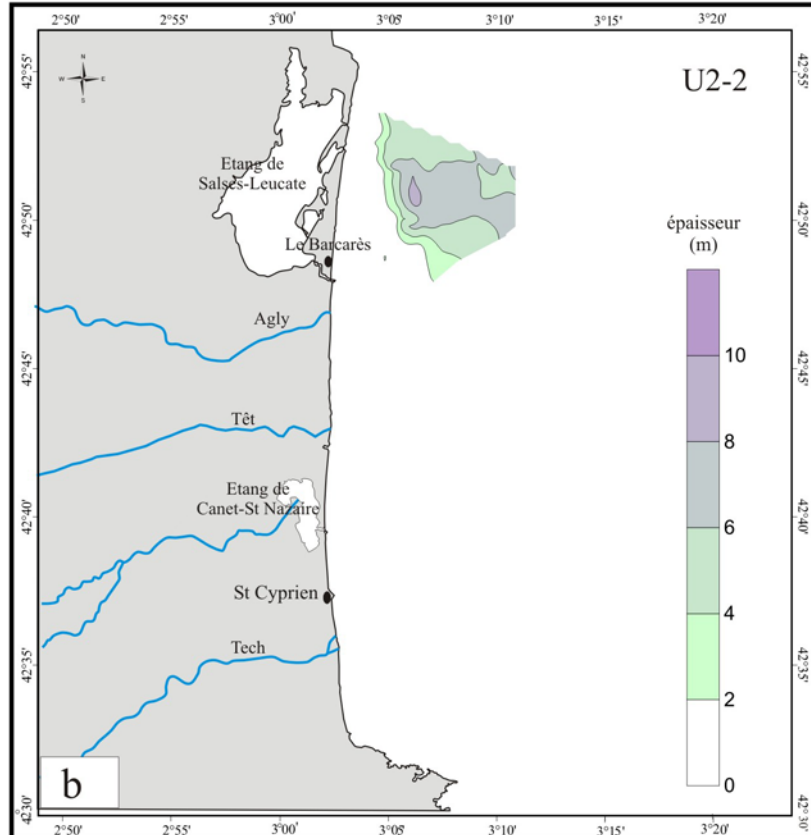
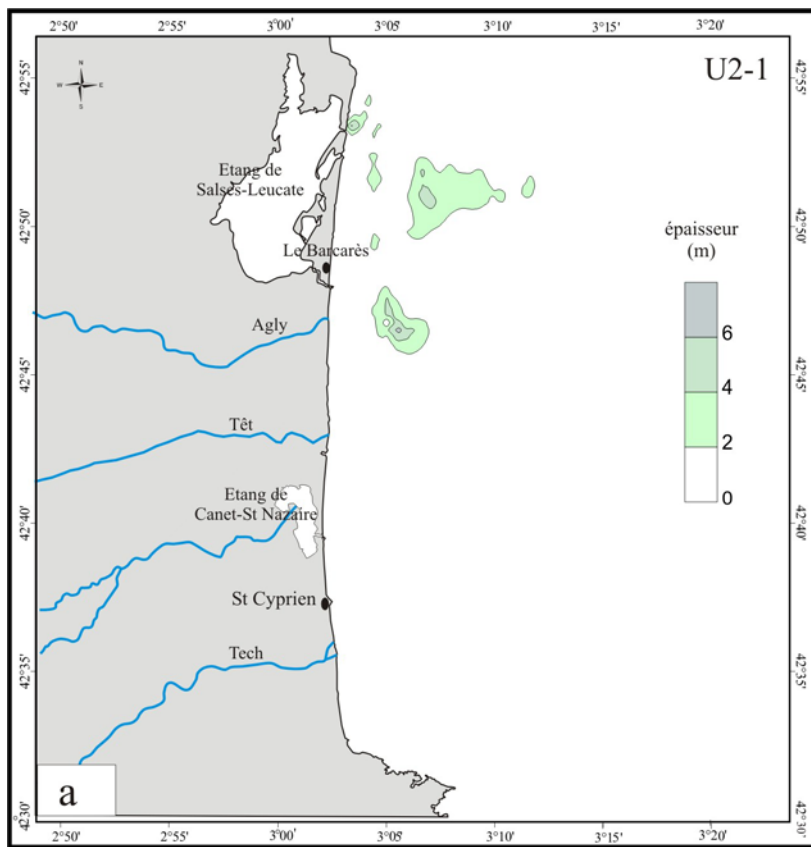


Figure 1.7. Cartes isopaques des unités U2-1 (a) et U2-2 (b). Vs : 1750 m.s⁻¹

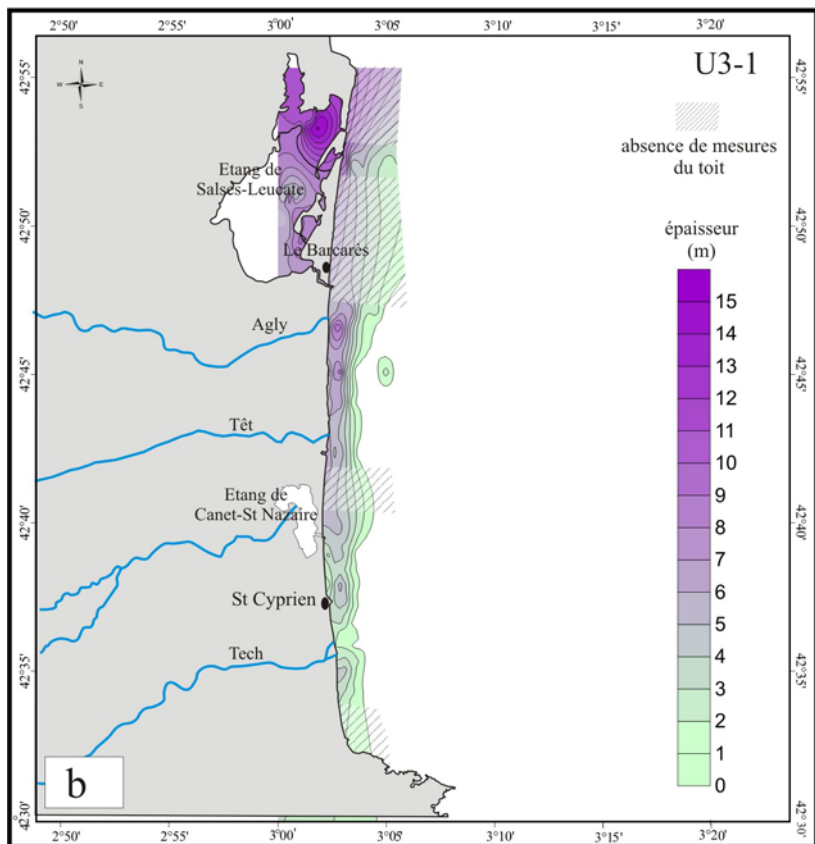
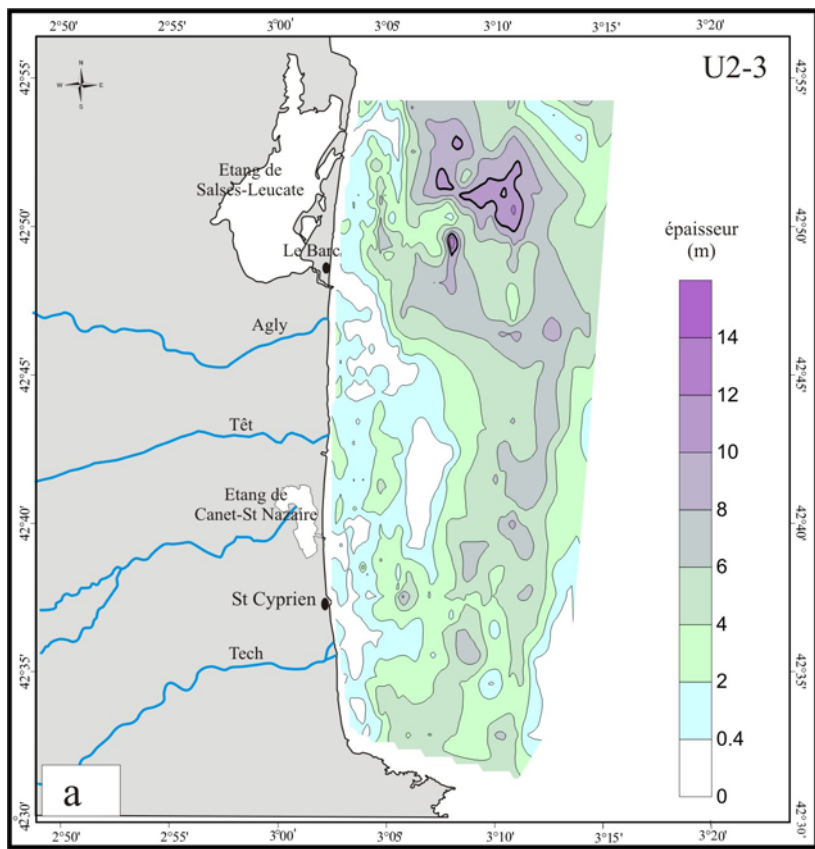


Figure 1-8. Cartes isopaques des unités U2-3(a) et U3-1(b). Vs : 1750 m.s⁻¹

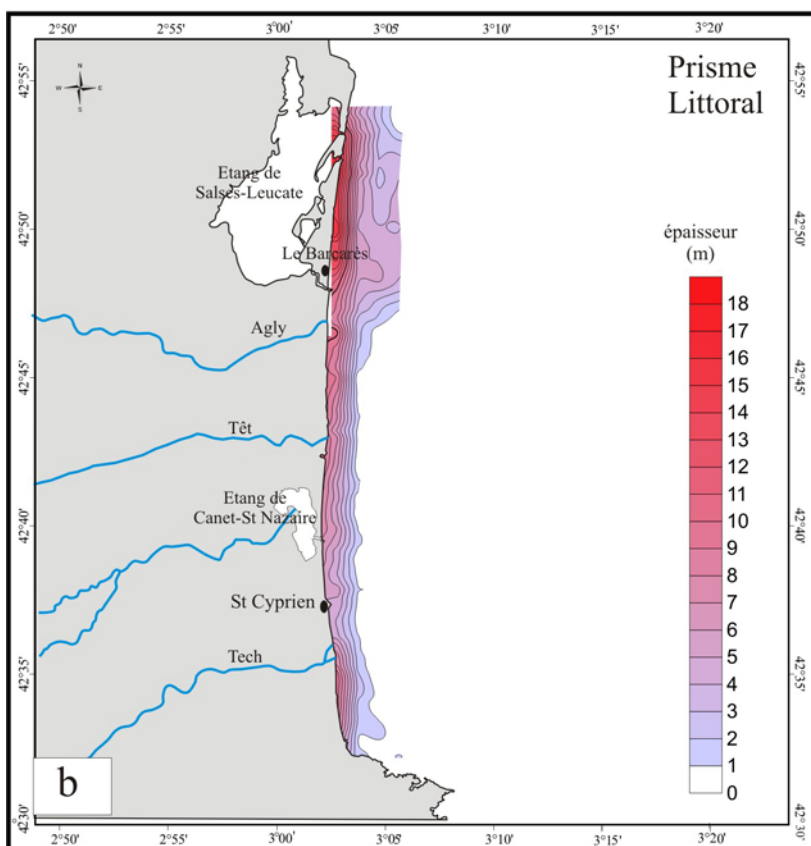
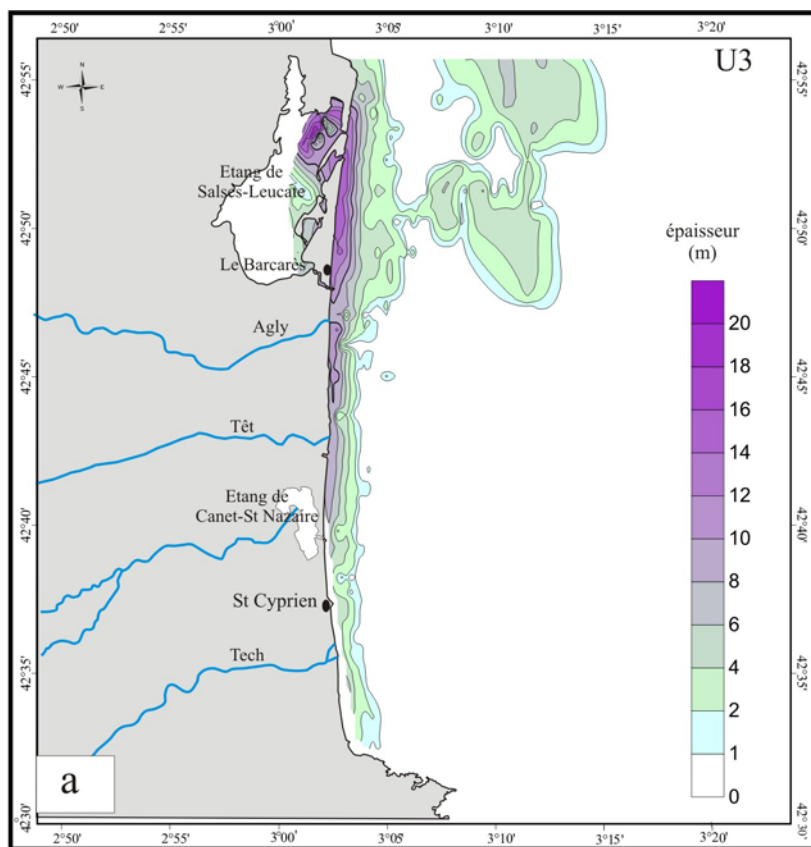


Figure 1.-9. Cartes isopaques des unités U3 (a) et prisme littoral (b). Vs : 1750 m.s⁻¹

La plate-forme du Rhône et son extension occidentale

Les cartes isobathes des principales discontinuités

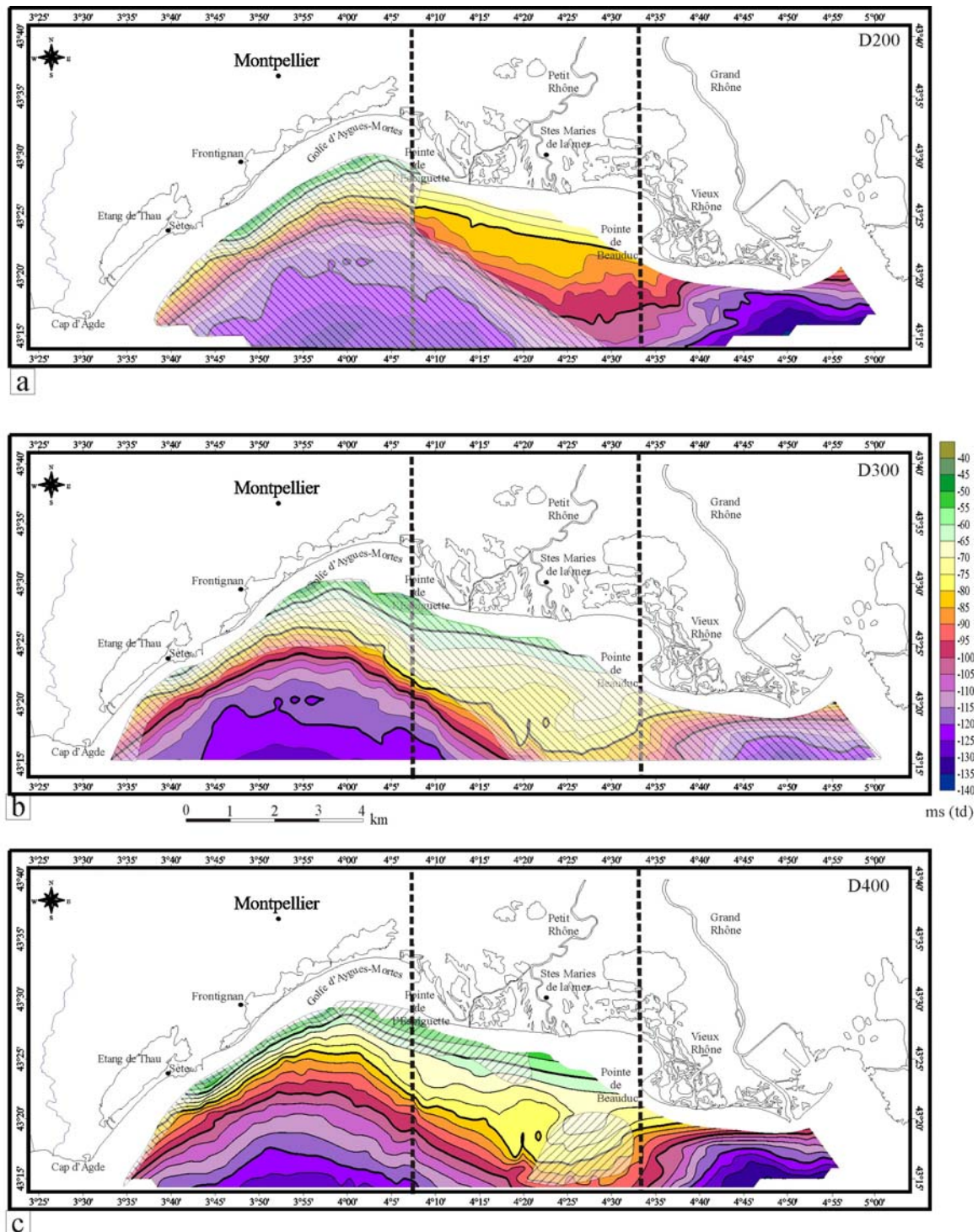
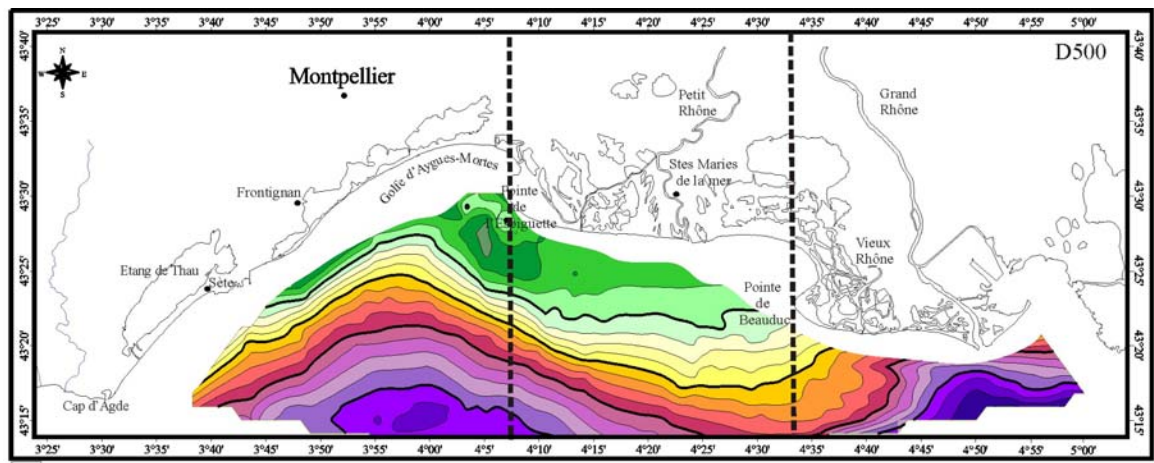
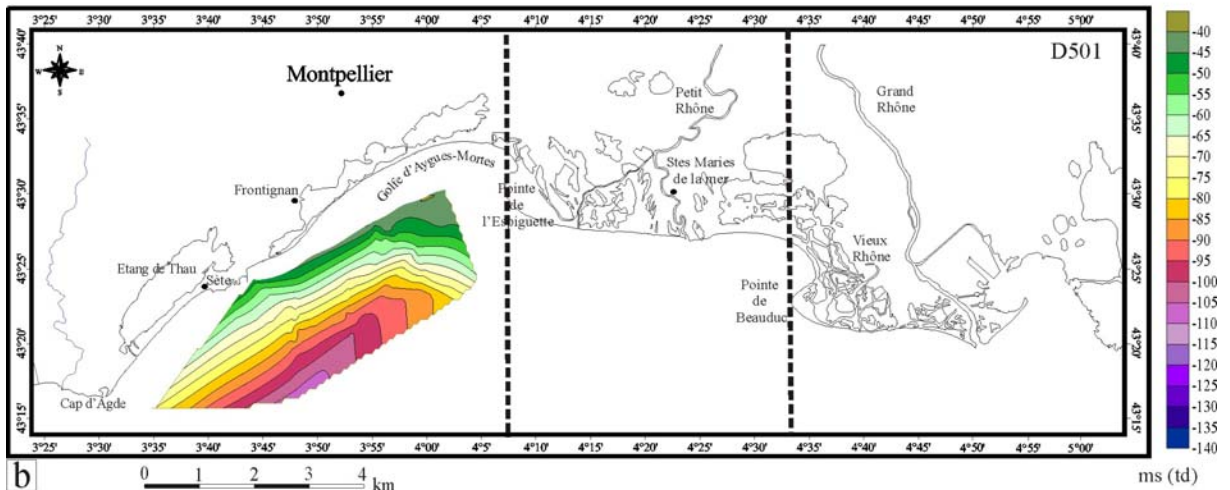


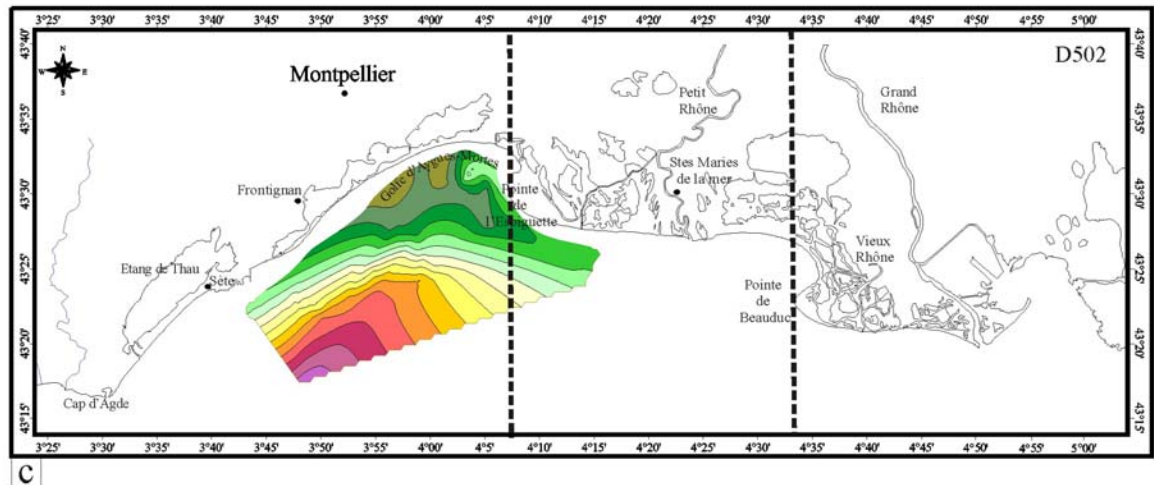
Figure 2.1. Cartes isobathes (en mètres) des discontinuités D200 (a), D300 (b) et D400 (c). Ve : 1500 m.s⁻¹ et Vs : 1600 m.s⁻¹. Les zones hachurées correspondent aux zones où les discontinuités sont amalgamées avec la discontinuité supérieure.



a



b



c

Figure 2.2. Cartes isobathes (en mètres) des discontinuités D500 (a), D501 (b) et D502 (c). Ve : 1500 m.s⁻¹ et Vs : 1600 m.s⁻¹.

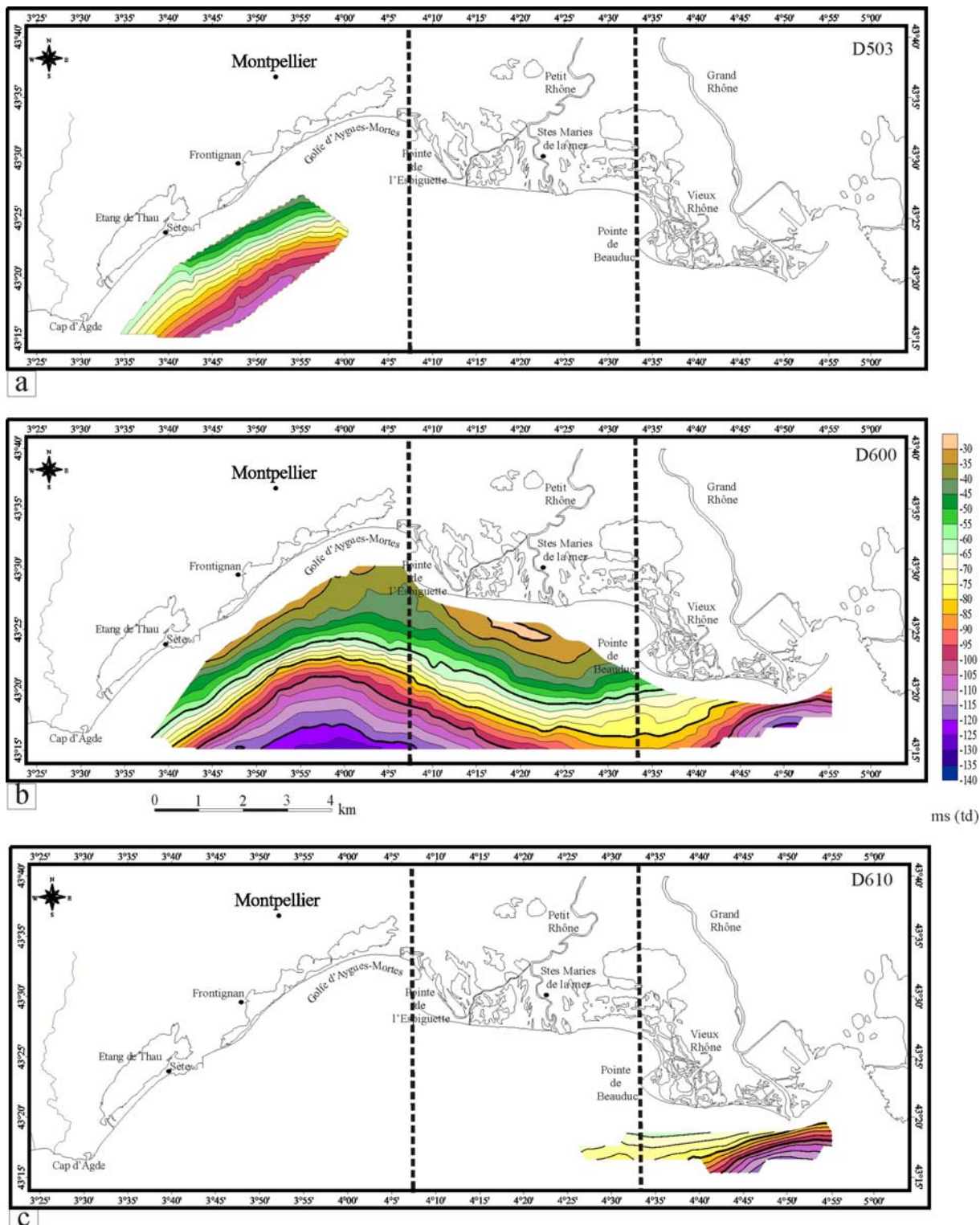


Figure 2.3. Cartes isobathes (en mètres) des discontinuités D503 (a), D600 (b) et D610 (c). Ve : 1500 m.s⁻¹ et Vs : 1600 m.s⁻¹.

Les cartes isopaques des unités sismiques

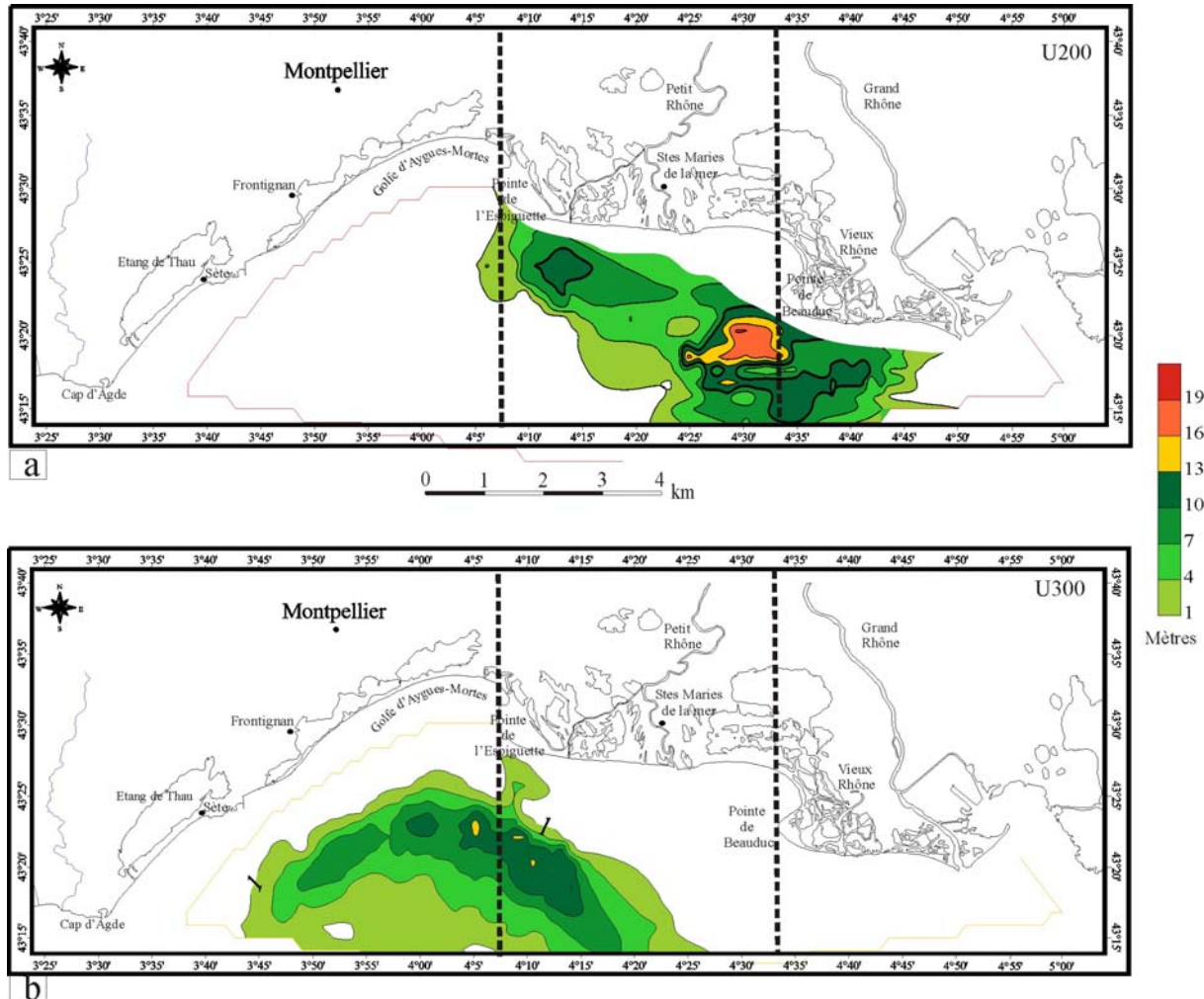


Figure 2.4. Cartes isopaques (en mètres) des unités U200 (a) et U300 (b). Vs : 1600 m.s-1.

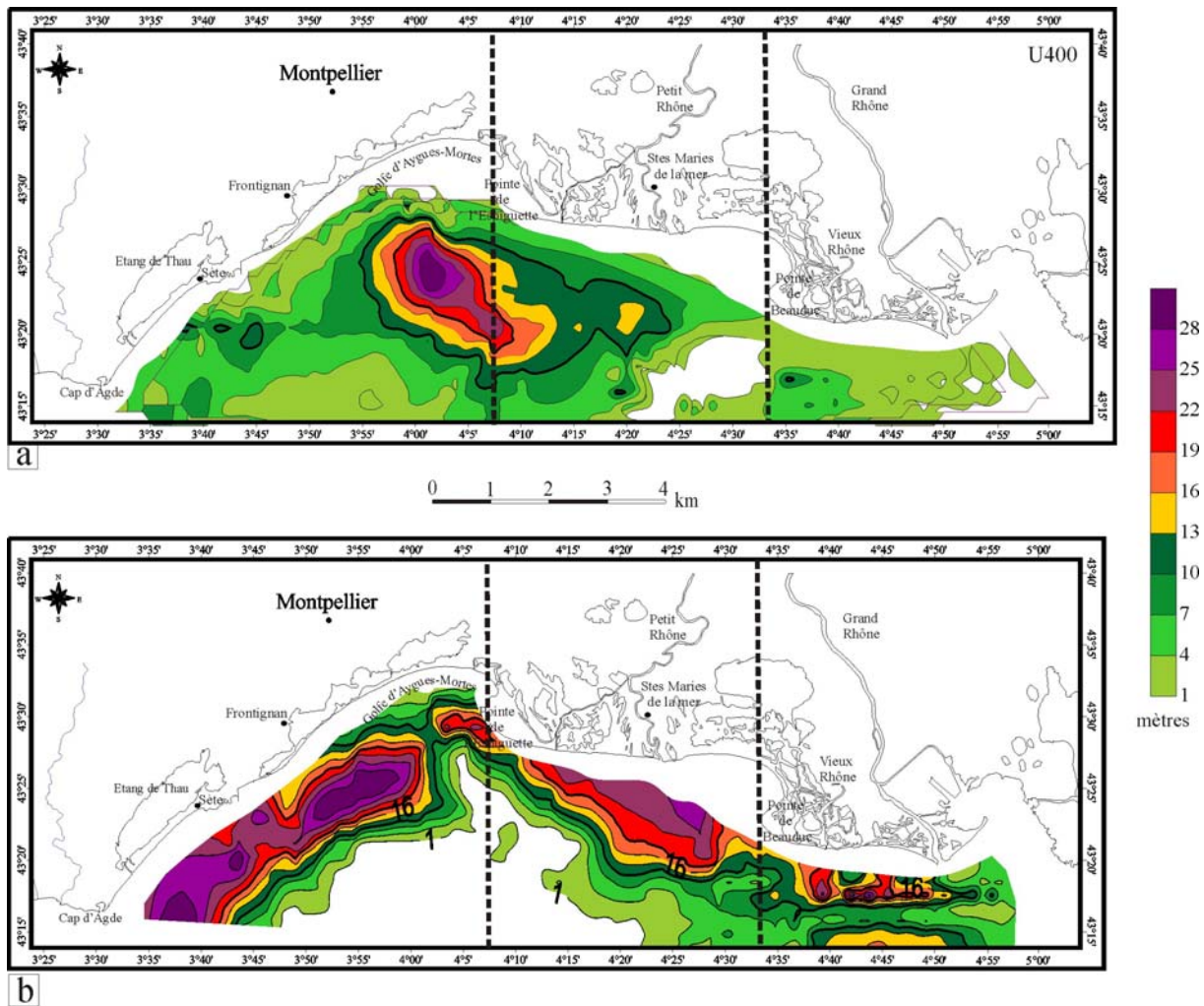


Figure 2.5. Cartes isopaques (en mètres) des unités U400 (a) et U500 (b). Vs : 1600 m.s⁻¹.

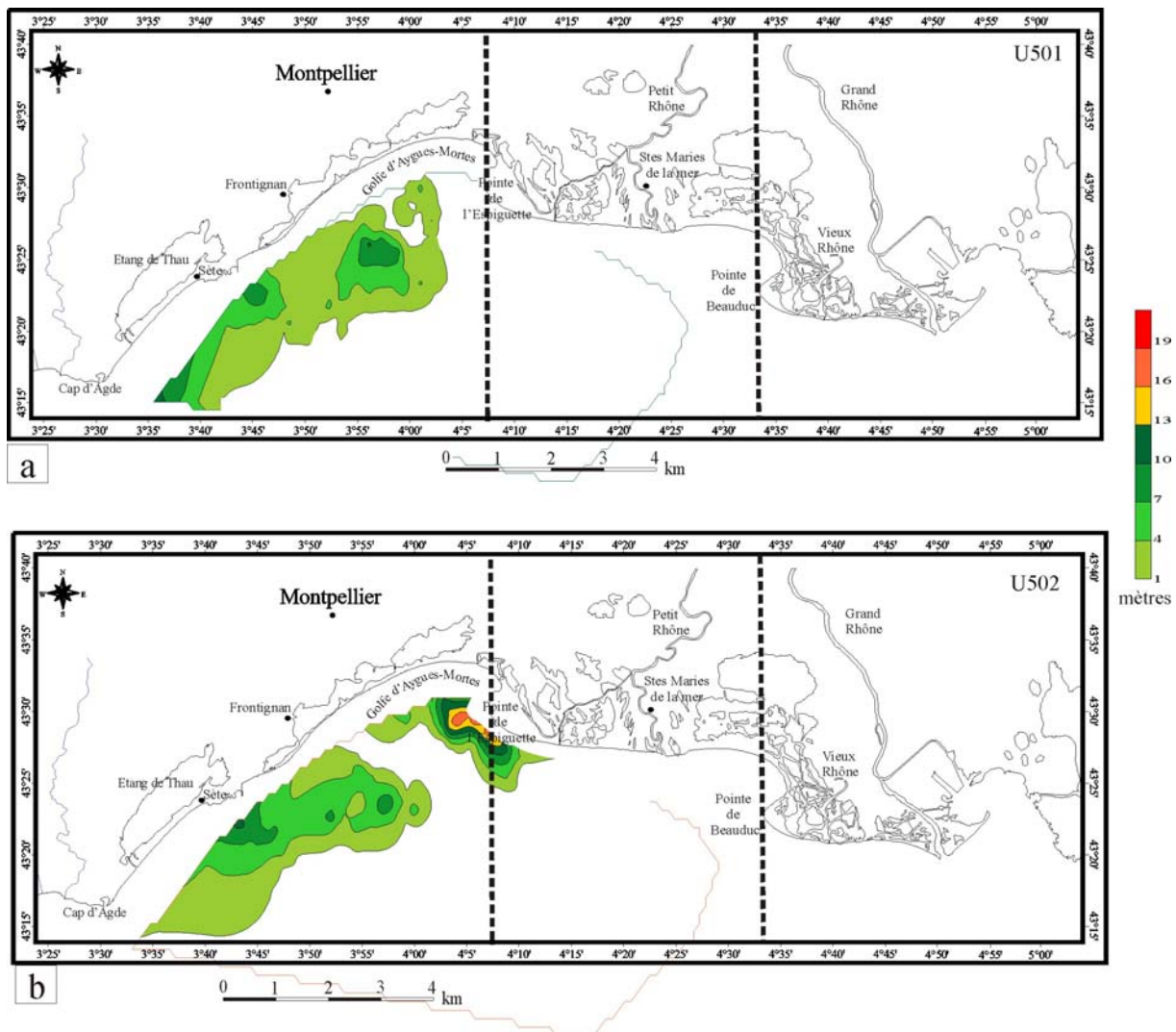


Figure 2.6. Cartes isopaques (en mètres) des unités U501 (a) et U502 (b). Vs : 1600 m.s-1.

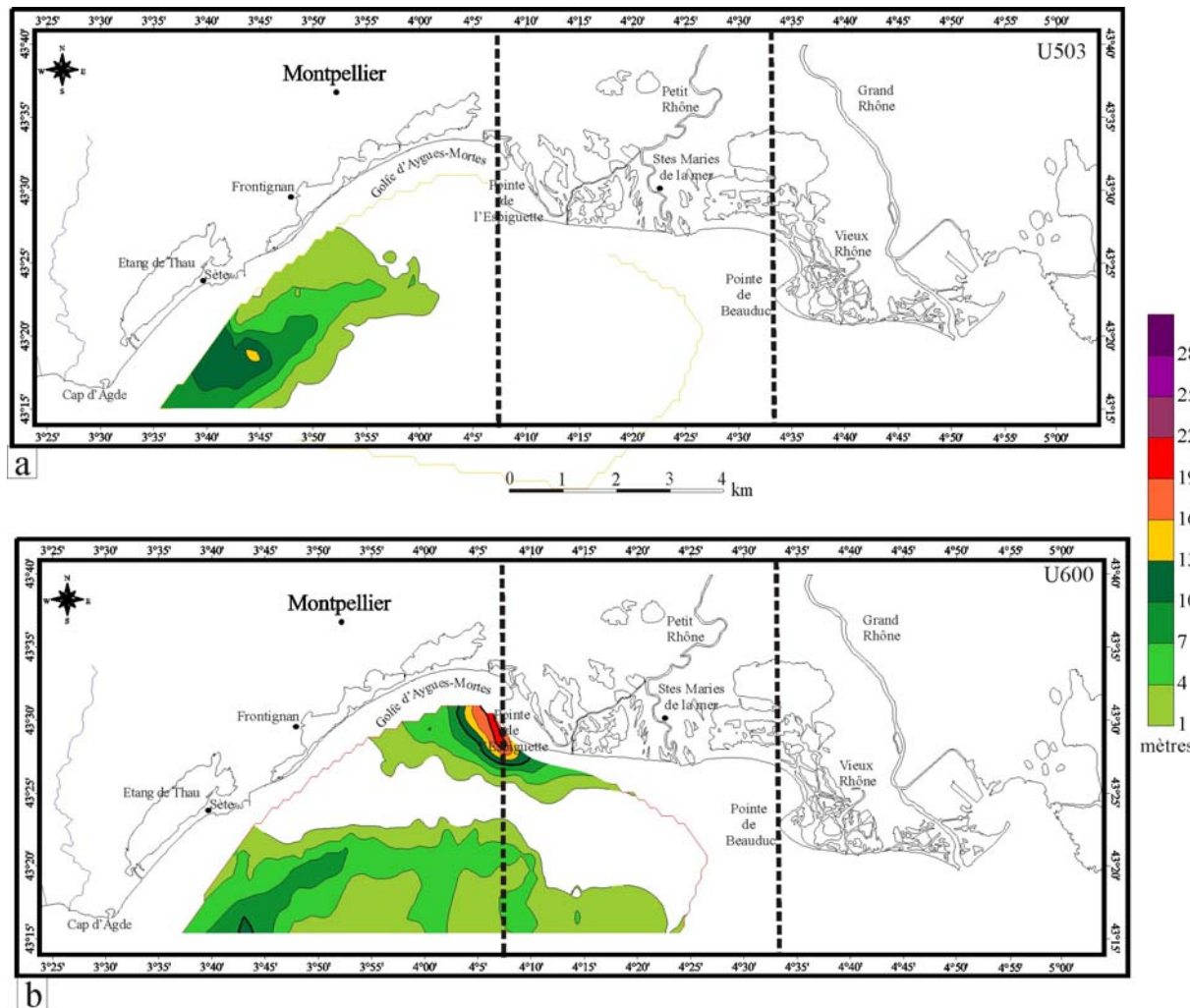


Figure 2.7. Cartes isopaques (en mètres) des unités U503 (a) et U600 (b). Vs : 1600 m.s-1.

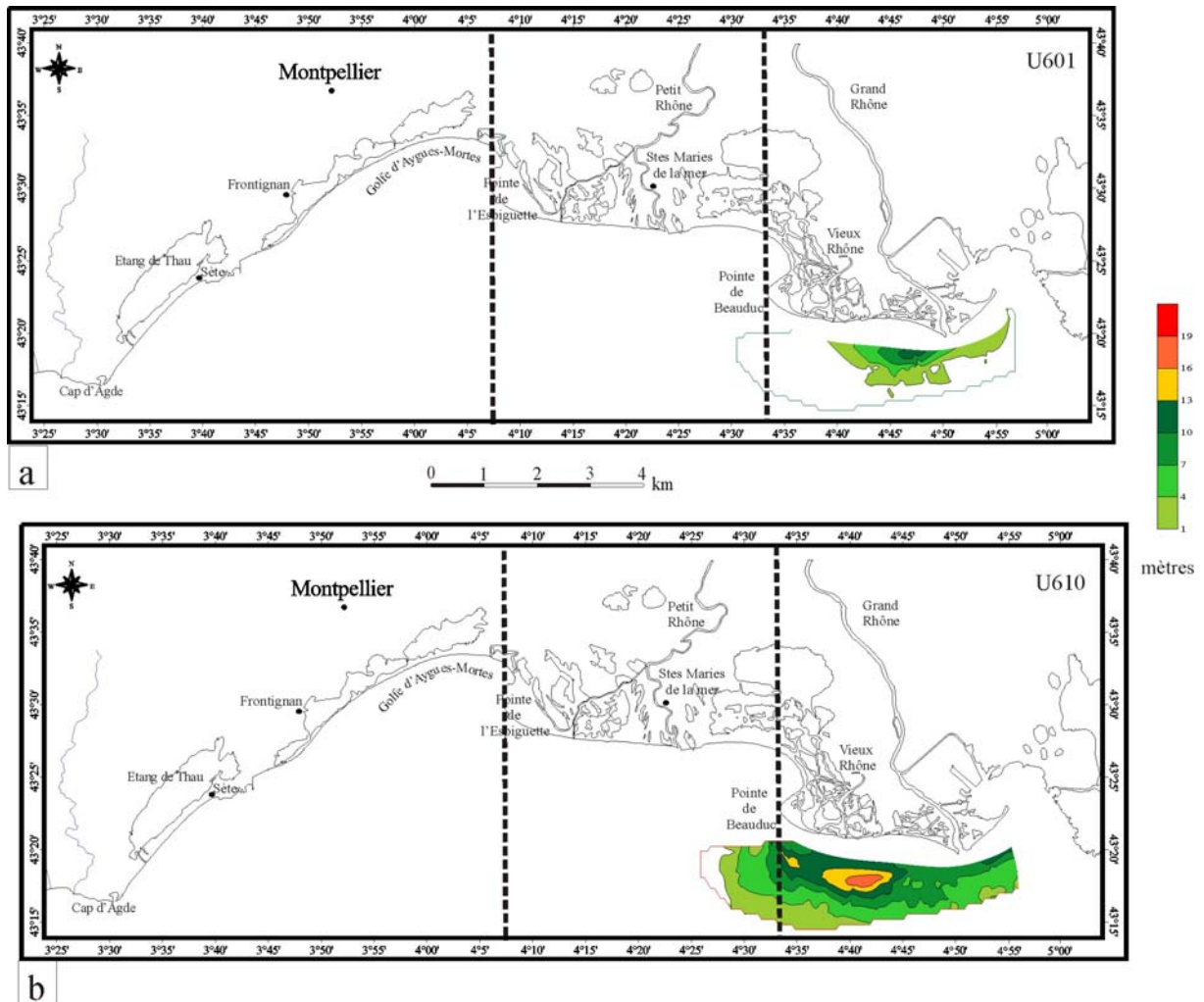
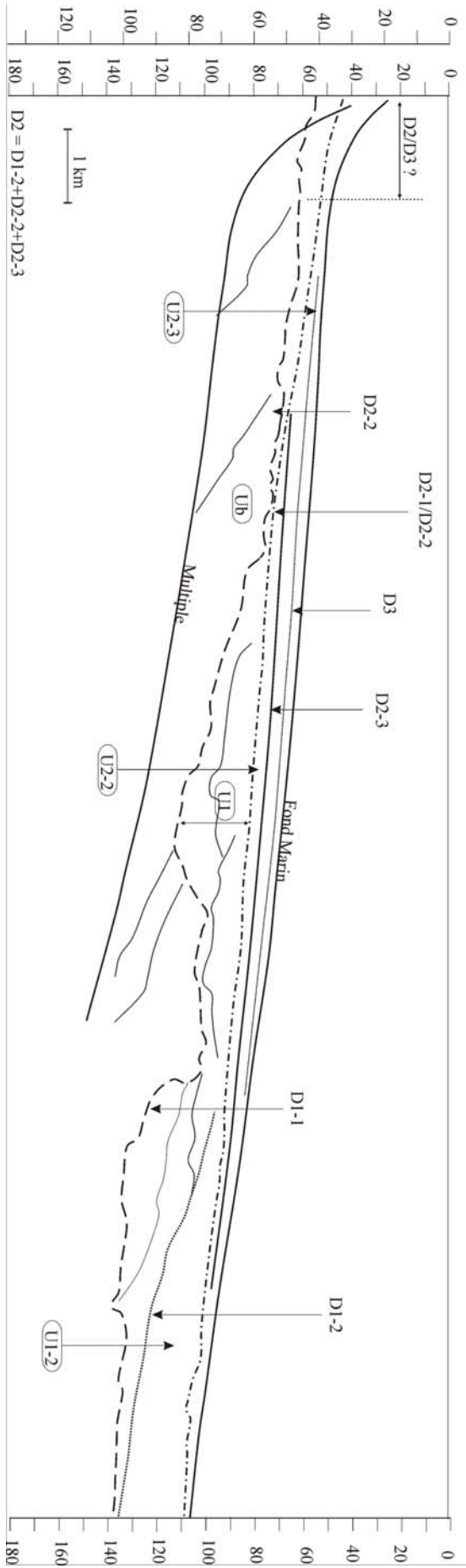
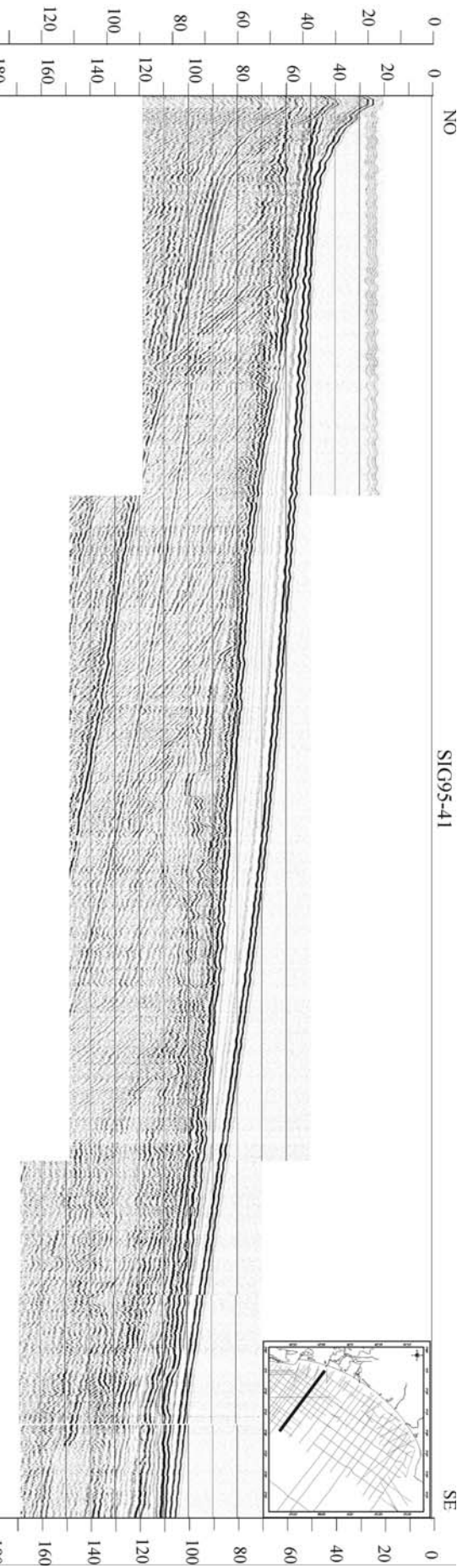


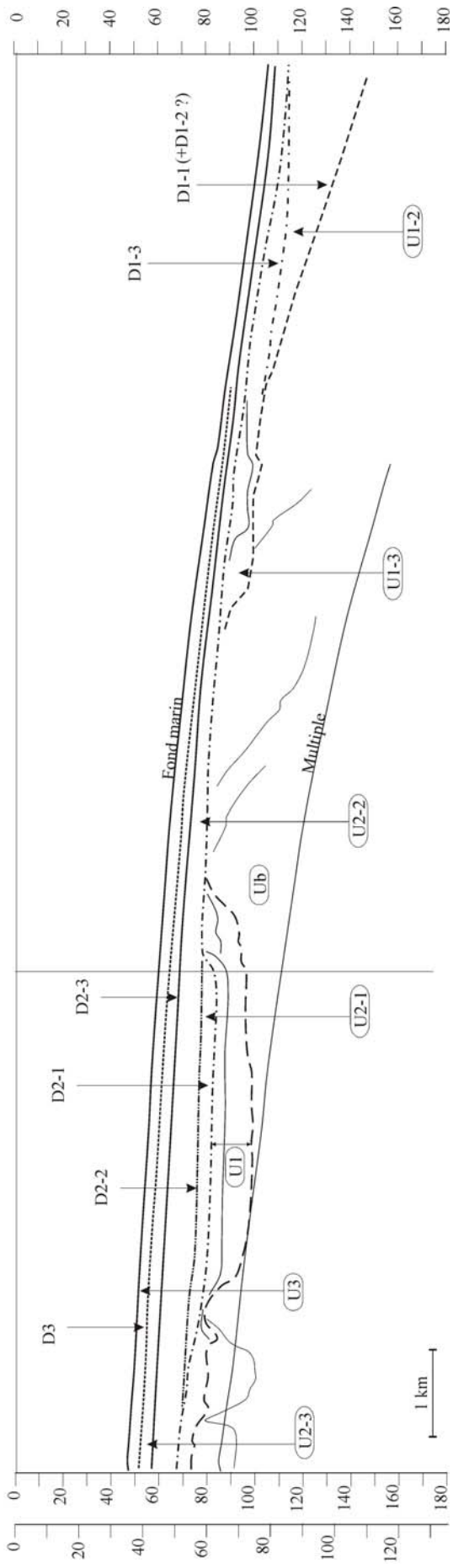
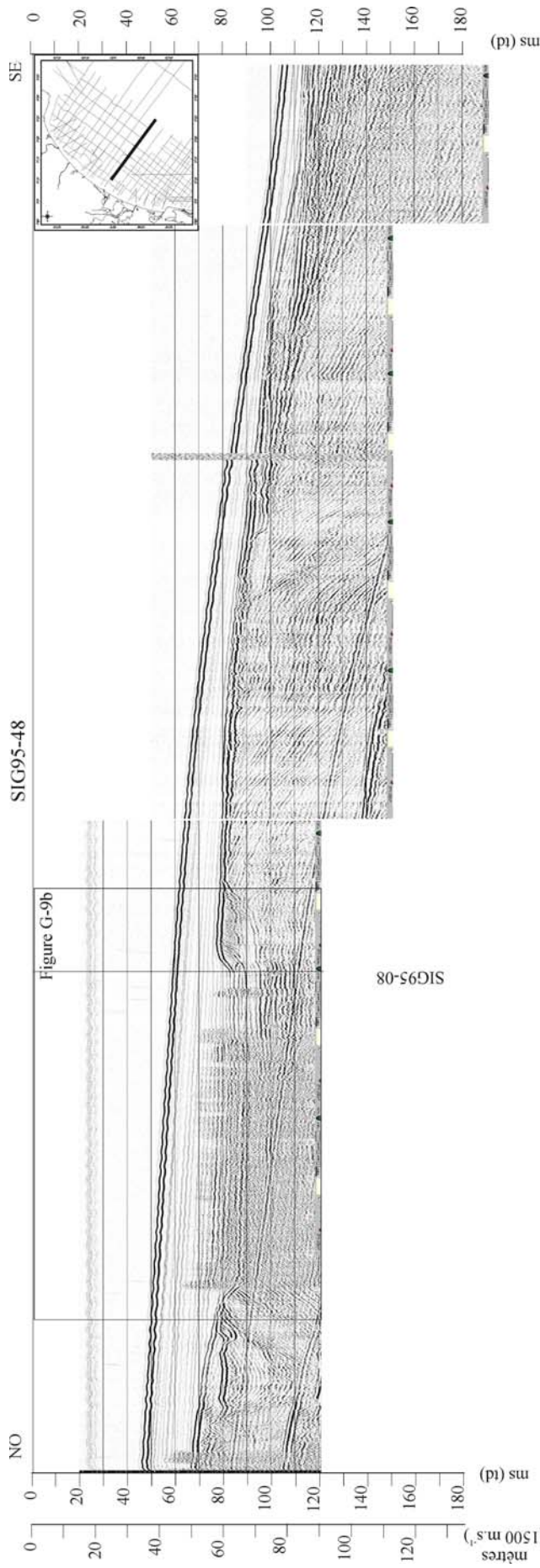
Figure 2.8. Cartes isopaques (en mètres) des unités U601 (a) et U610 (b). Vs : 1600 m.s-1.

Le Sud-Languedoc

Les profils sismiques et leur pointé

SIG95-41





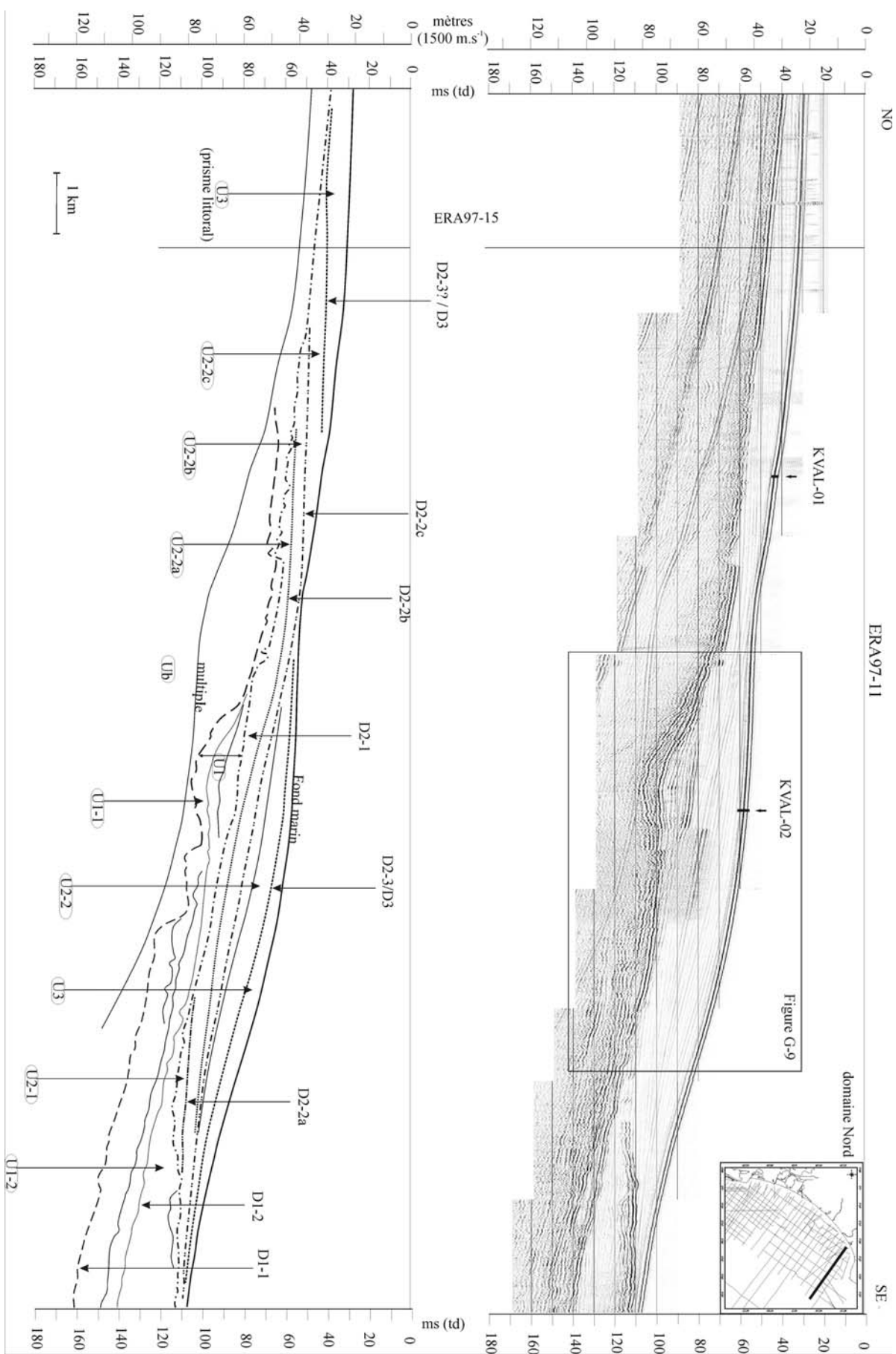
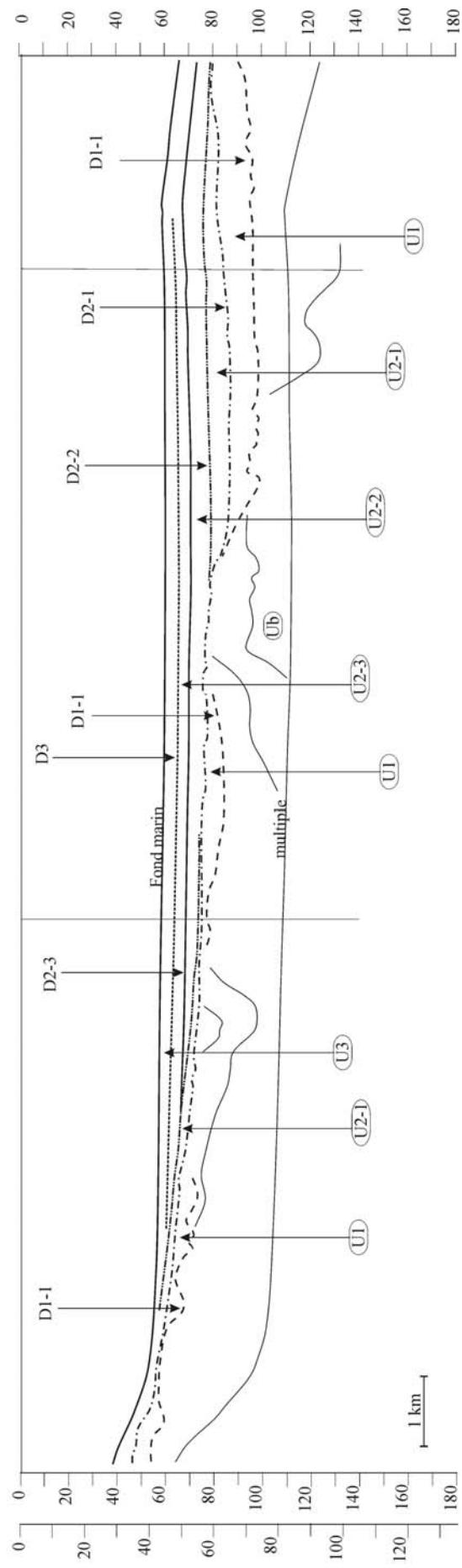
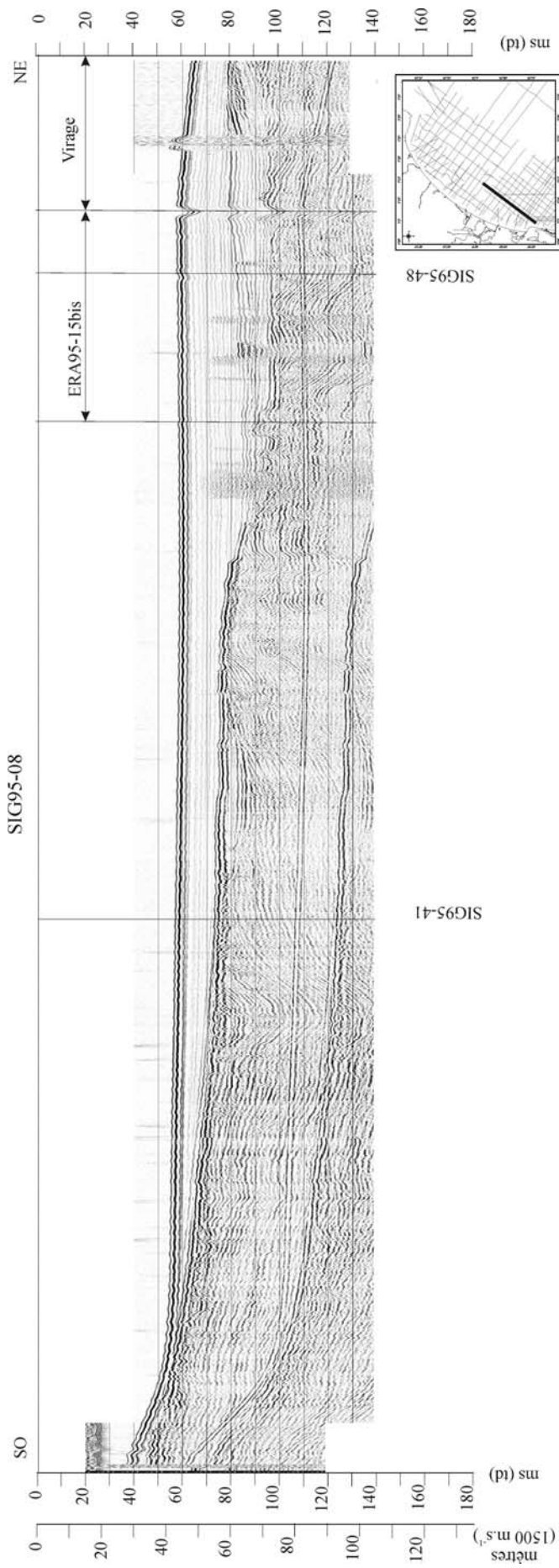
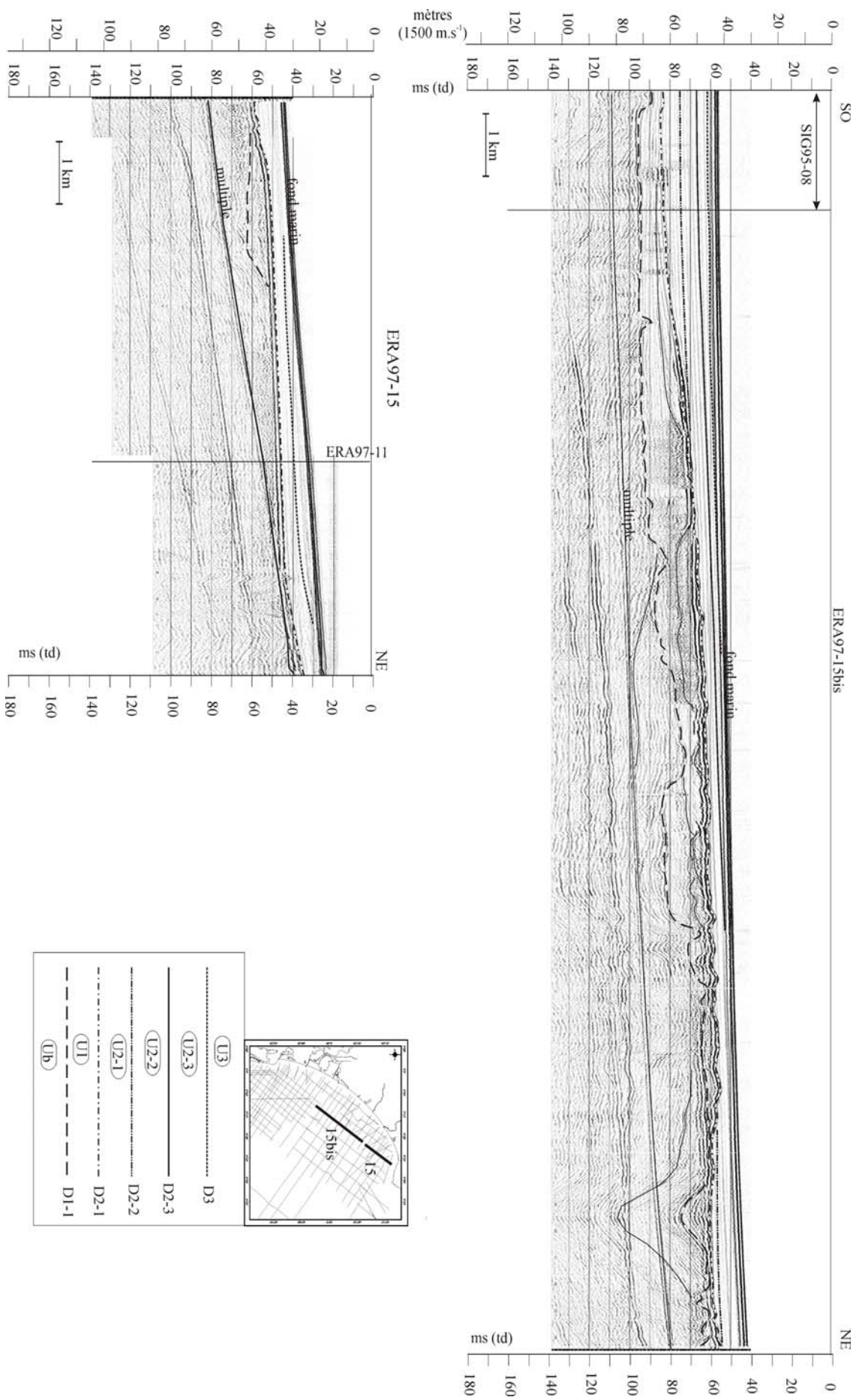


Figure G-9





Les cartes isobathes des principales discontinuités

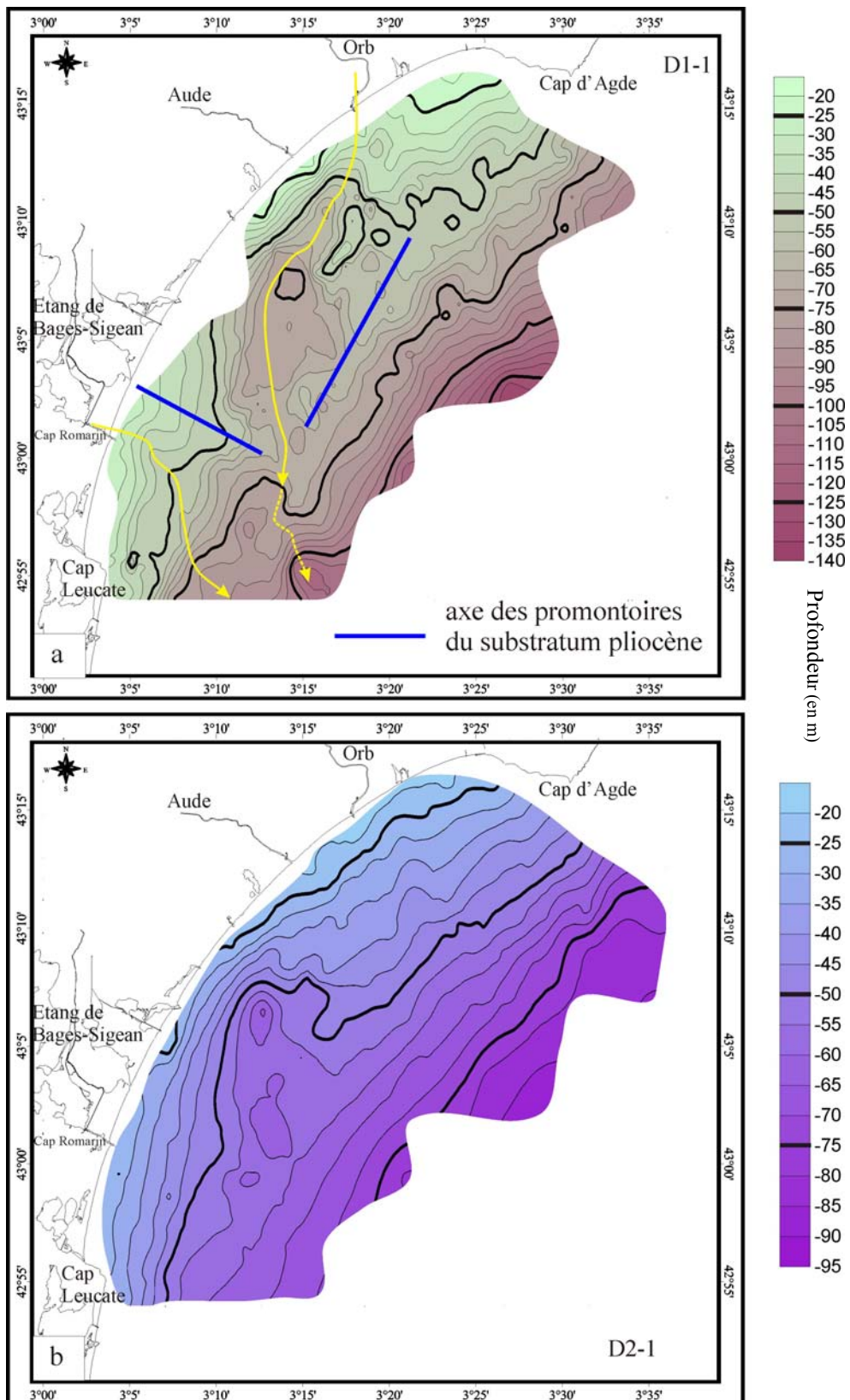


Figure 3-1. Cartes isobathes des discontinuités D1-1 (a) et D2-1 (b)

→ Réseau des paléo-vallées

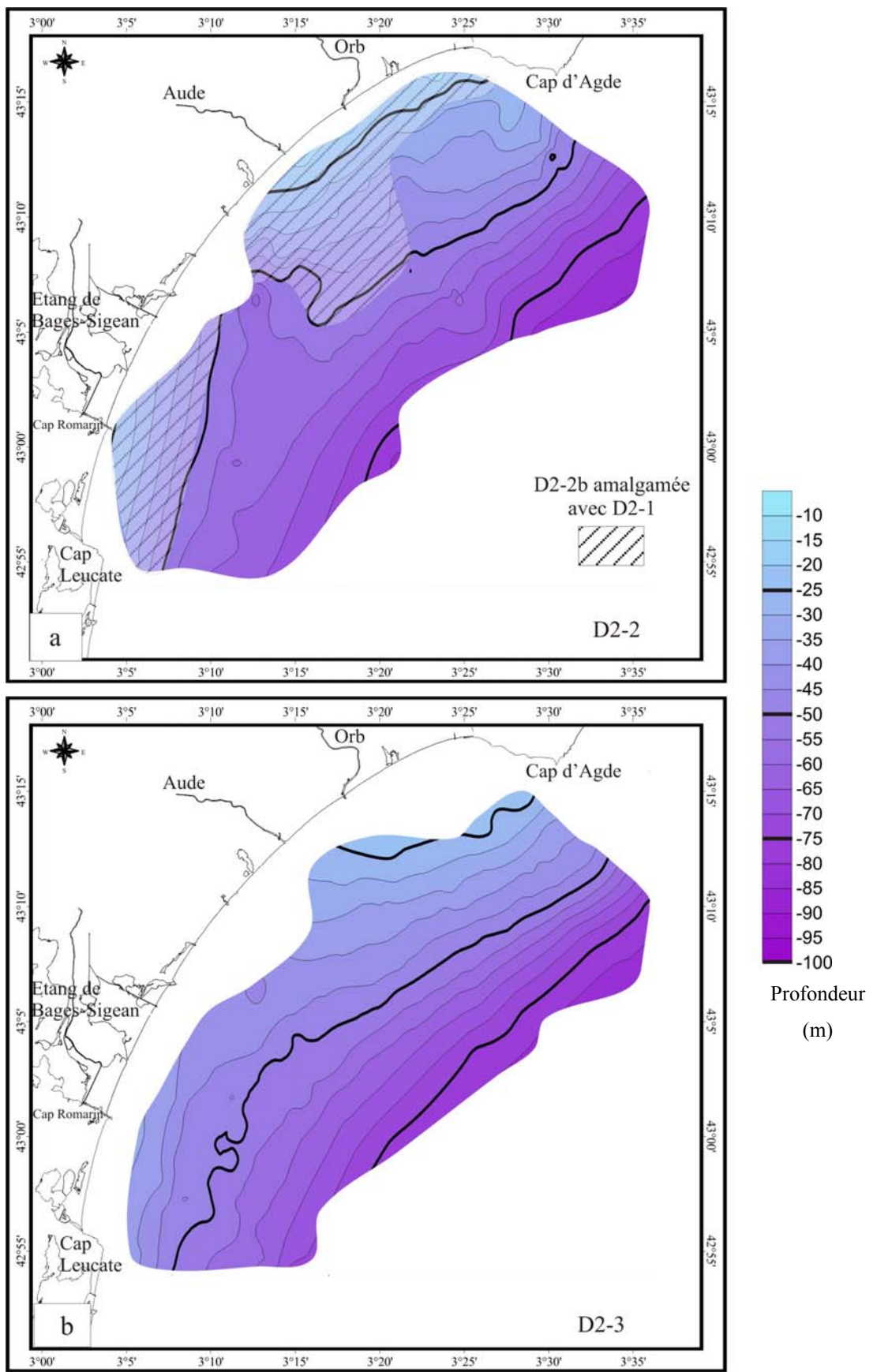


Figure 3-2. Cartes isobathes des discontinuités D2-2b (a) et D2-3 (b)

Les cartes isopaques des unités sismiques

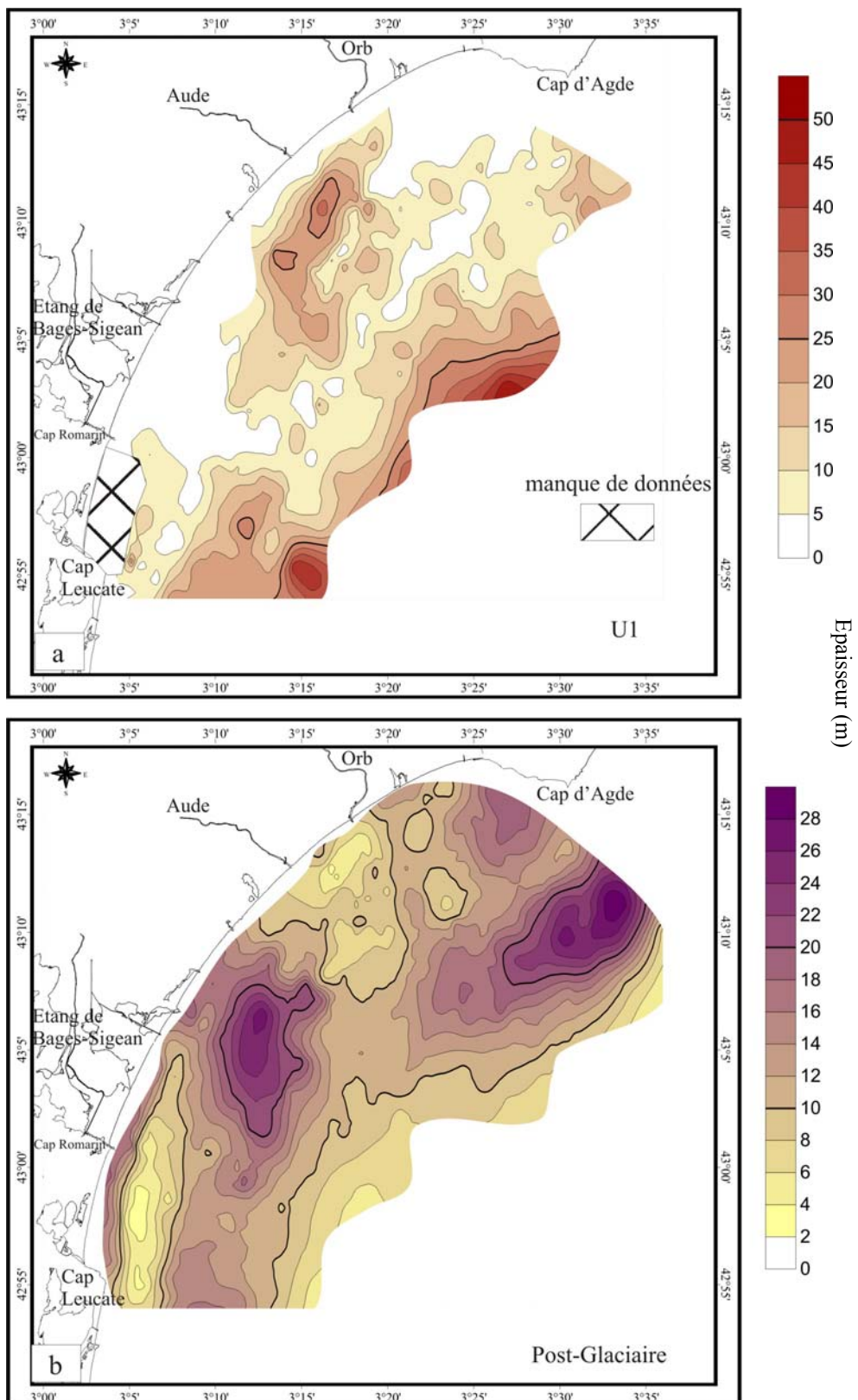


Figure 3-3. Cartes isopaques de l'unité U1 (a) correspondant aux dépôts anté post-glaciaires et du Post-Glaciale (b).

ANNEXE III

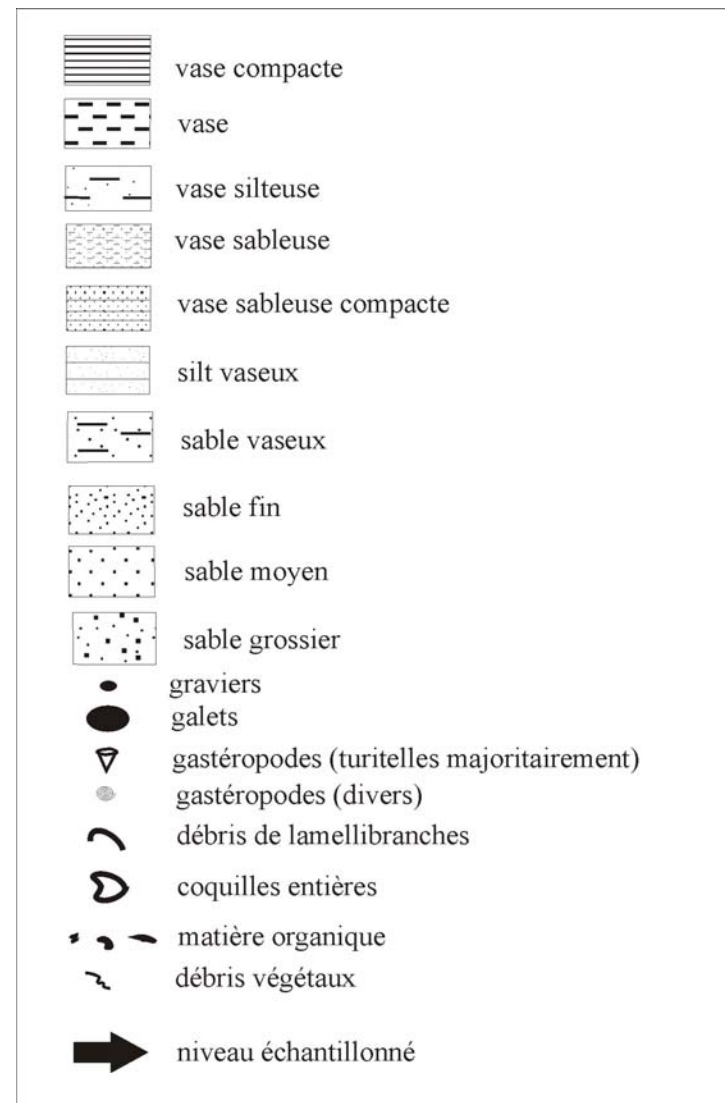
DESCRIPTION DETAILLEE DES CAROTTAGES ET

VIBROCAROTTAGES REALISES SUR LE SECTEUR

ROUSSILLON

Pour chacun des carottages effectués et analysés, nous avons réalisé au minimum un log lithologique présentant les différents niveaux observés. Pour les vibrocarottages, nous présentons, en plus du log lithologique, le montage photographique et les résultats des analyses par rayon X effectuées à l'université de Bordeaux I, UMR EPOC. Les carottages seront présentés par mission ce qui correspond aussi à une répartition géographique. Les carottages du secteur Roussillon effectués au cours de la mission TRANSLIT-2004 ont été réalisés sur les fonds d'environ 40 m bsl au droit de l'étang de Salses-Leucate. Les carottages de la mission LIPPER-2003 ont été réalisés sur l'extension distale du prisme littoral, soit sur les fonds entre 25 et 30 m bsl. Les vibrocarottages de la mission LITTO ont quant à eux été effectuées à la fois dans l'étang de Salses-Leucate et sur le cordon externe.

Des analyses granulométriques, granulométrie-laser et observations de la fraction grossière, ont été effectuées sur des échantillons prélevés sur les vibrocarottages et sur les carottes acquises pendant la mission LIPPER2003 (carotte LK03-x). Les résultats seront présentés en annexe IV.



Légende des carottes

Mission TRANSLIT-2004 : carottage Kullenberg

TRANSK-01 (Figure III-1)

Métadonnées :

Coordonnées : Longitude : 3°06,128 Profondeur : 37,7 m
Latitude : 42°52,017 Longueur : 1,04 m

Description :

La carotte TRANSK-01 est divisée en 4 niveaux montrant une tendance évolutive granodécroissante. On passe des sables fins à la base (niveau TR1-1) à des vases silteuses au sommet (niveau TR1-3 et TR1-4). Les trois niveaux de base (de 1,04 à 0,10 m) contiennent des coquilles et des débris coquilliers alors que le niveau sommital montre plutôt des traces de matière organique.

Interprétation :

L'empilement granodécroissant est un indice d'accroissement de la profondeur d'eau. Seul le niveau de base TR1-1 pourrait être associé à un environnement de dépôt peu profond. La présence de coquilles et de débris coquilliers dans l'ensemble de la carotte montre l'influence marine permanente.

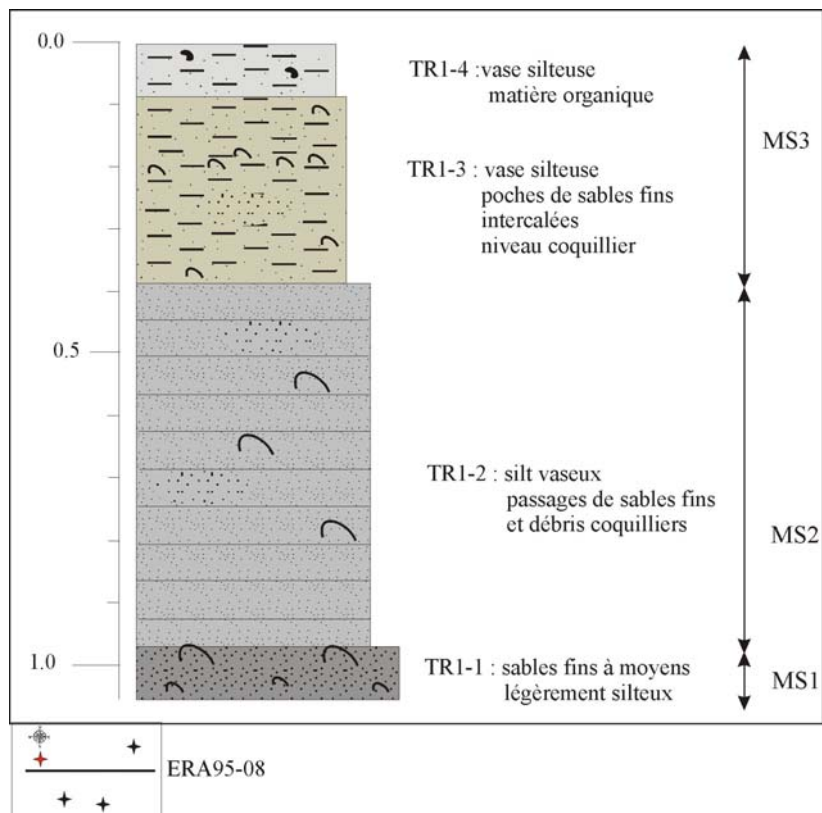


Figure III-1. Log lithologique de la carotte TRANSK-01.

TRANSK-01bis (Figure III-2)

Métadonnées :

Coordonnées : Longitude : 3°06,159 Profondeur : 37,5 m
Latitude : 42°51,984 Longueur : 1,08 m

Description :

La carotte TRANSK-01bis, située à environ 100 m au Sud de TRANSK-01, est divisée en trois niveaux avec une tendance évolutive granodécroissante. On retrouve des sables fins à la base, sable silteux du niveau TR2-1. Au-dessus, les niveaux TR2-2 et TR2-3 sont beaucoup plus vaseux que leurs équivalents sur la carotte précédente, les passages sableux et coquilliers sont cependant observés au sein du niveau TR2-2.

Interprétation :

Pour la carotte TRANSK-01bis, les conditions de mise en place supposées seraient similaires à celle de la carotte TRANSK-01 : accroissement progressif de la profondeur d'eau.

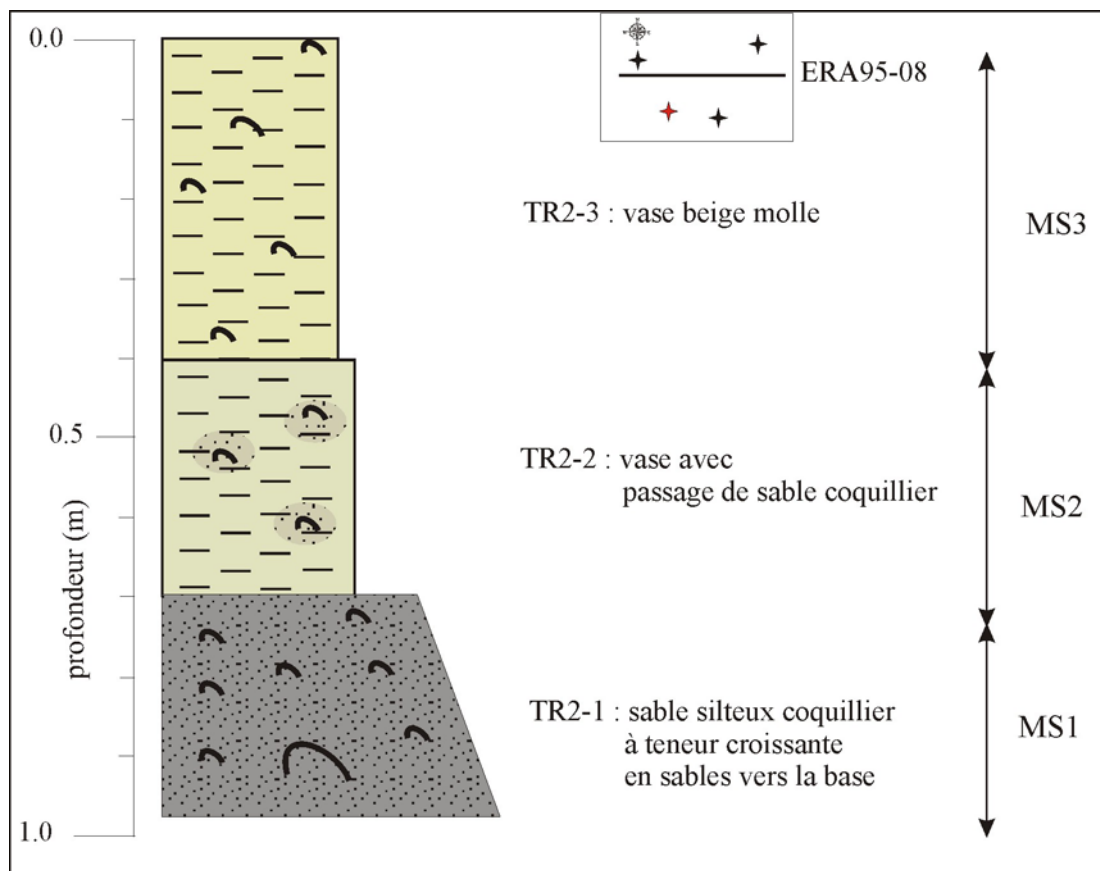


Figure III-2. Log lithologique de la carotte TRANSK-01bis.

TRANSK-01ter (Figure III-3)

Métadonnées :

Coordonnées : Longitude : 3°06,229 Profondeur : 38 m
Latitude : 42°52,020 Longueur : 2,26 m

Description :

La carotte TRANSK-01ter, située à environ 200 m à l'Est de TRANSK-01, a permis un échantillonnage sur une plus grande profondeur. Quatre niveaux sont observés de bas en haut, TR3-1 à TR3-4. Sur la base d'une observation visuelle uniquement, la granulométrie paraît plus grossière et plus homogène sur l'ensemble de la carotte. Les niveaux sommitaux ne sont plus composés de vase silteuse mais de vase silto-sableuse. La présence de coquilles est notée pour les deux niveaux supérieurs uniquement, TR3-3 et TR3-4, le niveau TR3-3 étant le plus riche en coquilles et débris coquilliers.

Interprétation :

L'approfondissement de la tranche d'eau est moins net au sein de cette carotte. Le log lithologique indique uniquement l'influence d'un environnement marin du fait de la présence de débris coquilliers.

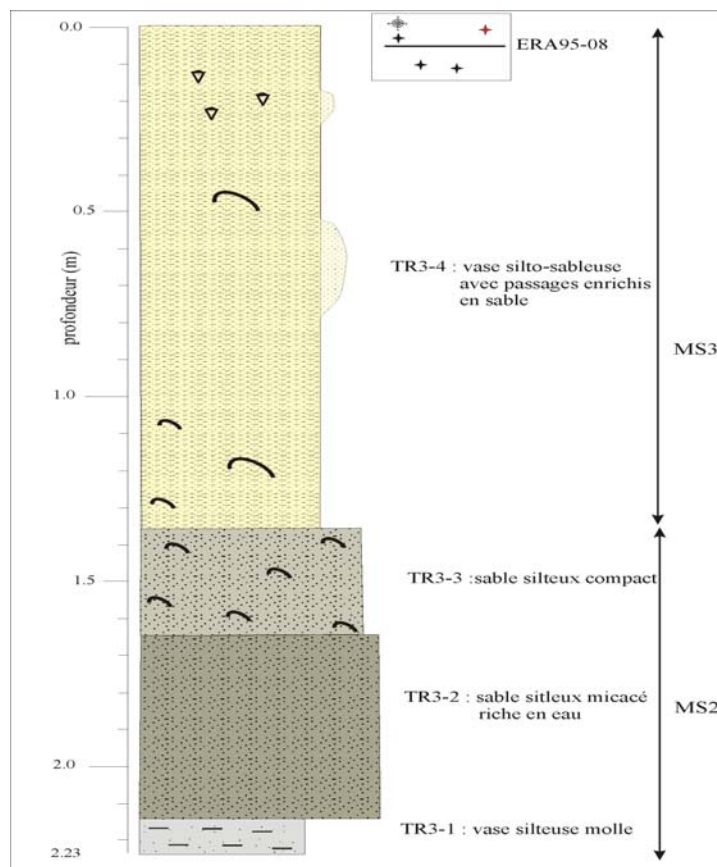


Figure III-3. Log lithologique de la carotte TRANSK-01ter.

TRANSK-01quat (Figure III-4)

Métadonnées :

Coordonnées : Longitude : 3°06,189 Profondeur : 38 m
Latitude : 42°51,580 Longueur : 2,00 m

Description :

La carotte TRANSK-01quat, située à environ 150 au Sud-Est de TRANSK-01, est divisée en 8 niveaux. A la base, on observe un niveau vaso-sableux riche en coquilles de gastéropodes, type turitelles. Seuls les trois niveaux sommitaux (TR4-6 à TR4-8 situés entre 0,55 et 0,30 m) ne semblent pas contenir de coquilles ou de débris coquilliers visibles à l'œil nu. L'ensemble de la carotte est relativement homogène, essentiellement composé de vase silteuse à sableuse avec toutefois des passées sableuse (niveau TR4-2 entre 1,35 et 1,55 m ; niveau TR4-8 entre 0,05 m et le fond marin).

Interprétation :

On notera cette fois encore un approfondissement de la tranche d'eau entre les niveaux TR4-2 et TR4-7. Le niveau de base TR4-1 s'est également mis en place dans un milieu à influence marine sans doute plus protégé, indiqué par la présence de vase. Le niveau supérieur est attribué à un épisode de tempête ayant permis le transport de sédiments plus grossiers en limite de zone d'action de la houle.

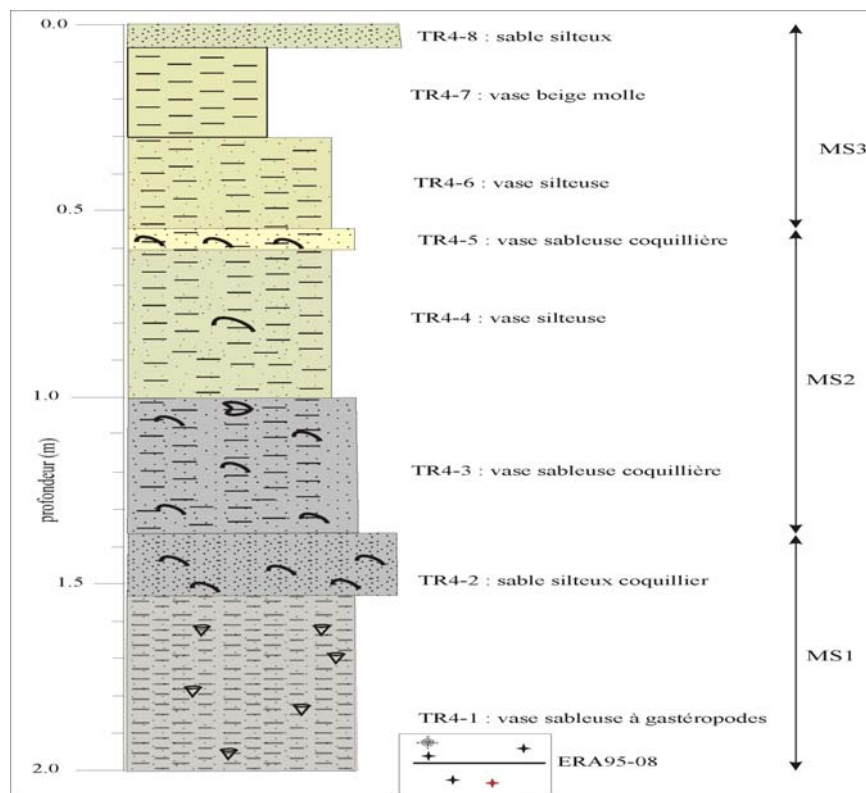


Figure III-4. Log lithologique de la carotte TRANSK-01quat.

Mission LIPPER-2003 : carottage Kullenberg

LK03-01 (Figure III-5)

Métadonnées :

Coordonnées : Longitude : 3°05,435 Profondeur : 29,8 m

Latitude : 42°51 ,977 Longueur : 1,45 m

Description :

La carotte LK03-01 présente 4 niveaux différents. L'ensemble de la carotte est de nature lithologique relativement sableuse. Seul le niveau de base (LK01-1 entre 1,45 et 1,28 m) contient quelques débris coquilliers visibles à l'œil nu.

L'évolution du mode principal (annexe IV Figure IV-1) et celle de la répartition des classes granulométriques (annexe IV Figure IV-2) ont tendance à montrer une alternance entre niveaux granocroissants et granodécroissants (LK01-2 et LK01-4). La courbe de variation du classement indique un très mauvais classement du niveau basal et des deux niveaux supérieurs ($S_0 > 2 \Phi$). Il reste très mauvais pour le sommet du niveau LK01-2 et s'améliore légèrement pour le reste de ce niveau. Le classement étant relativement mauvais, on ne tiendra pas compte des classes indiquées dans le Tableau IV.2 en annexe et basées sur la moyenne. Au niveau de l'asymétrie, le niveau basal présente une forte asymétrie vers les sédiments les plus grossiers, de même que la base du niveau sommital. Pour les deux autres niveaux et pour sommet de la carotte, on note une assez bonne symétrie.

Interprétation :

Par rapport au mode et au pourcentage de chacune des classes granulométriques (annexe IV Figure IV-1 et IV-2), l'ensemble des niveaux semble s'être mis en place dans un milieu à énergie relativement faible. De plus, le classement relativement mauvais pour l'ensemble des échantillons indique lui aussi une quasi absence de l'action de la houle. L'asymétrie voisine de 0 n'a pas une valeur très significative. L'ensemble de ces caractéristiques indique une mise en place sous une tranche d'eau supérieure à la limite d'action de la houle.

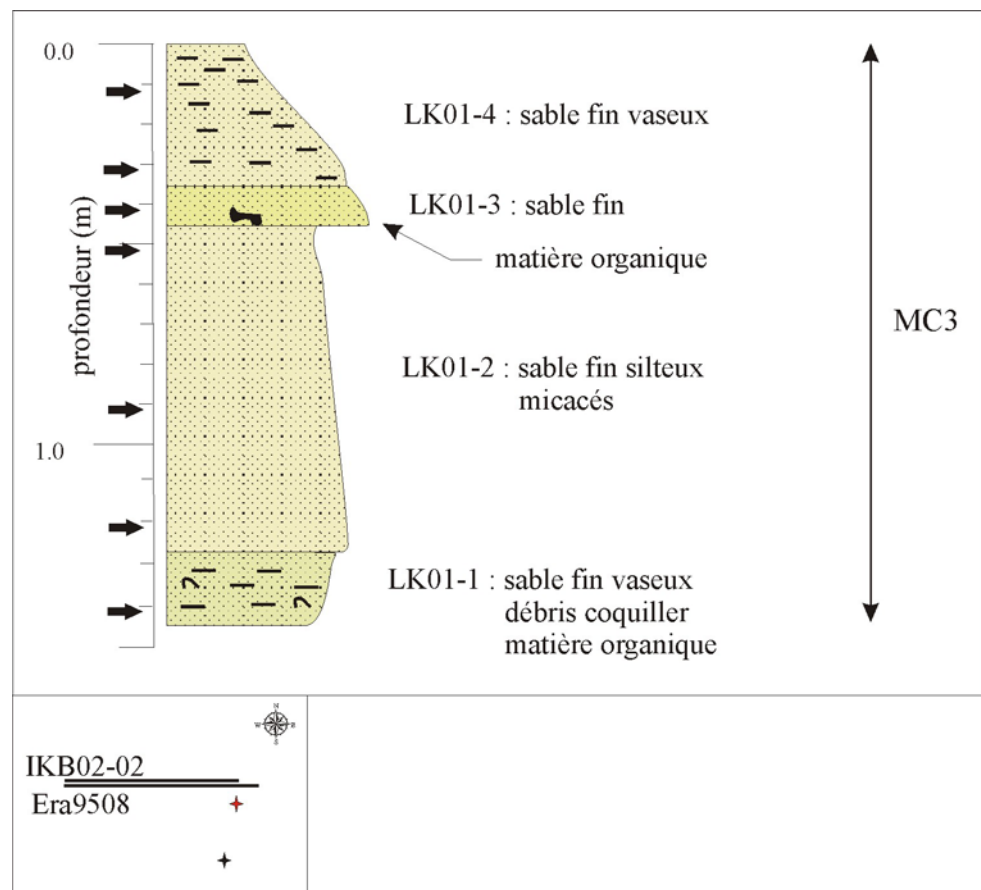


Figure III-5. Log lithologique de la carotte LK03-01.

LK03-01bis (Figure III-6)

Métadonnées :

Coordonnées : Longitude : 3°03,444 Profondeur : 24,5 m

Latitude : 42°44 ,051 Longueur : 1,36 m

Description :

La carotte LK03-01bis, située à environ 200 m au Sud de LK03-01, a été effectuée sur une zone de plus faible profondeur. Elle est divisée en 9 niveaux pour la plupart composés de sable fin. Il n'existe pas de tendance évolutive générale granocroissante ou décroissante. Le niveau LK01b-3 est en fait composé d'une alternance entre des passées sableuses et des passées coquillières. Une datation a été réalisée au sein de l'une de ces passées coquillères. Le niveau LK01b-5 constitue une limite assez nette entre les niveaux inférieurs et supérieurs, il est essentiellement composé de coquilles et débris coquilliers.

La courbe représentant l'asymétrie (annexe IV Figure IV-1) indique une assez bonne symétrie pour la plupart des échantillons. Elle se détériore cependant vers la base de la carotte où on observe une déviation vers la fraction fine. A l'exception du niveau LK01b-6, le classement est très mauvais.

Interprétation :

Cette carotte est constituée d'un ensemble de niveaux relativement hétérogènes indiquant une variation des modes et/ou des environnements de dépôts au cours du temps. Le mauvais classement indique cependant une faible action de la houle et donc un environnement soit abrité, soit aux limites du domaine d'action de la houle. La très légère amélioration du classement observée à la base semble indiquer une plus forte influence de la houle et un transport par charriage des sédiments. Les indices granulométriques devront cependant être modérés étant donné que la plupart des échantillons sont bimodaux. Ces niveaux doivent s'être mis en place dans la zone infralittorale soumise à l'action des houles de tempête.

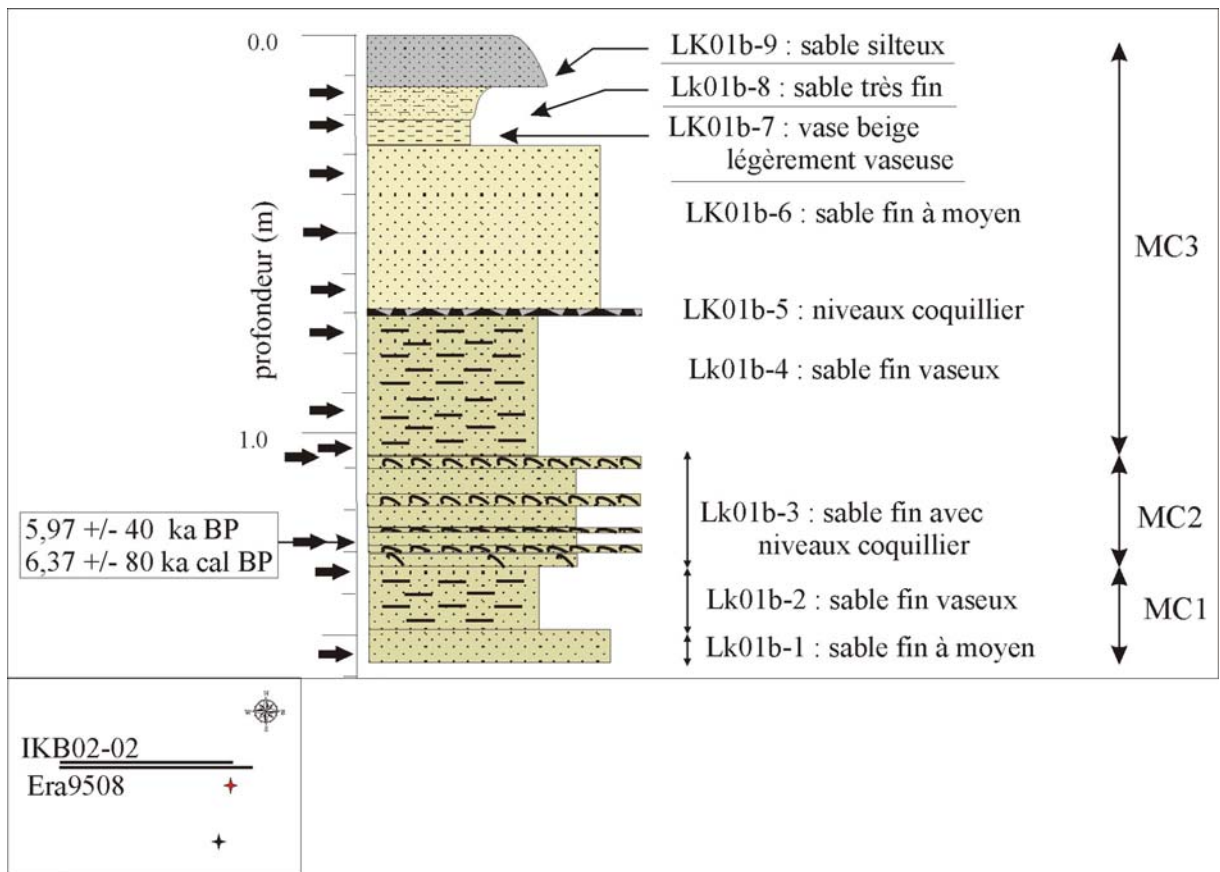


Figure III-6. Log lithologique de la carotte LK03-01bis.

LK03-03 (Figure III-7)

Métadonnées :

Coordonnées : Longitude : 3°04,570

Profondeur : 29 m

Latitude : 42°44 ,037

Longueur : 1,10 m

Description :

La carotte LK03-03, située au Nord de l'embouchure de la Têt, est divisée en 6 niveaux de type essentiellement sablo-vaseux. Seuls les deux niveaux de base, LK03-1 et LK03-2, contiennent des coquilles et des débris coquilliers. La pénétration a été limitée par la présence de grès et de galets retrouvés dans l'ogive. Les trente premiers centimètres montrent une variabilité très rapide dans le type de sédiments observés.

Les courbes des différents paramètres granulométriques (annexe IV Figure IV-5) montrent une grande homogénéité pour le classement (globalement très mauvais) et pour l'asymétrie qui présente une assez forte déviation vers la fraction fine. De même, le graphique de répartition des différentes classes granulométriques pour chacun des échantillons est très homogène. Les proportions de chaque classe granulométrique sont pratiquement identiques pour tous les échantillons. La sédimentation semble être de type aggradante. Là encore, le mauvais classement rend la valeur de la moyenne peu significative.

Interprétation :

La carotte LK03-03 composée essentiellement de sédiments fins et relativement homogène, mis à part la présence de débris coquillier ou de matière organique, semble correspondre à une sédimentation dans un milieu de faible énergie. L'asymétrie positive ne paraît pas, dans ce cas, significative d'un net remaniement par la houle. La proportion égale de silt et de sable très fin indique un dépôt sous une tranche d'eau où l'influence de la houle, bien qu'encore présente, reste relativement faible.

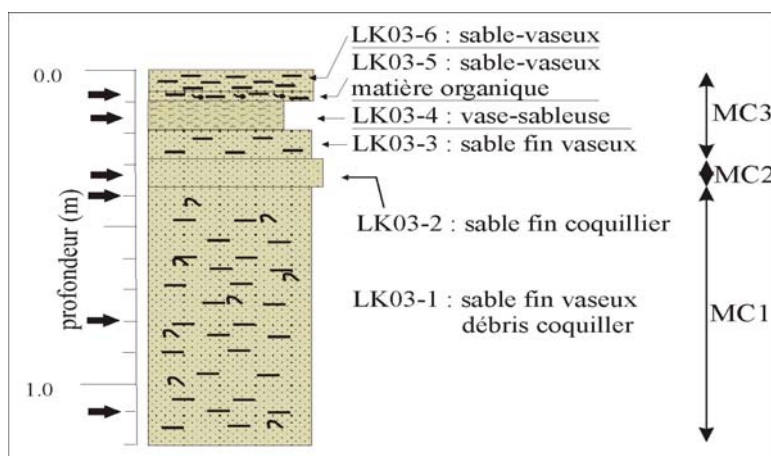


Figure III-7. Log lithologique de la carotte LK03-03.

LK03-04 (Figure III-8)

Métadonnées :

Coordonnées : Longitude : 3°03,444 Profondeur : 24,5 m

Latitude : 42°44 ,051 Longueur : 1,36 m

Description :

La carotte LK03-04, située plus près de la côte que la LK03-04, montre une plus grande hétérogénéité avec une division en 11 niveaux. Le niveau basal LK04-0 a été prélevé dans l'ogive. L'observation visuelle n'a pas permis de noter la présence de coquilles ou de débris coquilliers dans les différents niveaux. Des débris coquilliers extrêmement fins ont cependant été observés à la loupe binoculaire dans les niveaux LK04-0 à LK04-3, LK04-9 et LK04-10. Une datation a été effectuée sur le niveau LK04-0. On notera une variation importante entre les dépôts de la base, plutôt grossiers et de couleur beige à jaune et le reste de la carotte qui présente une sédimentation plus fine alternant entre les sables-vaseux et la vase-sableuse de couleur grise.

Le graphique de répartition des classes granulométriques (annexe IV Figure IV-8), ainsi que la courbe d'évolution du mode principal (annexe IV Figure IV-7), montrent une alternance entre un empilement granocroissant (pour les 4 niveaux de base et du sommet) et décroissant (pour les trois niveaux médians). Le classement est encore une fois mauvais à très mauvais. On note une asymétrie vers la fraction fine pour l'ensemble des échantillons mais elle n'est importante que pour le niveau sommital (LK04-10) et le niveau LK04-3. Il est du à la présence d'un second mode décalée vers la fraction fine.

Interprétation :

La sédimentation relativement hétérogène et grossièrement granodécroissante semble indiquer une mise en place sous des conditions dynamiques variables. Les niveaux grossiers et les grès observés à la base indiquent un milieu littoral. Les alternances de sable-vaseux et de vase-sableuse au-dessus indiquent une influence épisodique de l'action de la houle. Les dépôts se forment sans doute dans la zone d'action de la houle de tempête.

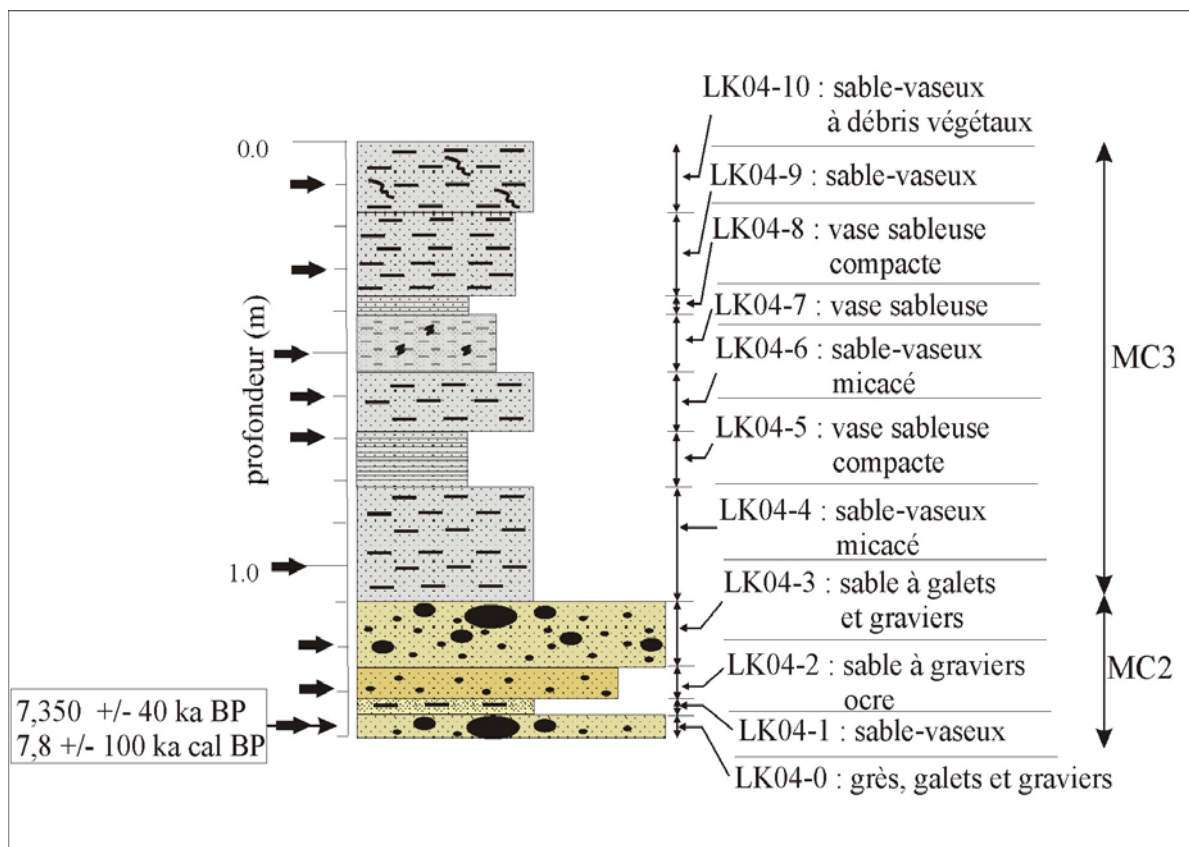


Figure III-8. Log lithologique de la carotte LK03-04.

Mission LITTO-2003 : vibrocarottage petits fonds

03VK01 (Figure III-9)

Métadonnées :

Coordonnées : Longitude : 3°02,310 Profondeur : 0 m

Latitude : 42°52,527 Longueur : 5,9 m

Description :

La carotte 03VK01, située sur la bordure Est de l'étang de Salses-Leucate est divisée en 8 niveaux. La première remarque concerne une évolution dans les teintes, avec passage des teintes jaunes à la base à des teintes grises au sommet. L'ensemble de la carotte est composé essentiellement de sédiments sableux. A la base, les niveaux VK01-1, VK01-2 et VK01-3 sont de type sableux granodécroissant avec la présence de galets à la base de chacun. Ces niveaux ne contiennent pas de débris coquilliers. Dans les niveaux sableux supérieurs, de couleurs grises (niveaux VK01-5 à VK01-8), nous n'observons plus ni galets ni graviers. Le niveau VK01-5 contient quelques débris coquilliers mais ceux-ci sont essentiellement présents dans les 3 niveaux supérieurs.

La répartition des classes granulométriques (annexe IV Figure IV-10) confirme le caractère globalement granodécroissant de chacun des niveaux de sables jaunes. Le niveau VK01-5 est lui aussi très légèrement granodécroissant. A l'exception du sommet du niveau VK01-7, le classement (annexe IV Tableau IV-5 et Figure IV-9) est de type modéré. Seul les deux échantillons sommitaux, l'un dans le niveau VK01-8 et l'autre au sommet du niveau VK01-7, présentent une assez forte dissymétrie négative dans le premier cas et positive dans le deuxième.

Interprétation :

Les caractéristiques lithologiques et les paramètres granulométriques des niveaux sableux VK01-1 à VK01-4 indiquent une mise en place dans un milieu d'assez forte énergie, type cordon dunaire. Le niveau sableux VK01-5 qui présente une sédimentation légèrement plus fine et contenant des débris coquilliers s'est également mis en place dans un environnement littoral, le classement indique une action de la houle non négligeable. Les deux niveaux supérieurs très riches en coquilles et débris coquilliers et présentant une diminution de l'action de la houle pourrait correspondre à un dépôt dans un milieu confiné. Il faut cependant noté que le sommet de la carotte, prélevé sur le cordon interne, est fortement influencé par les remaniements anthropiques. De nombreux travaux en bordure de l'étang de Salses-Leucate ont été réalisés au cours de ces cinquante dernières années.

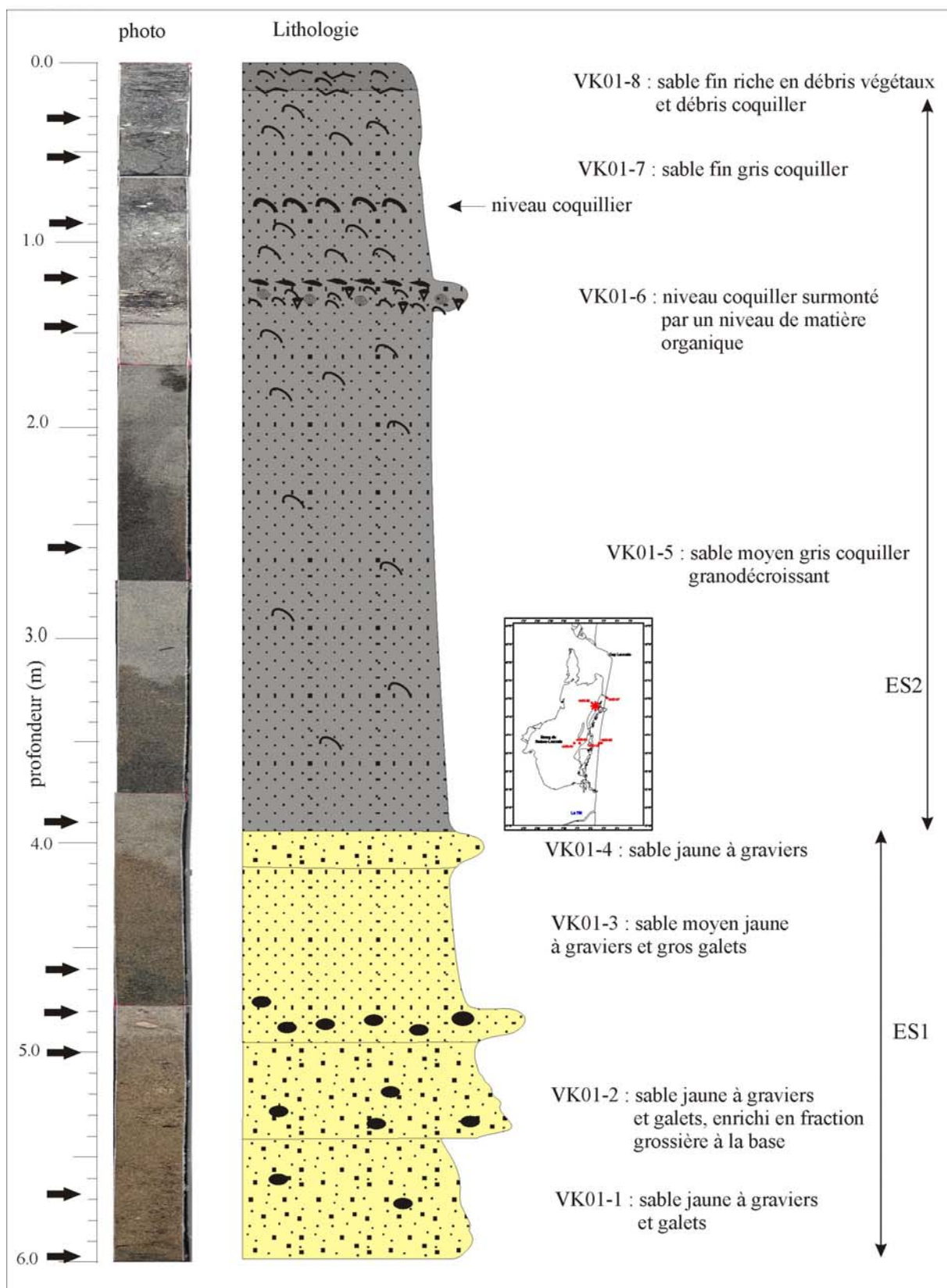


Figure III-9. Log lithologique et photographie de la carotte 03VK01.

03VK02 (Figure III-10)

Métadonnées :

Coordonnées : Longitude : 3°02,088	Profondeur : 1 m
Latitude : 42°52,740	Longueur : 1,8 m

Description :

La carotte 03VK02, située dans le bassin Nord de l'étang de Salses-Leucate, est divisée en 7 niveaux. Les niveaux VK02-1 à VK02-3 montrent une évolution de type granodécroissant avec des galets à la base et des sables fins au sommet. Ce point est confirmé par les résultats de la radioscopie. On notera la présence de débris coquilliers sur l'ensemble de ces niveaux. Une datation a été réalisée à la base du niveau VK02-2. Ces niveaux sont surmontés par une alternance de sable vaseux gris coquillier à débris végétaux (VK02-5 et VK02-7) et de vase grise relativement compacte (VK02-4 et VK02-6). Les résultats de la radioscopie montre une très grande hétérogénéité au sein de ces niveaux supérieurs.

La répartition des classes granulométriques (annexe IV Figure IV-12) dans les échantillons du niveau VK02-3 indique une sédimentation relativement constante, type aggradante. La base de la carotte ainsi que les niveaux gris supérieurs présentent un classement relativement médiocre (annexe IV Tableau IV-6 et Figure IV-11). Le niveau sableux jaune, VK02-3, présente un bon classement ainsi qu'une répartition relativement symétrique.

Interprétation :

Les niveaux VK02-1 à VK02-3 sont considérés par rapport à la lithologie et aux analyses granulométriques comme étant une sédimentation de cordon littoral externe, sable de plage pour le niveau VK02-3. La base de la carotte paraît soumise à une influence fluviatile. Les niveaux VK01-4 à VK01-7 moins bien classés et plus fins semblent moins soumis à la dynamique marine et sont associés à une sédimentation en milieu fermé.

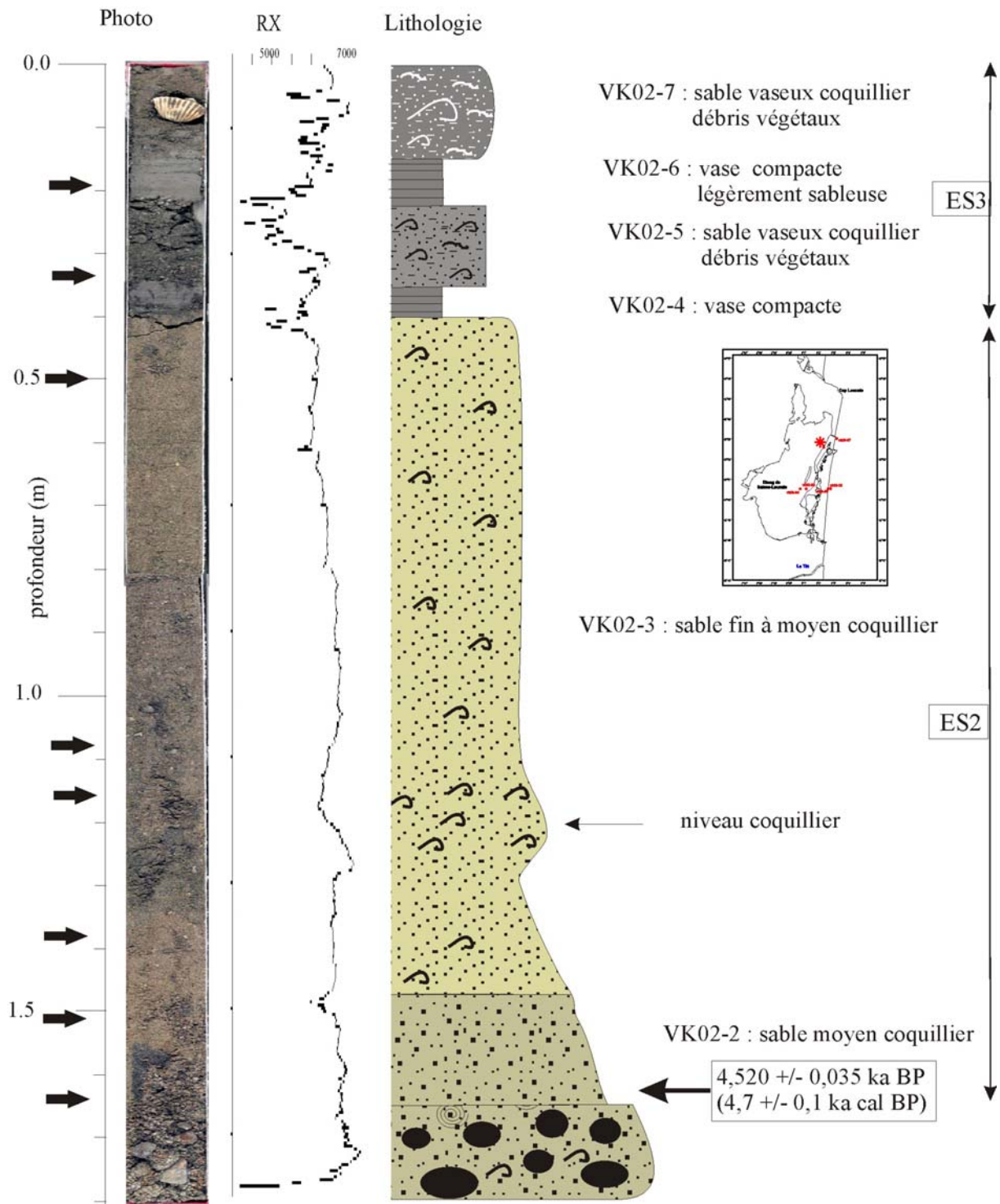


Figure III-10. Log lithologique, photographie et rayon X de la carotte 03VK02.

03VK03 (Figure III-11)

Métadonnées :

Coordonnées : Longitude : 3°01,170 Profondeur : 2,1 m
Latitude : 42°50,514 Longueur : 2,6 m

Description :

La carotte 03VK03, située dans le bassin Sud, est divisée en 9 niveaux plutôt sableux pour les niveaux inférieurs (VK03-1 à VK03-4) et vaseux pour les niveaux supérieurs (VK03-5 à VK03-9). Les niveaux inférieurs sont relativement riches en fraction grossière type graviers et galets. Les débris coquilliers apparaissent dans les niveaux VK03-4 à VK03-9. L'analyse effectuée sur le banc radioscopique montre une grande hétérogénéité de l'ensemble de la carotte.

La répartition des classes granulométriques (annexe IV Figure IV-14) reflète également la grande hétérogénéité des différents niveaux. Le classement (annexe IV Tableau IV-7 et Figure IV-13) est mauvais à très mauvais pour l'ensemble de la carotte. On notera également une asymétrie vers la fraction fine. La majorité des échantillons sont bimodaux, voir plurimodaux, les indices granulométriques sont donc à considérer avec précaution.

Interprétation :

L'ensemble de la sédimentation semble indiquer un dépôt dans un milieu relativement protégé mais soumis à des variations rapides des conditions. Par rapport à la localisation de la carotte, on peut supposer une forte influence anthropique.

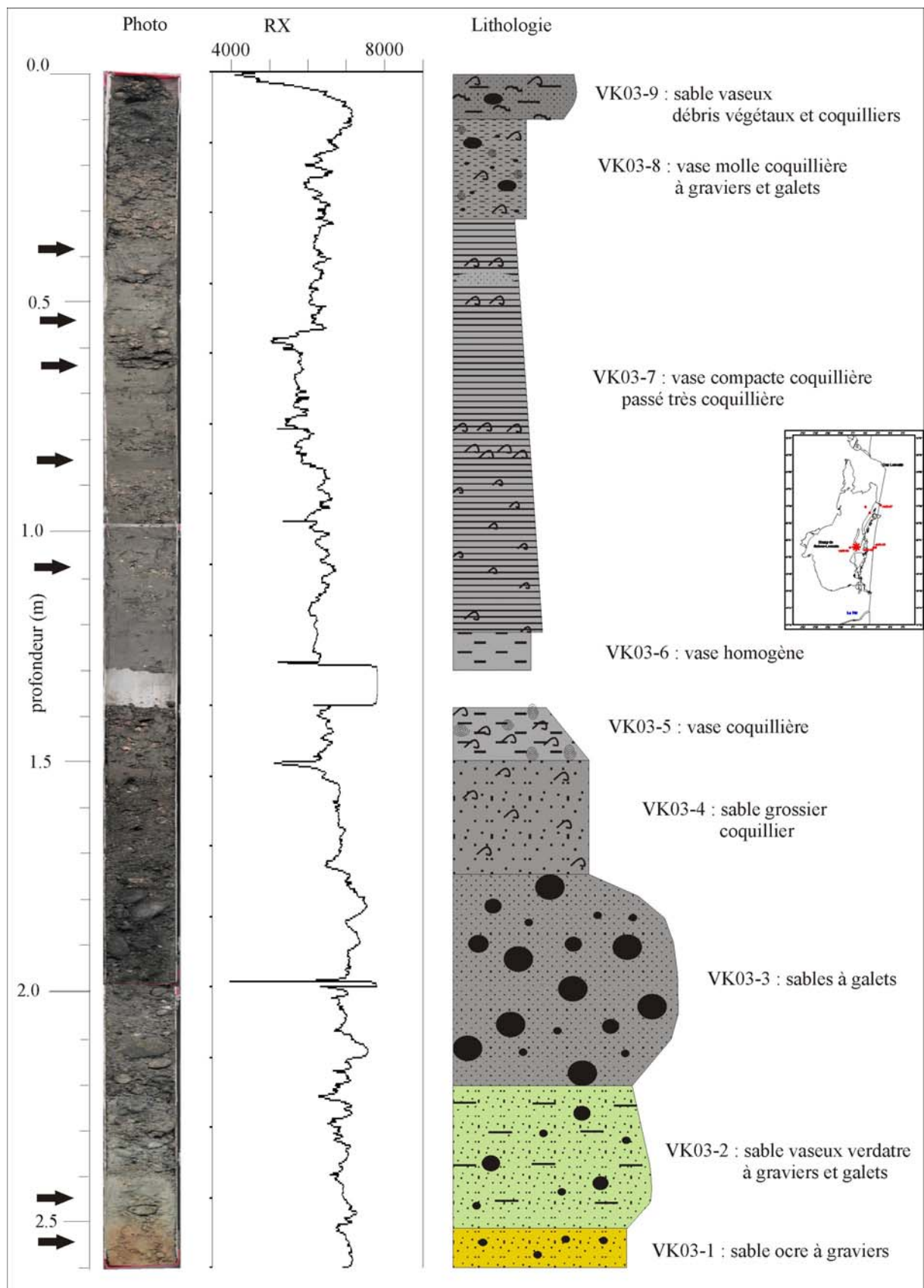


Figure III-11. Log lithologique, photographie et rayon X de la carotte 03VK03.

03VK04 (Figure III-12)

Métadonnées :

Coordonnées : Longitude : 3°00,763	Profondeur : 3,6 m
Latitude : 42°50,512	Longueur : 4,1 m

Description :

La carotte 03VK04, située dans le bassin Sud de l'étang de Salses-Leucate, est divisée en 8 niveaux. Les 5 niveaux de base sont de nature sableuse et délimités par des passées à galets. L'observation à l'œil nu ne permet pas de repérer la présence de coquilles et débris coquilliers. L'analyse sur le banc radioscopique indique la succession de niveaux granodécroissants (de VK04-2 à VK04-5). Les trois niveaux supérieurs (VK04-6 à VK04-8) sont de nature plus vaseuse et coquillière pour VK04-6 et VK04-8.

La répartition des classes granulométriques (annexe IV Figure IV-16) indique une tendance granodécroissante pour l'ensemble de la carotte. Le classement (annexe IV Tableau IV-8 et Figure IV-15) est mauvais pour les niveaux sableux et très mauvais pour les sédiments vaseux. On notera une dissymétrie négative, vers la fraction grossière, pour les niveaux sableux VK04-2 à VK04-5. Cette asymétrie est associée à un second mode situé au niveau des sables grossiers.

Interprétation :

Les niveaux sableux semblent soumis à une influence fluviatile à leur base et marine à leur sommet. Ils correspondent à une migration du cordon littoral. Les dépôts vaseux sommitaux sont associés à une sédimentation fine de type lagunaire.

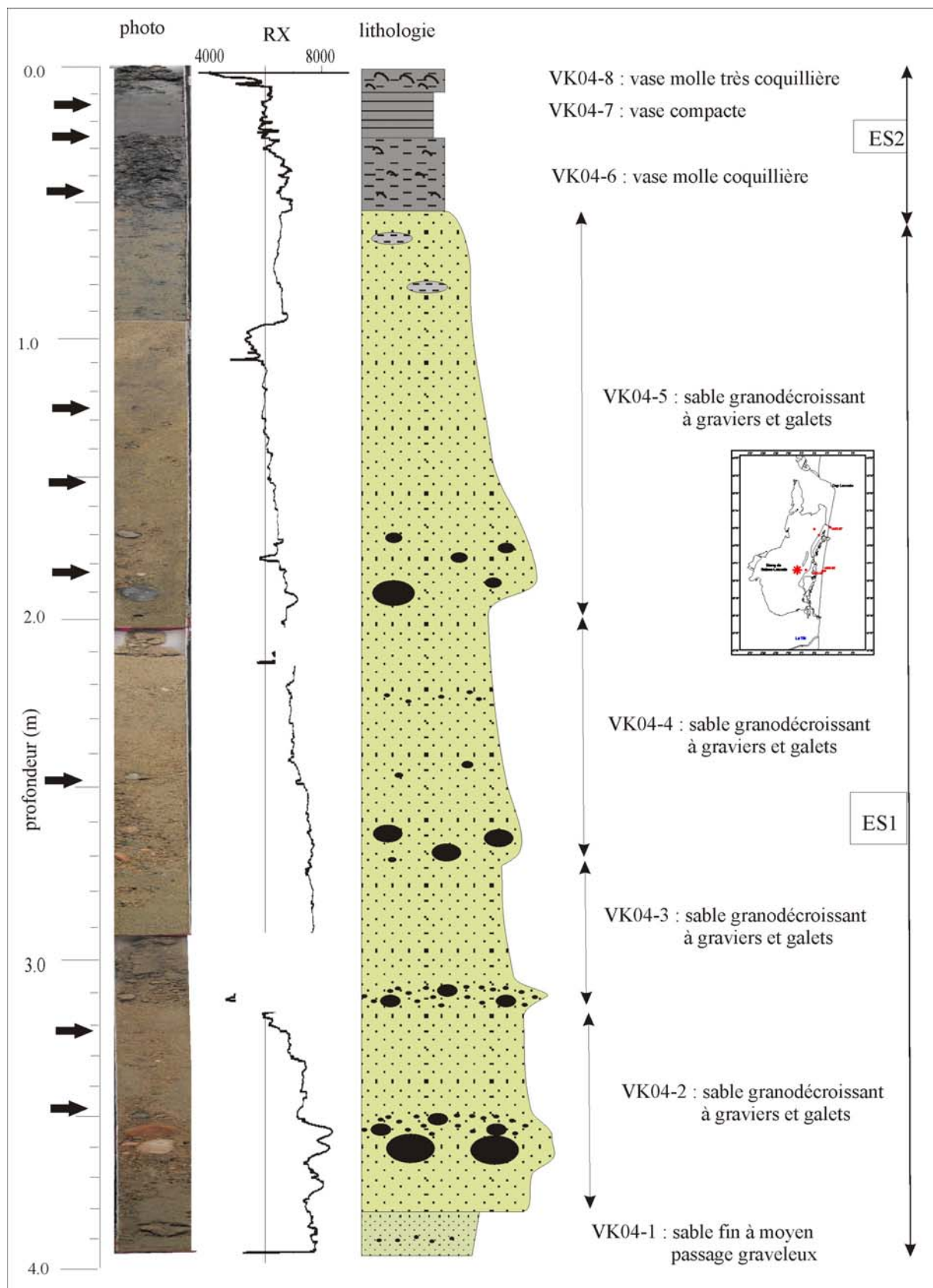


Figure III-12. Log lithologique, photographie et rayon X de la carotte 03VK04.

03VK05 (Figure III-13)

Métadonnées :

Coordonnées : Longitude : 3°02,642 Profondeur : 0 m
 Latitude : 42°50,520 Longueur : 2,6 m

Description :

La carotte 03VK05, située sur la plage, est divisée en trois niveaux à dominance sableuse. Seule le tronçon supérieur a été passé sur le banc radioscopique, les résultats indiquent une légère granodécroissance. On notera la présence de deux niveaux de graviers au sein du niveau VK05-3.

La répartition des classes granulométriques (annexe IV Figure IV-17) montre une granodécroissance dans le dernier mètre du niveau VK05-3. Le classement reste relativement correct et constant sur l'ensemble de la carotte (annexe IV Tableau IV-9 et Figure IV-18). De même, la symétrie est également relativement constante et bonne. Les échantillons sont tous unimodaux.

Interprétation :

La sédimentation est typique des sables de plage avec vraisemblablement une influence fluviatile à la base de la carotte.

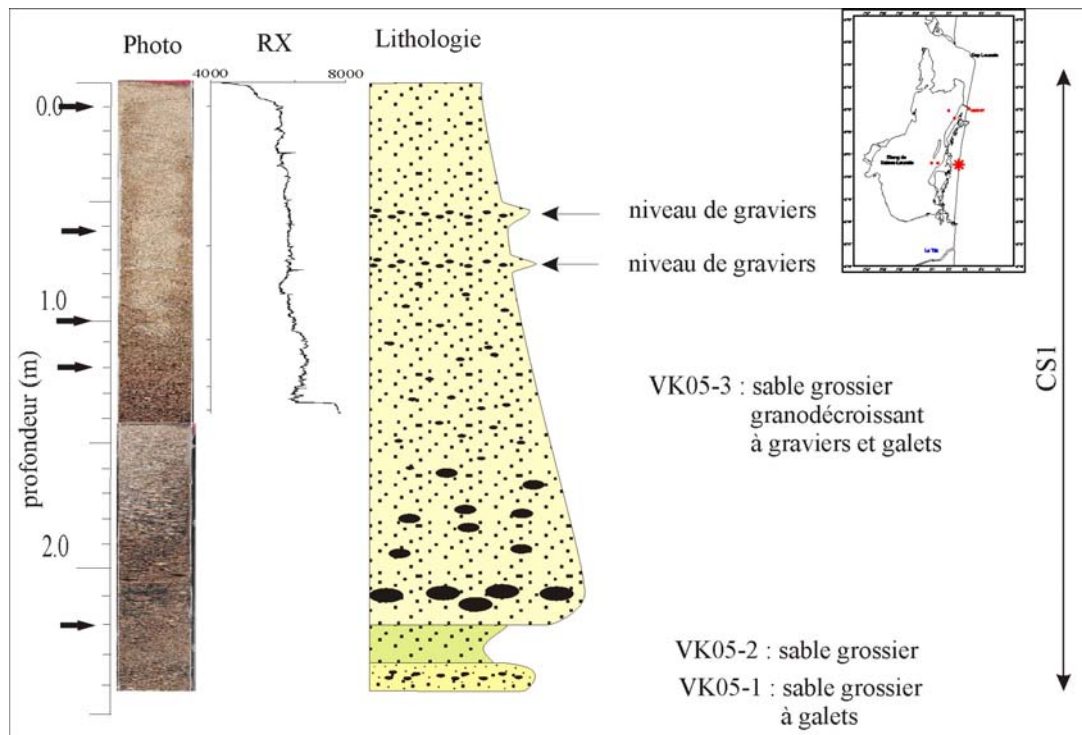


Figure III-13. Log lithologique, photographie et rayon X de la carotte 03VK05.

03VK06 (Figure III-14)

Métadonnées :

Coordonnées : Longitude : 3°02,816 Profondeur : 3,9 m
Latitude : 42°50,520 Longueur : 1,7 m

Description :

La carotte 03VK06, située sur la barre d'avant-côte interne, présente une sédimentation extrêmement homogène de type sable moyen à grossier jaune sans trace de coquilles ou de débris coquilliers. Ceci est confirmé par les analyses granulométriques. La symétrie et le classement sont relativement bons. Les échantillons sont tous unimodaux.

Interprétation :

L'ensemble des caractéristiques de cette carotte est associé à celles d'un sable de plage typique.

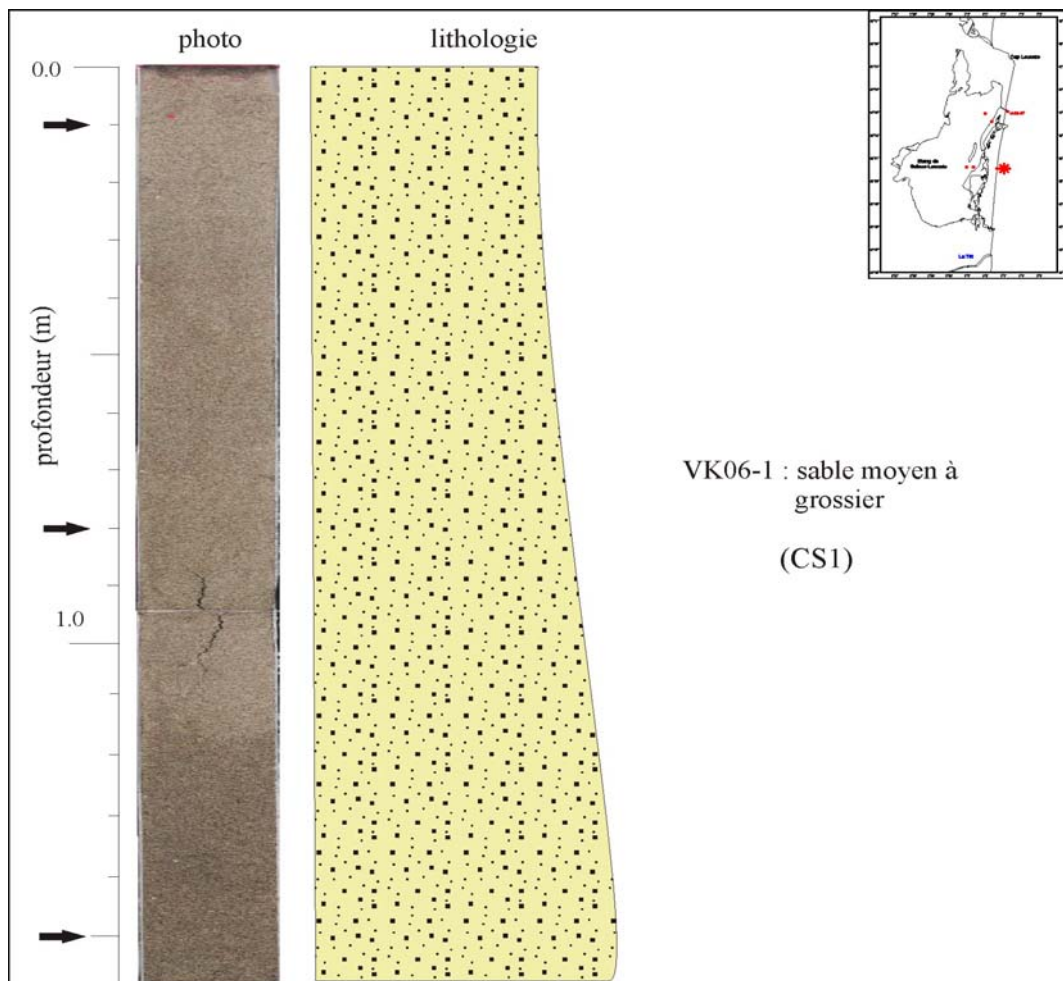


Figure III-14. Log lithologique et photographie de la carotte 03VK06.

03VK07 (Figure III-15)

Métadonnées :

Coordonnées : Longitude : 3°03,227	Profondeur : 2,7 m
Latitude : 42°53,004	Longueur : 4,2 m

Description :

La carotte 03VK07, située également sur la barre d'avant-côte interne, présente également une sédimentation relativement homogène. On distingue cependant trois niveaux différents limités par des passées à graviers. Des coquilles et débris coquilliers ont pu être observés au sein des trois niveaux de sable jaune.

La répartition des classes granulométriques (annexe IV Figure IV-22) et la courbe d'évolution du mode principal montre trois types d'empilement. Le niveau VK07-1 est de type granodécroissant, au-dessus, le niveau VK07-2 est plutôt granocroissant et au sommet le niveau VK07-3 présente une bonne homogénéité. Les trois niveaux sont relativement bien classés et présentent une répartition symétrique. A une exception près, Les échantillons sont tous unimodaux.

Interprétation :

Comme pour la carotte précédente, les trois niveaux correspondent à des sables de plage soumis à l'action de la houle. Les passages plus grossiers pourraient correspondre à une sédimentation au niveau des fosses de lévigation présentes entre les barres d'avant-côte.

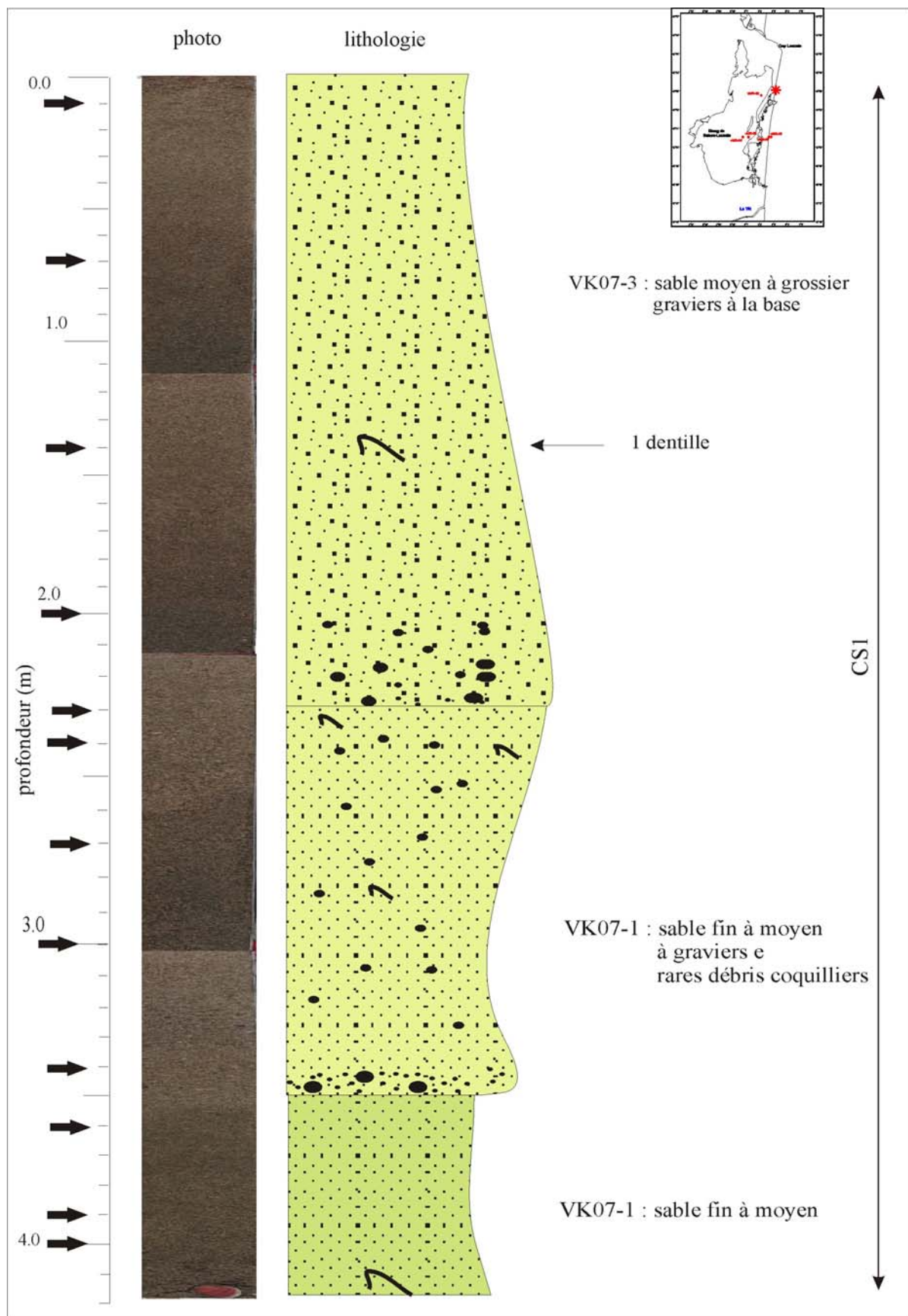


Figure III-15. Log lithologique et photographie de la carotte 03VK07. Figure 3-3. Cartes isophaques de l'unité U1 (a)correspondant aux dépôts anté post-glaciaires et du Post-Glaciale (b).

ANNEXE IV

PRESENTATION DES RESULTATS DES ANALYSES

GRANULOMETRIQUES

Présentation des résultats :

1. Tableau récapitulatif des paramètres granulométriques pour chaque échantillon. La première ligne indique les profondeurs d'échantillonnage. Signification des abréviations :

L : lamellibranches ; G : gastéropodes

sf : sable fin ; sm : sable moyen ; sg : sable grossier ; stg : sable très grossier

gr : graviers ; ga : galets ; ag : agrégats

Pour certains échantillons les débris coquilliers n'ont pas pu être identifiés, nous avons donc juste indiqué leur abondance relative.

Les valeurs des paramètres granulométriques sont données en unité phi.

2. Figure présentant les courbes d'évolution des paramètres granulométriques établies par rapport aux échantillons.

— mode 1 ; — moyenne ; — classement (S_0 ; graphic standard deviation) ; — asymétrie (S_k ; inclusive graphic skewness).

Les valeurs des paramètres granulométriques sont données en unité phi (axe des ordonnées).

3. Figure présentant la répartition des classes granulométriques (à l'exception de la fraction grossière, supérieure à 2 mm) pour les différents échantillons. Les sondes correspondent aux profondeurs d'échantillonnage en cm.

LK03-01

Tableau IV.1. Résultats de la granulométrie laser : paramètres granulométriques

	11	31	41	51	91	121	141
$\varnothing 5$	3,45	2,4	2,85	2	2,15	1,7	2,2
$\varnothing 16$	4,45	2,6	3,2	2,7	2,6	2,3	2,5
$\varnothing 25$	5,3	2,8	3,85	3,05	2,75	2,55	2,78
$\varnothing 50$	6,82	3,3	6,05	3,6	3,1	2,95	3,2
$\varnothing 75$	8,35	6,3	7,8	4	3,5	3,35	4,9
$\varnothing 84$	9	7,45	8,6	4,3	3,75	3,58	6,7
$\varnothing 95$	10,1	9,4	10,1	6,1	5,2	4,4	8,38
moyenne	6,76	4,45	5,95	3,53	3,15	2,94	4,13
graphic standard deviation	2,15	2,27	2,45	1,02	0,75	0,73	1,99
inclusive graphic skewness	-0,01	0,36	0,06	0,11	0,19	0,04	0,33
mode1	7,3	2,85	3,15	3,7	3,15	3,1	2,9
%	2,6	7,5	3,9	8	9,8	9,3	8
mode 2	6	7,4	7,4	1,8			
%	2	1	2	1			
mode 3	4,6		4,3				
%	1,6		1,7				
> 2mm (%)	0	0	0	0	0	0	0
coquille							
débris	oui	oui	oui			oui	
foram							
gravier							
classe	silt	silt	silt	silt	silt	s. fin	silt

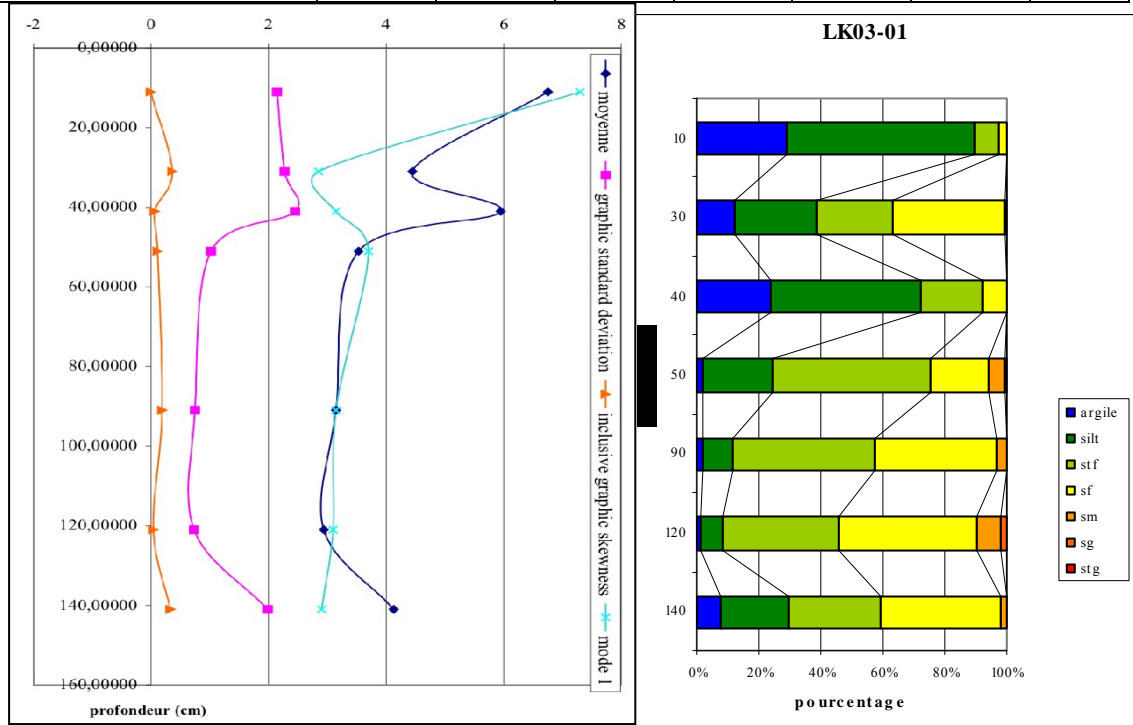


Figure IV.1. Courbes d'évolution des paramètres granulométriques

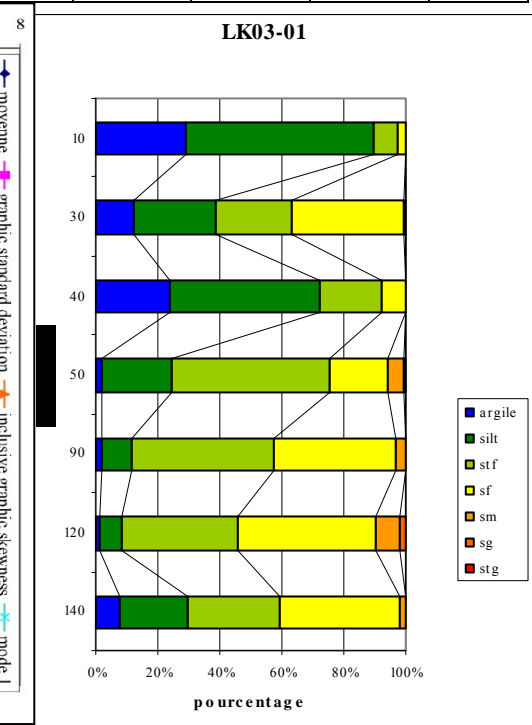


Figure IV.2. Répartition des classes granulométriques

LK03-01b

Tableau IV.2. Résultats de la granulométrie laser : paramètres granulométriques

	15	22	35	50	65	75	95	105	108	125	135	155
Ø5	2,85	3,25	2,4	2,4	1,7	2,6	3,65	2,1	-5	2,15	2,4	2,42
Ø16	3,45	4,3	2,65	2,78	2,55	3,05	4,38	2,55	0,05	2,38	2,6	2,78
Ø25	4	5,05	2,75	2,95	2,85	3,6	5	2,8	0,75	3,05	2,78	2,85
Ø50	6,1	6,7	3,05	3,35	3,45	5,62	6,55	3,3	2,7	4,15	3,1	3,2
Ø75	7,8	8,15	3,45	3,75	3,9	7,7	8,05	5,5	3,3	6,98	3,8	3,85
Ø84	8,45	8,85	3,62	4	4,15	8,55	8,8	7	4	7,9	5,2	5
Ø95	10	10,2	4,9	6	5,25	10	10,1	9	7,62	9,6	8,6	8,1
moyenne	6,00	6,62	3,11	3,38	3,38	5,74	6,58	4,28	2,25	4,81	3,63	3,66
S0	2,33	2,19	0,62	0,85	0,94	2,50	2,08	2,16	2,90	2,51	1,59	1,42
Sk	0,05	0,00	0,24	0,24	0,01	0,09	0,05	0,32	-0,11	0,23	0,38	0,35
mode1	3,35	7,3	3	3,3	3,7	3	7,2	3	2,82	3,2	3	3,1
%	2,5	2,4	11	9,5	7,9	4	2,4	6,5	5,9	4,4	9,8	9,9
mode 2	7,35	6			2	7,4	4,4		-0,3	2,25		
%	2,2	2,1			1,8	1,9	2,2		2,8	2,1		
mode 3	5,95	3,35				6	6			7,35		
%	1,7	1,9				1,4	2,15			1,4		
> 2mm (%)	0	0	0	0	0	0	0	0	0	0	0	0
coquille												
débris	oui		rare	rare	rare	riche						
foram												
gravier												
classe	silt	s. fin	silt	silt	silt							

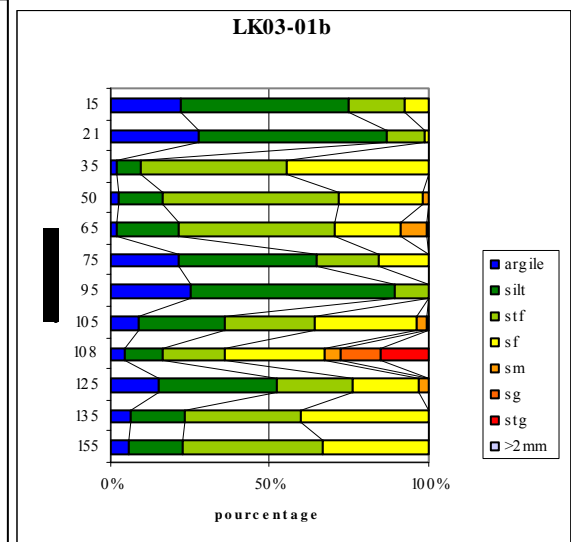
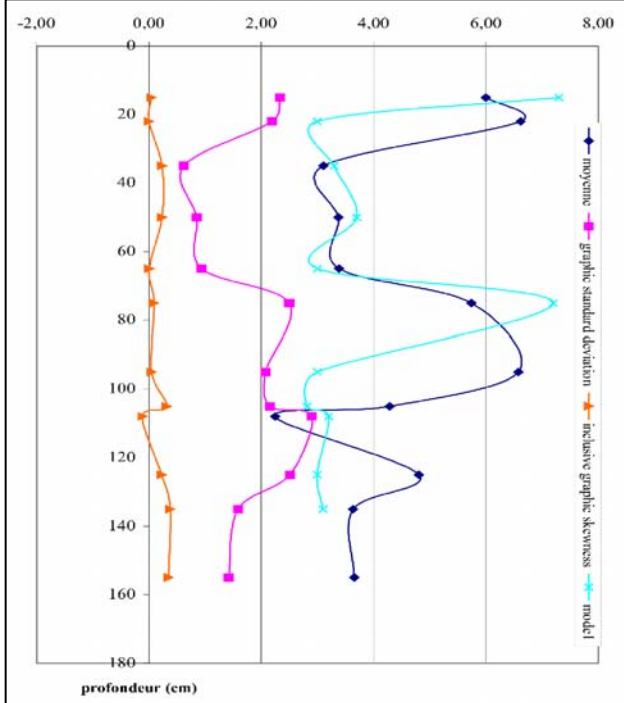


Figure IV.4. Répartition des classes granulométriques

Figure IV.3. Courbes d'évolution des paramètres granulométriques

LK03-03

Tableau IV.3. Résultats de la granulométrie laser : paramètres granulométriques

	7	15	33	40	80	110
$\varnothing 5$	2,75	2,85	2,9	2	2,8	2,78
$\varnothing 16$	3,2	3,3	3,2	2,8	3,2	3,1
$\varnothing 25$	3,4	3,6	3,4	3,1	3,45	3,5
$\varnothing 50$	3,9	4,4	3,9	3,6	4	3,9
$\varnothing 75$	5,35	6,8	6,3	4,45	5,6	5,15
$\varnothing 84$	6,9	7,85	7,6	6	7,22	6,6
$\varnothing 95$	9	9,2	9,3	8,8	9,2	9
moyenne	4,67	5,18	4,90	4,13	4,81	4,53
graphic standard deviation	1,87	2,10	2,07	1,83	1,97	1,82
inclusive graphic skewness	0,31	0,25	0,33	0,26	0,31	0,31
mode1	3,7	3,75	3,4	3,85	3,6	3,6
%	6,9	5	7	6,8	6,5	6
mode 2	7,2	7,3	7,3	2	7,3	7,2
%	0,9	1,2	0,9	1	0,95	0,8
mode 3		7,65				
%		1,2				
> 2mm (%)	0	0	0	0	0	0
coquille						
débris	oui	trace	traces	traces	traces	traces
foram						
gravier						
classe	silt	silt	silt	silt	silt	silt

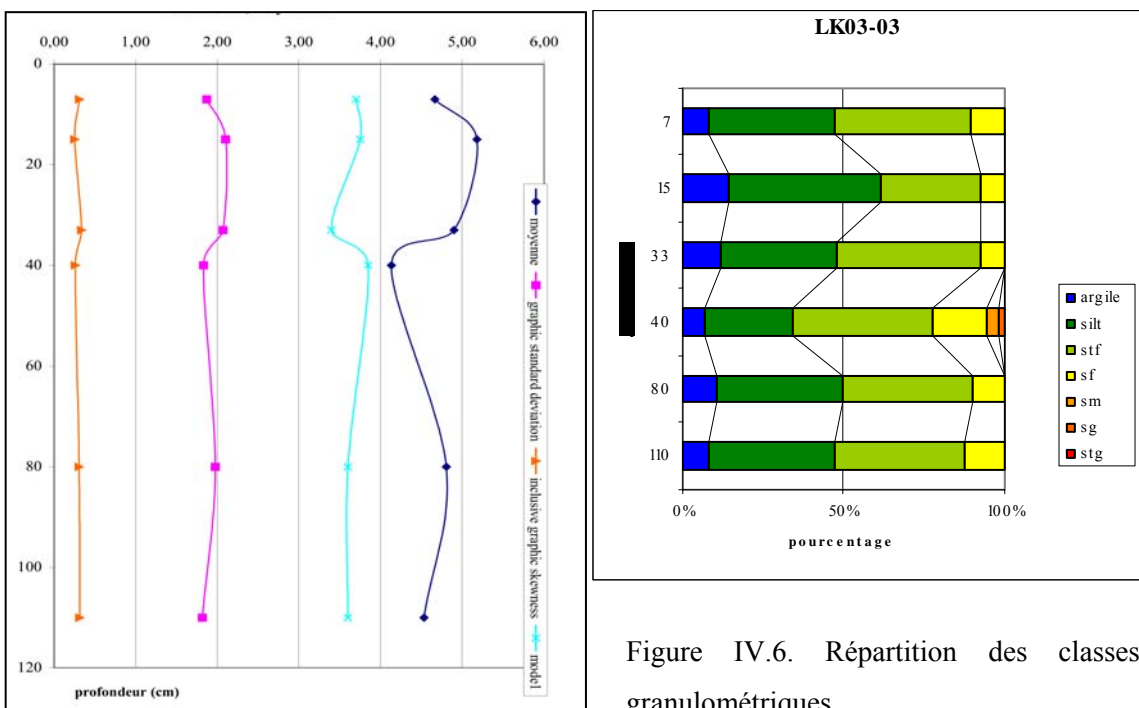


Figure IV.5. Courbes d'évolution des paramètres granulométriques

Figure IV.6. Répartition des classes granulométriques

LK03-04

Tableau IV.4. Résultats de la granulométrie laser : paramètres granulométriques

	10	30	50	60	70	100	119	129	134
Ø5	3,05	2,4	3,58	1,7	3,22	1,2	-0,65	-0,5	2,6
Ø16	3,4	3,22	4,1	2,6	3,65	2,3	-0,4	0,15	3,7
Ø25	3,6	3,65	4,55	2,95	4,05	2,85	-0,15	0,7	4,2
Ø50	4,38	5	5,8	3,5	5,4	3,62	0,45	2,2	5,2
Ø75	6,4	6,9	7,5	4,3	6,8	4,35	3,5	3,35	6,6
Ø84	7,5	7,8	8,35	5,6	8	4,8	4,65	5,2	7,25
Ø95	9,1	9,3	9,9	8,4	9,62	6,9	6,9	8	9
moyenne	5,09	5,34	6,08	3,90	5,68	3,57	1,57	1,90	5,38
graphic standard deviation	1,94	2,19	2,02	1,77	2,06	1,49	2,41	1,66	1,86
inclusive graphic skewness	0,27	0,12	0,15	0,23	0,16	0,08	0,35	0,03	0,09
mode1	3,7	3,9	4,65	3,5	3,85	3,85	-0,1	2,5	4,6
%	6	3,1	3,1	6,5	3,6	5,4	6	6	3,2
mode 2	7,2	5,9	7,1		5,8	1,85	4	0,4	2,5
%	1,2	1,8	1,8		2	1,4	1,1	2,5	1,1
mode 3		6,8						-0,4	
%		1,7						2,4	
> 2mm (%)	0,00	0,00	0,00	0,00	0,00	0,00	73,14	41,93	0,00
coquille									
débris	traces	traces					traces	traces	
foram									
gravier								oui	ag
classe	silt	silt	silt	silt	silt	silt	s. moyen	s. moyen	

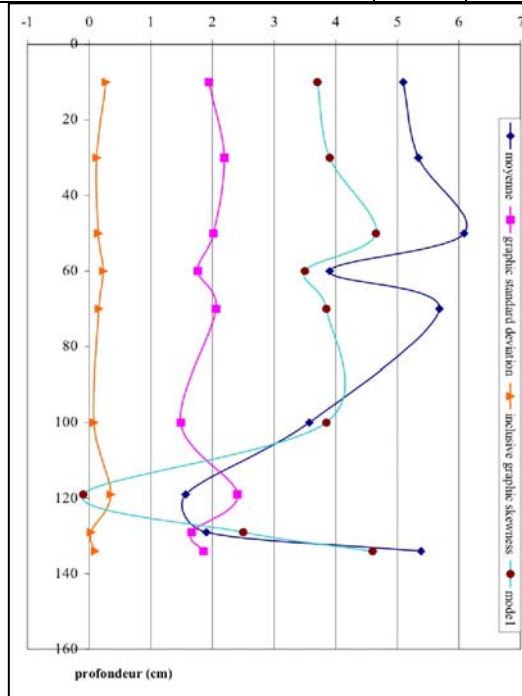


Figure IV.7. Courbes d'évolution des paramètres granulométriques

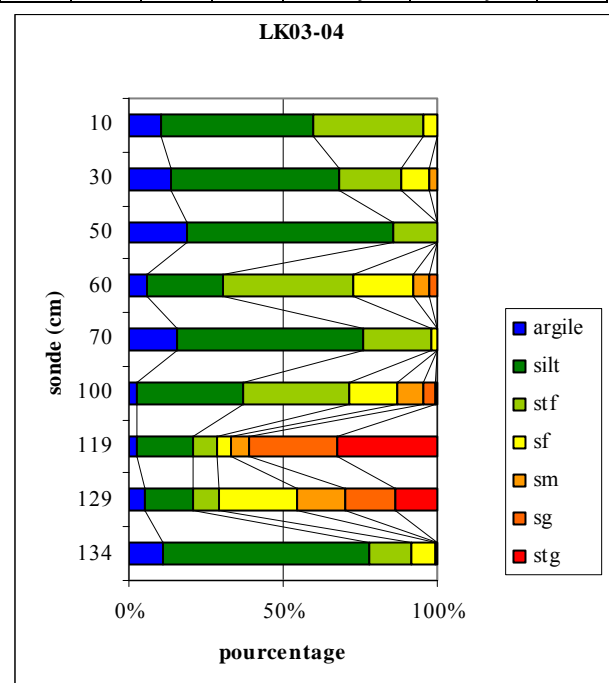


Figure IV.8. Répartition des classes granulométriques

03VK01

Tableau IV.5. Résultats de la granulométrie laser : paramètres granulométriques

	30	52	90	120	148	260	390	460	480	500	578	598
05	-0,55	0,1	0,38	0,4	0,4	-0,15	-0,4	0,2	-0,7	-0,4	0,15	-0,05
016	-0,13	0,85	0,65	0,8	0,8	0,4	0,15	0,78	-0,4	0,05	0,8	0,55
025	0,4	1,2	0,8	0,9	0,9	0,65	0,45	0,95	-0,15	0,4	1	0,85
050	0,98	1,7	1,15	1,25	1,2	1,1	1	1,3	0,55	1,15	1,35	1,3
075	1,2	2,3	1,45	1,55	1,6	1,4	1,4	1,6	1,2	1,6	1,7	1,6
084	1,45	2,65	1,6	1,75	1,65	1,6	1,6	1,75	1,5	1,7	1,8	1,8
095	1,85	5,55	1,95	2	2	1,9	1,9	2,1	1,85	2,1	2,15	2,3
moyenne	0,77	1,73	1,13	1,27	1,22	1,03	0,92	1,28	0,55	0,97	1,32	1,22
graphic standard deviation	0,76	1,28	0,48	0,48	0,45	0,61	0,71	0,53	0,86	0,79	0,55	0,67
inclusive graphic skewness	-0,14	0,21	0,01	-0,03	0,00	-0,11	-0,11	-0,08	0,01	-0,12	-0,10	-0,08
mode1	1,75	1,75	1,2	1,75	1,2	1,25	1,25	1,4	1,2	1,4	1,3	1,5
%	9,5	9,5	12	7	11,5	10	9	11	5,5	7,5	10	9,5
mode 2	-0,55	-0,55		0,38			-0,6	-0,2	0	0,15		0,15
%	2,2	2,2		2			1,8	1	5	4		2
mode 3												
%												
> 2mm (%)	28,30	33,03	15,09	11,95	13,13	0,56	6,68	0,00	48,74	8,38	36,33	0,00
coquille	L	G	L	L	L							
Débris coquillier	L	L	L	L	L+G	L			traces			
Fraction grossière	gr						gr		gr+ga	gr+ga	gr+ga	
Classe	sg	sm	sm	sm	sm	sm	sg	sm	sg	sg	sm	sm

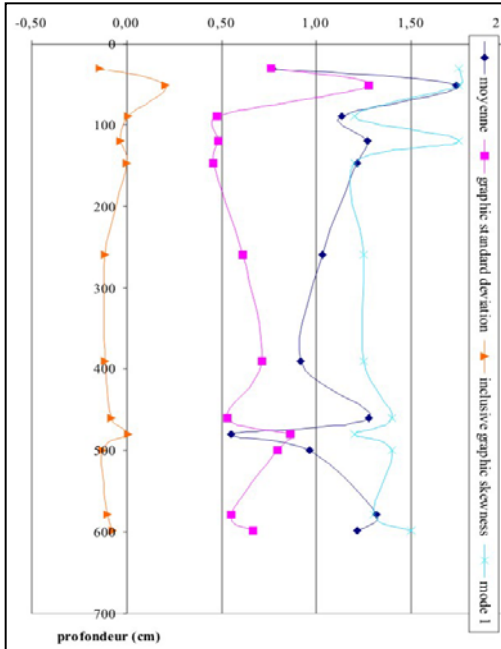


Figure IV.9. Courbes d'évolution des paramètres granulométriques

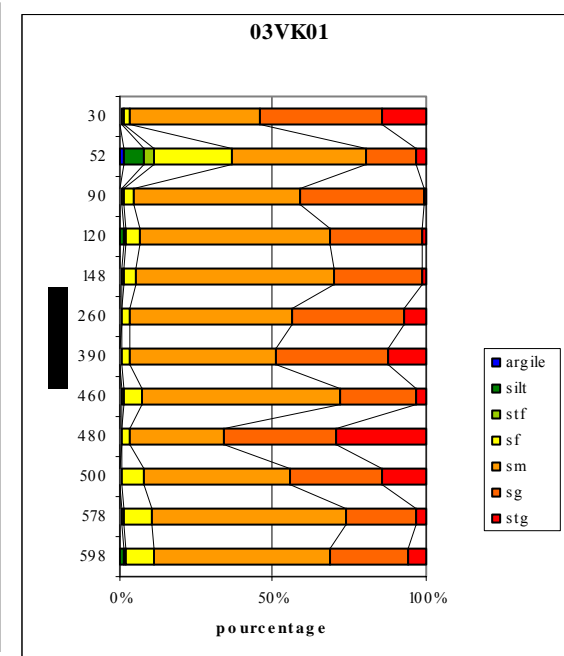


Figure IV.10. Répartition des classes granulométriques

03VK02

Tableau IV.6. Résultats de la granulométrie laser : paramètres granulométriques

	18	33	38	50	107	116	138	151	165
Ø5	2,7	-0,1	0,9	0,6	-0,15	0,35	0,3	-0,6	-0,45
Ø16	3,85	0,85	1,6	1,1	0,7	1,05	1	-0,35	0,1
Ø25	4,45	1,3	2	1,25	1	1,2	1,2	0	0,5
Ø50	6,05	1,8	4,1	1,6	1,4	1,6	1,55	1	1,2
Ø75	7,6	2,25	6,6	1,9	1,8	1,85	1,8	1,58	2,4
Ø84	8,4	2,8	7,55	2,05	2	2	1,98	1,8	3,85
Ø95	9,9	6,4	9,4	2,85	2,5	2,45	2,2	2,05	6,7
moyenne	6,10	1,82	4,42	1,58	1,37	1,55	1,51	0,82	1,72
graphic standard deviation	2,23	1,47	2,78	0,58	0,73	0,56	0,53	0,94	2,02
inclusive graphic skewness	0,03	0,21	0,12	0,06	-0,09	-0,10	-0,16	-0,11	0,27
mode1	5,85	1,9	1,8	1,6	1,6	0,3	1,6	1,5	1,45
%	2,2	8,5	4	11,5	11,5	11,5	12	7	4,5
mode 2	7	0,3	5,9	0,35	0,35	1,55	-0,15	-0,5	0,2
%	2,1	2	1,5	1	1	1	1	4,5	3
mode 3	4,7	-0,4	4,8					-0,3	
%	2,1	1	1,4					4,5	
> 2mm (%)	0	0	0	0	0	0	0	0	0
coquille	0	0	0	0	0	0	0	0	0
débris									
type	silt	sm	silt	sm	sm	sm	sm	sg	sm

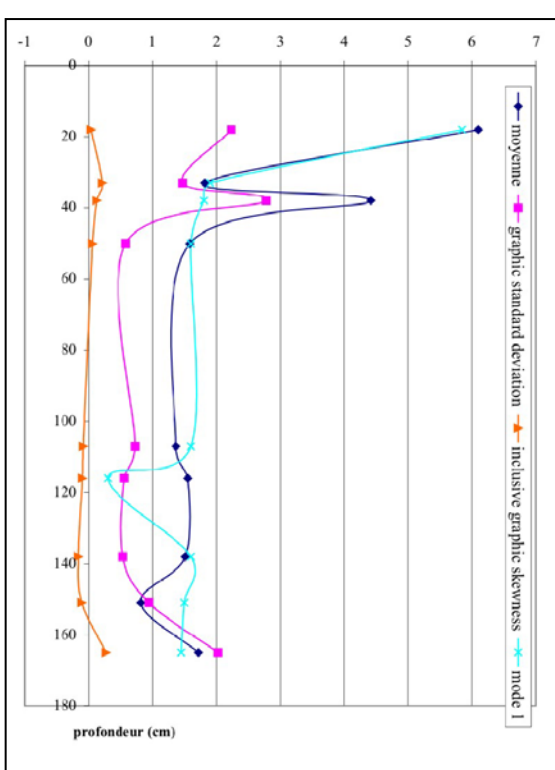


Figure IV.11. Courbes d'évolution des paramètres granulométriques

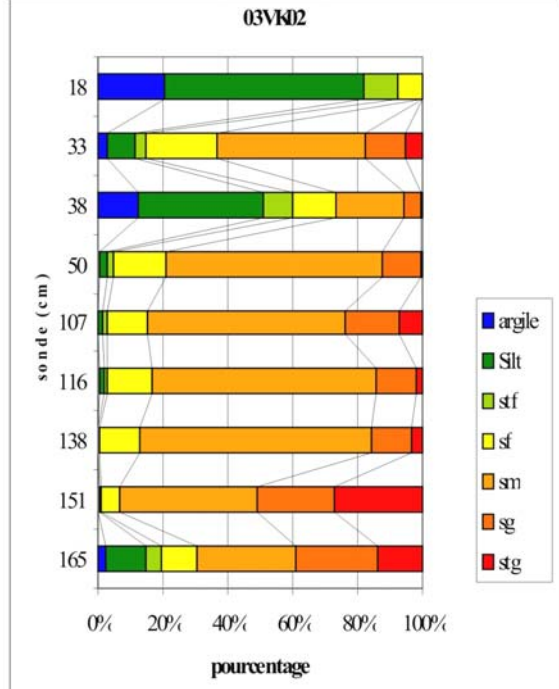


Figure IV.12. Répartition des classes granulométriques

03VK03

Tableau IV.7. Résultats de la granulométrie laser : paramètres granulométriques

	39	53	63	85	107	246	253
Ø5	-0,2	0,85	0,1	-0,6	0,35	-0,4	-0,2
Ø16	0,75	2	0,8	-0,35	1,22	0,1	0,45
Ø25	1,2	2,8	1,2	0,2	1,75	0,4	1,05
Ø50	2	4,35	2	1,2	2,8	1,3	1,8
Ø75	3,3	6,55	3,4	2	4,05	3,9	4,15
Ø84	4,4	7,3	4,8	2,45	5,1	5,15	5,45
Ø95	6,8	8,8	7,2	5,25	7,3	7,6	8
moyenne	2,38	4,55	2,53	1,10	3,04	2,18	2,57
graphic standard deviation	1,97	2,53	2,08	1,59	2,02	2,47	2,49
inclusive graphic skewness	0,18	0,06	0,23	0,19	0,15	0,28	0,25
mode1	1,7	3	1,5	-0,6	2,8	1,3	1,8
%	4	2	4	4,7	3,4	3,8	4,7
mode 2	0,2	6		1,45	2	0,4	0,35
%	1,8	1,8		4,6	3,4	3,75	2,2
mode 3	-0,45	6		0,4	0,3	4,9	4,4
%	1,1	1,6		3,5	1,1	1,1	1
> 2mm (%)	27,80	28,32	60,39	14,68	7,60	23,37	61,48
coquille				riche	oui	0	0
débris	riche	riche	riche	riche	oui		
foram							
gravier						riche	riche
classe	s. fin	silt	s.fin	s. moyen	silt	s.fin	s. fin

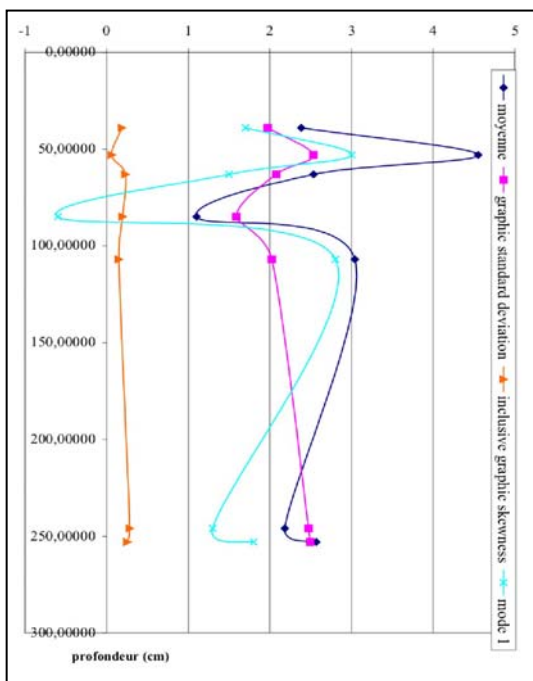


Figure IV.13. Courbes d'évolution des paramètres granulométriques

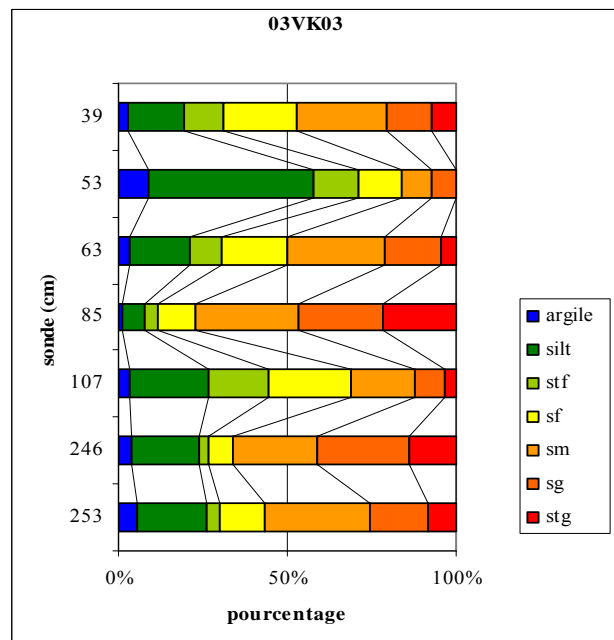


Figure IV.14. Répartition des classes granulométriques

03VK04

Tableau IV.8. Résultats de la granulométrie laser : paramètres granulométriques

	16	26	47	126	151	182	249	321	349
Ø5	2,9	-0,15	0,1	-0,1	0	0,35	-0,5	-0,35	-0,5
Ø16	3,6	1,05	1,2	0,4	0,55	1,4	0,45	0,1	-0,15
Ø25	4	2,05	1,7	0,85	1	1,8	0,85	0,4	0,05
Ø50	5,35	3,8	3,25	1,7	1,8	2,2	2,7	1,4	0,55
Ø75	7,15	5,15	5,4	2,38	2,4	2,65	2,4	2,35	1,8
Ø84	7,85	6	6,6	2,6	2,65	2,8	2,6	2,6	2,35
Ø95	9,4	8,2	8,6	3,2	3,2	3,2	3,3	3,1	3
moyenne	5,37	3,33	3,28	1,49	1,58	2,08	1,85	1,28	0,73
graphic standard deviation	1,64	1,96	2,03	0,90	0,86	0,68	0,96	1,01	0,92
inclusive graphic skewness	0,01	-0,14	0,02	-0,17	-0,19	-0,26	-0,60	-0,09	0,13
mode1	4,1	4,15	1,85	2,1	2,25	2,4	2,1	2,4	0,35
%	3	2,8	3	5,5	6	9,5	5,5	5,1	7
mode 2	5,8	-0,1	4,1	0,35	0,4	0,4	0,35	0,4	2,45
%	2	2,6	1,7	2,95	2,6	1,5	3	4,4	3
mode 3		1,9	0	0	0				
%		1,5	1,55						
> 2mm (%)	0,00	49,58	36,52	14,57	27,37	4,25	4,10	20,73	12,87
coquille		(lam, gast)							
debris		riche	present						
foram									
gravier			ag	oui	oui	oui	oui	oui	oui
galet									
classe	silt	silt	silt	sm	sm	sf	sm	sm	sg

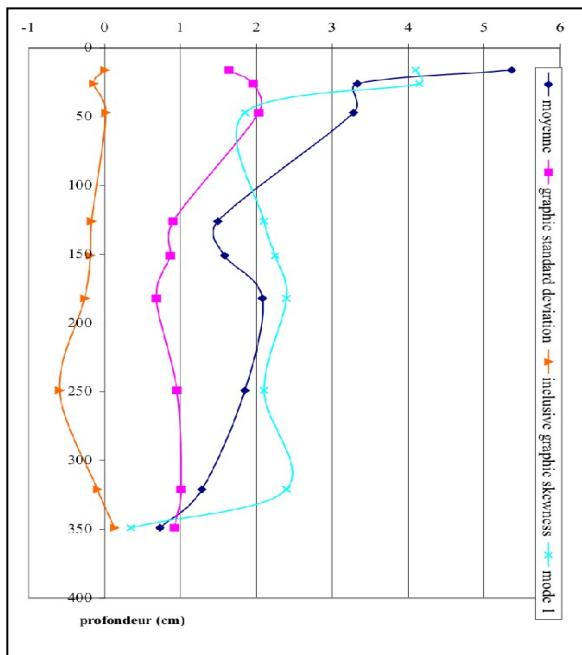


Figure IV.15. Courbes d'évolution des paramètres granulométriques

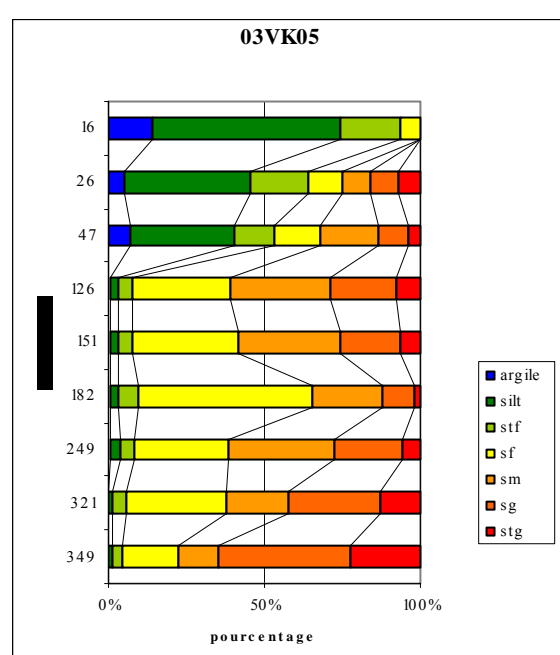


Figure IV.16. Répartition des classes granulométriques

03VK05

Tableau IV.9. Résultats de la granulométrie laser : paramètres granulométriques

	10	61	100	120	220
Ø5	-0,35	-0,7	-1	-0,75	-0,65
Ø16	0,1	-0,45	-0,8	-0,5	-0,45
Ø25	0,2	-0,35	-0,75	-0,4	-0,3
Ø50	0,55	0	-0,3	0	0,1
Ø75	0,89	0,35	0	0,4	0,45
Ø84	1,1	0,45	0,15	0,6	0,65
Ø95	1,45	0,85	0,65	1,1	0,8
moyenne	0,58	0,00	-0,32	0,03	0,10
graphic standard deviation	0,52	0,46	0,49	0,56	0,49
inclusive graphic skewness	0,00	0,05	0,08	0,09	-0,02
mode1	0,65	0,2	-0,5	-0,1	0
%	10,5	11	15,5	9,5	9
mode 2					
%					
mode 3					
%					
> 2mm (%)	0,60	18,70	43,36	22,76	44,63
coquille					
débris					
foram					
gravier	oui	oui	riche	oui	oui
classe	sg	sg	stg	sg	sg

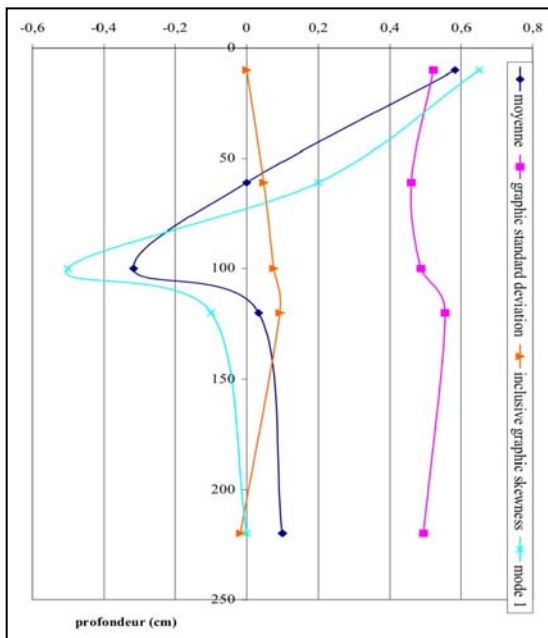


Figure IV.18. Répartition des classes granulométriques

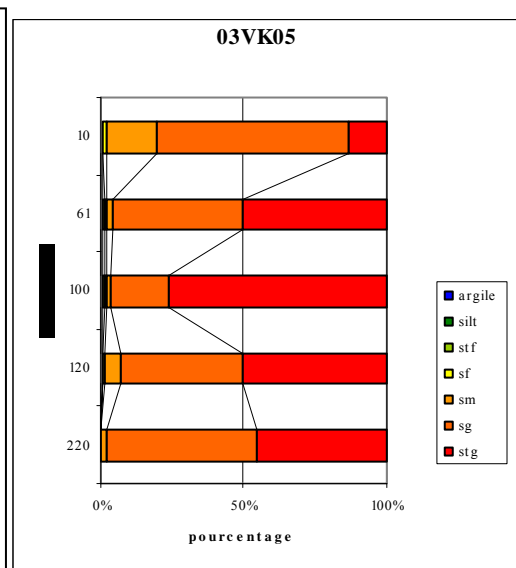


Figure IV.17. Courbes d'évolution des paramètres granulométriques

03VK06

Tableau IV.10. Résultats de la granulométrie laser : paramètres granulométriques

	10	80	150
Ø5	0,48	0,38	0,15
Ø16	0,7	0,75	0,45
Ø25	0,8	0,9	0,7
Ø50	1,2	1,22	1,05
Ø75	1,58	1,62	1,45
Ø84	1,65	1,8	1,65
Ø95	2,05	2,3	2,05
moyenne	1,18	1,26	1,05
graphic standard deviation	0,48	0,55	0,59
inclusive graphic skewness	0,04	0,06	0,03
mode1	1,2	1,25	1,1
%	10,1	10	9,5
mode 2			
%			
mode 3			
%			
> 2mm (%)	0	0	0
coquille			
débris			
foram			
gravier			
classe	s. moyen	s. moyen	s. moyen

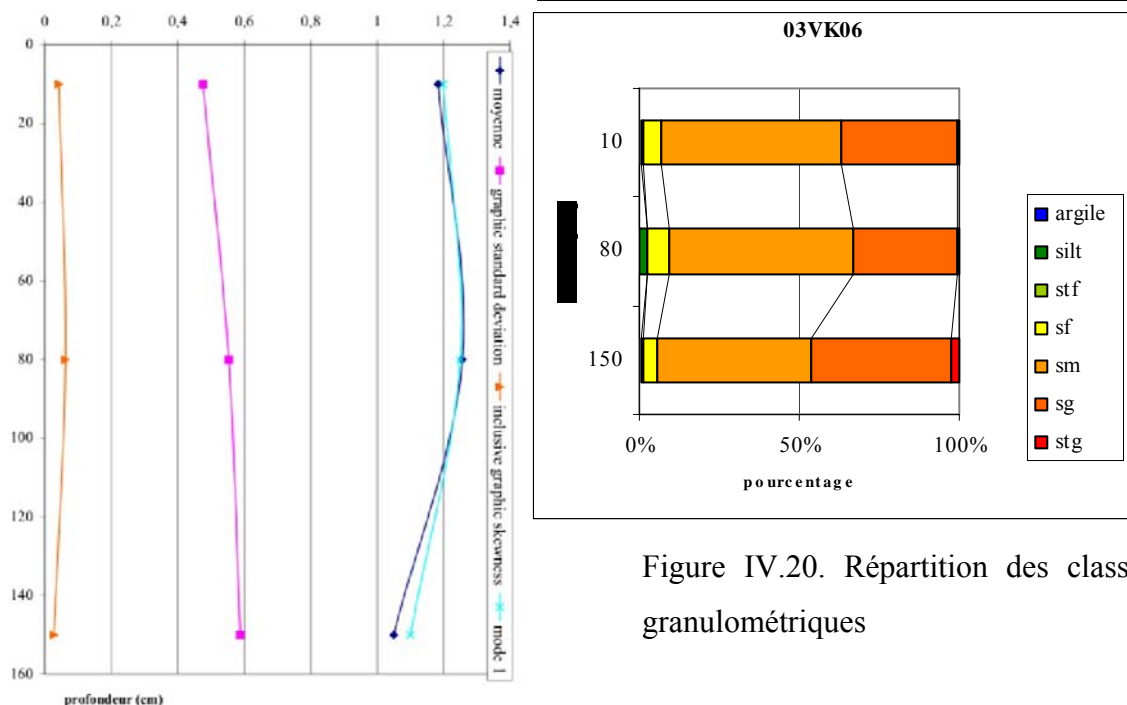


Figure IV.20. Répartition des classes granulométriques

Figure IV.19. Courbes d'évolution des paramètres granulométriques

03VK07

Tableau IV.11. Résultats de la granulométrie laser : paramètres granulométriques

	10	70	140	200	230	240	270	300	340	360	390	400
$\varnothing 5$	0,2	0,3	0,1	0	-0,65	-0,45	-0,1	-0,1	-0,1	0,38	0,45	-0,15
$\varnothing 16$	0,6	0,7	0,5	0,4	-0,3	-0,1	0,25	0,3	0,4	0,85	0,8	0,3
$\varnothing 25$	0,8	0,85	0,78	0,7	-0,1	0,1	0,45	0,5	0,6	1,1	1	0,6
$\varnothing 50$	1,2	1,2	1,15	1,2	0,5	0,6	0,85	0,9	1,05	1,4	1,3	1,1
$\varnothing 75$	16	1,6	1,55	1,6	1	1,05	1,3	1,3	1,4	1,55	1,6	1,5
$\varnothing 84$	1,8	1,8	1,75	1,75	1,25	1,2	1,55	1,55	1,6	1,95	1,8	1,7
$\varnothing 95$	2,2	2,25	2,05	2,15	1,65	1,6	1,95	1,9	2	2,3	2,15	2,05
moyenne	1,20	1,23	1,13	1,12	0,48	0,57	0,88	0,92	1,02	1,40	1,30	1,03
S0	0,60	0,57	0,61	0,66	0,74	0,64	0,64	0,62	0,62	0,57	0,51	0,68
Sk	0,00	0,04	-0,04	-0,06	0,00	-0,01	0,04	0,00	-0,05	-0,03	0,00	-0,07
mode1	1,3	1,3	1,2	1,35	0,7	0,7	1,05	1,05	1,22	1,6	1,4	1,25
%	9,2	9	9	8	6,5	7,5	8,2	8,2	8,8	10,2	11	8,1
mode 2					-0,55							
%					4							
mode 3												
%												
> 2mm (%)	0,00	0,00	0,00	0,00	13,82	0,00	0,00	0,00	0,00	0,00	0,00	0,00
coquille					oui							
débris	rare				oui							
foram												
gravier					riche							
classe	sm	sm	sm	sm	sg	sg	sg	sg	sm	sm	sm	sm

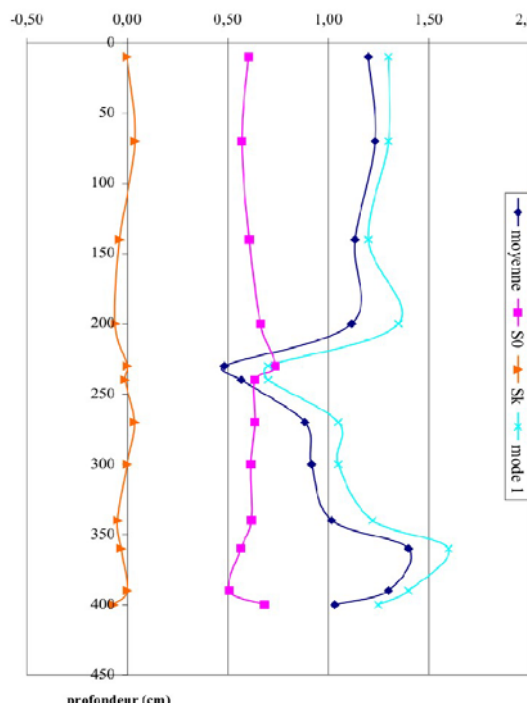


Figure IV.21. Courbes d'évolution des paramètres granulométriques

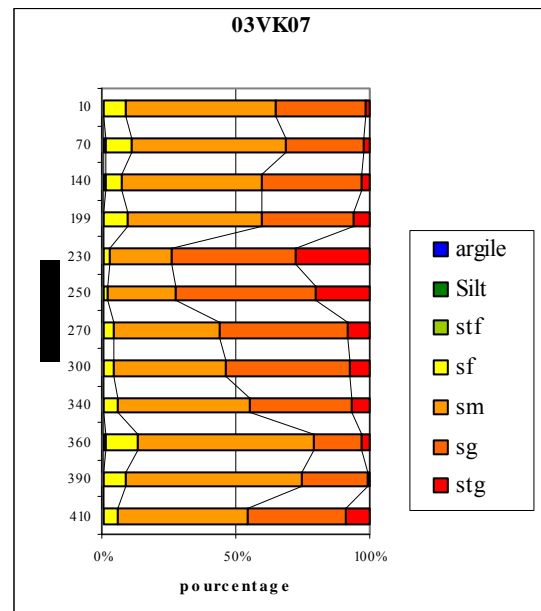


Figure IV.22. Répartition des classes granulométriques

COMMUNICATIONS ET PUBLICATIONS

Articles en préparation ou soumis :

Labaune, C., Duvail, C., Tesson, M., Le Strat, P., Gensous, B., en preparation. Plio-Quaternary stratigraphic pattern in the littoral of Roussillon: well-log, high and very high resolution seismic reflection from land to sea. A soumettre à Continental Shelf Research.

Articles de rang A sous-presse ou publiés :

Labaune, C., Jouet, G., Berne, S., Gensous, B., Tesson, M., Leroux, E., Duval, F., 2005. Seismic stratigraphy of the deglacial deposits of the Rhône prodelta and adjacent shelf. *Marine Geology*, 222-223 : 299-311

Tesson, M., **Labaune, C.**, Gensous, B., 2005. Small rivers contribution to the Quaternary evolution of a mediterranean littoral system: the Western Gulf of Lion, France. *Marine Geology*, 222-223: 313-334

Labaune, C., Tesson, M., Gensous B, In press. Integration of High and Very High Resolution Seismic reflection profiles to study late Quaternary deposits of a coastal area in the western Gulf of Lions, SW France. *Marine Geophysical Researches*.

Rapport :

Satra, C., Boyer, J., **Labaune, C.**, Berné, S., Tesson, M., Gensous, B. 2004a. Evaluation des stocks sédimentaires dans le Golfe du Lion. Phase B : Synthèse des données sur les ateliers potentiellement exploitable. Partie 1 : présentation des données. DRO/GM/R.2004-15, Ifremer, BDSI.

Communications orales :

Labaune, C., Tesson, M., Gensous, B., Jouet, G., Berné, S., Vella, C., 2004. Seismic stratigraphy and chronostratigraphy of the Deglacial deposits of the Rhône prodelta and the adjacent shelf. Joint EURODELTÀ-EUROSTRATAFORM annual meeting, 20-23 Oct., Venice, Abstract: 53.

Labaune C., Delpeint A., Berne S., Gensous B., Tesson M., Leroux E. and Duval F., 2003. Seismic stratigraphy of the deglacial deposits of the Rhône prodelta and adjacent shelf,

COMDELTA Open Conference on Comparing Mediterranean and Black Sea prodeltas,
26-28 Octobre, Aix en Provence, Abstract: 62-63.

Labaune, C., Tesson, M. et Gensous, B., 2003. Architecture des dépôts postglaciaires du littoral du Roussillon : lagune, cordon et plate-forme interne. 9 ème congrès ASF, 14-16 Octobre, Bordeaux, Livre des résumés 38 : 85-86.

Posters :

Gensous, B., Tesson, M., and **Labaune, C.**, 2003. The deglacial deposits of the Rhône shelf : Stratigraphic organisation and controlling factors COMDELTA Open Conference on Comparing Mediterranean and Black Sea prodeltas, 26-28 Octobre, Aix en Provence, Abstract : 32-33.

Labaune, C., Tesson, M. and Gensous, B., 2003. The late Holocene deposits of the Coastal area (lagoon, shoreface and inner shelf) of the SW part of the Gulf of Lions (Roussillon area): exploration with high and very high resolution 2D seismic system. Prodeltal Technology Forum, DELTECH International Workshop, 5-9 may, Venice.

Labaune, C., Tesson, M. and Gensous, B., 2003. Languedoc Roussillon littoral system (western Gulf of Lion, France): Late Quaternary stratigraphic organisation. COMDELTA Open Conference on Comparing Mediterranean and Black Sea prodeltas, 26-28 Octobre, Aix en Provence, Abstract: 64-65.

Tesson, M, **Labaune, C.** and Gensous, B., 2003. Land to sea stratigraphic correlations: A buried incised valleys complex of the western gulf of Lion (France). Late Quaternary and Holocene. 9 ème congrès ASF, 14-16 Octobre, Bordeaux. Livre des résumés 38: 491-492.



ELSEVIER

Marine Geology 222–223 (2005) 299–311

**MARINE
GEOLOGY**
INTERNATIONAL JOURNAL OF MARINE
GEOLOGY, GEOCHEMISTRY AND GEOPHYSICS

www.elsevier.com/locate/margeo

Seismic stratigraphy of the Deglacial deposits of the Rhône prodelta and of the adjacent shelf

Caroline Labaune ^{a,*}, Gwenael Jouet ^b, Serge Berné ^b, Bernard Gensous ^a, Michel Tesson ^a, Arnaud Delpeint ^b

^aUniversité de Perpignan, Laboratoire de Biophysique et Dynamique des Systèmes Intégrés, 52 avenue Paul Alduy,
66860 Perpignan, France

^bIfremer, DRO/GM Technopôle Brest-Iroise, P.O.Box 70, 29280, Plouzané, France

Accepted 15 June 2005

Abstract

In order to achieve a synthesis of the stratigraphic organization of the Deglacial deposits of the inner/middle shelf in front of the Rhône delta plain, we merged high resolution (Mini-sparker and Sparker), and very high resolution (chirp and mud-penetrator) seismic data into a single seismic database. Thus, the merged seismic database improves the lateral correlation between eastern and western parts, separated by the Rhône Incised Valley deposits. As a result the interpretation of seismic units in relation to local and global environmental changes was refined.

The Deglacial deposits rest on a basal erosional discontinuity capping a complex of Pleistocene prograding wedges. The identified units make up Transgressive and Highstand Systems Tracts, and are bounded by flooding surfaces. The main flooding surfaces are (1) the transgressive surface (D200) which forms the lower boundary of the Deglacial deposits and (2) the maximum flooding surface which forms the boundary between the Transgressive and Highstand Systems Tracts. Regarding the data set the study area is divided into three parts depending on the stacking pattern and main control factors. In the western area the units present an aggradational stacking pattern and the rate of sediment supply and dynamic conditions seems coupled with glacio-eustacy role on sedimentary units building and evolution. In the central area the units present an overall backstepping pattern mainly controlled by glacio-eustacy. In the eastern area the units present an aggradational stacking pattern and both the glacio-eustacy and rate of sediment supply have an important role.

The lower parasequence of the Transgressive Systems Tract (U200) is due to the reworking of Würmian terraces. Above, the parasequence U300 is a transgressive body formed during a rapid sea-level rise. The two upper parasequences are interpreted as ancestral coastal systems with a backstepping pattern. The first coastal system (U400) is due to a decrease in the rate of sea-level rise that occurred during the Younger Dryas. The second coastal system (U500) may be due to a similar event or to an increased rate of sediment supply during a constant sea-level rise.

* Corresponding author. Tel.: +33 336 66 68 21 12.
E-mail address: labaune@univ-perp.fr (C. Labaune).

Finally the Highstand Systems Tract is composed of three units: (i) unit U601, located to the West and interpreted as a subaqueous delta, (ii, iii) units U600 and U610, located to the East and interpreted as prograding deltaic lobes.
 © 2005 Published by Elsevier B.V.

Keywords: Rhône shelf; Deglacial deposits; seismic stratigraphy; glacio-eustacy; sediment supply

1. Introduction

During the last three decades, Deglacial deposits of shelf areas have been the field of numerous geological studies. On many inner continental shelves, shallow water depth and landward thickening prisms, several tenths of meter thick, provide expanded records of Deglacial deposits. The Rhône continental shelf, in particular, allows detailed analysis of various local and global factors controlling formation of depositional sequences formed during the last post-glacial hemi-cycle.

Several previous works deal with the Deglacial deposits of the northern part of the Gulf of Lions, including Aloisi et al. (1975); Marsset and Bellec (2002) and Gensous and Tesson (1997, 2003). Those papers defined a set of progradational, aggradational and/or backstepping units. Some differences

appear about the extension of the transgressive units and essentially about the interpretation and identification of the upper units of the prodelta system.

Through the “Eurodelta” European concerted action (Trincardi, 2003), the main prodeltas of the northern Mediterranean Sea and Black Sea are objects of synthesis of previous works and data. In this context, a synthetic study of the Deglacial Rhône prodelta and adjacent shelf deposits was done, using a large seismic database. The present study is based on the analysis of high and very high resolution (HR and VHR) seismic data acquired both by Ifremer and Perpignan University (GDARGO) on the inner and middle shelf of the northern part of the Gulf of Lions (Fig. 1).

The objectives were to achieve a synthesis of the stratigraphic organization of the Deglacial deposits, to improve the lateral correlation between eastern and

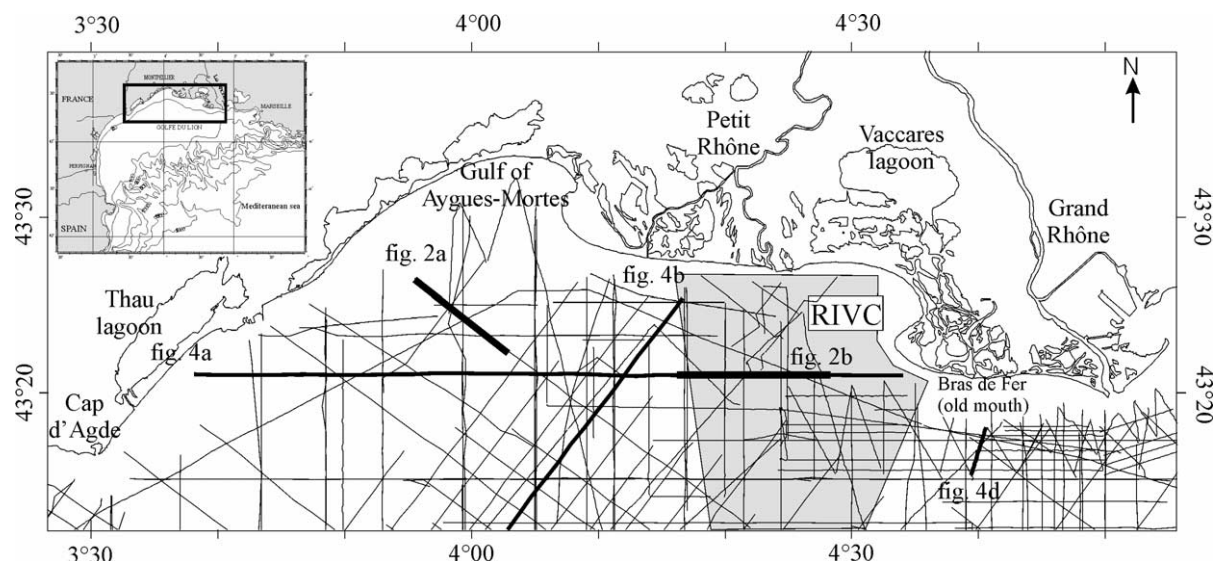


Fig. 1. Map of the northern part of the Gulf of Lion and location map of seismic sections acquired both by Ifremer and Perpignan University (GDARGO). The grey area indicates the location of the Rhône Incised Valley Complex (RIVC) which delimits the eastern from the western area.

western parts of the delta system, and to refine the interpretation of seismic units in terms of genetic factors.

2. Regional setting

The Gulf of Lions is a siliciclastic passive margin stretched between the Pyrenean and Alpine orogenic belts in the Northern part of the Western Mediterranean Basin (Fig. 1). The development of the margin was initiated by Oligocene rifting (Gueguen, 1995; Sioni, 1997) followed by oceanic opening during the Miocene (Speranza et al., 2002). The accumulation of the sedimentary wedge mainly occurred during the Plio-Quaternary period, principally controlled by glacio-eustacy (Bessis, 1986).

The Gulf of Lions is a wave-dominated area with, at the shoreline, extensive sand barriers isolating shallow lagoons (“étangs”). The Rhône sediment supply represents 80%, about 7.4×10^6 tons/yr, of the total sediment budget to the continental shelf (Pont et al., 2002) and forms a large delta system. At the coast, the southeasterly dominant wave-regime drives a south-westward longshore drift. The general oceanographic circulation is dominated by the geostrophic Liguro-Provencal current (Millot, 1994). The specific study area is bounded at the South by the $43^{\circ}15'$ parallel.

From the mid-shelf to the shelf break, Pleistocene deposits are represented by a complex of superimposed prograding wedges thickening seaward. Those wedges are interpreted as prodeltaic deposits (Aloïsi, 1986; Tesson and Allen, 1995; Rabineau et al., 1998) that accumulated during falling-stage and lowstand sea-level episodes (Tesson et al., 2000; Posamentier et al., 1992). In the central part of the study area, the Pleistocene deposits are interrupted by an important incised valley system: the Rhône Incised Valley Complex—RIVC (Fig. 1). It extends from the deltaic plain down to the Petit Rhône canyon. The RIVC formed by successive Quaternary eustatic cycles (Tesson and Allen, 1995). The stacking pattern of Pleistocene units differs between the western and eastern parts of the RIVC. In the western area, some well-developed intercalated units appear between the prograding wedges at the mid/outer shelf. They represent near-shore sand bodies that accumulated either during the periods of maximum relative sea level lowstand and/or

or during stillstands that occurred during overall sea-level rises (Berne et al., 1998; Rabineau et al., 1998; Tesson et al., 2000).

3. Data and methodology

The location map of all seismic sections used for this study is presented in Fig. 1. The database represents both the Ifremer and the University of Perpignan seismic data collected since 1990. The 5000 km seismic data comprise high resolution (HR) profiles, acquired with a mini-sparker (50 J) and a sparker (700 J). Very high resolution (VHR) seismic data were acquired with a chirp system (2–5 kHz) and a mud penetrator working at 3.5 kHz. Most of the data were digitally recorded using a Delph seismic system. Other data were recorded on analogic format, and were subsequently digitized. The navigation was based on GPS (100 m accuracy) and DGPS (about 10 m accuracy).

The following section summarizes key observations based on these data, especially on HR seismic data. The principles of seismic analysis are those described by Mitchum and Vail (1977) and Mitchum et al. (1977) who describe the key seismic facies and terminations (Fig. 2).

4. Seismic stratigraphy

The main characteristics of seismic surfaces and units are summarized in Tables 1 and 2.

4.1. Discontinuities

Nine surfaces, labeled D200 to D610 from base to top, are identified through the study area (Figs. 3 and 4). Each surface is defined as regional or local depending both on their correlation with previous works and on the correlation through the seismic database used in this study. Generally, the bounding surfaces present a flat morphology, except those located in the RIVC area. The basal discontinuity, D200, is amalgamated with D300 in the western area and is well-defined in the central and eastern areas where it overlays toplap terminations. D200 is an erosional discontinuity which is correlated down to

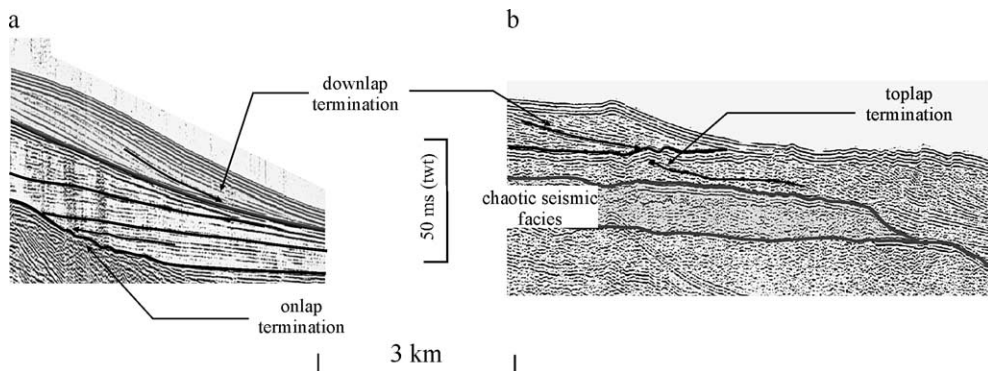


Fig. 2. Several types of seismic reflector terminations, after the terminology defined by Mitchum et al. (1977).

the shelf break by Gensous and Tesson (2003) and thus it is considered as a regional surface. D300 is defined by onlap terminations onto the RIVC to the east, and by coastal onlap onto Pleistocene deposits landward. The underlying reflectors show toplap terminations. It is an erosional and regional discontinuity amalgamated with D400 in the eastern area. D400 is a regional surface observed through the whole seismic database. It is an erosional discontinuity defined by toplap and essentially downlap terminations, and lateral sub-concordant reflectors. The surface D401 shows toplap terminations and is observed only in the north of the Gulf of Aigues-Mortes. D402 is a downlap surface restricted to the westernmost coast. D500 is an erosional and regional surface, observed through the whole seismic database. It is characterized by toplap terminations below and downlap terminations above except in the western end of the RIVC area where it is outcropping. The upper boundary surfaces, D600 and D610, are only identified in the eastern area as downlap surfaces. D601 is an erosional discontinuity characterized by toplap terminations. It

extends only in the western area. It is also a downlap surface.

4.2. Seismic units

Ten seismic units (from U200 to U610 from base to top) bounded by the above described unconformities have been identified.

Unit U200 is located in the central and eastern areas. Its maximum thickness is about 10 m (Fig. 5a). It erosionally overlies the deposits of the RIVC in the central area and the Pleistocene wedges in the eastern area. Its stratal pattern evolves from discontinuous reflectors or chaotic seismic facies in the axial part to continuous, slightly convex-upward reflectors which downlap eastward onto the underlying surface.

Unit U300 is observed in the western area from the middle shelf up to 30 m water depth. The isopach map (Fig. 5b) shows a crescent shape with a maximum thickness of about 20 m in the proximal part of the unit. Its internal structure is characterized by horizontal to sub-horizontal parallel continuous reflectors onlapping landward onto Pleistocene deposits and laterally onto U200 deposits and incised valley deposits. It is a regional seismic unit.

The prograding units U400 and U500 are superimposed or slightly backstepping. Both are regional units but they mainly developed in the western and central area where they outcrop on the inner shelf between 30 and 60 m of water depth. In the eastern area, in front of the present Rhône river mouth, U400 and U500 are relatively thin and arranged in an aggrading pattern; the presence of gas prevents seismic penetration and further observation.

Table 1
Main characteristics of seismic surfaces

Surfaces	Terminations	Type	Extent
D610	downlap	?	local
D601	toplap/downlap	erosional	local
D600	toplap/downlap	erosional	local
D500	toplap/downlap	erosional	regional
D402	downlap	?	local
D401	toplap	erosional	local
D400	toplap/downlap	erosional	regional
D300	toplap/onlap	erosional	regional
D200	toplap	erosional	regional

Table 2

Main characteristics of seismic units and named correspondence with previous works of Marsset and Bellec (2002) and Gensous and Tesson (2003)

Units	Seismic facies	Thickness	Extent	Area	Marsset and Bellec (2002)	Gensous and Tesson (2003)
U610	prograding clinoforms to sub-horizontal reflectors	up to 25 m	local	East	U8–U11	
U601	prograding sigmoids	up to 10 m	local	West		T4
U600	prograding clinoforms to sub-horizontal reflectors	up to 10 m	local	East	U8–U11	
U501	sigmoid to oblique-tangential reflectors	up to 20 m	local	West		
U500	prograding clinoforms to sub-horizontal reflectors	up to 30 m	regional	West	U7	T4
U402	oblique-tangential reflectors	up to 15 m	local			T3
U401	landward prograding clinoforms	up to 15 m	local	North-West	U6	T3
U400	prograding clinoforms to sub-horizontal reflectors	up to 30 m	regional		U5	T3
U300	sub-horizontal reflectors	up to 30 m	“regional”		U4b–U4c	
U200	chaotic to continuous reflectors	up to 10 m	local	RIVC/East	U4a	T2

Unit U400 is mainly developed in front of the Gulf of Aigues-Mortes (Fig. 5c). On cross section it appears as a lenticular to prismatic body, about 30 m thick, thinning seaward and eastward. Seismic facies pattern is oblique-tangential with high angle toplap terminations (1° to 1.5°). The distal toes of clinoforms gently downlap onto the lower boundary and merge with sub-parallel reflectors of U300. Shoreward, the inner part of U400 is erosionally overlaid by unit U401 (Fig. 5d) showing landward prograding clinoforms. In the eastern area U400 is thin (maximum 15 m) and is composed of horizontal to sub-horizontal reflectors. It rests on Pleistocene deposits or U200.

Unit U500 spreads on the inner shelf shoreward of U400. In the central area, it is a shore parallel lenticular to prismatic body (Fig. 6f), of up to 30 m thick, and presenting an offlap break. It shows seaward prograding clinoforms to sub-horizontal tangential reflectors. Towards the east, U500 prolongs under the modern delta plain; only the distal part of the

unit, composed of horizontal to sub-horizontal reflectors, is observed on the inner shelf.

Unit U402 and unit U501 are located at the westernmost part of the study area, close to Cap d'Agde (Figs. 5e and 6g). Based on correlation of seismic profiles, they are considered as lateral equivalents of U400 and U500, respectively. Unit U402 is a lenticular body (Fig. 5e), 15 m thick, with prograding oblique-tangential reflectors onlapping onto the Pleistocene deposits. They present an accentuated dip in the proximal area.

Unit U501 (Fig. 6g) is a prismatic body up to 20 m thick. Its seismic facies presents sigmoid to oblique-tangential reflectors.

Units U600 and U610 are stacked units that develop in the eastern part of the study area, in front of the Rhône delta plain (Fig. 6h). Both units are wedge shaped thinning progressively offshore and thickening landward. They show prograding oblique-tangential reflectors. Maximum observed thick-

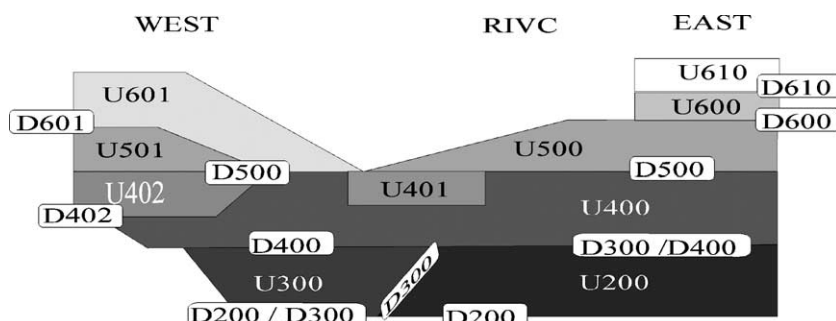


Fig. 3. Schematic stratigraphic organization of the Deglacial deposits and discontinuities in the western, RIVC and eastern parts of the study area (not scaled).

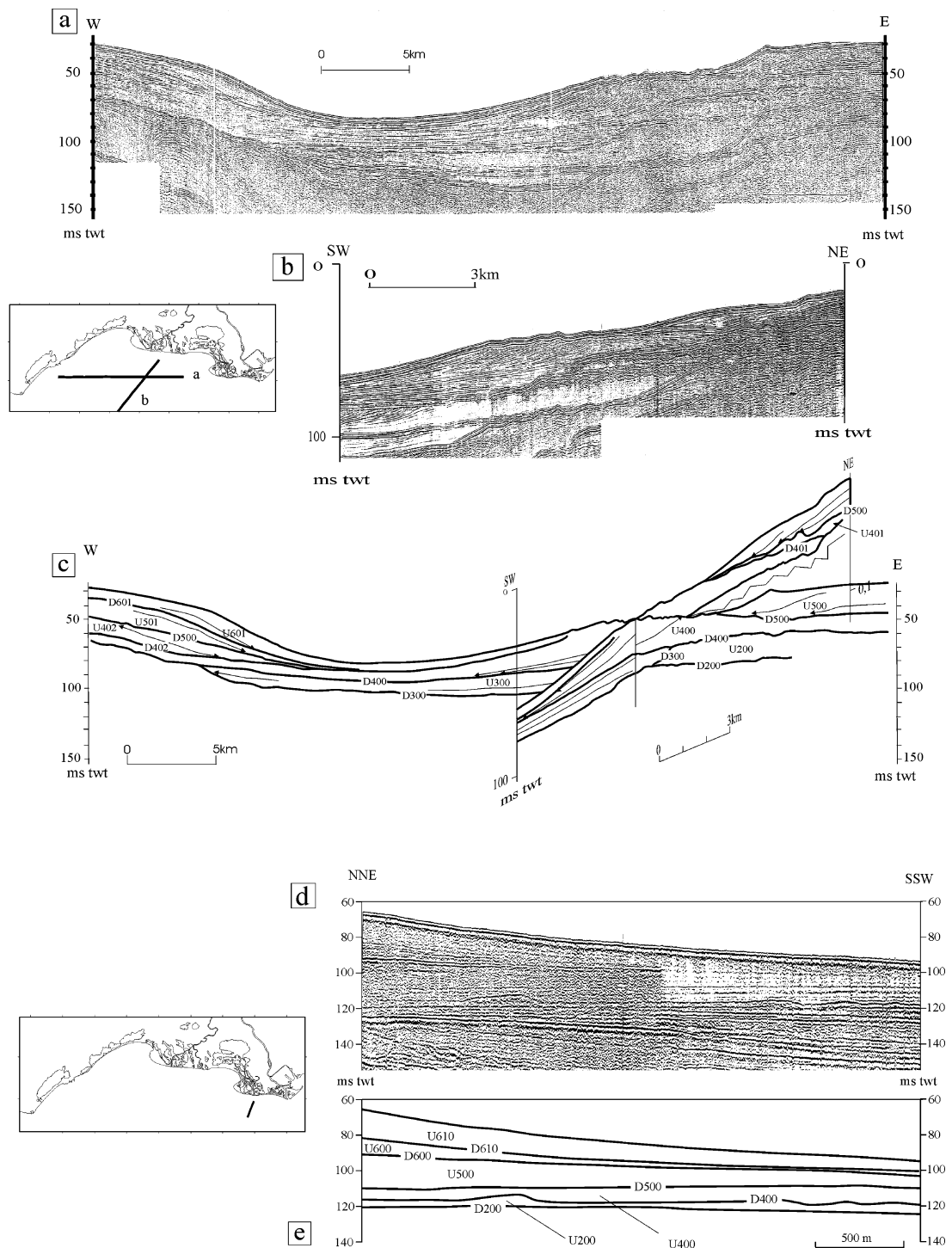


Fig. 4. Uninterpreted (a, b, d) and interpreted (c, e) seismic sections illustrating the main units and discontinuities, respectively, in the western area (a, b, c) and eastern area (d, e).

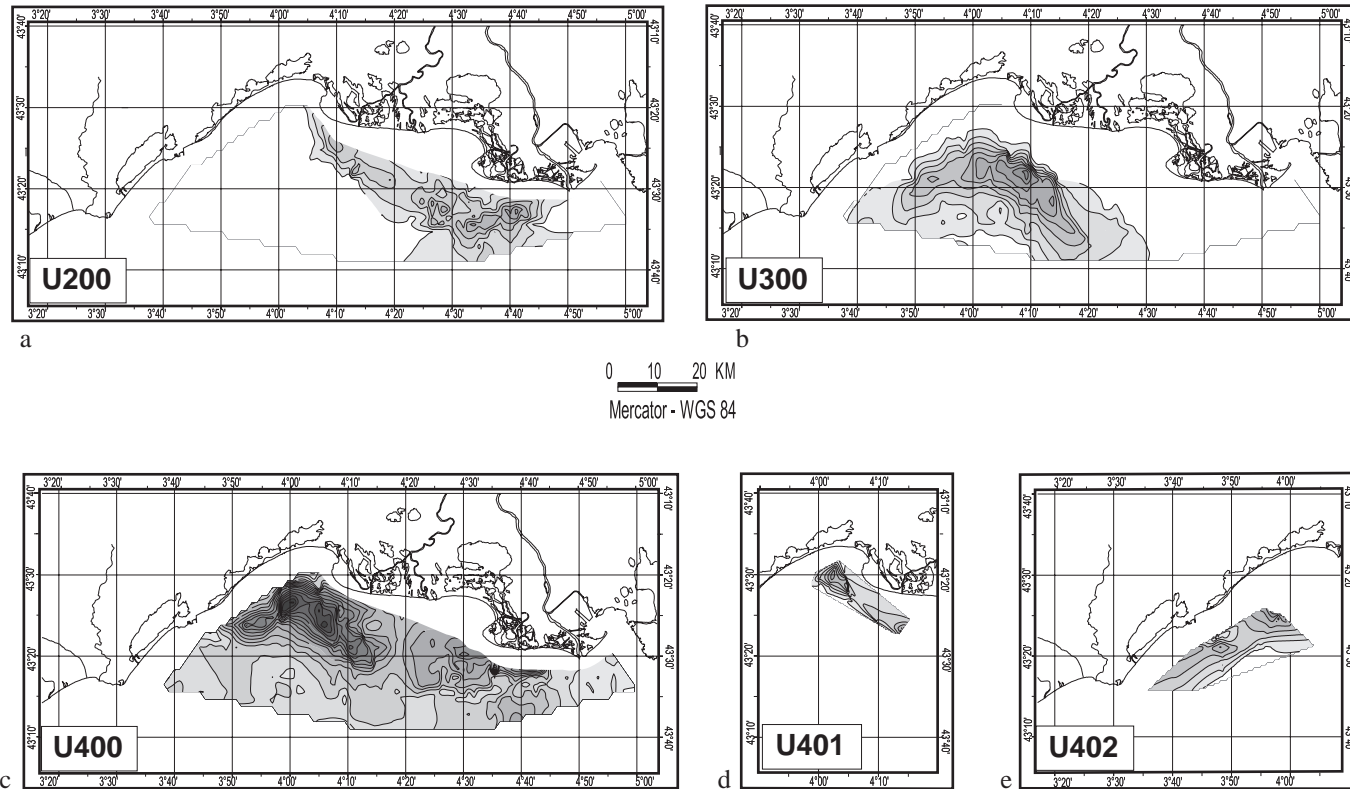
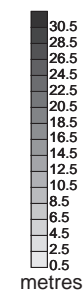


Fig. 5. Isopach maps of some of the units identified in the Rhône prodelta and adjacent shelf. The isopach maps from the basal to the fifth unit identified (from a to e) are here shown. Thickness in meters, based on an acoustic waves velocity of 1600 m/s in sediment.

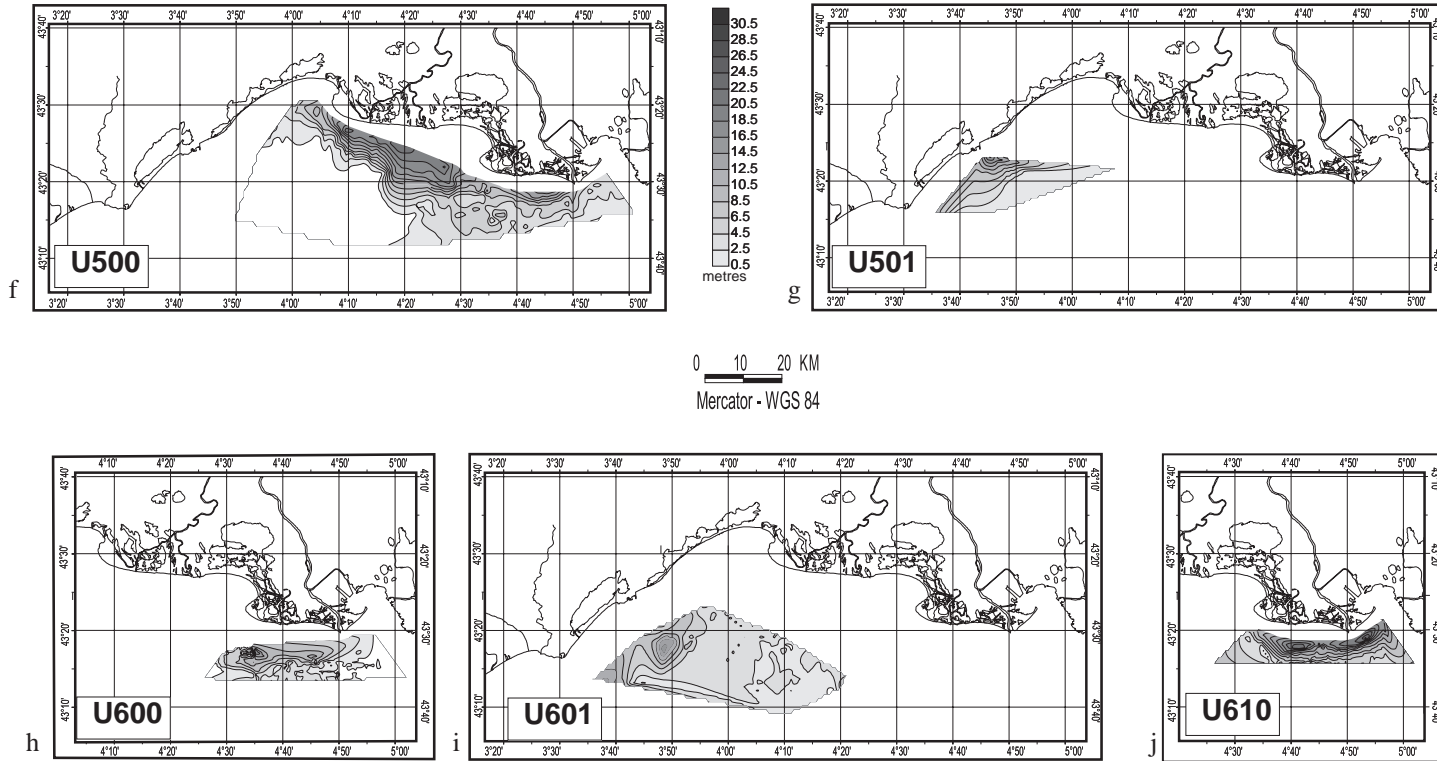


Fig. 6. Isopach maps of some of the units identified in the Rhône prodelta and adjacent shelf. The isopach maps from the sixth unit to the upper unit identified (from f to j) are here shown. Thickness in meters, based on an acoustic waves velocity of 1600 m/s in sediment.

ness is 10 m for U600 and 25 m for U610 in front of the “Grand Rhône” and “Bras de Fer” mouths.

Unit 601 is the uppermost unit in the western area (Fig. 6i). It appears as a lenticular body with a maximum thickness of 10 m. U601 shows clearly prograding sigmoids.

5. Interpretation

5.1. Stratigraphic interpretation

Two mains unconformities (Fig. 7) have been identified in terms of sequence stratigraphy (Mitchum et al., 1977).

(i) D200, which is merged with D300 in the western area, is located at the base of the Deglacial deposits. It is interpreted at once as the lowstand

erosional discontinuity (Marsset and Bellec, 2002) and as the Transgressive Surface (TS).

(ii) The unconformity D600 which separates backstepping units from aggrading/prograding units is a maximum flooding surface (mfs). In the central area, this surface is outcropping. In the western area the lateral equivalent of D600 (mfs) is represented by D601.

The other unconformities (D400, D500, D610) represent flooding surfaces.

On either side of the deltaic plain, the units rest on a Pliocene and Mesozoic substrate which has a relatively high gradient (1% to 3%). Three types of stacking pattern are observed (Fig. 7): (a) aggrading pattern in the eastern area, (b) backstepping pattern with mfs outcropping in the central area and (c) aggrading pattern with mfs outcropping in the westernmost area.

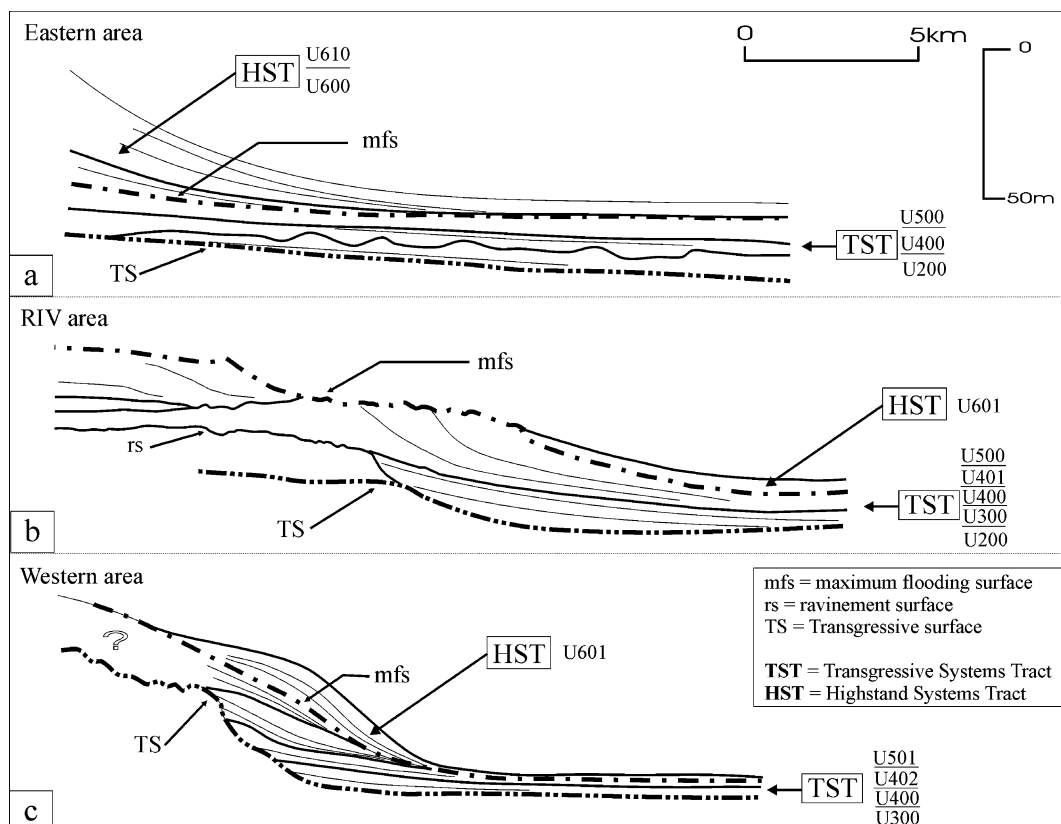


Fig. 7. Schematic patterns of the Deglacial deposits in each identified areas (a: eastern area, b: RIV area, c: western area). Location of key stratigraphic surfaces and systems tracts.

5.2. Depositional processes (environments)

The basal seismic unit, U200, built along the retreat path of the Rhône mouth across the shelf. In the central part, seismic facies indicate coarse-grained deposits probably resulting from the reworking of alluvial deposits of the RIVC (Würmian terraces). To the east, the continuous reflectors are interpreted as medium to fine grained overflow deposits.

The transgressive pattern within unit U300 suggests that this unit developed during a period of rapid landward migration of the shoreline.

The two prograding units, U400 and U500, have similar attributes to modern coastal depositional systems. The seaward prograding clinoforms are typical of a sandy coastal barrier, with lagoonal deposits possibly preserved (Fig. 5b) landward. Locally, the sudden acoustic wipe out of seismic reflections observed seaward of the coastal barrier (Fig. 5d) is attributed to the effects of shallow gas. It is commonly found in rapidly deposited sediments with a high organic content such as prodelta environments. U400 and U500 are interpreted as coastal systems resulting from the progradation of deltaic lobes which have been subsequently reworked and reshaped into coastal barriers as it can be observed in the modern Rhône delta (Oomkens, 1967). Unit U401 may represent either backbarrier deposits synchronous of the U400 coastal system, or washover deposits associated with reworking of the top of U400 during the subsequent flooding event.

Units U400 and U500 prograded during periods of decreasing rate of sea level rise and/or increased sediment supply. These units are parasequences of the Transgressive Systems Tract (TST) bounded by flooding surfaces in the sense of Van Wagoner et al. (1988); locally, the boundary of U400/U500 is a wave ravinement surface (D500). They are arranged in a backstepping pattern which reflects the transgressive character of the late Deglacial period. Because of their present bathymetric location (30 to 60 m), below storm wave base, they are not presently subject to reworking.

Units U402 and U501 are considered as the lateral equivalents to U400 and U500, respectively. Regarding their shapes and internal reflectors, they are compared to ancestral “subaqueous deltas” in the sense of Cattaneo et al. (2003). They would have formed under the effect of westward littoral drift and regional cir-

culation, considered similar to the present-day oceanographic regime.

Units U600 and U610 constitute prodeltaic lobes. They correlate onshore with deposits of the upper part of the delta plain. They prograded onto the late transgressive deposits (U400 and U500) and they are interpreted as sedimentary bodies of the Highstand Systems Tract. Their lower boundary (D600) is the maximum flooding surface (mfs). Recent studies on the Rhône delta plain (Vella, 2002) show that at least two major Highstand delta complexes prograded during the last 4000 yr. The first one (Saint Ferreol complex) prograded between 4000 and 2000 yr BP in the western part of the Rhône delta plain, in front of units U400 and U500. The most recent system (Vieux Rhône complex) prograded since 2000 yr BP in the eastern part of the delta plain and correlates seaward with units U600 and U610. The upper prodeltaic lobe, U610, shows two depocentres. The first depocentre is correlated with the “Bras de Fer” deltaic lobe and the second depocentre with the presently active lobe (Roustant lobe).

Unit U601 is also interpreted as a modern “subaqueous delta” in the sense of Cattaneo et al. (2003) because there is no direct sediment supply source in the vicinity. The Rhône would therefore be the main sediment source of U601, sediment being transported by a southwestward current generated by the Liguro-Provencal current.

6. Discussion

6.1. Glacio-eustacy

Given the short time-span represented by the Deglacial deposits, and the moderate effect of tectonic subsidence in the area (Bessis, 1986) we consider that the main controlling factor on stratal architecture is related to glacio-eustatic sea-level changes. Nevertheless other controlling factors, especially sediment supply, ocean dynamics and the pre-existing morphology may have had an effect on the stacking pattern of the prodeltaic units.

It is now well-known that the last Deglacial sea level rise was not continuous and regular but was punctuated by steps (Fairbanks, 1989; Bard et al., 1993; Bard et al., 1996). In Lambeck and Bard

(2000), two sea-level variation models are presented. The first model represents a predicted relative sea-level curve which shows a regular relative sea-level rise along the French Mediterranean coast. The second model presents a corrected relative sea-level curve based on field observations and shows increased and decreased rate of relative sea-level rise.

On the Rhône shelf, the good correlation between the bathymetry of the upper boundaries of the transgressive units and the Deglacial sea-level curve suggests that glacio-eustatic changes are the main controlling factor.

6.2. Deglacial development

Unit U200, located along the axis of the paleo-Rhône, is observed all over the shelf (Gensous and Tesson, 2003), representing the retreating path of the Rhône delta.

Unit U300 built up during a period of rapid migration of the shoreline from outer to inner shelf (from -90 m to -70 m). We correlate it with the meltwater pulse 1A (MWP-1A) that started at around 14,200 yr Cal. BP and occurred during 500 yr (Fig. 8). Moreover, the low gradient of the middle shelf, inherited from the previous lowstand period, favored the rapid landward shift of the shoreline, when the rate of eustatic sea-level rise increased dramatically.

Units U400 and U500 prograded during periods of slowing down of eustatic rise. Age dating from cores cutting across U400 gives 9860 yr ^{14}C BP/11,300 yr Cal. BP (Aloisi et al., 1975) and $10,475 \pm 40$ yr ^{14}C BP/12,600 yr Cal. BP (Berne et al., 2003). From these data, it is assumed that U400 built up during the Younger Dryas after MWP 1A. Similarly, it would be proposed that U500 prograded during the period of decreased rate of sea-level rise that occurred after MWP 1B. However, the importance of this second meltwater pulse (MWP-1B) is controversial (Bard et al., 1996), and it is not absolutely certain that the backstepping pattern between U400/U500 is related to a changing rate of sea-level rise. Another possibility is that the progradation of U500 would be related to climatically induced increase in river supply.

Units U600 and U610 have prograded onto the late transgressive deposits since the period of reduced rate of sea-level rise at the end of the Holocene. A previous study of sea-level changes during the Highstand

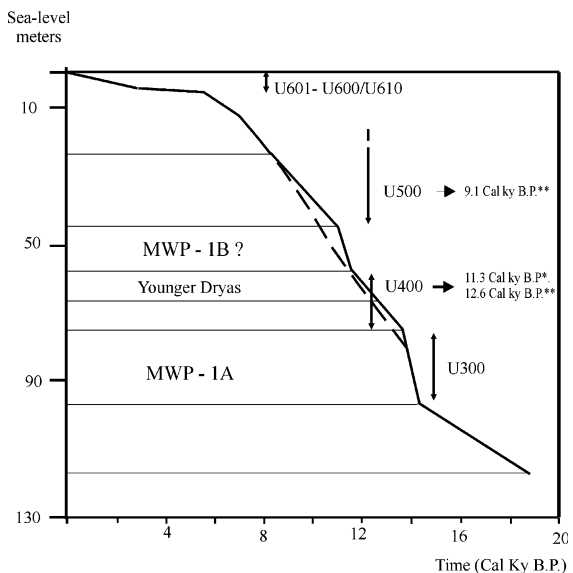


Fig. 8. Relation between glacio-eustacy and Deglacial units. Eustatic curves from Bard et al. (1996), showing the alternating period of increase and decrease rates of sea-level rise. MWP-1A and MWP-1B: brief periods of accelerated melting (i.e., meltwater pulse) of the continental ice and increase of sea-level rise. The continuous line presents the two MWP events whereas the dashed line presents a single MWP. YD: periods corresponding to the Younger Dryas cold period. *Age dating from Berne et al. (2003) corresponding to the unit U400, **age dating from Aloisi et al. (1975) corresponding to the units U500 and U400.

period that occurred in the delta plain (Vella and Provansal, 2000) indicates two periods of rapid sea-level rise. The first occurred between 6295 and 4585 yr ^{14}C BP (about 2 mm/yr) and the second, between 2120 and 1200 yr ^{14}C BP (1.9 mm yr). These periods were separated by a period of stability between 4085 and 2260 yr ^{14}C BP during which the Saint Ferréol lobe prograded in the western part of the delta plain. From studies carried out on the delta (Vella, 2002), the two depocentres of Unit 610 are correlated with the “Bras de Fer” delta lobe that prograded during the 17th and 18th Century (that is the Little Ice Age period) during a period of enhanced sediment supply and the presently active “lobe de Roustang”, that was artificially channelled at the end of the 19th century.

6.3. Other controlling factors

In the western area, units U402, U501 and U601 represent subaqueous deltas. In this work, they are

considered as time correlative (synchronous) of units U400, U500 and U600/U610, respectively.

The development of a large prograding body rather than a subaqueous delta is correlated to the hydrodynamic conditions and to the variation in sediment supply. In front of the Rhône mouth the sediment discharge was sufficient to build up an important prograding deltaic depositional system with continuity between the deposits of the delta plain, delta front and prodelta. Westward to the Rhône mouth the sediment supply decreased. Nevertheless the general oceanographic circulation could lead to a westward transport of suspended sediment of the Rhône which enabled to build up a prograding body, the relict subaqueous delta which is disconnected from the modern coastal barrier.

In the central part, off the deltaic plain, the shelf has a low gradient (0.1% to 0.5%) inherited from the deltaic plain environment of the previous lowstand period (and similar to the gradient of the Rhône river of the modern delta plain). This inherited topography favored the rapid landward migration of the shoreline during a phase of accelerated sea-level rise and the drowning of parasequences that are arranged in a retrogradational pattern (Fig. 7b).

7. Conclusions

From the synthesis of existing seismic data, a succession of 10 units separated by flooding surfaces have been observed on the Rhône delta shelf. The first seven are associated to the Transgressive Systems Tract and the last three are associated to the Highstand Systems Tract (HST).

From base to top the TST is composed of (i) reworking deposits of Würmian terraces due to the first step of the Deglacial transgression, (ii) transgressive deposits due to the rapid sea-level rise and landward migration of the shoreline and (iii) two backstepping coastal systems. The first coastal system is due to a decrease in the rate of sea-level rise associated to the Younger Dryas event. The second coastal system is due to a decrease in the rate of the sea-level rise or to an important increase in the rate of sediment supply associated to a constant rate of sea-level rise.

The HST is composed of prograding delta lobes in the eastern area and subaqueous delta in the western area. The prograding delta lobes are due to minor sea-

level variations during a stillstand sea-level, or, more probably, to lobe switching that could be linked to rapid climatic changes. The subaqueous delta is mainly fed by sediment supply reworked through the hydrodynamic circulation.

Glacio-eustacy seems to be the main factor controlling the overall stratigraphic organization of units. Good correlation exists between the shape of the global sea-level curve and the position of the units. Moreover, lateral variability observed within the Rhône sedimentary units would result from the ratio between the rate of sea-level rise and fluvial sediment supply, the location of the sediment input and differing slope gradients.

Without a detailed chronostratigraphic framework, it is difficult to disentangle effects from global (eustatic) changes and those due to local (climatic) changes. However, this study provides the first comprehensive view of the stratigraphic architecture of the Rhône prodelta, and provides the framework for future detailed sedimentological and paleoenvironmental studies.

Acknowledgments

This project was carried out within the Eurodelta Concerted Action funded by the European Community (Contract EVK3-CT-2001-20001).

The seismic data acquisition was supported by the French INSU-CNRS and Ifremer. Additional support came from the French “margins” program (GDR MArges). A regional grant supported by the Languedoc-Roussillon Region was attributed to C. L.

References

- Aloïsi, J.C., 1986. Sur un modèle de sédimentologie deltaïque. Contribution à la connaissance des marges passives. Thèse d'état, Université de Perpignan. 161 pp.
- Aloisi, J.C., Monaco, A., Thommeret, J., Thommeret, Y., 1975. Évolution paléogéographique du plateau continental languedocien dans le cadre du golfe du Lion. Analyse comparée des données sismiques, sédimentologiques et radiométriques concernant le Quaternaire récent. Rev. Géogr. Phys. Géol. Dyn. XXXII (1), 13–22.
- Bard, E., Arnold, M., Fairbanks, R.G., Hamelin, B., 1993. ^{230}Th – ^{234}U ^{14}C ages obtained from mass spectrometry on corals. Radiocarbon 35, 191–199.

- Bard, E., Hamelin, B., Arnold, M., Montaggioni, L., Cabioch, G., Faure, G., Rougerie, F., 1996. Deglacial sea-level record from Tahiti corals and the timing of global meltwater discharge. *Nature* 382, 241–244.
- Berne, S., Lericolais, G., Marsset, T., Bourillet, J.F., De Batist, M., 1998. Erosional offshore sand ridges and lowstand shorefaces: examples from tide and wave dominated environments of France. *J. Sediment. Res.* 69 (4), 540–555.
- Berne, S., Baton, J.M., Delpeint, A., Dennielou, B., Duval, F., Field, M., Lericolais, G., Le Roux, E., Satra, C., Taviani, C., 2003. Deglacial history of the Rhône prodelta form detailed morphology and preliminary stratigraphic data. ComDelta: Open conference on Comparing Mediterranean and Black Sea Prodeltas. Aix-en-Provence, France, 26–28 October 2003.
- Bessis, F., 1986. Some remarks on the study of subsidence of sedimentary basins. Application to the Gulf of Lions margin. *Mar. Pet. Geol.* 3, 37–63.
- Cattaneo, A., Correggiari, A., Langone, L., Trincardi, F., 2003. The late-Holocene Gargano subaqueous delta, Adriatic shelf: sediment pathways and supply fluctuations. *Mar. Geol.* 193 (1–2), 61–91.
- Gensous, B., Tesson, M., 1997. Les dépôts postglaciaires de la plate-forme rhodanienne: organisation stratigraphique et conditions de mise en place. *C. R. Acad. Sci., Paris II* (317), 803–810.
- Gensous, B., Tesson, M., 2003. L'analyses des dépôts postglaciaires et son application à l'étude des séquences de dépôt du Quaternaire terminal sur la plate-forme au large du Rhône (Golfe du Lion). *Bull. Soc. Géol. Fr.* 174, 401–419.
- Gueguen, E., 1995. La Méditerranée Occidentale: un véritable océan. Exemple de segmentation des marges et de hiatus cinématiques. Implications sur les processus d'amincissement crustal. Thèse de doctorat, Université de Bretagne Occidentale.
- Fairbanks, R.G., 1989. A 17000-year glacio-eustatic sea level record: influence of glacial melting rates on the Younger Dryas event and deep-ocean circulation. *Nature* 342 (6250), 637–642.
- Lambeck, K., Bard, E., 2000. Sea-level change along the French Mediterranean coast for the past 30000 years. *Earth Planet. Sci. Lett.* 175 (3–4), 203–222.
- Marsset, T., Belloc, V., 2002. Late-Pleistocene–Holocene deposits of the Rhône inner continental shelf (France): detailed mapping and correlation with previous continental and marine studies. *Sedimentology* 49, 255–276.
- Millot, C., 1994. Models and data: a synergetic approach in the Western Mediterranean sea. In: Malanotte-Rizzoli, P. (Ed.), *Ocean Processes in Climate Dynamics: Global and Mediterranean Examples*. Kluwer Academic Publishers, pp. 407–425.
- Mitchum, J.R., Vail, P.R., 1977. Seismic stratigraphy and global changes of sea level: Part 7. Seismic stratigraphy interpretation procedure. In: Payton, C.E. (Ed.), *Seismic Stratigraphy—Applications to Hydrocarbon Exploration*, 26, Mem. AAPG, pp. 135–143.
- Mitchum, J.R., Vail, P.R., Sangree, J.B., 1977. Seismic stratigraphy and global changes of sea level, part: stratigraphic interpretation of seismic reflection patterns in depositional sequences. In: Payton, C.E. (Ed.), *Seismic Stratigraphy—Applications to Hydrocarbon Exploration* (Ed. Payton, C.E.), 26, Mem. AAPG, pp. 117–133.
- Oomkens, E., 1967. Depositional sequences and sand distribution in a deltaic complex. *Geol. Mijnb.* 46, 265–278.
- Pont, D., Simonnet, J.-P., Walter, A.V., 2002. Medium-term changes in suspended sediment delivery to the ocean: consequences of catchment heterogeneity and river management (Rhône River, France). *Estuar. Coast. Shelf Sci.* 54 (1), 1–18.
- Posamentier, H., Allen, G., James, D.P., Tesson, M., 1992. Forced regressions in a sequence stratigraphic framework: concepts, examples, and exploration significance. *AAPG Bull.* 76, 1687–1709.
- Rabineau, M., Berne, S., Ledrezen, E., Lericolais, G., Marsset, T., Rotunno, M., 1998. 3D architecture of lowstand and transgressive Quaternary sand bodies on the outer shelf of the Gulf of Lion, France. *Mar. Pet. Geol.* 15 (5), 439–452.
- Sioni, S., 1997. Mer Ionienne et Apulie depuis l'ouverture de l'Océan Alpin. Thèse de Doctorat, Univ. Bretagne Occidentale.
- Speranza, F., Villa, I.M., Sagnotti, L., Florido, F., Cosentino, D., Cipollari, P., Matei, M., 2002. Age of the Corsica-Sardinia rotation and Liguro-Provencal Basin spreading: new paleomagnetic and Ar/Ar evidence. *Tectonophysics* 347, 231–251.
- Tesson, M., Allen, G., 1995. Contrôle tectonique et eustatique haute-fréquence de l'architecture et de la stratigraphie de dépôts de plate-forme péricatonique. Exemple du Golfe du Lion (Méditerranée, France) et des dépôts quaternaires. *C. R. Acad. Sci., Paris IIa* (320), 39–46.
- Tesson, M., Posamentier, H., Gensous, B., 2000. Stratigraphic organization of the Late Pleistocene deposits of the western part of the Golfe du Lion shelf (Languedoc shelf), western Mediterranean Sea, using high resolution seismic and core data. *AAPG Bull.* 84 (1), 119–150.
- Trincardi, F., 2003. The impact of short term supply fluctuations on margin shaping over the last 20,000 years. Ocean Margin Research Conference, Paris 15th–17th September 2003.
- Van wagoner, J.C., Posamentier, H.W., Mitchum Jr., R.M., Vail, P.R., Sarg, J.F., Loutit, T.S., Hardenbol, J., 1988. An overview of the fundamentals of Sequence Stratigraphy and key definitions. In: Wilgus, C.K., Hastings, B.S., Kendall, C.G.St.C., Posamentier, H., Ross, C.A., Van Wagoner, J. (Eds.), *Sea Level Changes—An integrated approach*. SEPM Special Publication, vol. 42, pp. 39–46.
- Vella, C., 2002. Edification pulsée d'un appareil prodeltaïque progradant: le lobe de St. Ferréol, delta du Rhône. Colloque général du GDR marges, Reuil Malmaison.
- Vella, C., Provansal, M., 2000. Relative sea-level rise and neotectonic event during the last 6500 yr on the southern eastern Rhône delta. *Mar. Geol.* 170, 27–39.



ELSEVIER

Marine Geology 222–223 (2005) 313–334

**MARINE
GEOLOGY**
INTERNATIONAL JOURNAL OF MARINE
GEOLOGY, GEOCHEMISTRY AND GEOPHYSICS

www.elsevier.com/locate/margeo

Small rivers contribution to the Quaternary evolution of a Mediterranean littoral system: The western gulf of Lion, France

Michel Tesson ^{*}, Caroline Labaune, Bernard Gensous

BDSI, Biophysique et Dynamique des Systèmes Intégrés, Perpignan University, 52, Av. Paul Alduy, 66 860 Perpignan, France

Accepted 15 June 2005

Abstract

Along the Mediterranean coasts and the Atlantic French coast, former and actual research programs focused on major river systems, estuaries and deltas, characterized by a last Glacial relative sea level lowstand and incision and a well developed sedimentary incised valley infilling deposited during the following sea level rise and highstand. This paper presents the preliminary results of a program focused on a particular area of the Gulf of Lion coast with a thin sedimentary cover over the substratum and only minor rivers with non-apparent and important sedimentary contribution during the Late Quaternary. The results show that in this area the best Pliocene to Actual sedimentary record is preserved. The paper rests on the analysis of an extensive database of recent high resolution and very high resolution seismic reflection lines and previously published core data. Seismic data show that a major complex of paleovalleys connected with the Orb, Aude and Agly rivers is preserved on the inner shelf and adjacent coastal plain. On the inner shelf, the separated incised valleys merged in a unique broad and shoreparallel incision dipping southward. At the southward extremity, the incision turns eastward and seaward. The basal surface of this incision extends seawards under six to seven Late Quaternary depositional sequences preserved on the mid and outer shelf. The infilling of the complex of paleovalleys is characterized by aggrading deposits attributed to periods of relative sea level rise (transgressive systems tracts), organized into several subunits bounded by internal discontinuities locally deeply incising. The discontinuities are amalgamated surfaces, including successive sequence boundaries (indicative of phases of relative sea level falls) merged with transgressive surfaces (indistinct tidal and wave ravinement surfaces). The subunits are the part of Late Quaternary depositional sequences preserved in estuarine environments. They are the lateral equivalents of landward fluvial terraces and seaward coastal and prodeltaic deposits on the shelf. Using borehole dataset, the underlying and eroded deposits below the basal unconformity are correlated with Pliocene deposits outcropping landward in the hinterland. The top of the incised valleys complex is capped by the last Glacial lowstand surface of erosion (18 ky B.P.) reworked by the postglacial transgressive surface (TS), dissociated near the shoreline into a tidal and a wave ravinement surfaces. Above the TS, the very high resolution (VHR) seismic data in the lagoons, the tidal channels and cores, reveal in details the stratigraphic architecture of the deposits. At the base, a small wedge constitutes the postglacial transgressive systems tract (TST) locally thinning in the areas distant of the sediment point sources. The TST is capped by a flat surface of wave reworking (maximum flooding surface or mfs) prolongating under the Leucate lagoon and merging offshore at the seafloor. Boreholes and VHR seismic lines through the coastal barrier and in the lagoon show that the shoreline probably migrated far landward at the end of the transgression. When

^{*} Corresponding author.

E-mail address: tesson@univ-perp.fr (M. Tesson).

the rate of sea level rise decreased strongly, the shoreline migrated seaward and prograding and aggrading sandy material, with landward muddy lateral equivalent facies, deposited early highstand systems tract (HST) above the MFS. Offshore, fine material deposited as a sigmoidal blanket of mud originating in part from the north-east and Rhône river under oceanic circulation (equivalent to a subaqueous prodelta). Subsequently, the modern beach barrier built up by wave reworking of the early HST. This new study of the western part of the Gulf of Lion inner shelf and littoral illustrates an incised valley complex and thus presents the best preserved example of the sedimentary record of the effects of the relative sea level changes during the Pliocene to Actual period. For the first time, the land to sea transition is preserved and the Late Quaternary depositional sequences are in a great part observed. The last post Glacial deposits present a simplified but very different organisation compared to a record front of the adjacent Rhône river. Consequently a synthesis is now possible.

© 2005 Published by Elsevier B.V.

Keywords: incised valley fill; Late-Quaternary; land/sea correlation; high resolution seismic

1. Introduction

Relative sea level changes, among others factors, control the deposition and architecture of onshore coastal plain and adjacent shelf deposits respectively organized into terraces and marine depositional sequences. In the Gulf of Lion margin as everywhere, marine and continental systems have been initially studied separately (Boyer et al., 2003a,b; Duvail and Le Strat, 2002; Lobo-Sánchez, 2000; Posamentier et al., 1992; Rabineau et al., 1998; Tesson et al., 1990, 1993, 2000; Tesson, 1996). Correlation between continental and marine systems have been achieved for Upper Miocene and Pliocene deposits (Duvail and Le Strat, 2002; Lofi et al., 2003) from industrial and Ecors (French CNRS national program studying the mantel/crust structure) seismic data. However regarding the high frequency glacio-eustatic cycles of the Upper Quaternary, the connections between marine and continental studies in the present day coastal zone are not yet established because of: 1 — the difficulty to use seismic devices in shallow waters (presence of multiples, critical choices between resolution and penetration); 2 — the sedimentary cover above Pliocene substrate is thin and the occurrence of numerous amalgamated surfaces reduces the thickness of the sedimentary units below the seismic resolution; and 3 — outcropping pebbly deposits induce an acoustic diffraction.

In this study, we tentatively correlate marine and continental Quaternary deposits along an incised valley complex that has deeply carved the Pliocene substrate. The infilling deposits of these incised valleys are assumed to have been better preserved than the deposits between the incised valleys. In the marine area, we

implemented various high resolution (HR) and very high resolution (VHR) seismic tools which are well suited for studies in shallow water environments (Labaune et al., 2003d). Onland, studies were carried out in collaboration with the “Bureau de la Recherche Géologique et Minière” (BRGM) which provided cores data from the national subsurface data bank (BDSS).

The Rhône postglacial deposits of the delta plain and prodelta rest directly on a thick level of coarse alluvial deposits which probably represent the remnants of the Quaternary transgressive-regressive cycles. Thus we concentrated our study on the Langue-doc-Roussillon coastal system (Fig. 1) and the incised valleys (Hérault, Orb, Aude and Agly) and their landward extension buried under coastal plains. Preliminary results (Tesson et al., 2003) show evidences of a broad incised valley complex due to the merging of these rivers in the offshore area (Fig. 2) and presenting two branches: 1 — a “north” branch, oriented from north to south and shore parallel from Cap d’Agde to Cap Leucate; 2 — a “south” branch, shore transverse from west to east, and overlain by the Leucate lagoon and coastal plain. Direct relationships between the depositional sequences on the continental platform and the coastal plain deposit architecture are well exposed. In this paper we shall focus on the part linked to the Agly river.

2. Regional setting

2.1. Morphology

The coastline between the Rhône delta to the east and the Pyrenean mountains to the west is crescent

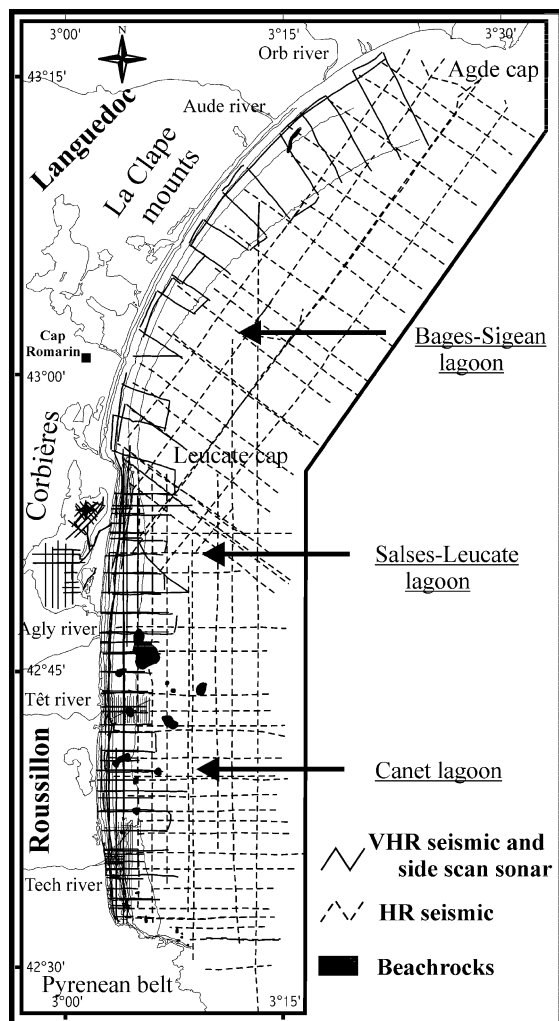


Fig. 1. Map of the Western part of the Gulf of Lion, south of France (Northwestern Mediterranean Sea) showing the study area and the acoustic survey tracklines (extract from the ARGO database). VHR seismic=very high resolution seismic; HR seismic=high resolution seismic.

shaped. It presents extensive beach barriers isolating backbarrier lagoons or “étangs” (from North to South: Bages-Sigean, Salses-Leucate and Canet “étangs”). The beach barrier continuity is interrupted by rocky caps (Agde, Leucate) and fluvial mouths (Hérault, Orb, Aude, Agly, Tech, Têt). In the southern part of the study area, the Roussillon coastal plain develops between the Pyrenean mountains to the south and the Mesozoic limestone of the “Corbières” to the north. To the north of Cap Leu-

cate, Mesozoic and Cenozoic limestones prolongate near the shoreline (Massif de la Clape) delimiting several minor coastal plains.

2.2. Geology

The construction of the Rhône passive margin was initiated in Upper Oligocene to Lower Miocene times during a phase of rifting, followed by an oceanic spreading (Gorini, 1993; Guennoc et al., 2000). From the Lower/Mid Miocene, the interaction between the post-rift subsidence and the high sedimentary supply from the Rhône hinterland led to the accumulation of a thick wedge of clastic sediments which seals the rift structure.

The constructional process of the shelf was interrupted at the end of Miocene (Messinian) when the Mediterranean Basin was isolated from the Atlantic ocean. Sea level dropped drastically and the margin was deeply eroded by valley incision. Subsequently, at the beginning of the Lower Pliocene, the margin was flooded and the valleys became rias.

Later during the Pliocene, the rias were filled by the progradation of Gilbert type deltas (Clauzon et al., 1987; Lofi et al., 2003), presently outcropping in the upstream part of the Roussillon coastal plain (Fig. 3a). These deposits prolongate under the actual shelf where they have been identified (Lofi et al., 2003; Duvail and Le Strat, 2002). They were incised during Quaternary eustatic changes and present an irregular upper boundary under the Roussillon coastal plain (Fig. 3b), seaward dipping under Quaternary deposits of the shelf. The last synthesis of BRGM core database (Duvail et al. 2001) describes two east–west oriented major incisions (50 m b.p.s.l.) under the Canet and Salses–Leucate lagoons. Under the Canet lagoon, the incision is bounded seaward by a Pliocene topographic high (5 m b.p.s.l.) (Martin et al., 1981). Under the Salses Leucate lagoon, the precise location and depth of the Pliocene upper boundary is now reinterpreted by our both teams. In the coastal plain out of the lagoons, the Pliocene upper boundary is sub-outcropping. Due to this erosion, the Upper Pliocene would be missing.

The continental Quaternary deposits in the river valleys are preserved and form imbricated terraces due to the interaction of base level drops during the Late-Quaternary sea level cycles and tectonic (uplift). The

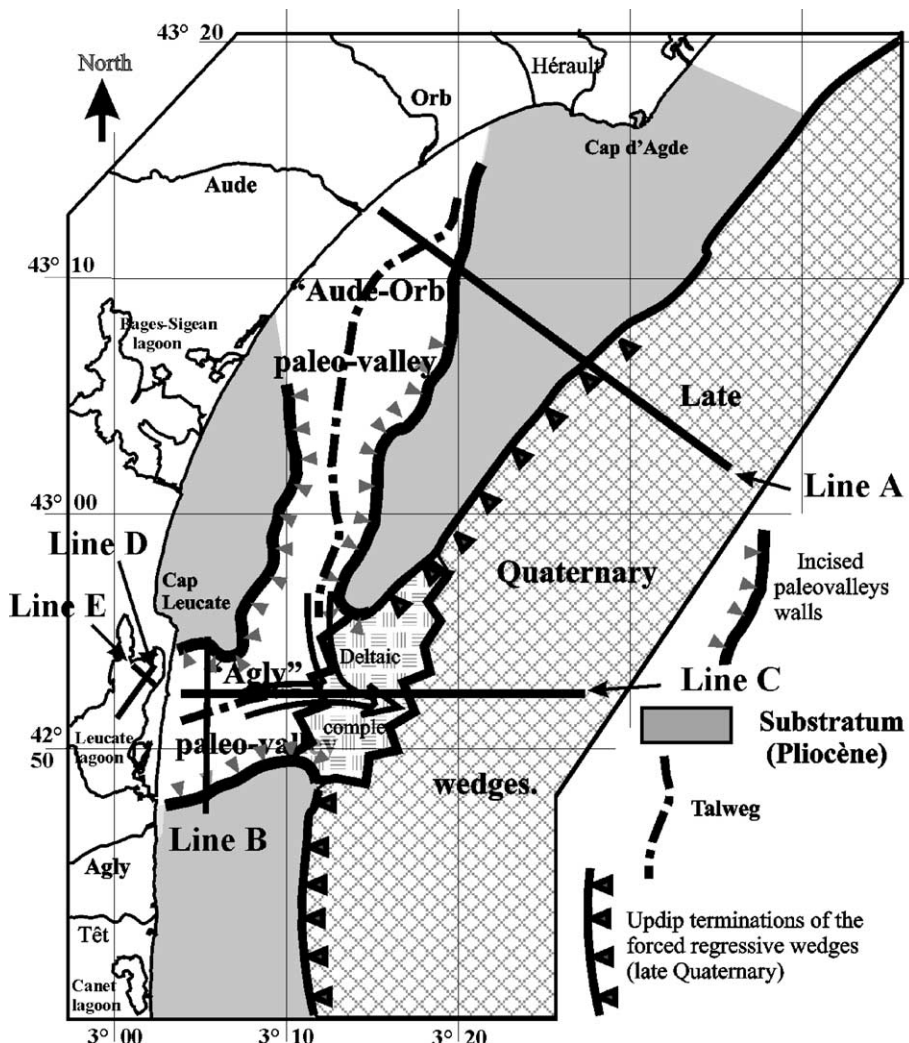


Fig. 2. The Languedoc-Roussillon paleovalley complex incised in the Pliocene of the Gulf of Lion. There is no direct relationship between the incised valley complex and the present Hérault river in the north. Location of the seismic examples used in Figs. 4–8 is indicated.

different terrace surfaces merge in the coastal plain, near the modern littoral (Duvail et al., 2001). Mixed continental/marine deposits are described in the two incisions under the Canet and Salses-Leucate lagoons. Their precise facies and age dating are discussed below.

Under the Canet lagoon, the deposits filling the Pliocene incision consist of marine sands dated of 4–5 ky BP age, overlain by marine clays and beach barrier sands of less than 2 ky BP old. The top of the sandy deposits is located at 10-m b.p.s.l. (Martin et al., 1981). In the northern part of the Leucate lagoon,

a short core shows a lower level of red sands (from 13.80 to 2.80 m) dated 8.2 ky BP but this value was considered as not valuable (Martin, 1978). At the base of the 0.60 m uppermost lagoonal clays, a shelly layer has been dated to be 2.1 ky BP. At the North of Cap Leucate (Cap Romarin area, location Fig. 1), drilling data across the coastal plain show (Fig. 4) a sandy prograding unit with a base at about 20 m b.p.s.l., developed between a cliff of Cenozoic rocks and the present shoreline 1 km eastward. It deposited since 4–6 ky BP (Aloisi et al., 1978).

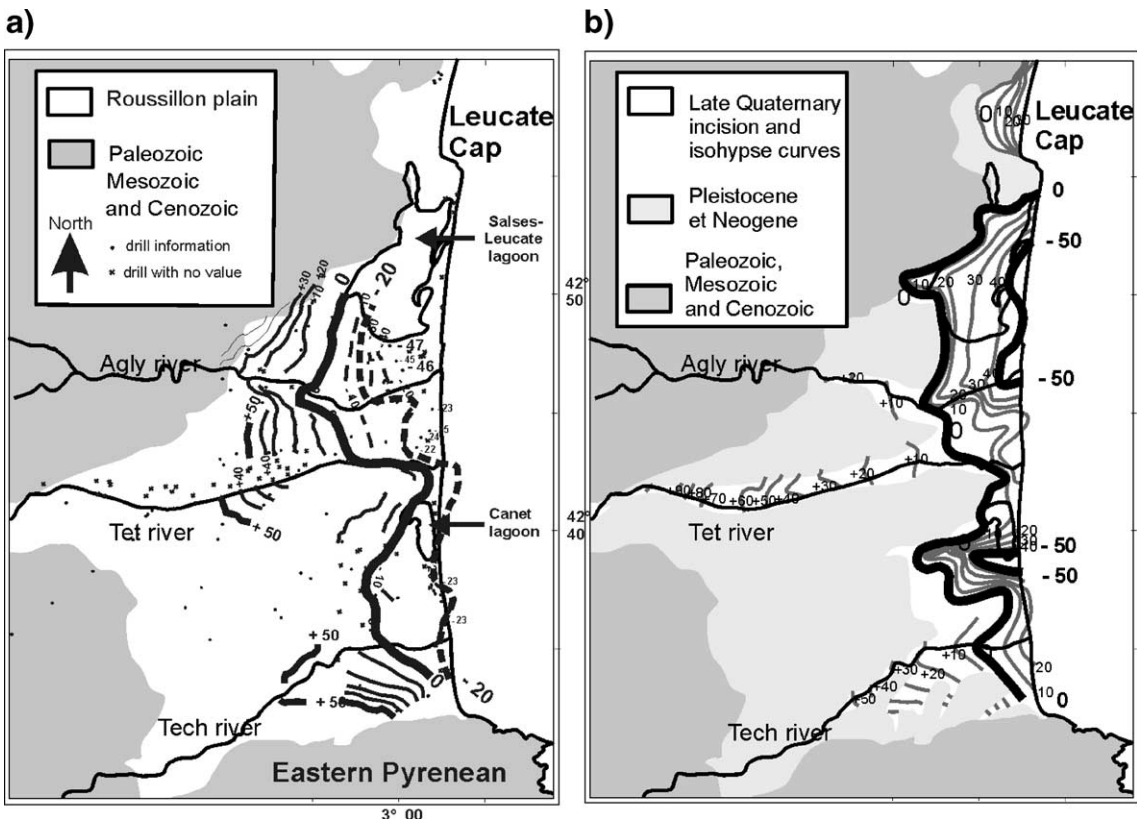


Fig. 3. The Pliocene upper boundary map (a) shows that the Pliocene is mainly seaward dipping north of the Têt river and under the Salses–Leucate lagoon. Map (b) shows the two main Quaternary incisions at the top of the Pliocene deposits, under the Salses–Leucate and Canet lagoons. Near the shoreline, the Pliocene deposits are globally at 50 and 20 m, respectively below sea level surface in these two areas. The best preservation of Quaternary deposits in the nearshore domain is expected in the Salses–Leucate area as confirmed by offshore seismic data. Modified from Duvail et al., 2001.

2.3. Quaternary stratigraphy of the mid/outer shelf

The deposits are organized into depositional sequences assumed to be of Late Quaternary age. The boundary between Early and Late Quaternary is not well known. The sequences are stacked in an aggrading pattern and form a major sedimentary complex wedge (Fig. 5) referred to as “Pleistocene wedge”. This wedge is thickening seaward (Tesson et al., 1990, 1993). Its shape has been explained by a synsedimentary differential subsidence (Tesson and Allen, 1995). It pinches landward at the middle shelf (Fig. 2) onto a substrate showing seaward dipping and/or folded reflectors with high amplitude. The upper boundary of the wedge is an erosional and polygenic surface located at the sea floor or overlain

by postglacial deposits. Due to the seaward dipping architecture, the more recent sequences are located at the outer shelf, the older sequences are observed at the inner-shelf where they may outcrop. The upper polygenic surface developed during the last relative sea-level fall and lowstand (18 ky BP) and was reworked during the postglacial sea level rise and transgression. In the nearshore area northward of this study area, the postglacial deposits (Gensous and Tesson, 2003) form a sedimentary body comprising the retrograding part of the transgressive systems tract or TST (sometimes unobserved or reduced) bounded by the maximum flooding surface (mfs) and overlain by the prograding deposits of the highstand systems tract (HST). In the study area, the landward boundary of the Pleistocene wedge is located at about 20 km seaward of the

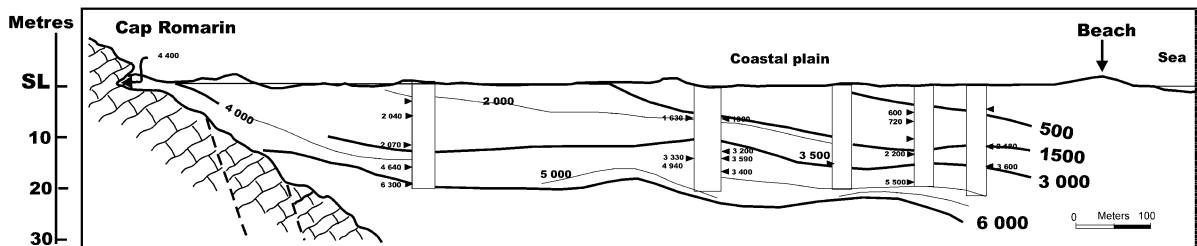


Fig. 4. The Romarin coastal plain initiation of progradation, north of Cap Leucate (location Fig. 1), is dated from about 6000 yr. BP. It represents the last post Glacial highstand systems tract (HST) with a thickness up to 20 m b.p.s.l. No direct fluvial input is known in this area. From Aloisi et al., 1978.

shoreline between Cap d'Agde and Cap Leucate and comes closer the shoreline south of Cap Leucate. The precise architecture of the last postglacial deposits is a part of the research program exposed in this paper. The Quaternary depositional sequences are not well dated on the shelf.

The more recent shelf perched lowstand wedge (Posamentier et al., 1992; Tesson et al., 2000) outcropping at the outer shelf is dated 40 ky cal. BP. It was deposited during the Wurmian sea level lowering phase (Gensous et al., 1993). For the previous lowstand wedges, data are not available however the hypothesis of control of deposition by 4th and/or 5th order glacio-eustatic cycles is proposed (Tesson

et al., 1993) and is supported by modelling studies (Rabineau, 2001).

3. Data and methods

3.1. Seismic data

HR and VHR seismic data used in this study are retrieved from the ARGO database (West area, Fig. 1). Seismic devices used were: the Minisparker SIG 50 Joules, the Uniboom EGG 300 joules, and the 2.5 and 3.5 Edo Western mud penetrator. New data since 2001 were acquired using a special IKB Seistec boomer in

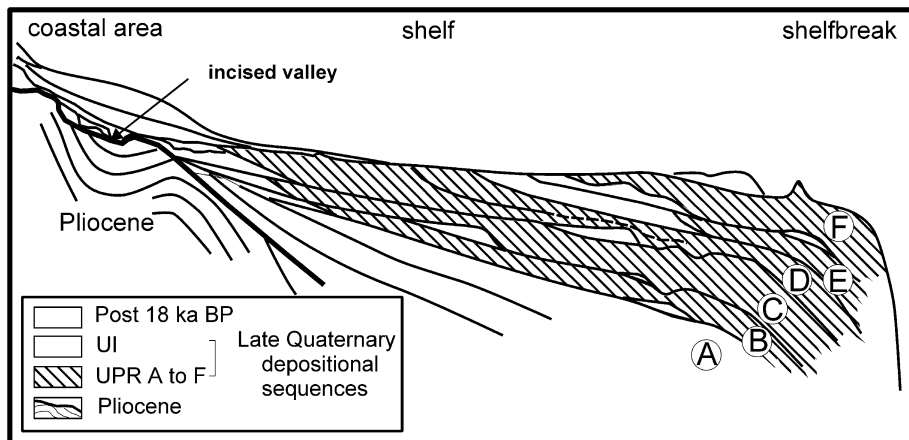


Fig. 5. Simplified sketch of the shelf stratigraphic architecture of the Plio-Quaternary deposits of the Gulf of Lion (modified from Tesson et al., 2000). Each Quaternary depositional sequence consists of a couplet of UPR/UI units. The couples are considered to represent the Late Quaternary deposits organised in an overall sedimentary wedge, thinning landward. Between the Pliocene and the Late Quaternary wedge, deposits should represent the Early to Mid Quaternary. The schematic representation in the coastal area is based on the present study. UPR=forced regressive wedge or “Unité Progradante Régionale” made of low energy deposits and developed on the whole continental shelf. UPR is considered as a “shelf-perched lowstand” (Posamentier et al., 1988). The mappable UPR are labelled from A to F. UI=“unité intercalée” made dominantly of high energy deposits (sandy paleocoastline on the outer shelf) and irregularly preserved. UI are considered mainly as transgressive deposits, excepted on the outer shelf where they should be in part maximum lowstand deposits.

the near offshore band (Liper cruise, *N/O Téthys II*, 2001) and the submarine beach and lagoon (Litto cruises, 2001–2003). The IKB Seistec boomer ([Simpkin and Davis, 1993](#)) has the source and receiver devices included in the same catamaran (offset is reduced to 0.5 m). The technical capacities of the new boomer led to highly increase the seismic resolution and were particularly suitable for studies in very shallow water environment ([Labaune et al., in press](#)).

Until 1994, data were recorded in an analogical mode while after 1994 in a digital and georeferenced mode using the Delph 2 system of Triton Erics ([Girault and Mathevov, 1990](#)). Time to depth conversion is based on acoustic velocity of 1500 m/s in water and 1875 m/s in sediment which are standard value used in similar previous studies of the Gulf of Lion and Gulf of Mexico ([Suter et al., 1987](#)). On seismic line figures, time is expressed in milliseconds two way travel time (ms T.W.T.) The offset between the source and the streamer (very sensitive in shallow depths) has been corrected when needed.

Positioning was acquired with a metrical precision with an onboard GPS and DGPS associated to a navigation system. The metadata concerning the properties of seismic devices and navigation may be consulted on the European database “PANGEA” where they are combined with the Institut Français de Recherche en Mer (Ifremer) metadata base and on the website of the BDSI (<http://www.univ-perp.fr/see/rch/bpc/present.htm>).

Seismic data analysis were made using the principles of seismic stratigraphy analysis ([Mitchum et al., 1977](#)) with some adaptations to HR and VHR seismic.

3.2. Core data

Previous core data consist of 2 cores in the southern and northern parts of the Salses–Leucate lagoon ([Martin, 1978](#)), 8 cores in the Canet lagoon ([Martin et al., 1981](#)) and more than 275 long cores in the emerged coastal plain, referenced into the BRGM databank or BDSS (<http://infoterre.brgm.fr>). Here we use only a part of these core data.

The S1 core, in the northern Salses–Leucate lagoon ([Fig. 6](#)), is 13.80 m long. The top of the core is at about 2.80 m below sea-level. It comprises from base to top: marine sand with very few shells, with increasing pebble content towards the top (13.80 to 2.80 m,

thickness 11 m); pebble/gravel level with sand (2.80 to 1.40 m, thickness 1.4 m); pebble and gravel in a muddy sand (1.40 to 0.50 m, thickness 0.9 m); mud with high shell content decreasing upwards (thickness 0.5 m). The levels 0.6/0.8 and 1.4/2.8 m are dated respectively at 2100 and 8200 yr B.P. The last value is considered as doubtful. HR and VHR seismic lines have been acquired just near the core location ([Fig. 1](#)).

The S2 core of the BRGM data bank, on the Salses–Leucate beach-barrier ([Fig. 6](#)), is 26 m long. The top of the core is at about 1.0 m above sea-level. It comprises from base to top: coarsening up silty sand (28.3 to 22.9 m, thickness 5.4 m); level of pebble in a sandy matrix (22.9 to 21.1 m, thickness 1.8 m); fine sand (21.1 to 18.8 m, thickness 2.3 m); pebble/gravel level (18.8 to 15.2 m, thickness 3.6 m); coarse sand (15.2 to 13 m, thickness 2.2 m); fine sand coarsening up to coarse sand (13 to 5.5 m, thickness 7.5 m); pebble/gravel level (5.5 to 4.3 m, thickness 1.2 m); sandstone (4.3 to 3.5 m, thickness 0.8 m); pebbly coarse sand (3.5 m to surface, thickness 3.5 m). No age calibration is available in the core data bank.

The C1, C2 and C3 cores, in the Canet lagoon ([Fig. 7](#)) are 19.8, 15 and 15 m long, respectively ([Martin et al., 1981](#)). From base to top, C1 core comprises Pliocene compact clay or marly clay (19 to 8.7 m) and coarsening up sand until surface. C2 core comprises Pliocene compact clay or marly clay (15 to 7.8 m), medium sand (7.8 to 0.5 m, thickness 7.3 m) and clay (0.5 m to surface). C3 core comprises sand fining up to clay (15 to 7 m), clay coarsening up to medium sand (7 to 0.5 m, thickness 6.5 m) and clay (0.5 m to surface). There is no Pliocene at the base of core C3.

The topographic maps of the Pliocene upper boundary and the Quaternary surface of incision in the Roussillon plain have been constructed (Duvail et al., 2001), using the BRGM BDSS data bank. The Pliocene upper boundary maps ([Fig. 3](#)) shows that, in the coastal area, the 0 and –20 m curves are located near the coast in the southern part and shifted landward in the north (Salses–Leucate area). The overlying Quaternary deposits have a reduced potential of preservation in the south. The Late Quaternary surface of incision is not clearly dated or correlated with the relative sea level changes. Nevertheless the depth of the incision is locally important and confirms that the places where a part of the Quaternary deposits should

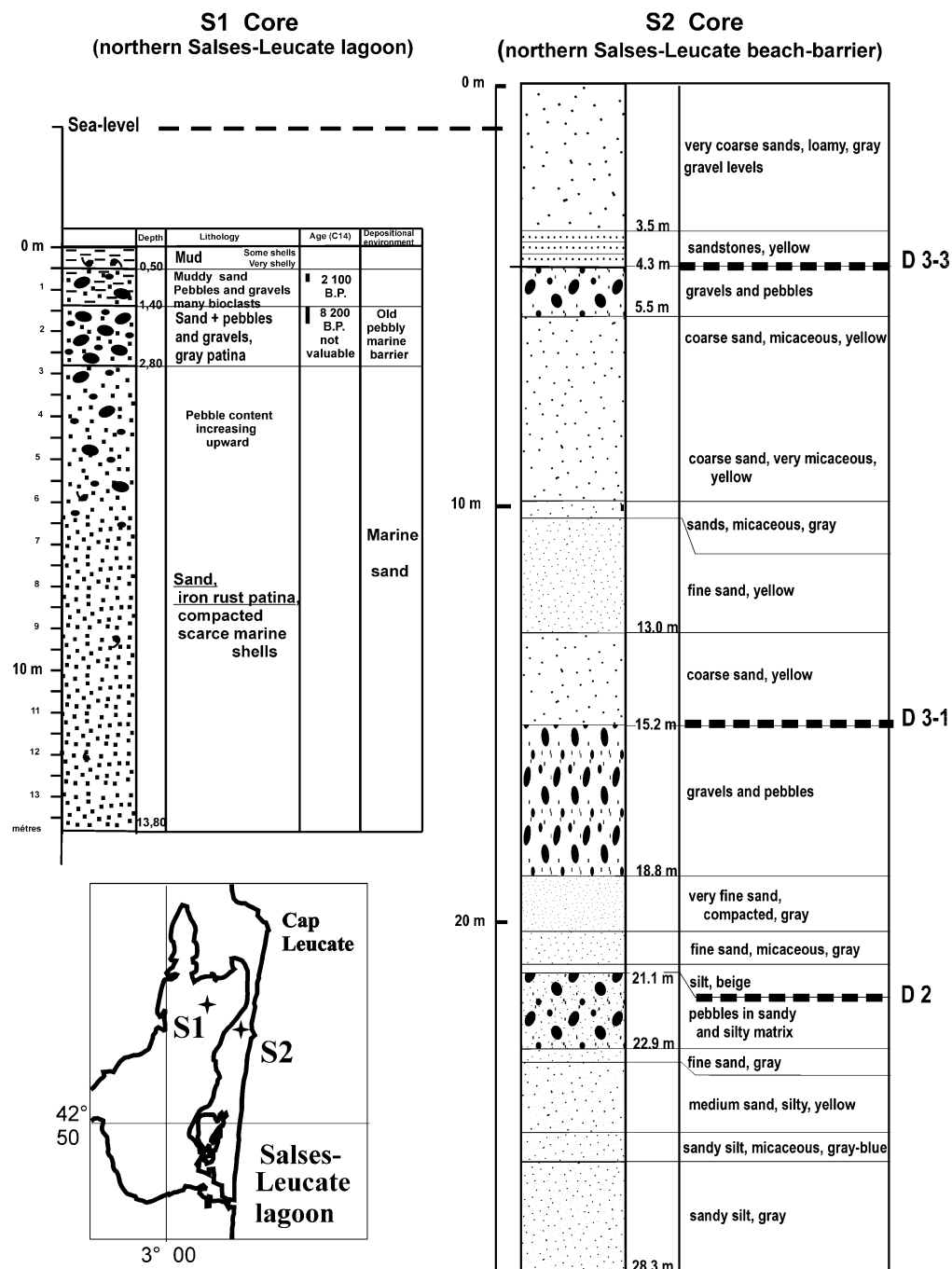


Fig. 6. The S1 core in the Salses–Leucate lagoon is located just at the boundary of the rocky and Tertiary Cap Leucate. The age dating of the upper pebbles and gravels (8200 yr. BP) have been considered as not valuable (Martin, 1978). Above, there are marine sands. The S2 core description (Labaune et al., in press) is from the BRGM databank. This core is adjacent to our seismic lines (Fig. 2) and the tops of the three pebbly levels are strong acoustic reflectors that correlate with our seismic discontinuities (D2, D3-1 and D3-3) on Figs. 10b, 11 and 12.

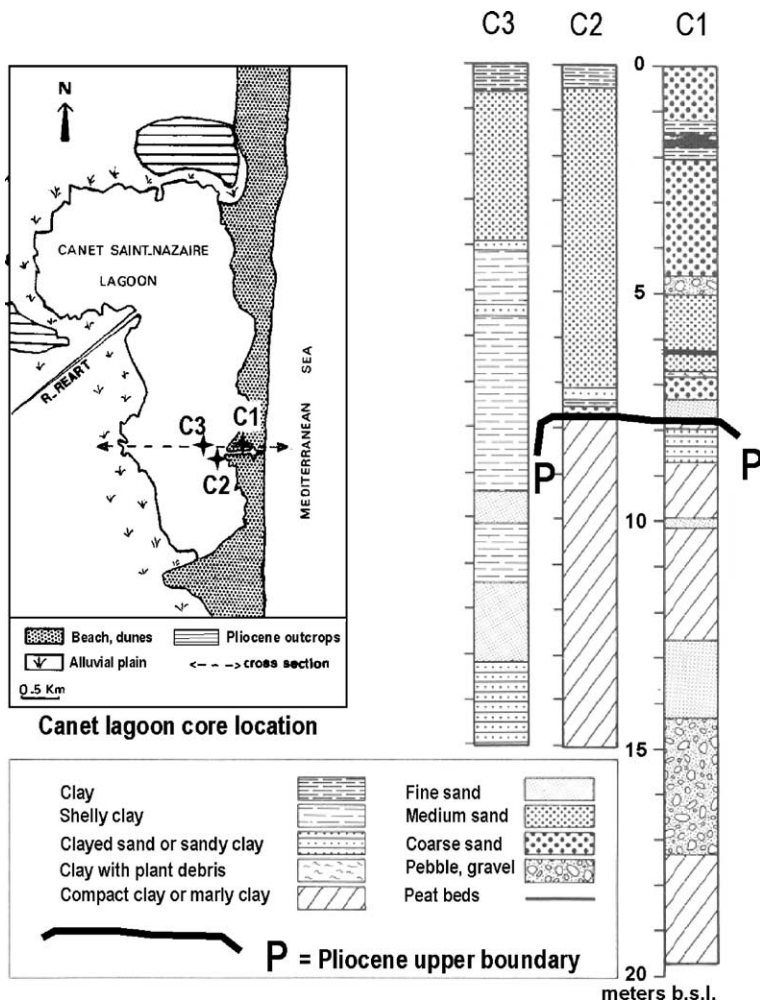


Fig. 7. South of the Tête river, around the Canet lagoon, the Pliocene deposits are outcropping or sub-outcropping as shown by the C1 and C2 cores. The Pliocene topography is very irregular (C3 core does not reach the Pliocene) has previously indicated by the maps of Fig. 3.

have been preserved are two valley axis located below the Salses–Leucate and the Canet lagoons.

4. Seismic analysis

We present a simplified analysis because the reduction scale does not allow to preserve all the original information. Description is essentially based on four HR seismic lines acquired with the minisparker (Fig. 2) and crossing the two main branches of the incised valley complex. Lines A and B are transverse sections. Lines C and D are longitudinal sections superimposed to the talweg and respectively located on the

inner shelf and Leucate lagoon. A VHR line (Boomer IKB Seistec) is also presented to show the detailed stratigraphic organization of the upper sedimentary bodies of the coastal and lagoonal Leucate complex (line E).

4.1. Transverse lines

Line A (Fig. 8), oriented SE/NW, crosses the “north” branch of the incised valleys system (Aude–Orb paleovalley). It shows a basal seismic unit (Ub) with high amplitude, low frequencies and continuous reflectors dipping seaward. They are affected by folding structures with S/SW–N/NE axis. The upper

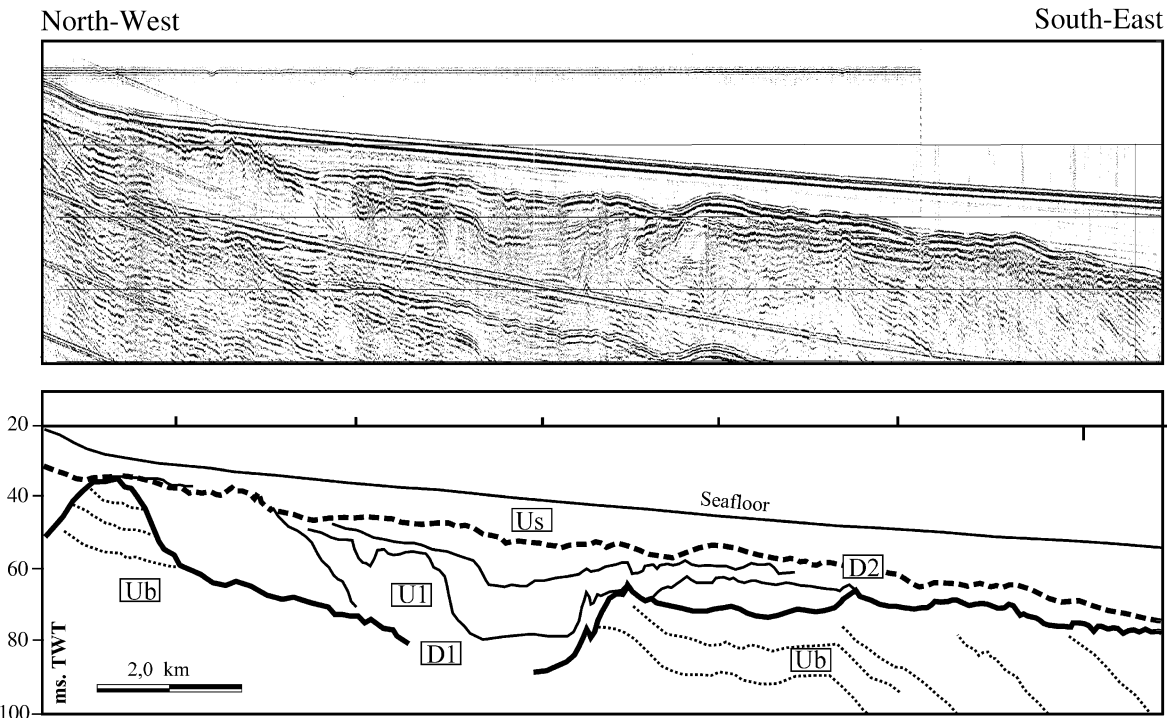


Fig. 8. Transverse line (A) of the “north” branch of the incised valley complex: reprocessed minisparker seismic line and interpreted line-drawing. Location on Fig. 2. Us=upper unit; Ub=basal unit (Pliocene); D1=basal incision; U1=incised valley infilling.

boundary (D1) is an erosional discontinuity. It is located at about 35 to 50 ms b.p.s.l. at the shoreline and deepens seaward (75 ms at the east end of line). Near the shoreline, it is truncated at more than 80 ms depth by a trough NS oriented. The filling of the trough is a composite seismic unit (U1) made of sub-units bounded by erosional discontinuities that merge laterally at the edges of the trough. The discontinuities are sub-horizontal with local U-shaped incisions. The sub-units present subhorizontal internal reflectors. The upper boundary of unit U1 is an erosional truncation (D2) that laterally merges with the basal boundary D1. It is marked by truncated terminations of the underlying reflectors. The overlying unit Us appears as relatively transparent but it is probably due to a technical problem.

Line B (Fig. 9), oriented N–S and shoreline parallel, runs across the “south” branch of the incised valleys system (Agly paleovalley). The basal unit Ub is folded in a syncline 12 km wide. The erosional discontinuity D1 at the top of unit Ub is marked by a major incision which axis superimposed to the axis of

the syncline. It is located 50 ms b.p.s.l. in the central part and rises laterally until the sea floor. In the northern part, the incision fill (unit U1) is clearly divided into two subunits by an erosional discontinuity. Near the top, several discontinuities, most of them amalgamated, present U-shaped erosional features. At the top of the complex infilling, we observed the D2 discontinuity identified in the previous section but in this section it is underlined clearly by downlap terminations of the overlying Us internal reflectors. The Us seismic facies is characterized by large sigmoidal clineforms gently dipping to the south. The upper boundary of Us is the seafloor that shows an upward convex (mounded) morphology.

4.2. Longitudinal lines

Line C (Fig. 10a), oriented east–west, follows the axis of the “south” branch of the incised valleys system in the open sea area. The erosional discontinuity D1, at the top of the basal unit Ub is located at 70 ms b.p.s.l. under the shoreline and beach barrier

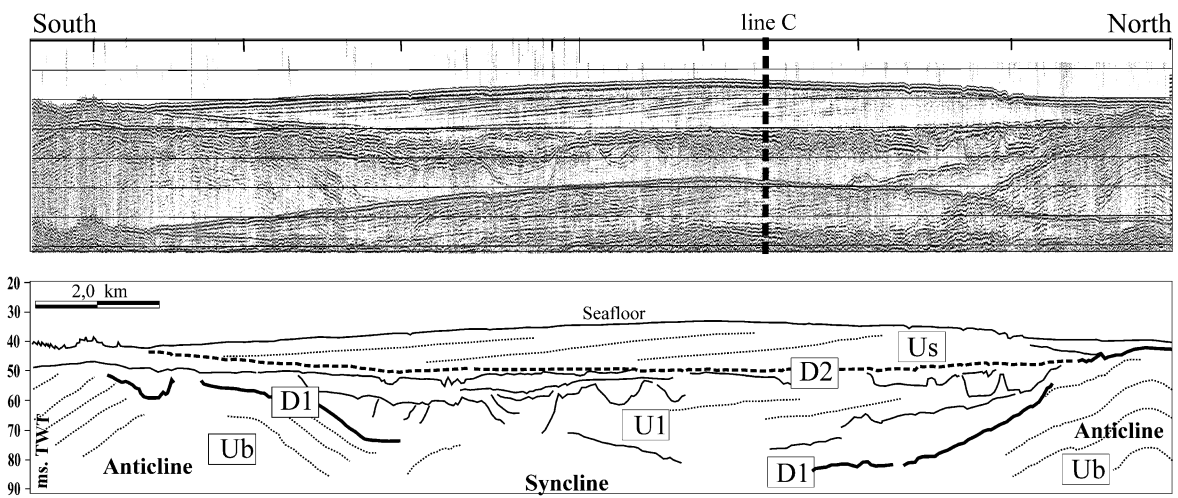


Fig. 9. Transverse line (B) of the “south” branch of the incised valley complex: reprocessed minisparker seismic line and interpreted line-drawing. Location on Fig. 2. TWT ms.=two way travel time in milliseconds.

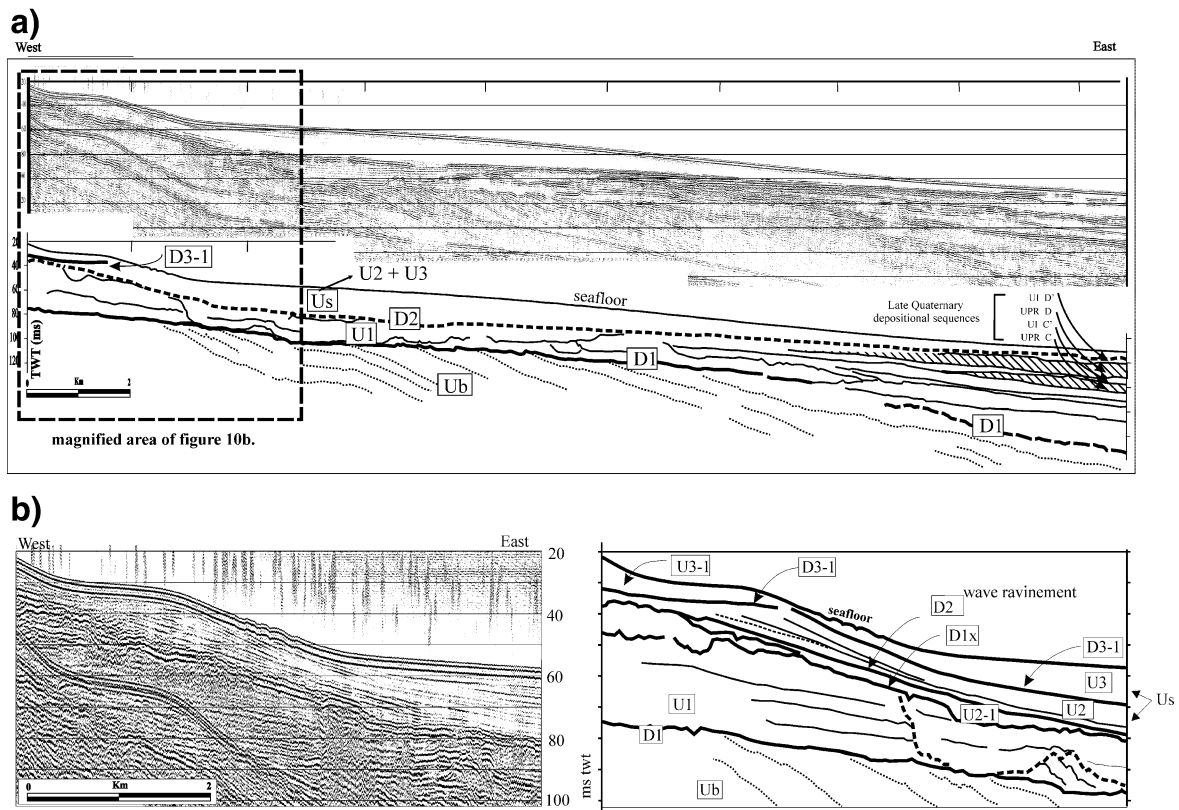


Fig. 10. a) Longitudinal line (C) of the “south” branch of the incised valley complex: reprocessed minisparker seismic section and line-drawing. Location on Fig. 2. The erosional discontinuity at the top of Ub (Pliocene) represents the base of the incised valley complex and extends seaward below the Late Quaternary depositional sequences. b) Magnified nearshore part of the minisparker line presented in Fig. 6a. Minisparker seismic line to the left and line-drawing to the right.

(Labaune et al., 2003b,c, in press). D1 deepens seaward and the overlying unit (U1) thickens. The unit U1 is composed of several encased subunits more or less preserved. They are bounded by discontinuities strongly erosional with escarpments up to 20 ms t.w.t. These subunits present subhorizontal and continuous internal reflectors. Seaward, the discontinuity D1 underlies the Late Quaternary depositional sequences described by Tesson (1996) and Lobo-Sanchez (2000). However direct correlation between the subunits of the U1 unit and the seaward depositional sequences are not precisely ensured. At the top of U1, the D2 discontinuity is a composite surface rising at 25 ms b.p.s.l. under the shoreline. It is overlain by unit Us.

The detailed analysis of the landward section of the Line C (Fig. 10b) allows to follow the uppermost discontinuity (D1x) through the unit U1. It is an erosional and irregular discontinuity. The overlying sedimentary filling is capped by D2 which can locally merge with D1x. Above, the unit Us is subdivided by an erosional discontinuity (D3-1) which

appears continuous and subhorizontal nearshore and beneath the beach. Below D3-1, the unit (U2) shows strong cliniform toplaps. Seaward, U2 converges and the reflectors become “paraconcordant”. Unit U2 pinches landward. Above D3-1, in the nearshore area, a locally prograding unit (U3-1) thickens landward. It is considered as the basal part of the present coastal wedge (Labaune et al., 2003b,c). Above D3-1 and seaward of the coastal wedge, a lenticular unit (U3) is identified (Fig. 10a and b). South of Cap Leucate, it is not connected with U3-1, but at the north it prolongates this unit up to the Cap d'Agde. In the southern area a direct relation may exist near Saint Cyprien area.

Line D (Fig. 11) prolongates line C under the northern part of the Leucate lagoon, in the axis of the incised valley. Three discontinuities are identified and correlated with those of line C. The basal discontinuity is located at 70–80 ms t.w.t. below the beach barrier at the Port-Leucate entrance and at 70–60 ms t.w.t. under the lagoon. It is the discontinuity D1. Above D1, the underlying unit is semi-

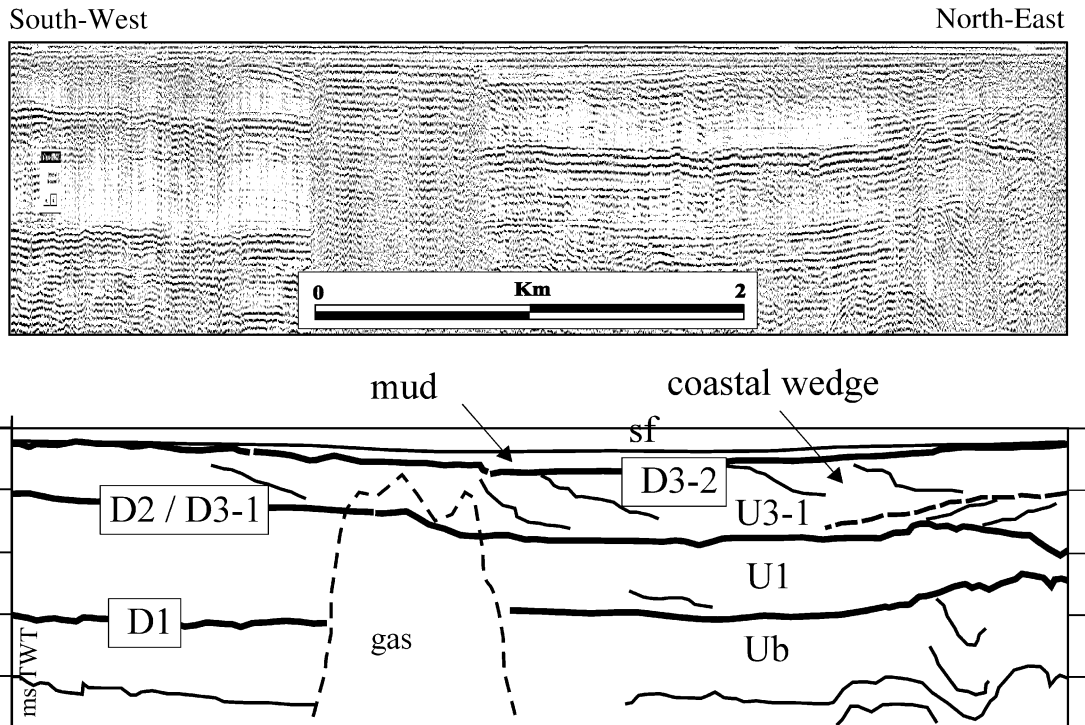


Fig. 11. Longitudinal line of the “south” branch of the incised valley complex under the Salses–Leucate lagoon: reprocessed minisparker seismic line and interpreted line-drawing. Location on Fig. 2. sf=seafloor.

transparent with eastward dipping clinoforms at the top. It is thinning northward, near the Cap Leucate. It is considered as equivalent of unit U1 and its subunits which are not well marked under the lagoon, perhaps due to lower seismic resolution. Its upper boundary is a discontinuity located at 25 ms t.w.t. near the beach barrier and sometimes 30 ms t.w.t. in the mid-lagoon. It would represent the lateral equivalent of the more or less amalgamated discontinuities D2 and D3-1. The upper part of the overlying unit (U3-1) shows oblique-tangential to sigmoidal reflectors. They are seaward dipping and organized in a progradational/aggradational pattern. The lower part shows subhorizontal reflectors. These two distinct seismic facies may characterize two distinct subunits or may be interpreted as upper (topset and foreset) and lower (bottomset) part of a single unit. In the southern part

of the lagoon, the unit comprises seaward prograding to aggrading subunits in place of the single reflectors of the northern part. This unit U3-1 is equivalent of the coastal wedge previously documented by line C. Its upper boundary (D3-2) is located at 15 ms t.w.t. in the mid lagoon and rises toward the beach barrier where it merges with the lagoon bottom. A thin sedimentary cover of lagoonal mud can reach 10–15 ms t.w.t. of maximum thickness in its central part.

Line E (Fig. 12), perpendicular to the beach barrier, gives a detailed insight of the upper lagoonal deposits organization. At the base, the equivalent unit of the coastal wedge exhibits a prograding and aggrading pattern under the discontinuity D3-2. This discontinuity rises toward the beach barrier (5 ms t.w.t. at the shoreline) and evolves into an erosional truncature. Between D3-2 and the lagoon bottom, a wedge

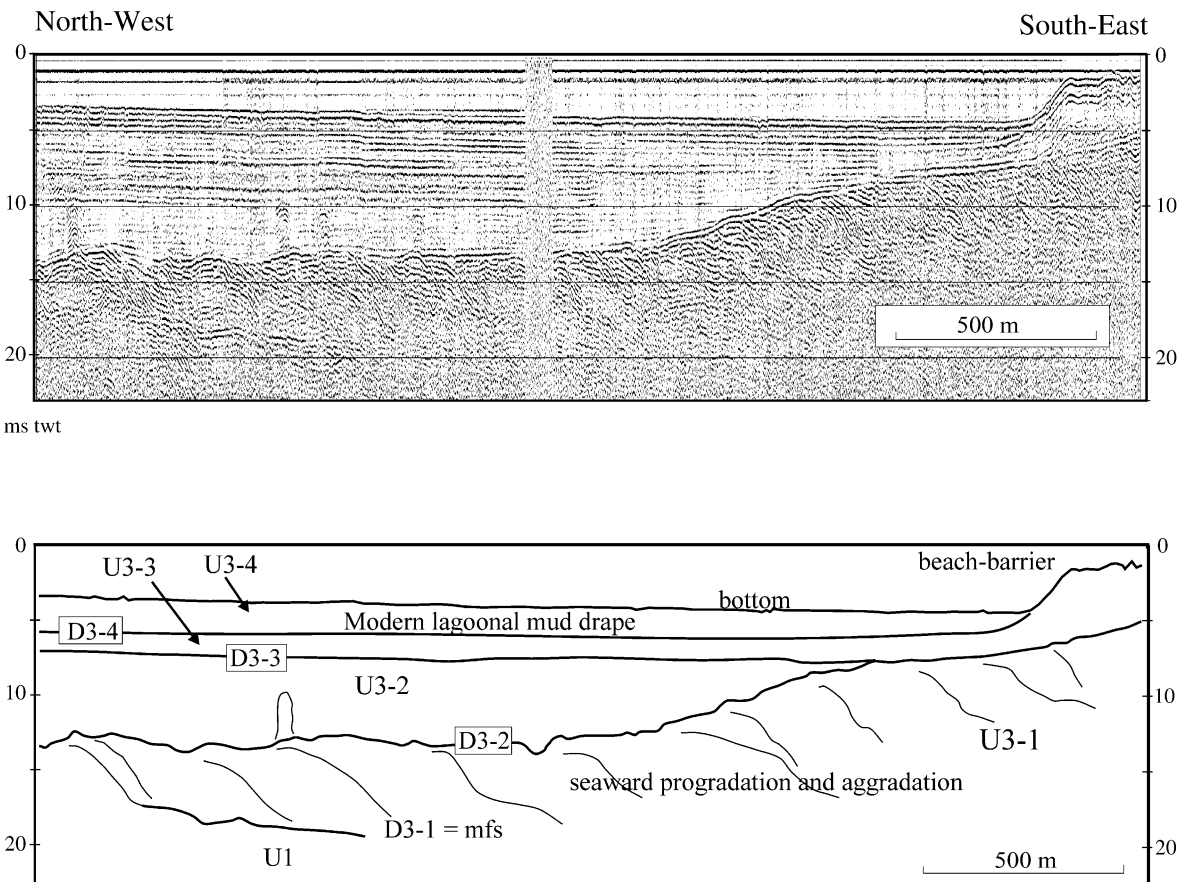


Fig. 12. Lagoonal reprocessed seismic line and line-drawing obtained with VHR IKB-Seistec boomer showing the detailed architecture of the littoral prism. VHR=very high resolution; mfs=maximum flooding surface.

shaped unit with high frequency internal reflectors has a maximum thickness of 10 ms t.w.t. The reflectors are subhorizontal, concordant and onlap onto D3-2. Two internal paraconcordant surfaces (D3-3 and D3-4) evolve toward the beach barrier to discontinuities. They bound a wedge shaped body with diffracting facies representing the beach barrier. At the barrier, D3-3 merges with D3-2 and D3-4 rises until the surface. The three units bounded by D3-2, D3-3, D3-4 and the lagoon bottom are labeled U3-2, U3-3 and U3-4.

5. Interpretation

In a first part, seismic, sedimentologic and chronologic data will be combined to assume an interpretation about the evolution of environmental parameters (such as water depth, oceanic regime and forces, fluvial input, landward and/or seaward shoreline migration) which can induce key surfaces and seismic units characteristics. In a second part, a stratigraphic model will be proposed.

5.1. Depositional environments and base level changes

The basal unit Ub spreads from the Pyrenean apron until the Cap d'Agde with similar characteristics. Synthetic studies of BRGM, onland, indicate a Pliocene age, probably Lower/Middle Pliocene (Duvail and Le Strat, 2002). The deformations cannot be imputed to compression, unknown during Pliocene, but probably result from local variations of the differential subsidence. The Pliocene substrate is made up of blues silty clays and/or yellow marls.

Erosional discontinuity D1 is the lower boundary of the incised complex infilling which has been excavated by the base level lowering during the Late Quaternary cyclic sea level changes (Van Wagoner et al., 1990; Weimer, 1984). This discontinuity rises upstream in the incised valleys. It appears that, at least in marine area, it preferentially incises the synclinal axis of Pliocene substrate. The incision occurred after the folding episode. Under the Leucate lagoon, the talweg of the incision diverts southward. Therefore, it seems that the Agly paleovalley was located more northward and that the present day course, which is

located at the southern edge of the incised system, is very recent. This was observed by Martin (1978) for recent periods, but it appears as a more general trend.

The infilling unit U1 is developed inside the incised valley complex and its extension under the coastal plain. It is interpreted as an infilling with successive stages of aggrading deposition in protected environment and underwent erosion during sea level lowering episodes. The infilling shows laterally accretional structures with high energy diverging reflectors which remind spit sand bars (Chaumillon et al., 2002). This suggests an estuarine environment and the lateral marine and fluvial equivalents. We propose that the complex infilling was deposited into a trough acting as a conduit for continental sediment yield (estuarine system) under control of Upper Quaternary relative sea level changes. Each aggrading subunit would be deposited at the end of a lowering sea level phase followed by a flooding episode due to a base level rise. It comprises a lower part with fluvial lowstand deposits overlain by transgressive deposits. Each internal discontinuity is a composite surface including the upper boundary of the aggrading transgressive infilling and the channel incision of the following phase of the base level lowering (sequence boundary). Under the Leucate lagoon, the “south” branch of the incised valley complex seems to be essentially filled with a single seismic unit without well marked reflectors. The interpretation of this unit as Agly fluvial terrace is consistent with the lithologic descriptions (sands and pebbles levels of the BDSS cores by Duvail and Le Strat, 2002; green sands by Martin, 1978).

The uppermost surface of incision in the infilling deposits (D1x) is considered as a lowstand surface which should correspond with the last relative sea level fall. The infilling is resumed by the ravinement surface D2 (transgressive surface). Beyond the banks of the main incision, D2 merges with the upper boundary of the Pliocene. This would explain the low thickness of Quaternary deposits on the inner shelf outside of the incised valleys areas. Moreover, this surface merges with the sea floor at middle shelf. It is interpreted as a polygenic surface generated during the last sea level lowstand from 50 to 18 ky BP and reworked during the postglacial transgression finished near 5 ky BP.

The unit U2, wedge shaped and prograding/aggrading, is the remnant of a transgressive sedimen-

tary body. It accumulated at the boundary of the inner-shelf during a phase of decreasing rate of sea level rise and/or increasing rate of sediment yield in the context of the last postglacial transgression. The proximal part with high energy facies evolves seaward to fine grained deposits.

The surface D3-1 is an erosional surface of truncature reworking the top of U2 in the nearshore area (Fig. 10b) and evolving laterally to a seaward dipping and conform surface. Under the beach barrier and the lagoon, D3-1 is also a basal surface of seaward progradation. After U2 deposited, the following sea level rise and wave reworking of U2 upper part developed a ravinement surface and simultaneously a lag deposit of coarse material and a healing phase of fine material (Posamentier and Allen, 1993). The fine material of the healing phase should have been redistributed seaward and downward, above the lateral conform equivalent of D3-1. The healing phase constitutes the base of the sigmoidal unit U3. D3-1 properties under the lagoon led to consider that it represents the last Holocene flooding surface (mfs).

The unit U3-1, seaward prograding and aggrading over D3-1 in the nearshore area (Fig. 8), probably developed during the last part of the Holocene sea-level rise. The shoreline migrated progressively until its recent location. The core S1 (Fig. 6) in the north of the Leucate lagoon shows (Martin, 1978) yellow marine sands equivalent to U3-1, with a top located at 3 m b.p.s.l. In the upper part, an age dating of 8.2 ky BP has not been confirmed by Martin (1978). Under the recent coastal wedge and submarine beach, these sands present a semi-transparent seismic facies with few thin downlaps. This facies is contrasting with the true sigmoidal facies observed under the lagoon. The first facies is assumed to correspond to homogeneous sands with their muddy distal termination; the second facies is assumed to correspond to sands strata intercalated with coarse or muddy layers, often observed in semi-enclosed environments. The unit U3-1 probably formed in an open bay environment previously located in the northern part of the Leucate lagoon. In the southern part of the lagoon, a more enclosed environment probably existed but progradation remained (Labaune et al., 2003a,b,c).

Well developed channels are not observed through U3-1 and it may indicate that the Agly river had previously migrated towards the south to its recent

location. Backward and behind the seaward prograding beach barrier thin sediments would be deposited. The base of the muddy deposits between D3-2 and D3-3 (Fig. 12) represents those sediments (unit U3-2). Despite a different seismic facies and the discontinuity observed, the prograding sands and mud would be synchronous. Doubts remain about the source of the sediment supply. The eastward/north-eastward progradation leads to exclude a supply due to a southward longshore drift. Moreover, the important volume of deposits excludes a direct supply by the small rivers located in the north/northwest of the Leucate lagoon. Progradation may be attributed to accretion due to the reworking of the old Agly terraces.

Above U3-1 (south-east limit, Fig. 12) the recent beach barrier developed during the stable highstand sea-level period (Fig. 13). It results from the reworking of the top of U3-1. This reworking surface would be correlated seaward with the discontinuity observed under the nearshore (Certain et al., 2004; Labaune et al., 2003b) and under the lagoon with its extension D3-3. This recent beach barrier would essentially consist of sandy deposits and levels of gravels provided by wave granulometric sorting. Toward the lagoon, its lateral extension (U3-3) may consist of tidal inlets sediment reworked by strong waves

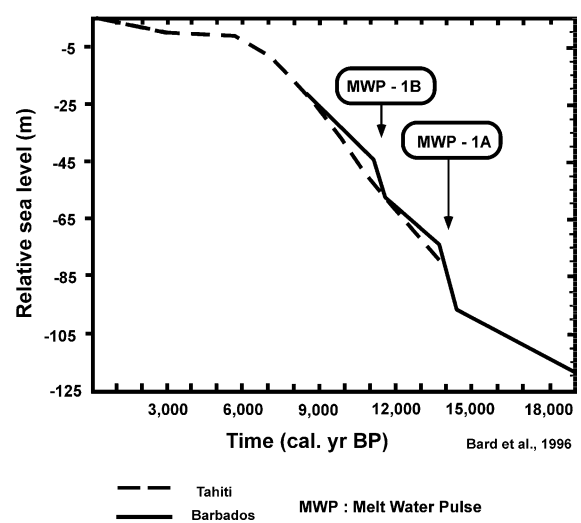


Fig. 13. Eustatic curve showing the alternate periods of increase and decrease rates of sea level rise. MWP are melt water pulses. From Bard et al., 1996. Sea level stabilized at about 6000 yr. BP and most of the coastal and deltaic plains deposits started to prograde.

induced by north-westward wind and/or of washover fan deposits. Above D3-4, the recent mud (U3-4) is deposited in an enclosed environment, the present Leucate lagoon. Some laminated sandy deposits would be locally intercalated.

Beyond of the seaward extension of U3-1 (*Fig. 10b*), unit U3 would be composed of thin deposits at the base, the healing phase concordant above D3-1. Those deposits, labelled U2b, were formed during the last sea-level rise. In the exposed line, the unit U3 is not clearly connected with U3-1. Nevertheless, it prolongates U3-1 northward of Cap Leucate. It probably developed during the last highstand period and would be an equivalent to U3-1 (thin deposits). It would be also correlated to unit U601 ([Labaune et al., 2005, Fig. 3](#)) clearly identified northward of Cap d'Agde.

*5.2. Sequence stratigraphy interpretation (*Fig. 14*)*

In sequence stratigraphic terms, the basal discontinuity D1 is a sequence boundary (SB) of 4th order, related to the oldest base level lowering which has been recorded. Due to the possibility of reworking during successive base level falls, its age is not precisely known. In the incised complex infilling, the internal discontinuities may represent younger sequence boundaries, generated during the periods of falling relative sea level which have punctuated the Upper Quaternary.

The subunits bounded by these sequence boundaries represent the remnants of depositional sequences in the complex. Because of aggrading seismic facies, they are interpreted as deposited in protected, semi-enclosed areas during a period of RSL rise. Thus the preserved part of the sequences is attributed to the TST. The number of preserved sequences is a main goal for the future which implies to fully correlate the seismic units along the incised valley complex (a new cruise has been carried out in July 2004).

The upper boundary of the incised complex infilling is wave ravinement surface which marks the final step of the eustatic sea-level rise in the nearshore area. The prograding wedge U2 would be a sedimentary body of the late TST. The healing phase (U2b), reworked top deposits of U2, is also interpreted as a part of the TST. The U2 wedge and the U2b healing phase are not observed within the whole studied area.

The upper erosional surface, D3-1 is a ravinement surface and also a flooding surface.

The deposits of the highstand systems tract (HST) overlay the flooding surface and its seaward lateral conform equivalent. The flooding surface is interpreted as the maximum flooding surface (mfs). The lower prograding part of the HST and its lateral conform equivalents (lower lagoonal mud deposits and basal part of U3, above the healing phase) represent the early HST (decreasing rate of sea level rise until the stillstand). The recent beach barrier overlies a wave ravinement surface and its lateral conform equivalent through lagoonal mud. Our data do not show clear internal reflectors of the beach barrier. Hypothesis of a seaward accretion by reworking of previous deposits should be assumed. In this case, the surface is also a downlap surface.

To date, the age of this surface is not precisely defined and it cannot be correlated with an allocyclic event. The beach barrier and its lateral conform equivalent (upper lagoonal mud and upper part of U3) may be interpreted as late HST.

6. Discussion

The Plio–Quaternary record in the littoral area, from onshore core data, has been considered as reduced to a landward uplifting Pliocene boundary covered with Holocene prograding marine mud and continental sand deposited under stable highstand sea level conditions ([Duval and Le Strat, 2002](#)). Two major incisions of the Upper Pliocene boundary were identified, with one located under the Leucate lagoon. In fact, the Pliocene boundary in the Leucate area is probably deeper than expected, and our geometric model (*Fig. 14*) shows that between this boundary and the uppermost prograding unit considered as the early modern HST, there is a preservation of sedimentary units attributed to several Quaternary relative sea level cycles and depositional sequences. The north to south irregular topography of the Upper Pliocene boundary is responsible for the more or less preserved record of the Quaternary transgressive-regressive cycles.

The location and drawing of the incised valley complex associated with the Aude, Orb and Agly

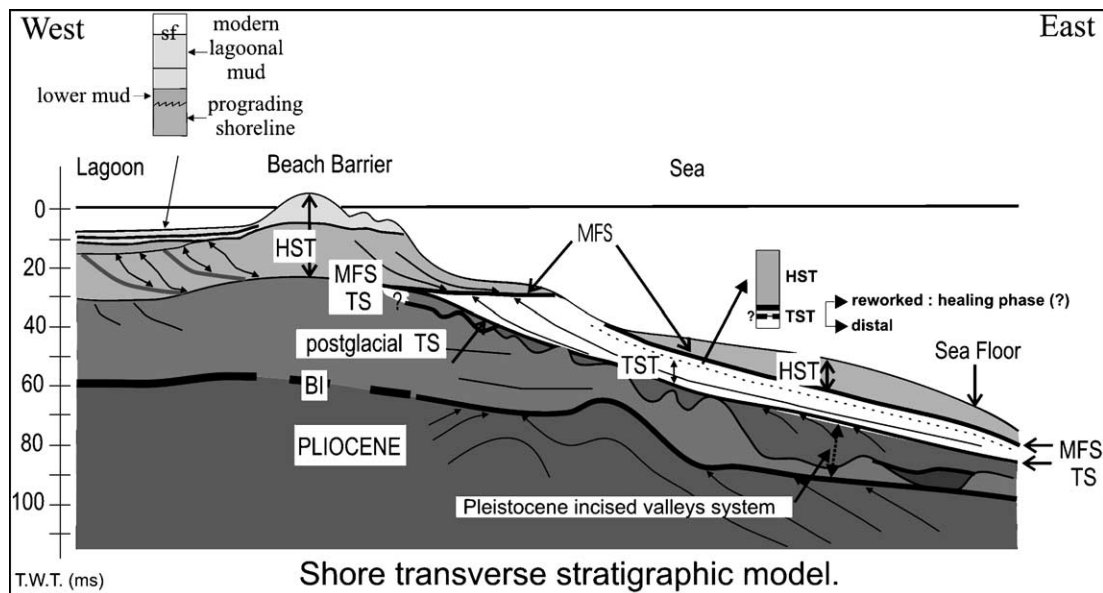


Fig. 14. Shore transverse stratigraphic model according to data of the Languedoc-Roussillon littoral and its buried incised valley complex. BI=basal incision; TS=transgressive surface; mfs=maximum flooding surface; sf=seafloor; TST=transgressive systems tract; HST=highstand systems tract.

rivers seems to have been induced in part by structural control of the underlying Pliocene strata, perhaps associated with lithologic parameters (Pliocene is mainly marly). The west–east oriented Leucate incised valley is superimposed with a syncline axis of the Pliocene substratum. The north–south oriented branch under the inner shelf is also superimposed with 2nd order deformations of the seaward dipping Pliocene strata and protected behind a kind of Pliocene high. The drawing of the incised valley complex shows that during sea level drops, the northern Languedoc-Roussillon rivers shifted southwards with alongshore course and merged. Thus, the drainage morphology was strongly modified and the rivers contribution to shelfal sediment supply evolved from linear to point source. During successive sea level drops of the Late Quaternary, the Gulf of Lion shelf was sediment supplied from only two drainage basins: the Rhône drainage basin in the north and the Languedoc-Roussillon single basin in the east. Consequently, the small Roussillon rivers had no meaningful effect on the strata development on the shelf. A similar change of the drainage system geometry has been described in the west of the Gulf of Mexico (Suter, 1994; Thomas and Anderson, 1991)

where the Nueces river became a tributary of the Rio Grande on the shelf.

Preservation of several transgressive system tracts and sequence depositional units in the incised valley complex is not common. They are generally drowned and filled by sediment during the last sea level rise and subsequent highstand (Ashley and Sheridan, 1994; Dalrymple et al., 1992; Zaitlin et al., 1994). On the French Atlantic coast, the incised valley infilling comprises mostly the lowstand fluvial coarse material overlying the sequence boundary, the transgressive estuarine and marine sands with several key surfaces (tidal and wave ravinement surfaces) and the highstand prograding muds over the mfs. The sequence boundary has been incised during the Wurm sea level drop and the incised valley fill (IVF) thickness is rapidly decreasing seaward so that the direct relationship with the stacked depositional sequences on the inner and mid shelf is not clear (Allen and Posamentier, 1993, 1994; Chaumillon et al., 2000; Lericolais et al., 2001; Weber et al., 2003). On the Mediterranean coast, the Rhône river delta shows a similar stratigraphic pattern with a thick pebble and gravel basal level above Pliocene strata, a postglacial TST and a modern HST (Boyer et al.,

2003a,b; Gensous et al., 2003; Oomkens, 1967). The pebble level is thick (several 10th of metres) and prevents from accurate drilling operation. Thus it remains possible that this level should be made of several relict and imbricated lowstand units of coarse material. Offshore of the delta, the architecture and the direct link with the Quaternary depositional sequences is not observable because of seismic pulse diffraction and attenuation, due to coarse material and occurrence of gas in the upper deposits. On the mid-outer shelf, there are deposits related to transgressive-regressive cycles (Tesson, 1996) on the western flank of the Rhône incised valley. It may be assumed that the Rhône incised valley fill would have recorded the Late Quaternary sea level drops. The record of these drops is preserved and observed more seaward than in the case of the Languedoc–Roussillon incised valley complex. Similar record is well documented for the Gulf of Mexico (Suter, 1986; Thomas and Anderson, 1994) or Virginia inner shelf (Foyle and Oertel, 1997) where several phases of deep incision have been mapped and the sedimentary infilling is mainly composed of stacked transgressive systems tracts. In our study area, the successive incisions reach great depths.

The tectonic control on the preservation potential of deposits relative to successive sea level drops, in our study area, may exist at the Late Quaternary scale. The fluvial terraces in the hinterland are well preserved and organized in a pattern indicative of a landward uplift (Duvail and Le Strat, 2002). In the Languedoc–Roussillon incised valley complex infilling, the level reached by the successive incisions progressively decreases. If we consider that the base level reached more or less similar depths during the successive Late Quaternary maximum sea level lowstands, then it suggests that the littoral area was slowly subsiding. This is in good agreement with the stratigraphic architecture on the mid-outer shelf and the effects of the control exerted by tectonic has been previously presented (Tesson and Allen, 1995). The hinge point should be located more or less landward, depending on local structural trends (Posamentier et al., 1988). Tectonic controlled the Late Quaternary sedimentation by the means of: 1—the previous deformations of the Pliocene substratum which led to uplifted and lowered areas on which the space needed for sedimentation was reduced or increased, and constrained the river talweg location during the phases of lowering and rising base level,

2—the synsedimentary differential subsidence and uplift during the Late Quaternary. This tectonic control has several major consequences on the depositional units in the littoral area by controlling the geometry and lithology of the deposits, with importance for littoral environment engineering, and also it may be indicative of large scale trend of the fluvial behaviour under sea level oscillations. Together with slope gradient, other factors control the fluvial response to eustasy (Blum, 1990). However the preservation potential here is mainly controlled by tectonics. The actual fluvial talweg location should be temporary and may returned to their “historical” location under catastrophic events.

Sedimentation during the last sea level rise, in this inner shelf/littoral area overlying the previous Agly incised valley, is particular because the present day river has shifted to the south. Above the presumed wave ravinement surface D2, the transgressive systems tract is reduced to a small prograding wedge that is usually indicative of a decrease or stillstand of the rate of sea level rise (Darigo and Osborne, 1986). The upper part of the last progradational clinoforms is at 35 ms b.p.s.l. (about 25 m). Considering a removed part of 5 m sediment, the sea level was at about 20 m b.p.s.l. and refers to about –8000 yr BP (Ters, 1986). If we consider that the progradation is due to decreasing rate of the sea level rise, then we have to explain the origin of the ravinement surface capping the wedge. Because this wedge is not common on the Gulf of Lion shelf and the study area is an active river front (Agly), we propose that the progradation is associated to a local increase of the sediment supply. The initial point of progradation is believed to have been somewhere landward from the actual shoreline. It should have been at the Mesozoic boundary (western side of the Leucate lagoon). The ravinement surface developed as the sediment flux decreased and the shoreline migrated landward again.

The prograding highstand systems tract (PL) observed under the Leucate lagoon developed probably before the end of the sea level rise. The documented coastal plain stratigraphy at the base of the Romarin cliff, a short distance north of the Cap Leucate, shows at the base a transgressive systems tract composed of gravelly sands. This first coastal construction is overlain by 15 m of prograding, well sorted and fine to medium sands with shells. The

transition from transgressive to highstand systems tracts occurred at the maximum sea level (prior to 4000 yr BP). The prograding unit PL under the Leucate lagoon is slightly different and downward shifted compared to the Romarin sketch. It progressively uplifts towards the beachbarrier so that the beginning of the highstand systems tract progradation probably started before the end of the sea level rise. This different timing of progradation is assumed to be in relation to a more important sediment supply in the Leucate area than in the Romarin area, that is believed to be induced by the Agly river proximity. This coastal progradation of an early highstand systems tract is in agreement with sequence stratigraphy models (Posamentier and Vail, 1988; Posamentier et al., 1988) and confirms a part of previous works around the Gulf of Lion (Aloisi et al., 1978; Martin, 1978).

The highstand systems tract located seaward and downward of the transgressive wedge and considered as an analog of the subaqueous delta as described by Cattaneo et al. (2003) is similar to the model of fine continental material dispersal and sedimentation on the western coast of the Adriatic sea. It has been mapped seaward of the Rhône delta (Labaune et al., 2003a, 2005) and the direct correlations are expected soon. It consists of fine material and we believe that under modern oceanic environmental conditions the coarse material is stored on the coastal area (with fluctuations depending upon seasonal oceanic climate changes), while the fine material supplied by rivers or delivered by wave reworking is dispersed seaward. A major contribution from the Rhône river sediment input using an along-shore drift is probable.

7. Conclusions

The incised valley fill complex on the Languedoc–Roussillon littoral and inner shelf is directly connected with the landward Quaternary fluvial terraces and the depositional sequences on the mid-outer shelf. Several sea-level drops and their associated key-surfaces and sedimentary units have been recorded. It represents the only area of the Gulf of Lion coast to study the land to sea relationship, their evolution during climate and sea level changes and the sedimentary budget.

The Languedoc rivers have greatly modified their courses during the phases of lowering and rising base level and merged at the inner shelf level. They constituted a shore-parallel estuary successively reoccupied during the Late Quaternary, with a seaward connection several 10th kilometers southward. Consequently the sediment supply that contributed to growth of the Gulf of Lion shelf was mainly delivered by two points sources: the Rhône drainage basin and the studied complex. The southwesternmost Roussillon rivers (Têt and Tech) had little influence on shelf and strata development.

The incised valley fill is largely constituted with Pleistocene transgressive deposits that were erroneously considered as part of the last transgressive system tract (Holocene period).

The preservation of Pleistocene transgressive deposits in the incised valley complex has probably a tectonic origin due to landward uplift and seaward subsidence, with an hinge point located landward of the littoral area.

A small prograding wedge that is sub-outcropping at the base of the littoral wedge is considered to represent a particular event (decreasing sea level rise rate/sediment supply) during the last transgression. Ravinement of its upper part contributed to an healing phase of fine material.

Progradation of the recent coastal plain deposits probably started shortly before the last sea level rise stopped. Complex depositional environments developed with some earlier low energy depositional systems back from the prograding shoreline (initial phase of lagoonal or semi enclosed bodies). This prograding phase constitutes a thinning seaward wedge of submarine beach and sandy coastal bars deposits. A more distal sigmoidal and muddy unit develops and thickens northeasterly constituting probably a subaqueous delta partly supplied with Rhône river fines. The actual system of beach barriers developed later when sea level stabilized and rested upon a wave ravinement surface. Remobilized sandy material from flood tidal delta and washover are intercalated within the lagoonal muds.

The Languedoc–Roussillon littoral area presents sedimentological and morphostructural trends which are in part inherited from the Pliocene and Quaternary. Consequently, the modern sedimentary processes are not the only key to understand the three dimensional

architecture and lithology and the past and future evolution.

Acknowledgements

Seismic data base acquisition on the shelf has been supported in part by French Insu-Cnrs (DBT and DYTEC) and national (GDR Marges) programs. New seismic and coring program on the coastal and lagoonal system has been realized by GD ARGO. Research grant of the Languedoc–Roussillon Region has been allocated. We wish to thank the crew and captains of the *CIRMED N/O Georges Petit* and *Téthys II*. We are particularly grateful to G.P. Allen and Ch. Ravenne which supported strongly the initial “STRAGLY” project on Gulf of Lion shelf. The collaboration with the BRGM Montpellier (MM. P. Le Strat and C. Duvail) has been very useful to improve our understanding of the land to sea relationship through drilling core results of the BDSS and future common research publications are forthcoming.

References

- Aloisi, J.C., Monaco, A., Planchais, N., Thommeret, J., Thommeret, Y., 1978. The Holocene transgression in the Golfe du Lion, southwestern France: paleogeographic and paleobotanical evolution. *Geogr. Phys. Quat.* XXXII (2), 145–162.
- Allen, G.P., Posamentier, H.W., 1993. Sequence stratigraphy and facies model of an incised valley fill: the Gironde Estuary, France. *J. Sediment. Petrol.* 63, 378–391.
- Allen, G.P., Posamentier, H.W., 1994. Transgressive facies and sequence architecture in mixed tide and wave-dominated incised valleys: example from the Gironde estuary, France. In: Dalrymple, R.W., Boyd, R.J., Zaitlin, B.A. (Eds.), *Incised Valley Systems: Origin and Sedimentary Sequences*, SEPM Spec. Publ., vol. 51, pp. 226–240.
- Ashley, G.M., Sheridan, R.E., 1994. Depositional model for valley fills on a passive continental margin. In: Dalrymple, R.W., Boyd, R., Zaitlin, B.A. (Eds.), *Incised Valley Systems: Origin and Sedimentary Sequences*, SEPM Spec. Publ., vol. 51, pp. 285–301.
- Bard, E., Hamelin, B., Arnold, M., Montaggioni, L., Cabioch, G., Faure, G., Rougerie, F., 1996. Deglacial sea-level record from Tahiti corals and the timing of global meltwater discharge. *Nature* 382, 241–244.
- Blum, M., 1990. Climatic and eustatic controls on gulf coastal plain fluvial sedimentation: an example from the Late Quaternary of the Colorado River, Texas. *SEPM Gulf Coast Section 11th Annual Research Conference, Sequences Stratigraphy as an Exploration Tool, Program with Abstracts*, December 2, pp. 71–83.
- Boyer, J., Le Strat, P., Duvail, C., 2003a. Le delta du Rhône: géodynamique de l’Holocène post-maximum glaciaire. Rapport BRGM/RP-52179-FR. 99 pp.
- Boyer, J., Duvail, C., Le Strat, P., Barrier, P., 2003b. Le delta du Rhône: géodynamique post-Glaciale. 9^e Congrès Français de Sédimentologie, Publ., vol. 38. ASF, pp. 83–85.
- Cattaneo, A., Correggiari, A., Langone, L., Trincardi, F., 2003. The Late-Holocene Gargano subaqueous delta, Adriatic shelf: sediment pathways and supply fluctuations. *Mar. Geol.* 193 (1–2), 61–91.
- Certain, R., Tessier, B., Courp, Th., Barusseau, J.P., Pauc, H., 2004. Reconnaissance par sismique très haute résolution du remplissage sédimentaire de la lagune de Leucate (Aude et Pyrénées-Orientales- SE France). *Bull. Soc. Géol. Fr.* 175 (1), 35–48.
- Chaumillon, E., Tesson, M., Weber, N., Garlan, T., 2000. Indication of the last sea level lowstand and Holocene transgression on the charente coast: preliminary results of the SIFADO seismic cruise. In: Trentesaux, A., Garlan, T. (Eds.), *Marine Sandwave Dynamics, International Workshop*, March 23–24 2000, vol. 1. University of Lille, France, pp. 43–46.
- Chaumillon, E., Gillet, H., Weber, N., Tesson, M., 2002. Evolution temporelle et architecture interne d’un banc sableux estuarien: la longe de Boyard (Littoral Atlantique, France). *C.R. Acad. Sci. (Paris)* 334, 119–126.
- Clauzon, G., Aguilar, J.P., Michaux, J., 1987. Le bassin Pliocène du Roussillon (Pyrénées Orientales, France): exemple d’évolution géodynamique d’une ria Méditerranéenne consécutive à la crise de salinité messinienne. *C.R. Acad. Sci. (Paris)* 304 (11), 585–590.
- Dalrymple, R.W., Zaitlin, B.A., Boyd, R., 1992. Estuarine facies models: conceptual basis and stratigraphic implications. *J. Sediment. Petrol.* 62, 1130–1146.
- Darigo, N.J., Osborne, R.H., 1986. Quaternary stratigraphy and sedimentation of the inner continental shelf, San Diego County, California. In: Knight, R.J., McClean, J.R. (Eds.), *Shelf Sand and Sandstone Reservoir*, Can. Soc. Pet. Geol., Mem., vol. 11, pp. 73–98.
- Duvail, C., Le Strat, P., 2002. Architecture et géométrie haute résolution des prismes sédimentaires Plio Quaternaires au droit du Roussillon suivant un profils terre-mer. Rapport BRGM/RP-51972-FR. 71 pp.
- Duvail, C., Le Strat, P., Bourgine, B., 2001. Atlas géologique des formations plio-quaternaires de la plaine du Roussillon (Pyrénées Orientales). BRGM report, BRGM/RP-51197-FR, 44 pp.
- Foyle, A.M., Oertel, G.F., 1997. Transgressive systems tract development and incised-valley fills within a Quaternary estuary-shelf system: Virginia inner shelf, USA. *Mar. Geol.* 137, 227–249.
- Gensous, B., Tesson, M., 2003. L’analyse des dépôts postglaciaires et son application à l’étude des séquences de dépôt du Quaternaire terminal sur la plate-forme au large du Rhône (Golfe du Lion). *Bull. Soc. Géol. Fr.* 174 (4), 401–419.
- Gensous, B., Williamson, D., Tesson, M., 1993. Late-Quaternary transgressive and highstand deposits of a deltaic shelf (Rhône Delta, France). *Spec. Publ. Int. Assoc. Sedimentol.* 18, 197–211.

- Gensous, B., Tesson, M., Labaune, C., 2003. The deglacial deposits of the Rhône shelf: stratigraphic organisation and controlling factors. COMDELT A Open Conference on Comparing Mediterranean and Black Sea prodeltas 26–28 Octobre, Aix en Provence, pp. 32–33 Abstract.
- Girault, R., Mathevon, G., 1990. Real time digital processing for high resolution seismic survey. 22nd Ocean Technology Conference, Houston, USA, pp. 591–596.
- Gorini, C., 1993. Géodynamique d'une marge passive: le Golfe du Lion (Méditerranée occidentale). Thèse, Univ. Paul Sabatier, Toulouse, 264 pp.
- Guennoc, C., Gorini, C., Mauffret, A., 2000. Histoire géologique du Golfe du Lion et cartographie du rift Oligo-Aquitainien et de la surface messinienne. *Géol. Fr.* 3, 67–97.
- Labaune, C., Delpoint, A., Berne, S., Gensous, B., Tesson, M., Leroux, E., Duval, F., 2003a. Seismic stratigraphy of the deglacial deposits of the Rhône prodelta and adjacent shelf. COMDELT A Open Conference on Comparing Mediterranean and Black Sea prodeltas 26–28 Octobre, Aix en Provence, pp. 62–63. Abstract.
- Labaune, C., Tesson, M., Gensous, B., 2003b. Architecture des dépôts postglaciaires du littoral du Roussillon: lagune, cordon et plate-forme interne. 9 ème congrès ASF 14–16 Octobre, Bordeaux.
- Labaune, C., Tesson, M., Gensous, B., 2001. Languedoc Roussillon littoral system (western Gulf of Lion, France): Late Quaternary stratigraphic organisation. COMDELT A Open Conference on Comparing Mediterranean and Black Sea prodeltas 26–28 Octobre, Aix en Provence, pp. 64–65 Abstract.
- Labaune, C., Tesson, M., Gensous, B., in press. High resolution compare to very high resolution seismic systems in a coastal area: Roussillon, West of Gulf of Lion, France. *Marine Geophysical Researches*.
- Labaune, C., Jouet, G., Berne, S., Gensous, B., Tesson, M., Leroux, E., Duval, F., 2005. Seismic stratigraphy of the deglacial deposits of the Rhône prodelta and adjacent shelf. *Mar. Geol.* 222–223, 229–311 (this issue) doi:10.1016/j.margeo.2005.06.018.
- Lericolais, G., Berné, S., Féries, H., 2001. Seaward pinching out and internal stratigraphy of the Gironde incised valley on the shelf (Bay of Biscay). *Mar. Geol.* 175, 183–197.
- Lobo-Sánchez, 2000. Estratigrafía de alta resolución y cambios del nivel del mar durante el Cuaternario del margen continental del golfo de Cádiz (S de España) y del Roussillon (S de Francia): estudio comparativo. Thesis Doctoral, Univ. de Cádiz, 618 pp.
- Lofi, J., Rabineau, M., Gorini, C., Berne, S., Clauzon, G., De Clarens, P., Dos Reis, A.T., Mountain, G.S., Ryan, W.B.F., Steckler, M.S., Fouquet, C., 2003. Plio-Quaternary prograding clinoform wedges of the western Gulf of Lion continental margin (NW Mediterranean) after the Messinian Salinity Crisis. *Mar. Geol.* 198, 289–317.
- Martin, R., 1978. Evolution Holocène et Actuelle des conditions de sédimentation dans le milieu lagunaire de Salses-Leucate. 210 pp.
- Martin, R., Gadel, F., Barusseau, J.P., 1981. Holocene evolution of the Canet-St Nazaire lagoon (Golfe du Lion, France) as determined from a study of sediment properties. *Sedimentology* 28, 823–836.
- Mitchum, J.R., Vail, P.R., Sangree, J.B., 1977. Seismic stratigraphy and global changes of sea level: Part 6. Stratigraphic interpretation of seismic reflection patterns in depositional sequences. In: Payton, C.E. (Ed.), *Seismic Stratigraphy—Applications to Hydrocarbon Exploration*, Mem. Am. Assoc. Pet. Geol., vol. 26, pp. 117–133.
- Oomkens, E., 1967. Depositional sequences and sand distribution in a deltaic complex. *Geol. En Mijnbouw* 46, 265–279.
- Posamentier, H.W., Allen, G.P., 1993. The “healing phase”—a commonly overlooked component of the transgressive systems tract. *Am. Assoc. Pet. Geol. Annu. Conv., Abstr. Prog.* 167.
- Posamentier, H.W., Vail, P.R., 1988. Eustatic controls on clastic deposition II: sequence and systems tract models. In: Wilgus, C.K., Hastings, B.S., Kendall, H.W., Posamentier, H.W., Ross, C.A., Van Wagoner, C. (Eds.), *Sea-Level Changes: An Integrated Approach*, vol. 42. Society of Economic Paleontologists and Mineralogists, Tulsa, pp. 125–154.
- Posamentier, H.W., Jersey, M.T., Vail, P.R., 1988. Eustatic controls on clastic deposition I: conceptual framework. In: Wilgus, C.K., Hastings, B.S., Kendall, H.W., Posamentier, H.W., Ross, C.A., Van Wagoner, C. (Eds.), *Sea Level Changes: An Integrated Approach*, vol. 42. Society of Economic Paleontologists and Mineralogists, Tulsa, pp. 109–124.
- Posamentier, H.W., Allen, G.P., James, D.P., Tesson, M., 1992. Forced regressions in a sequence stratigraphic framework: concepts, examples and exploration significance. *Am. Assoc. Pet. Geol. Bull.* 76, 1687–1709.
- Rabineau, M., 2001. Un modèle géométrique et stratigraphique des séquences de dépôt Quaternaires sur la marge du Golfe du Lion: enregistrement des cycles climatiques de 100 000 ans. Thèse Université, Univ. Rennes I, 455 pp.
- Rabineau, M., Berné, S., Ledrezen, E., Lericolais, G., Marsset, T., Rotunno, M., 1998. 3D architecture of lowstand and transgressive Quaternary sand bodies on the outer shelf of the Gulf of Lion, France. *Mar. Pet. Geol.* 12, 439–452.
- Simpkin, P.G., Davis, A., 1993. For seismic profiling in very shallow water, a novel receiver. *Sea Technology*, vol. 34(9), September.
- Suter, J.R., 1986. Ancient fluvial systems and Holocene deposits, southwestern Louisiana continental shelf. In: Berryhill, H.L. (Ed.), *Late Quaternary Facies and Structure, Northern Gulf of Mexico: Interpretations from Seismic Data*, Am. Assoc. Petrol. Geol., Studies in Geology, vol. 23, pp. 81–132.
- Suter, J.R., 1994. Late Quaternary sequence stratigraphy and fluvial architecture, northern Gulf of Mexico. *IAS Special meeting on High Resolution Sequence Stratigraphy*, Tremp, Spain, pp. 173–180.
- Suter, J.R., Berryhill, H.L., Penland, S., 1987. Late Quaternary sea-level fluctuations and depositional sequences, Southwest Louisiana Continental Shelf. In: Nummedal, D., Pilkey, O.H., Howard, J.P. (Eds.), *Sea Level Fluctuations and Coastal Evolution*, Soc. Econ. Paleont. Mineral., Spec. Publ., vol. 41, pp. 199–219.
- Ters, M., 1986. Variations in Holocene sea level on the French Atlantic coast and their climatic significance. In: Rampino, M.R. (Ed.), *Climate: History, Periodicity and Predictability*. Van Nostrand Reinhold, New York, pp. 204–237.

- Tesson, M., 1996. Contribution à la connaissance de l'organisation stratigraphique des dépôts d'une marge siliciclastique. Étude de la plate-forme continentale du Golfe du Lion. Mémoire d'Habilitation à Diriger des Recherches. 102 pp.
- Tesson, M., Allen, G.P., 1995. Contrôle tectonique et eustatique haute-fréquence de l'architecture et de la stratigraphie de dépôts de plate-forme péricratonique. Exemple du Golfe du Lion (Méditerranée, France) et des dépôts Quaternaires. C.R. Acad. Sci. (Paris) 320, 39–46.
- Tesson, M., Gensous, B., Allen, G.P., Ravenne, Ch., 1990. Late Quaternary deltaic lowstand wedges on the Rhône continental shelf, France. Mar. Geol. 91, 325–332.
- Tesson, M., Allen, G.P., Ravenne, Ch., 1993. Late Pleistocene shelf-perched lowstand wedges on the Rhône continental shelf. Spec. Publ. Int. Assoc. Sedimentol., vol. 18, pp. 183–196.
- Tesson, M., Posamentier, H.W., Gensous, B., 2000. Stratigraphic organization of Late Pleistocene deposits of the western part of the Rhône shelf (Languedoc shelf) from high resolution seismic and core data. Am. Assoc. Pet. Geol. Bull. 84, 119–150.
- Tesson, M., Labaune, C., Gensous, B., 2003. Land to sea stratigraphic correlations: a buried incised valleys complex of the western Gulf of Lion (France). Late Quaternary and Holocene 9 ème congrès ASF, 14–16 Octobre, Bordeaux.
- Thomas, M.A., Anderson, J.B., 1991. Late Pleistocene sequence stratigraphy of the Texas continental shelf: relationship to $\delta^{18}\text{O}$ Curves. GCSSEPM Foundation Twelfth Annual Research Conference, Program and Abstracts, pp. 265–270.
- Thomas, M.A., Anderson, J.B., 1994. Sea-level controls on the facies architecture of the Trinity/Sabine incised-valley system. Texas Continental Shelf, Spec. Publs., vol. 51. SEM, pp. 63–82.
- Weber, N., Chaumillon, E., Tesson, M., 2003. Variation of Quaternary stratigraphic pattern along an incised valley fill revealed by very high resolution seismic profiling: the paleo-Charente river (French Atlantic Coast). AAPG Annual Meeting May, 11–14, Salt Lake City, Utah.
- Weimer, R.J., 1984. Relation of unconformities, tectonics and sea level changes, Cretaceous of Western Interior, U.S.A. In: Schlee, J.S. (Ed.), Interregional Unconformities and Hydrocarbon Accumulation, Mem. Am. Assoc. Pet. Geol., vol. 36, pp. 7–35.
- Van Wagoner, J.C., Mitchum, R.M., Campion, K.M., Rahmanian, V.D., 1990. Siliciclastic sequence stratigraphy in well logs, cores and outcrops: concepts for high-resolution correlation of time and facies: Tulsa. Am. Assoc. Petrol. Geol. Methods Explor. Ser. 7 (55 pp.).
- Zaitlin, B.A., Dalrymple, R.W., Boyd, R., 1994. The stratigraphic organisation of incised valley systems associated with relative sea-level change. In: Dalrymple, R.W., Boyd, R., Zaitlin, B.A. (Eds.), Incised Valley Systems: Origin and Sedimentary Sequences, SEPM Spec. Publ., vol. 51, pp. 45–60.

2 **Integration of high and very high-resolution seismic reflection profiles
3 to study late Quaternary deposits of a coastal area in the western
4 Gulf of Lions, SW France**
5

6 Caroline Labaune*, Michel Tesson and Bernard Gensous

7 *Laboratoire de Biophysique et Dynamique des Systèmes Intégrés, BDSI Perpignan University, 52 avenue Paul
8 Alduy, 66860 Perpignan cedex, France;*

9 *Corresponding Author (Phone: +33-4-6866-2112; E-mail: labaune@univ-perp.fr)

10 Received 30 January 2004; accepted 5 June 2005

11 **Key words:** borehole, coastal plain, Gulf of Lions, HR, lagoon, late Quaternary deposits, near-shore,
12 seismic stratigraphy, VHR

13 **Abstract**

14 High resolution (HR – sparker) and very high resolution (VHR – boomer) seismic reflection data acquired in shallow water environments of the Roussillon coastal area are integrated to provide an accurate image of the stratigraphic architecture of the Quaternary deposits. The complementary use of the two systems is shown to be of benefit for studies of shallow water environments. The HR sparker data improved the landward part of a general model of Quaternary stratigraphy previously established offshore. They document an incised valley complex interpreted as the record of successive late Quaternary relative sea-level cycles. The complex is capped by a polygenetic erosional surface developed during the last glacial period (> 18 ky) and variably reworked by wave ravinement during the subsequent post-glacial transgression. The overlying transgressive systems tract is partly preserved and presents a varying configuration along the Roussillon coastal plain. The VHR boomer data provide information on the architecture of the uppermost deposits, both in the near-shore area and in the lagoon. These deposits overlie a maximum flooding surface at the top of the transgressive systems tract and constitute a highstand systems tract composed of two different architectural elements. In the near-shore area, a sandy coastal wedge is subdivided into a lower unit and an upper unit in equilibrium with present day dynamics. In the Salses-Leucate lagoon area, the sedimentary architecture is highly complex due to the closure of a former embayment and the formation of the present beach barrier.

27

28 **Introduction**

30 Most studies of near-shore areas have focused on
31 the hydrodynamic regime and its impact on recent
32 sedimentation (Nielsen et al., 2001; Stépanian and
33 Levoy, 2003). Integration over longer timescales
34 has usually been applied either to deposits onshore
35 in the coastal plain or offshore across the continental shelf. In particular, many studies have
36 addressed the late Quaternary architecture of continental shelves (Suter et al., 1987; Hernandez-Molina et al., 1994; Tesson et al., 2000; Ridente and Trincardi, 2002). However, few studies
41 have really dealt with the architecture of deposits across the coastal zone, i.e. the transition between
43 the continental and marine domains spanning the coastal plain to the inner continental shelf. One of

the first was proposed by Penland et al. (1988) in
46 the Mississippi delta area and focused essentially
47 on the post-glacial transgressive deposits and the
48 development of coastal barriers. Thomas and
49 Anderson (1994) carried out a study of a late
50 Quaternary incised valley system on the Texas
51 continental shelf and proposed a correlation with
52 coastal plain deposits. Locker et al. (2003) carried
53 out seismic studies on the post-glacial Florida
54 inner shelf and near-shore area. In most areas,
55 however, there remains a gap concerning the
56 geological evolution of the near-shore area due
57 to a lack of direct correlation between data from
58 the onshore and marine domains.

59 The Roussillon coastal plain (western part of
60 Gulf of Lions, France), its shoreface and the
61 adjacent continental shelf have been the subjects of

	Journal : MARI	Dispatch : 23-10-2005	Pages : 13
CMS No. :	D000023711	<input type="checkbox"/> LE	<input type="checkbox"/> TYPESET
MS Code :	MARI MI-03	<input type="checkbox"/> CP	<input checked="" type="checkbox"/> DISK

a number of sedimentological studies, none of which have integrated the transition from the coastal plain to the continental shelf. Several studies, based on borehole data or geomorphology, have dealt with the Quaternary fluvial terraces on the coastal plain (Carozza and Delcaillau, 1999; Duvail et al., 2001). The post-glacial infill of the Salses-Leucate and the Canet-St Nazaire lagoons were studied without real correlation to the marine area (Martin, 1978; Martin et al., 1981; Certain et al., 2004). Durand (1999) focused on the shore-face area in order to determine the recent evolution of the beaches attributed to present hydrodynamic conditions. A preliminary study of the onshore to inner shelf transition was presented by Monaco (1971), but was limited by a lack of near-shore data.

In order to fill the coastal data gap, several seismic acquisition cruises have been undertaken since 2000 along the Roussillon coast, both in shallow marine areas and in lagoons. The high and very high resolution (HR and VHR) seismic reflection data that were acquired supplement a HR seismic database previously acquired across the Gulf of Lions continental shelf (Tesson

et al., 2000; Gensous and Tesson, 2003). In this paper, an integration of the HR and VHR seismic data types is presented and used to discuss the evolution of the Roussillon coastal area during the Quaternary. The marine and lagoonal seismic profiles are correlated with a borehole previously acquired on the beach barrier, allowing us to relate the key seismic surfaces and facies to lithology and so improve the architectural model.

87
88
89
90
91
92
93
94
95
96

Regional setting

97

The Gulf of Lions is a passive margin that has developed since the Messinian salinity crisis (Hsü et al., 1973) under the influence of sea-level variations. In addition, during the Plio-Quaternary (Bessis and Burrus, 1986; Clauzon et al., 1987) differential landward uplift and seaward subsidence have led to a sedimentary architecture of deposits characterised onshore by an imbricate system of fluvial terraces (Duvail and Le Strat, 2002) and on the shelf by stacked marine depositional sequences (Lofi et al., 2003).

98
99
100
101
102
103
104
105
106
107
108

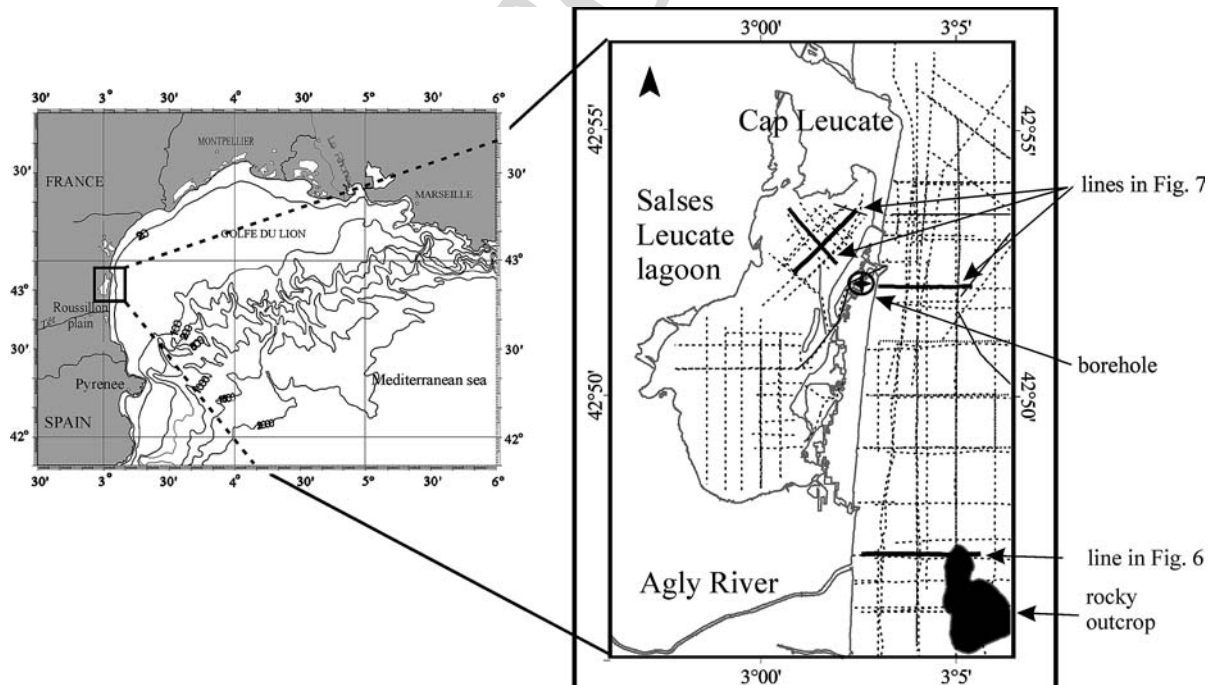


Figure 1. Architectural model of Plio-Quaternary deposits in the western part of the Gulf of Lions (Languedoc-Roussillon continental shelf, modified from Tesson and Gensous, 1998). IU: Intercalated Unit; RPU: Regional Prograding Unit.

109 The onshore area of Languedoc-Roussillon is
 110 characterised overall by a Pliocene substratum
 111 overlain by a system of imbricate Quaternary
 112 fluvial terraces that record a history of uplift
 113 movements (Duvail and Le Strat, 2002). The
 114 terraces have also been influenced by late Quater-
 115 nary glacio-eustatic cycles and associated changes
 116 in base level.

117 On the Roussillon coastal plain, lithological
 118 analysis of boreholes (Duvail et al., 2001) has
 119 contributed to a general stratigraphic model of the
 120 Plio-Quaternary deposits that is still in develop-
 121 ment. Pliocene strata underlie much of the Rous-
 122 sillon plain. Lower Pliocene deposits outcrop as
 123 Gilbert deltas (Clauzon, 1990) in the upstream
 124 parts of the plain as seaward-dipping marine muds
 125 overlain by marine sands and capped by continen-
 126 tal muddy-sands. The upper boundary of the
 127 Pliocene corresponds to a major unconformity at
 128 the base of Pleistocene alluvial terraces. The
 129 Holocene is represented by a prograding system
 130 comprising a succession of basal marine muds,
 131 marine sands and complex continental deposits
 132 (fluvial sands, conglomerates and/or lagoon
 133 muds).

134 On the shelf, the late Quaternary deposits
 135 comprise stacked marine depositional sequences,
 136 the upper of which are mainly related to the fourth-
 137 order glacio-eustatic cycles of sea level that punc-
 138 tuated the late Quaternary (Aloisi, 1986; Tesson
 139 et al., 1990; Tesson et al., 1993; Rabineau et al.,
 140 1998; Lobo et al., 2004). The sequences pinch out
 141 landward at about 80 m below sea level (Figure 1)
 142 except in the north of the Gulf where they seem to

143 extend below the recent lobes of the Rhone delta.
 144 Each sequence comprises a wedge-shaped prograd-
 145 ing unit, or RPU, of regional extent and locally an
 146 intercalated unit or IU (Figure 1). The RPUs are
 147 interpreted as lowstand wedges associated with
 148 relative sea-level fall and the following lowstand
 149 period. They provide an example of forced regres-
 150 sive deposits (Tesson et al., 1990; Posamentier
 151 et al., 1992). The IU represents near-shore sand
 152 bodies that accumulated either during the period of
 153 maximum relative sea level lowstand and/or during
 154 stillstands that occurred during the following
 155 period of rise (Tesson et al., 2000).

156 Throughout the study area, the Pleistocene
 157 deposits are capped by a polygenetic erosional
 158 surface that developed during the last relative sea
 159 level fall and the subsequent post-glacial relative
 160 sea level rise (Figure 1). The post-glacial deposits
 161 are concentrated along the outer and inner shelf as
 162 retrograding units of the transgressive systems
 163 tract. A regressive highstand systems tract devel-
 164 oped on the inner shelf but is poorly known because
 165 previous studies generally do not extend to less than
 166 20–25 m water depth (Monaco, 1971; Aloisi et al.,
 167 1975; Gensous and Tesson, 2003; Lobo et al.,
 168 2004). Onshore, the post-glacial deposits are mainly
 169 represented by alluvial plain deposits (Duvail et al.,
 170 2001).

171 The present Roussillon shoreline is sandy and
 172 interrupted from north to south by three rivers
 173 (Agly, Têt and Tech). Moreover two lagoons
 174 (Salses-Leucate and Canet-St Nazaire) are isolated
 175 behind a beach barrier subjected to microtidal and
 176 wave dynamics. Median grain size increases from

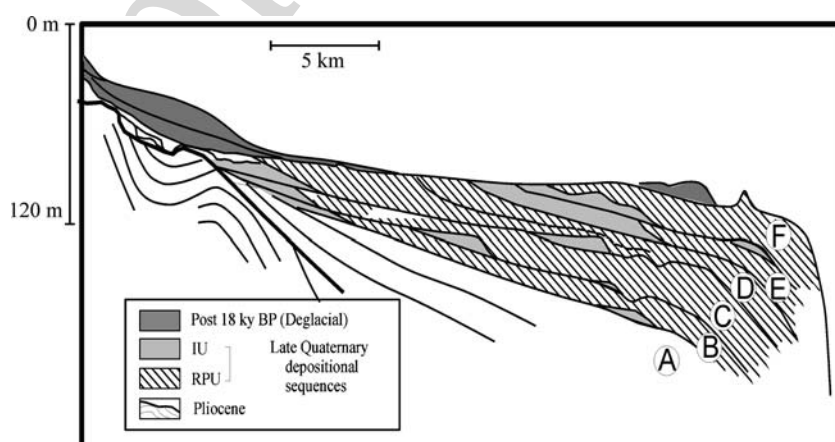


Figure 2. Simplified surficial sediment facies distribution across the study area (modified after Aloisi, 1986 and Gensous et al., 1993). Bathymetric contour shown is 20 m below sea level.

177 0.6 to 1.8 mm from north to south (Durand, 1999).
 178 Seaward, the sand to mud boundary lies near 30 m
 179 b.s.l. (Figure 2). Some beachrocks or sandstones,
 180 considered as relict Quaternary deposits, outcrop at
 181 up to 50 m b.s.l. (Monaco et al., 1972). In the
 182 lagoons, the uppermost deposits are muds (Martin,
 183 1978; Martin et al., 1981) that should represent the
 184 transgressive and highstand deposits of the late
 185 post-glacial period (Certain et al., 2004).

186 Data and methods

187 Two types of seismic reflection profiles, HR and
 188 VHR, were acquired, in some cases along the same
 189 lines. Seismic units identified in the lagoon were
 190 correlated to those in the near-shore area using a
 191 borehole previously acquired on the beach barrier.

192 The seismic acquisition was carried out using
 193 two different platforms: seaward of 15 m b.s.l., a
 194 conventional 25 m research vessel (N/O Tethys II

195 of CNRS-INSU) was used, whereas in shallower
 196 water and in the lagoon, a 5 m boat was used.
 197 About 200 km of HR seismic profiles and 1000 km
 198 of VHR profiles were acquired (Figure 3), both in
 199 the Salses-Leucate lagoon and in shallow marine
 200 environments. All seismic data were acquired
 201 digitally, using the Delphseismic 2.1 software,
 202 and geo-referenced using a differential global
 203 positioning system (DGPS).

204 The HR seismic data were acquired with a
 205 SIG™ mini-sparker composed of a multi-elec-
 206 trode sparker array and a single channel streamer
 207 with five hydrophones (Figure 4). The VHR seis-
 208 mic data were acquired with a novel type of
 209 boomer, the IKB Seistec™ boomer (Figure 5),
 210 developed for marine and lacustrine environments
 211 in 1987 (Simpkin and Davis, 1993). The innova-
 212 tions of the boomer are (i) the line-in-cone receiver
 213 array which reduces the resonance and distortion
 214 of the return signal and thus improves the resolu-
 215 tion; and (ii) the catamaran which supports both

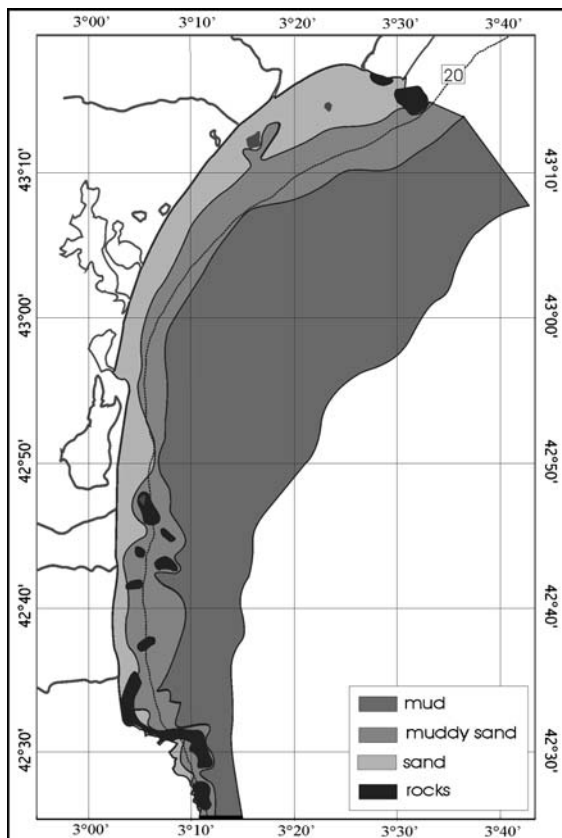


Figure 3. Map showing the locations of seismic profiles acquired in the study area. Highlighted lines correspond to seismic profiles shown in Figures 6 and 7.

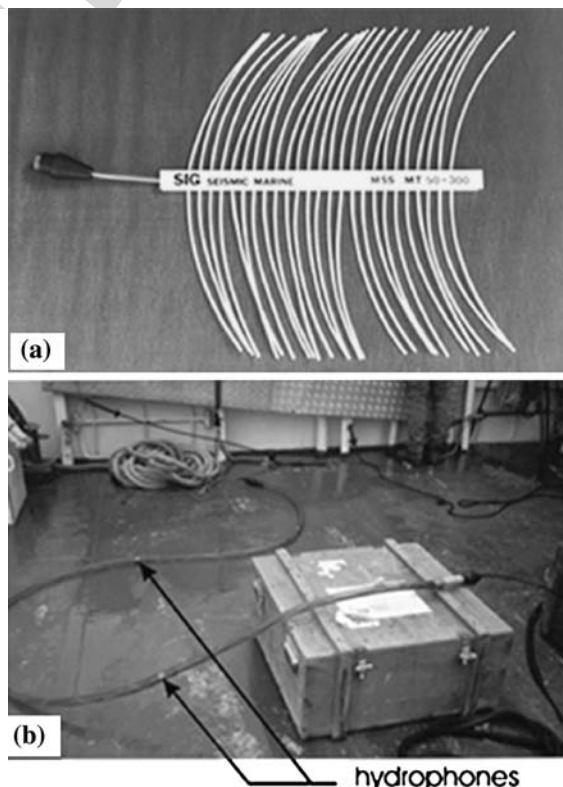


Figure 4. The SIG™ mini-sparker components: (a) the multi-
 electrode sparker array; (b) the single-channel streamer com-
 posed of five hydrophones at 1 m spacing.

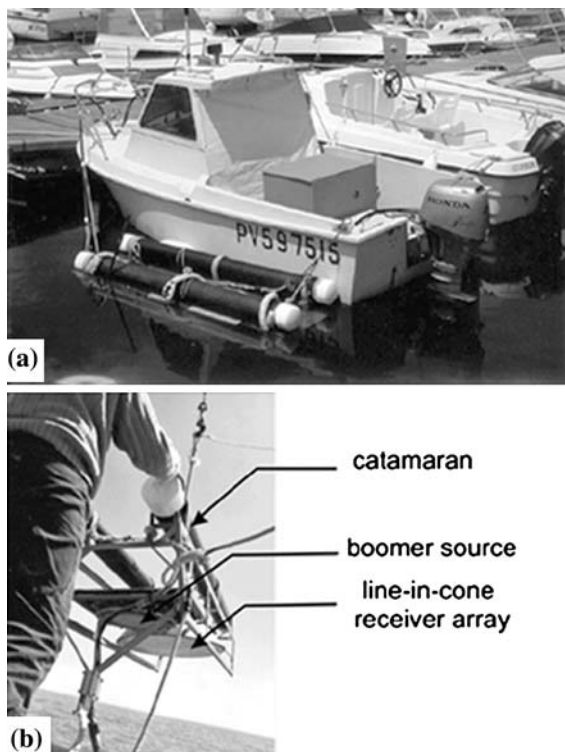


Figure 5. The IKB-Seistec™ boomer equipment: (a) the catamaran of the boomer on the side of the 5 m boat used for the coastal study; (b) main components of the boomer.

the receiver and the boomer source. The proximity of the source and of the receiver improves the definition of close targets. A filter removes frequencies below 1000 Hz directly at the top of the line-in-cone receiver.

Since the study focused both on the overall Quaternary stratigraphy and on the detailed post-glacial evolution, it was necessary to operate seismic systems that combined both penetration and resolution. This would normally imply acoustic pulses that are characterised by a broad bandwidth since higher frequencies are quickly attenuated during travel time but give HR, whereas lower frequencies give lower resolution but better penetration. The integration of the mini-sparker, HR system with relatively good penetration (up to 80 m), and the boomer, VHR system with good resolution (about 0.25 m) was found to be a good alternative. The technical and acquisition characteristics of each system are listed in Table 1.

For interpretation, the seismic profiles were converted from two-way time to depth in meters using 1700 m s^{-1} sound velocity in the sediments

and 1500 m s^{-1} in the water column. The interpretation was based on the seismic stratigraphic concepts and methods first outlined in AAPG Memoir 26 (Mitchum et al., 1977). These concepts were improved by Posamentier et al. (1988) and Posamentier and Vail (1988) and key terminology defined by Van Wagoner et al. (1988). The sequence stratigraphy concepts are based on the identification of regional discontinuities bounding stratigraphic units interpreted as sequences and/or their internal components (systems tracts). The genesis of the sequences and systems tracts is attributed to relative sea-level changes, and specific increments of the cycles and local variations are due to 2nd order controlling factors such as the sediment load. The identification of physical discontinuities and acoustic facies by seismic systems is essential to define the sequences and the systems tracts when boreholes are not available. This model was initially developed using conventional seismic exploration data and borehole calibration and further applied to HR and VHR seismic data. The key unconformities observed on the seismic profiles are interpreted as regressive and transgressive surfaces and maximum flooding surfaces that are related to relative sea-level cycles of 4th and 5th order, i.e. 100 and 20 ky cycles.

The borehole previously acquired for engineering purposes on the beach barrier in the mid-1970s was available from the national subsurface database (BDSS) of the BRGM (the French geological survey). Generally, little information is available on the boreholes of the BDSS and in this study, only the lithological log based on cuttings was available. This borehole log indicates strong

Table 1. SIG™ mini-sparker and IKB Seistec™ boomer systems; acquisition parameters and data characteristics

	SIG™ mini-sparker	IKB Seistec™ boomer
Frequency band	0.05–1.5 kHz	1–12 kHz
Input energy	50 J	140 J
Shooting rate	2 shots s^{-1}	2 shots s^{-1}
Sampling frequency	6 kHz	24 kHz
Band pass filter	0.4–1.1 kHz	1–3 kHz
Resolution	1–2 m	0.25 m
Penetration	Up to 80 m in study area	Up to 20 m in sands and muddy sands

275 contrasts in lithology, assumed to be significant
 276 enough to induce strong acoustic impedance
 277 variations in the seismic profiles.

278 Results

279 Seismic characteristics

280 Before describing the seismic surfaces and units
 281 identified across the study area, it is of interest to
 282 point out some characteristics of the boomer
 283 (VHR) and mini-sparker (HR) data. The VHR
 284 seismic data have a common vertical resolution of
 285 about 0.25 m that allows high frequency strati-
 286 graphic variations to be well identified. A “rever-
 287 beration” is often observed on the VHR data
 288 under the seafloor reflector that locally reduces the
 289 resolution. Its thickness varies from 4 to 2 ms
 290 below the seafloor (b.s.f.) and is represented by a
 291 set of “pseudo” parallel reflectors. Data acquired in
 292 the lagoon area are not affected by this “reverber-
 293 ation”.

294 The HR data are generally affected by acoustic
 295 ringing caused by the bubble oscillation of the
 296 sparker source. However, the data show a different
 297 acoustic response in the lagoon and near-shore
 298 areas where the data quality is improved with

299 reduced acoustic ringing (from 4 to 2 ms) and a
 300 weak first multiple arrival. This allows a better
 301 penetration, up to 70 m, that permits the deeper
 302 targets to be investigated.

Seismic stratigraphy

304 The main characteristics of the observed seismic
 305 surfaces and units are summarized in Table 2.
 306 From base to top, three main regional discontinuities,
 307 D1, D2 and D3-1, are observed on the HR
 308 and VHR seismic profiles (Figures 6 and 7).
 309 Locally, D2 is subdivided into D2-1 at the base
 310 and D2-2 at the top. Above D3-1, several discon-
 311 tinuities of local extent are observed especially in
 312 the lagoon (D3-2, D3-3 and D3-4). D3-3 seems to
 313 extend across the beach barrier in the shore-face
 314 area. The units bounded by these discontinuities
 315 are labelled Ub, Ur, U2 and U3.

Surface D1

316 The basal discontinuity D1 is observed on HR
 317 seismic data throughout the study area at about
 318 40–60 m b.s.l. and is relatively flat and seaward
 319 dipping. It truncates a basal unit, Ub, character-
 320 ized by oblique reflectors of high amplitude and
 321 low frequency. The unit Ub exhibits well-devel-
 322 oped folded structures.

Table 2. Properties of the observed seismic discontinuities and units

Discontinuities	Units	Properties of discontinuities	Type of discontinuities	Area of location
D3-4	U3-4	Para-concordant surface	Facies boundary	Lagoon
	U3-3	Erosional surface (marine area) Para-concordant (lagoon)	Wave reworking surface (marine)	Lagoon and near-shore
D3-3	U3-2	Seaward rising with topset below and onlap above	Facies boundary	Lagoon
	U3-1	Erosional and linear surface Toplap below, downlap above	Ravinement surface and maximum flooding surface	Lagoon and marine
D3-2	U2-b	Onlaps above	Wave ravinement	Lagoon and marine
D2-1	U2-a	Toplap/onlap terminations	Transgressive surface	Lagoon and marine
D1	Ur	Subaerial erosional surface Toplaps below	Unconformity: sequence boundary	Lagoon and marine

The discontinuity D2 mentioned in the text is subdivided into D2-1 and D2-2. The main discontinuities are highlighted in bold.



Journal : MARI

CMS No. : **DO00023711**

MS Code : **MARI MI-03**

Dispatch : **23-10-2005**

Pages : **13**

LE

TYPESET

CP

DISK

324 *Unit Ur*

325 Above D1, the HR seismic data show a set of
 326 erosional surfaces bounding seismic units globally
 327 labelled Ur (Figures 6 and 7b). The maximum
 328 thickness of the unit is about 20 m in front of the
 329 Salses-Leucate lagoon. The erosional surfaces are
 330 imbricate and comprise sub-horizontal parts and
 331 channel incisions from 1 m to about 10 m depth.
 332 The infill of major channels is characterized by
 333 aggrading sub-horizontal reflectors, whereas in
 334 smaller channels the seismic facies is rather chaotic
 335 (Figure 6b, d). Southward, the erosional surfaces
 336 tend to merge. Under the lagoon, only one sub-
 337 horizontal surface is observed between D1 and D2.
 338 The extension of unit Ur under the lagoon is not
 339 clearly observed on the seismic data (Figure 7c).

340 *Surface D2*

341 Ur is capped by an erosional surface D2 that is an
 342 unconformity. D2 is relatively flat in the south of
 343 the study area (Figure 6) and dips gently seaward
 344 in front of the Salses-Leucate lagoon (Figure 7b,
 345 d). D2 is a polygenetic surface, either merged or
 346 subdivided into D2-1 at the base and D2-2 at the
 347 top. The surface D2-1 is an erosional surface
 348 incised by small channels (Figure 7b), observed
 349 especially on the VHR seismic data. The surface
 350 D2-2 is identified in the shore-face zone in the
 351 southern part of the study area (Figure 6a) and
 352 beyond 20 m b.s.l. in front of the Salses-Leucate
 353 area (Figure 7b) and is an erosional surface that
 354 onlaps in distal areas and downlaps in proximal
 355 areas. In the lagoon, the penetration of VHR
 356 seismic profiles is not adequate to clearly identify
 357 D2 and the surface that is observed on the HR
 358 seismic data is too deep to represent D2. It is more
 359 likely that D2 is merged with the surface D3-1
 360 above.

361 *Unit U2*

362 The unit U2 is developed between D2 and D3-1
 363 (Figures 6a and 7b, d) in the area in front of the
 364 Salses-Leucate lagoon, at about 20 m b.s.l. It has
 365 a maximum thickness of 10 m and is subdivided
 366 into U2-1 at the base and U2-2 at the top. Unit
 367 U2-1 is relatively thin (maximum thickness 3–
 368 4 m) and contains small channels and chaotic
 369 facies (Figure 7b). Unit U2-2 is composed of
 370 truncated oblique clinoforms dipping seaward
 371 with upper terminations either as coastal onlap
 372 or toplap. On the HR seismic lines, the clinoforms

373 are characterized by low amplitude and low
 374 frequency. In the area located south of Salses-
 375 Leucate lagoon, U2 (Figure 6a, b) is also subdivided
 376 into U2-1 and U2-2 but with different
 377 properties and seismic facies. The unit U2-1 is
 378 only observed in the area below 20 m b.s.l., where
 379 its seismic facies evolve from chaotic to oblique
 380 reflectors. The unit U2-2 is present in the shore-
 381 face area and below 30–35 m b.s.l. where it is
 382 composed of oblique tangential reflectors with
 383 toplap and downlap terminations, whereas in
 384 distal areas, it is a thin unit with sub-horizontal
 385 reflectors. On the seismic profiles from the lagoon,
 386 U2 is not clearly defined.

387 *Surface D3-1*

388 The surface D3-1 is both an erosional surface at
 389 the top of the unit U2 (Figures 6a, b and 7b, c) and
 390 a downlap surface that dips gently seaward
 391 (between 15 and 30 m b.s.l.). Southwards, towards
 392 the Salses-Leucate lagoon, D3-1 truncated sea-
 393 ward on the seabottom (Figure 6a, b). Under the
 394 lagoon, D3-1 is also an erosional and downlap
 395 surface.

396 *Unit U3*

397 Overlying D3-1, unit U3 is wedge-shaped and
 398 pinches out seaward at about 30 m b.s.l. in the
 399 south of the area. In the northern part of the
 400 area, in front of the Salses-Leucate lagoon, it
 401 evolves seaward into a thin layer (3 m b.s.f.)
 402 detected only on the VHR seismic profiles. In the
 403 shoreface area, the U3 wedge is subdivided into
 404 unit U3-1 at the base and unit U3-3 at the top,
 405 separated by the seismic surface D3-3. U3-1 is
 406 composed of prograding clinoforms and its thick-
 407 ness reaches 15 m. Above, U3-3 corresponds to
 408 the near-shore sand ridges that constitutes the
 409 modern upper shoreface. The seismic facies of
 410 U3-3 is obscured by the first multiple arrival and
 411 the boomer reverberation due to the very shallow
 412 water (Figure 6b). In the Salses-Leucate lagoon,
 413 unit U3 is more complex and comprises four
 414 units (Figure 6a). The basal unit U3-1 is com-
 415 posed of a set of seaward prograding and
 416 aggrading sedimentary bodies characterised by
 417 sigmoidal clinoforms. It is the most developed
 418 unit with a maximum thickness of about 10 m.
 419 Above U3-1, three units with similar characteris-
 420 tics are stacked (U3-2, U3-3 and U3-4 from base
 421 to top). They are characterised by aggrading sub-

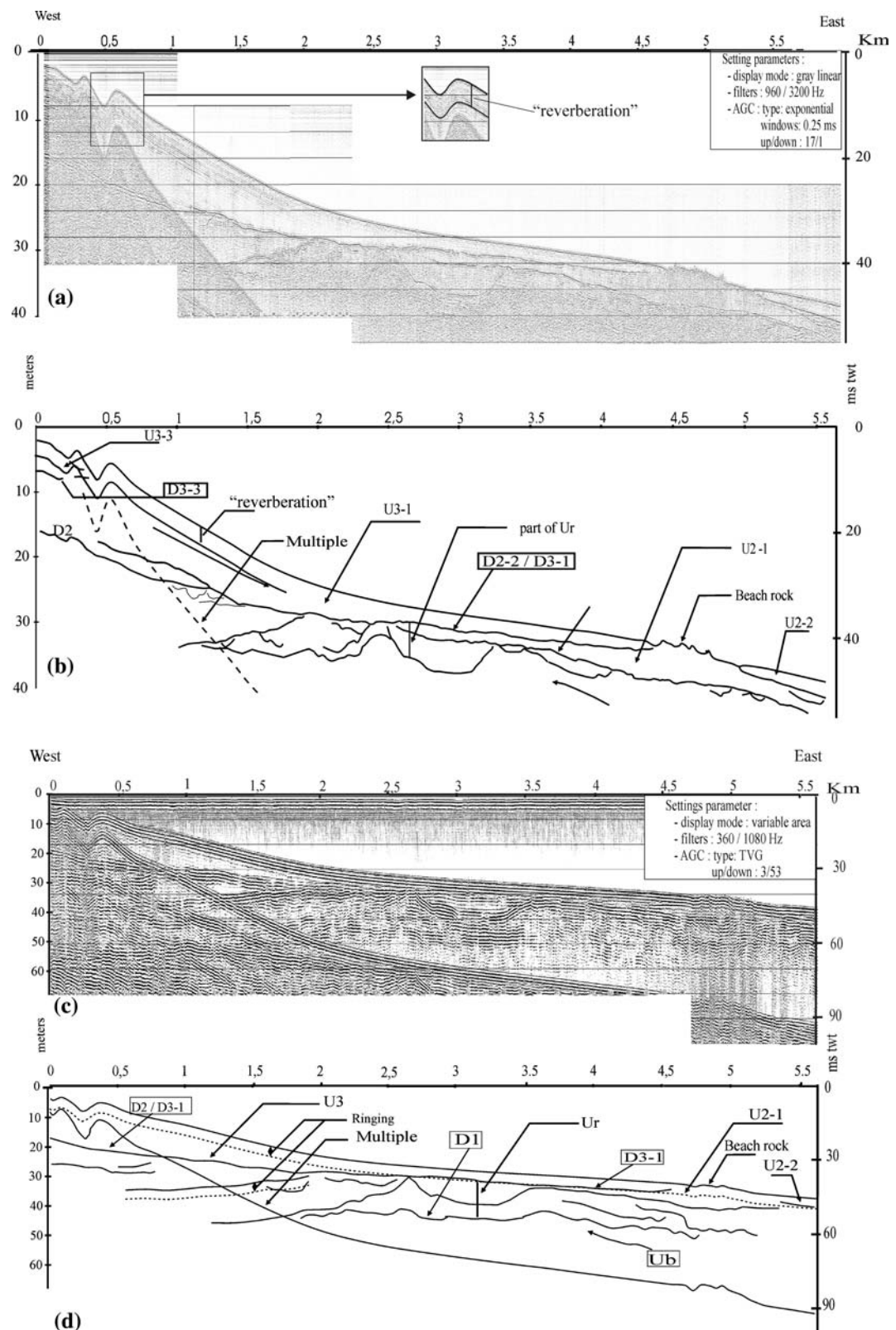


Figure 6. Seismic profiles showing the architecture of deposits in the southern part of the study area. Lines (a) and (b) represent the boomer profile and its line-interpretation. Lines (c) and (d) represent the mini-sparker profile and its line-interpretation. The main characteristics of the single channel seismic recording can be seen including the 'ringing' or the 'reverberation' and the first multiple arrival. Line (b) shows two discontinuities, D2 and D3-1, which merge in the near-shore area. They delimit two units U2 and U3. In line (d), a new basal discontinuity (D1) forms the lower boundary of unit Ur.

422 horizontal reflectors. The subdivision of U3-2,
 423 U3-3 and U3-4 is mainly based on seismic facies,
 424 amplitude and frequency variations. They are
 425 bounded by D3-2 at the base, an onlap surface,
 426 and the para-concordant surfaces D3-3 and D3-4
 427 and the bottom floor at the top. U3-2 is restricted
 428 to the central part of the lagoon and shows
 429 aggrading sub-horizontal reflectors onlapping
 430 toward the beach barrier. The two upper units,
 431 U3-3 and U3-4 do not exceed 2–3 m in thickness.
 432 Unit U3-3 extends through the beach barrier,
 433 whereas Unit U3-4 is restricted to the lagoonal
 434 area.

Correlation to borehole lithologies

435

The borehole (Figure 7e) was located on the beach
 436 barrier between the lagoon and the shelf (see
 437 Figure 3) with the top at about 1 m a.s.l. The total
 438 borehole penetration was 27 m. The lithological log
 439 shows prevailing sandy deposits interrupted by
 440 three thick levels of gravels and pebbles (from 1 to
 441 4 m thick) at about 4 m, 16 m and 21 m b.s.l.,
 442 respectively). Above the uppermost pebble level, the
 443 sands are coarsening upwards. Between 4 and 16 m
 444 b.s.l., two trends are observed, fining upwards at the
 445 base and then coarsening upwards. The lower two
 446

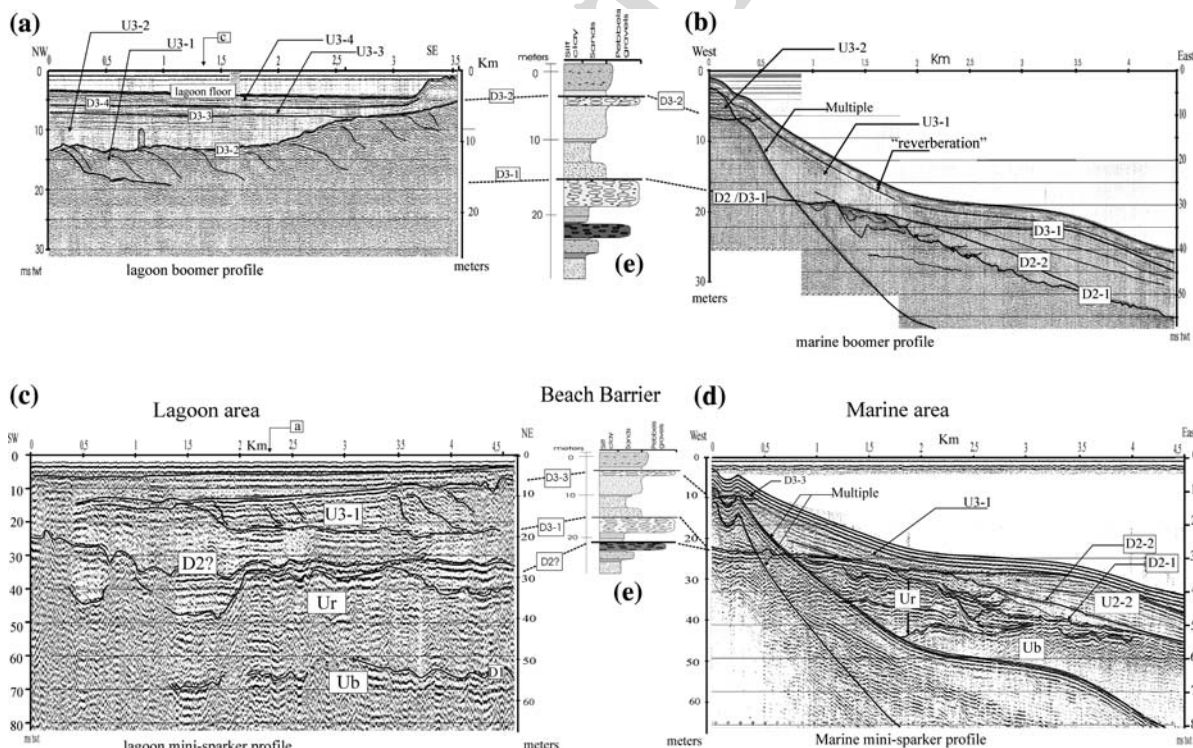


Figure 7. Seismic profiles showing the architecture of deposits in the lagoon area (a, c) and in the near-shore area (b, d) off the lagoon. The correlation is based lithologic information from a borehole (e), located on the beach barrier. In the lagoon, line (a) shows three upper discontinuities D3-2, D3-3 and D3-4, not identified in front of the Agly River. D3-3 is correlated via the borehole (e) to the marine environment (b). In the marine environment, the discontinuity D2 is divided seaward into D2-1 and D2-2 (b, d).

447 units, below the second and the lowermost pebble
 448 level, both coarsen upwards. Macrofaunal data are
 449 not referred to in the borehole log description, so
 450 the depositional environment could not be deduced.
 451 The sharp contacts between pebbles and overlying
 452 sands constitute major levels of acoustic impedance
 453 contrast and are correlated with major reflectors in
 454 the seismic profiles. The upper boundaries of the
 455 first level and second level of pebbles are correlated
 456 to D3-3 and D3-1 respectively. In the shoreface off
 457 the lagoon, D2 and D3-1 are amalgamated but it
 458 may be assumed that a subdivision occurred under
 459 the beach barrier and thus the pebble level at 21 m
 460 b.s.l may correlate to D2.

461 Discussion

462 Surficial sediment effect on seismic records

463 Considering information on the surficial sediment
 464 distribution from north to south along the shore-
 465 face area (Durand, 1999), and from the shoreline
 466 to the inner shelf (Aloisi, 1986), the “reverberation”
 467 seems to vary in correspondence with
 468 surficial sediment texture. The “reverberation” is
 469 amplified where the seafloor sediments are coarse-
 470 grained, whereas in the lagoon, where surficial
 471 sediment is of fine muds, the “reverberation” is not
 472 observed. The “reverberation” intensity would
 473 seem to be proportional to the grain size of the

surficial sediment, it could therefore be interpreted
 474 as a resonance phenomenon linked to the character
 475 of the surficial sediment immediately beneath
 476 the water bottom.

On the HR seismic data, the thin surficial muddy layer, which gives a reduced impedance
 477 contrast between the water column and the sea-
 478 bottom, also reduced the first multiple arrival and
 479 the ringing due to the bubble pulse oscillation.
 480 These effects improve the data quality in the
 481 lagoon, increasing both the penetration and the
 482 resolution.

486 Stratigraphic interpretation in relation to 487 sea level variation

The stratigraphic architecture is presented in
 488 Figure 8. The basal unconformity D1 is correlated
 489 landward to the upper boundary of the lower
 490 Pliocene (Duvail and Le Strat, 2002). Thus the unit
 491 underlying Ub also includes the lower Pliocene
 492 deposits that are the substratum of the Quaternary
 493 deposits. D1 is interpreted as a sequence boundary
 494 which probably marked the end of the last
 495 Pliocene 3rd order sea-level cycle (cycle 3.8, Haq
 496 et al., 1987).

The imbricated erosional surfaces and units
 497 (Ur) observed above D1 represent an Incised
 498 Valley Complex (IVC) and its infill, the latter not
 499 clearly resolved. Each erosional surface is a
 500 regressive surface + TS.

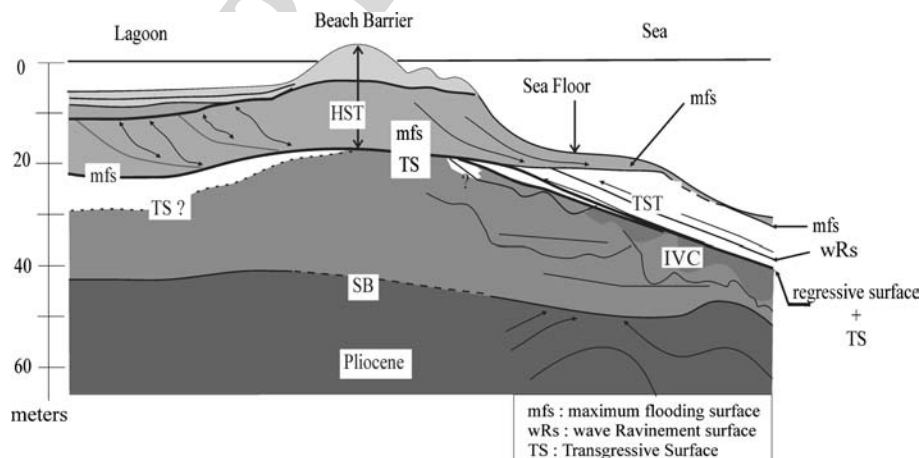


Figure 8. Stratigraphic model of the Roussillon coastal area. The Pliocene upper boundary is a sequence boundary (SB). The overlying Quaternary deposits are poorly developed except in the area of the incised valley complex (IVC). The IVC infill is truncated by a polygenetic erosional surface correlated to the regression and transgression of the last (fourth-order) sea-level cycle. The overlying transgressive systems tract (TST) and the highstand systems tract (HST) are separated by a maximum flooding surface (mfs).



502 sequence boundary, correlative to the successive
 503 falling sea-levels of the late Quaternary glacio-
 504 eustatic cycles of 4th order. The IVC may be
 505 laterally correlative to onshore fluvial terraces
 506 (Duvail and Le Strat, 2002) and lowstand wedges
 507 observed on the continental shelf (Lobo Sánchez,
 508 2000). Work by Thomas and Anderson (1994) on
 509 the Texas continental shelf led to a similar interpre-
 510 tation, whereas the infilling of the incised valley
 511 system of the Gironde (France) seems to record
 512 only the last glacio-eustatic hemi-cycle (Allen and
 513 Posamentier, 1993). This difference is probably due
 514 to dynamic conditions, in which a dominantly
 515 macro-tidal environment with large estuary develop-
 516 ment is not favourable to the preservation of
 517 deposits. A detailed study of the IVC is ongoing
 518 and the first results are the subject of a paper in
 519 preparation by the authors.

520 The sedimentary hiatus between the Pliocene
 521 and Quaternary deposits is likely related to the
 522 absence of important glacio-eustatic variations
 523 prior to the major late Quaternary glacio-eustatic
 524 variations (of about 120 m amplitude, Lambeck
 525 et al., 2002).

526 The IVC is capped by the polygenetic erosional
 527 surface D2, which we attribute to the last (4th-
 528 order) sea-level cycle. D2-1 is also a sequence
 529 boundary, interpreted as a lowstand surface attrib-
 530 uted to the late glacial maximum and probably
 531 merged with the post-glacial transgressive surface
 532 (TS). The overlying erosional surface D2-2 is
 533 assumed to be a wave ravinement surface (wRs)
 534 due to post-glacial shoreline transgression. Unit
 535 U2 overlies the TS and represents a transgressive
 536 systems tract (TST). It is composed of units U2-1
 537 and U2-2, which are variably preserved along the
 538 study area. As with the late Quaternary IVC infill,
 539 this TST is mainly developed off the Salses-
 540 Leucate lagoon, suggesting that this area has
 541 remained a persistent depocentre during shoreline
 542 retreat. The upper boundary of the TST is the
 543 surface D3-1 which is interpreted as the maximum
 544 flooding surface (mfs). In the north of the study
 545 area, ¹⁴C dating of shell layers indicates the mfs at
 546 about 20 m b.s.l. (Aloisi et al., 1978) which corre-
 547 sponds to the depth of D3-1 and confirms our
 548 interpretation.

549 The uppermost unit U3, composed of several
 550 sub-units of regional to local extent, represents a
 551 HST and exhibits different stratigraphic patterns
 552 on the seaward and the lagoonal sides of the beach

553 barrier. Seaward, a sandy coastal wedge is subdivided
 554 into two units: U3-1 and U3-3 (from base to
 555 top), considered to have been deposited during the
 556 early and the late highstand periods, respectively.
 557 No accurate age dating is available, but a transition
 558 between early and late highstand deposits is
 559 consistent with the facies analysis and the inferred
 560 dynamic conditions. The lower unit seems to not
 561 be affected by present day reworking, whereas the
 562 upper unit was subjected to wave reworking. This
 563 configuration is typical of wave dominated coastal
 564 areas (Tamura and Masuda, 2004). In the lagoon
 565 area, the stacking pattern is more complex due to
 566 the last phase of enclosure of the Salses-Leucate
 567 lagoon during the highstand period (Martin,
 568 1978). The basal prograding unit U3-1, correlated
 569 through the beach barrier, is associated with the
 570 construction of the barrier during the decreasing
 571 rates of sea-level rise that occurred at the begin-
 572 ning of the highstand period. It induced the final
 573 enclosure of the north basin of the Salses-Leucate
 574 lagoon, the south basin is presumed to have been
 575 previously closed (Martin, 1978; Certain et al.,
 576 2004). The overlying unit U3-2 is inferred to
 577 comprise the landward muddy sediments depos-
 578 ited synchronously with the build-up of the beach
 579 barrier. In such a case, these units are lateral facies
 580 variations rather than units having chronostrati-
 581 graphic significance. The two upper units U3-3
 582 and U3-4 correspond to the late highstand period
 583 and were deposited under low dynamic conditions.
 584 They are typical lagoonal deposits.

Other controlling factors

585 Fourth-order glacio-eustatic cycles of sea level are
 586 inferred to have been the first-order control on the
 587 stratigraphic architecture of the late Quaternary
 588 deposits. This is a relatively general statement for a
 589 passive continental margin. Superimposed fifth-
 590 order glacio-eustatic cycles can be recognised
 591 throughout the TST deposits, as will be detailed
 592 in forthcoming studies.

593 Over the timescale of the late Quaternary, the
 594 effects of subsidence can normally be neglected on
 595 passive margins. Nevertheless, the influence of
 596 differential subsidence is evident both on the
 597 continental shelf and across the Roussillon coastal
 598 plain. Seaward, net subsidence has controlled the
 599 stacking of prismatic units on the outer shelf
 600 (Tesson and Allen, 1995; Lofi et al., 2003). On the

602 inner shelf, the preservation of deposits of several
 603 successive sea-level lowstands implies some
 604 amount of subsidence. Onshore, the Roussillon
 605 plain has been affected by Quaternary uplift
 606 movements (Carroza and Delcaillau, 1999; Duvail
 607 and Le Strat, 2002). The hinge line between
 608 landward uplift and seaward subsidence is as-
 609 sumed to lie just landward of the present coastline.
 610 However, subsidence was probably more impor-
 611 tant during the Pliocene period, which is recorded
 612 by thicker deposits.

613 The late Quaternary depocentre off the Salses-
 614 Leucate lagoon, the IVC development and the area
 615 of maximum preservation of TST, together high-
 616 light the influence of palaeomorphology and sedi-
 617 ment supply. These factors have no real effect on the
 618 primary properties of the stratigraphic model, i.e.
 619 the key surfaces and systems tracts, but they affected
 620 the thickness and the seismic facies of the units. The
 621 similar location of successive palaeovalleys during
 622 sea level lowstands is probably due to an initial
 623 structural control and later geomorphologic trends.
 624 The palaeomorphology seem to have guided drain-
 625 age flow during base level falls. The occurrence of a
 626 thick TST depocentre off the Salses-Leucate area is
 627 probably due to a higher sediment supply from the
 628 Têt and Agly Rivers. Some Roman writers, in the
 629 period BC, spoke of an important river associated
 630 with the Têt River near the Salses-Leucate lagoon;
 631 the Têt River has probably moved southward in
 632 recent time. The lateral variability observed in the
 633 coastal area, and particularly in the recent post-
 634 glacial deposits of the Salses-Leucate lagoon, of
 635 thickness and stacking pattern variations, is attribut-
 636 ed to local evolution mainly controlled by hydro-
 637 dynamic factors, alternating river mouths and
 638 sedimentary spit formation.

639 Conclusions

640 This study represents one of the first attempts to
 641 integrate HR and VHR seismic reflection data
 642 across a coastal area, from the coastal plain to the
 643 inner shelf, in order to develop an architectural
 644 model of late Quaternary deposits. The use of the
 645 two acoustic systems, combining the penetration
 646 of HR seismic and the resolution of VHR seismic,
 647 proved very useful in a complex area such as a
 648 coastal zone. Nevertheless, areas of sandy seafloor
 649 remained more difficult to study than muddy

areas, because of the degradation of seismic data
 650 quality due to decreased penetration and the
 651 phenomena of reverberation and ringing.

652 The observations made in this study have
 653 allowed a model of the sedimentary architecture
 654 of the late Quaternary coastal deposits to be
 655 presented from the coastal plain to the inner shelf.
 656 Above the eroded Pliocene substratum, the late
 657 Quaternary deposits record several relative sea-
 658 level cycles represented by an IVC. This succession
 659 is capped by post-glacial deposits, interpreted to
 660 comprise a transgressive systems tract (TST),
 661 exhibiting lateral variability, and a highstand
 662 systems tract (HST).

663 The incised valley complex shows several ero-
 664 sional surfaces and depositional units that were
 665 probably linked to fourth-order fluctuations in base
 666 level. At this stage, we can assume a landward
 667 correlation with fluvial terraces and seaward corre-
 668 lation with lowstand wedges, without being able to
 669 identify the successive phases of genesis. Forthcom-
 670 ing work will attempt to clarify those correlations.

671 The uppermost transgressive and highstand
 672 deposits are well preserved above the incised valley
 673 complex but poorly preserved laterally. The ob-
 674 served pattern conforms to sequence stratigraphic
 675 concepts. The TST records the first steps of the late
 676 Holocene transgression and then the shoreline
 677 transgression, while the HST, composed of several
 678 units, reflects the complexity of the highstand
 679 period. This was initiated before the end of the
 680 relative sea-level rise and records the shoreline
 681 evolution that resulted in the current morphology.

682 The post-glacial coastal depocentres are lo-
 683 cated above late Quaternary point sources, i.e.
 684 incised valleys. This indicates that the main coastal
 685 depocentres during the late Quaternary have been
 686 repeatedly linked to palaeo-river mouths that are
 687 not systematically imprinted in the present-day
 688 morphology.

689 The interplay of eustatism with differential
 690 subsidence/uplift explains the changes of the
 691 stratigraphic record, from forced regressive wedges
 692 on the seaward side to fluvial terraces on the
 693 landward side.

694 Acknowledgements

695 C. Labaune is funded by a PhD fellowship from
 696 the Languedoc-Roussillon Region and by EU-

698 RODELTA Concerted Action. The geological
 699 database and new data of the Littoral program
 700 have been collected and furnished by GD ARGO
 701 research association. The authors thank the crew
 702 of the N/O Tethys II and the captain of Port-
 703 Leucate. They would also like to thank the
 704 reviewers, Daniel Praeg and Martina Busetti, and
 705 also the guest editor, Nigel Wardell, for their
 706 constructive comments.

707 References

- 708 Allen, G.P. and Posamentier, H.W., 1993, Sequence stratigraphy and facies model of an incised valley fill: the Gironde
 709 Estuary, France, *J. Sediment. Petrol.* **63**, 378–391.
 710 Aloisi, J.C., Monaco, A., Thommeret, J. and Thommeret, Y.,
 711 1975, Évolution paléogéographique du plateau continental
 712 languedocien dans le cadre du golfe du Lion. Analyse
 713 comparée des données sismiques, sédimentologiques et ra-
 714 diométriques concernant le Quaternaire récent, *Rev. Géogr.
 715 Phys. Géol. Dynam.* **XXXII**(1), 13–22.
 716 Aloisi, J.C., Monaco, A., Planchais, N.J., Thommeret, J. and
 717 Thommeret, Y., 1978, The Holocene transgression in the
 718 Golfe du Lion, southeastern France: paleogeographic and
 719 paleobotanical evolution, *Geogr. Phys. Quat.* **15**, 145–162.
 720 Aloisi, J.C., 1986, Sur un modèle de sédimentologie deltaïque.
 721 Contribution à la connaissance des marge passives. PhD
 722 thesis, Perpignan University, France.
 723 Bessis, F. and Burrus, J., 1986, Etude de la subsidence de la
 724 marge du Golfe du Lions, *Bull. Cent. Rech. Explor. Prod.
 725 Elf-Aquitaine* **10**, 123–141.
 726 Carozza, J.-M. and Delcaillau, B., 1999, Geomorphic record of
 727 Quaternary tectonic activity by alluvial terraces: example
 728 from the Tet basin (Roussillon, France, *C. R. Acad. Sci.
 729 Series IIA Earth Planet. Sci.* **329**(10), 735–740.
 730 Clauzon, G., Aguilar, J.P. and Michaux, J., 1987, The Pliocene
 731 Roussillon Basin (Eastern Pyrenees, France): a geodynamic
 732 evolution case of a Mediterranean Ria following the Messinian
 733 Salinity Crisis, *C. R. Acad. Sci., Série II* **304**, 585–590.
 734 Clauzon, G., 1990, Reconstitution de l'évolution géodynamique
 735 néogène du bassin du Roussillon et de l'unité adjacente des
 736 Corbières d'après les données éco-stratigraphiques et pal-
 737 éogéographiques, *Paléobiol. Continent.* **XVII**, 125–155.
 738 Certain, R., Tessier, B., Courp, T., Barusseau, J.P. and Pauc,
 739 H., 2004, Reconnaissance par sismique très haute résolution
 740 du remplissage sédimentaire de la lagune de Leucate (Aude
 741 et Pyrénées-Orientales - SE France), *Bull. Soc. Géol. Fr.* **175**,
 742 35–48.
 743 Durand, P., 1999, L'évolution des plages de l'Ouest du Golfe du
 744 Lion au XX^e siècle, cinématique du trait de côte, dynamique
 745 sédimentaire, analyse prévisionnelle. PhD thesis, Lyon 2
 746 University, France.
 747 Duvail, C., Le Strat P. and Bourgine, B., 2001, Atlas géologique
 748 des formations plio-quaternaires de la plaine du Roussillon
 749 (Pyrénées-Orientales). In *BRGM Report RP-51197-FR.*
 750 Duvail, C. and Le Strat, P., 2002, Architecture et géométrie
 751 haute résolution des prismes sédimentaires plio-quaternaires
 752 au droit du Roussillon suivant un profil terre-mer. In
 753 *BRGM Report RP 51972-FR.*
- 754 1 Gensous, B. and Tesson, M., 2003, L'analyse des dépôts
 755 postglaciaires et son application à l'étude des séquences de
 756 dépôt du Quaternaire terminal sur la plate-forme au large
 757 du Rhône (Golfe du Lion), *Bull. Soc. Géol. Fr.* **174**(4), 401–
 758 419.
 759 Haq, B.U., Hardenbol, J. and Vail, P.R., 1987, Chronology of
 760 fluctuating sea levels since Triassic (250 million years ago to
 761 present), *Science* **235**, 1156–1167.
 762 Hernandez-Molina, F.J., Somoza, L., Rey, J. and Pomar, L.,
 763 1994, Late Pleistocene-Holocene sediments on the Spanish
 764 continental shelves: model for very high resolution sequence
 765 stratigraphy, *Mar. Geol.* **120**, 129–174.
 766 Hsü, K.J., Cita, M.B. and Ryan, W.B.F., 1973, The origin of
 767 the Mediterranean evaporites, in Ryan, W.B.F. and Hsü,
 768 K.J. (Eds.), *Initial Reports of the Deep Sea Drilling Project*
 769 13, US Government Printing Office, Washington DC, pp.
 770 1203–1231.
 771 Lambeck, K., Esat, T.M. and Potter, E.K., 2002, Links between
 772 climate and sea levels for the past three million years, *Nature*
 773 **419**, 199–206.
 774 Lobo, F.J., Tesson, M. and Gensous, B., 2004, Stratral archi-
 775 tectures of late Quaternary regressive-transgressive cycles in
 776 the Roussillon Shelf (SW Gulf of Lions, France), *Mar.
 777 Petrol. Geol.* **21**(9), 1181–1203.
 778 Lobo Sánchez, F.J., 2000, Estratigrafía de alta resolución y
 779 cambios del nivel del mar durante el cuaternario del margen
 780 continental del golfo de Cádiz (S de España) y del Roussillon
 781 (S de Francia) : estudio comparativo. PhD thesis,
 782 Cádiz, Facultad de Ciencias del Mar, Spain.
 783 Locker, S.D., Hine, A.C. and Brooks, G.R., 2003, Regional
 784 stratigraphic framework linking continental shelf and
 785 coastal sedimentary deposits of west-central Florida, *Mar.
 786 Geol.* **200**, 351–378.
 787 Lofi, J., Rabineau, M., Gorini, C., Berne, S., Clauzon, G.,
 788 De Clarens, P., Tadeu Dos Reis, A., Moutain, G.S., Ryan,
 789 W.B.F., Steckler, M. and Fouchet, C., 2003, Plio-Quater-
 790 nary prograding clinoform wedges of the western Gulf of
 791 Lion continental margin (NW Mediterranean) after the
 792 Messinian Salinity Crisis, *Mar. Geol.* **198**, 289–317.
 793 Martin, R., 1978, Evolution Holocène et actuelle des conditions
 794 de sédimentation dans le milieu lagunaire de Salses-Leucate.
 795 PhD thesis, Perpignan University, France.
 796 Martin, R., Gadel, F. and Barusseau, J.P., 1981, Holocene
 797 evolution of the Canet-St Nazaire lagoon (Golfe du Lion,
 798 France) as determined from a study of sediment properties,
 799 *Sedimentology* **28**, 823–836.
 800 Mitchum, J.R., Vail, P.R. and Sangree, J.B., 1977, Seismic
 801 stratigraphy and global changes of sea level, part 6: Stratigra-
 802 phic interpretation of seismic reflection patterns in
 803 depositional sequences, in Payton, C.E. (Ed.), *Seismic
 804 Stratigraphy – Applications to Hydrocarbon Exploration*, pp.
 805 117–133. Mem. Am. Assoc. Petr. Geol. vol. 26.
 806 Monaco, A., 1971, Contribution à l'étude géologique et sédi-
 807 mentologique de plateau continental du Roussillon (Golfe
 808 du Lions). PhD Thesis, Université des Sciences et Tech-
 809 niques du Languedoc, France.
 810 Monaco, A., Thommeret, J. and Thommeret, Y., 1972, L'âge
 811 des dépôts quaternaires sur le plateau continental du
 812 Roussillon (Golfe du Lion), *C. R. Acad. Sci. Paris – série D*
 813 **274**, 2280–2283.
 814 Nielsen, P., Robert, S., Moller-Christiansen, B. and Oliva, P.,
 815 2001, Infiltration effects on sediment mobility under waves,
 816 *Coastal Eng.* **42**(2), 105–114.

- 818 Penland, S., Boyd, R. and Suter, J.R., 1988, Transgressive
819 depositional systems of the Mississippi delta plain: a model
820 for barrier shoreline and shelf sand development, *J. Sediment. Petrol.* **58**, 932–949.
821
- 822 Posamentier, H., Jersey, M. and Vail, P., 1988, Eustatic control
823 on clastic deposition I – Conceptual framework, in Wilgus,
824 C., Kendall, C., Posamentier, H., Ross, C. and Van Wag-
825 oner J. (Eds.), *Sea-level Changes: An Integrated Approach*,
826 pp. 109–124, SEPM Spec. Publ vol. 42.
827
- 828 Posamentier, H. and Vail, P., 1988, Eustatic controls on clastic
829 deposition II sequence and systems tract models, in Wilgus,
830 C., Kendall, C., Posamentier, H., Ross, C. and Van Wag-
831 oner J. (Eds.), *Sea-level Changes: An Integrated Approach*,
832 pp. 125–154, SEPM Spec. Publ vol. 42.
833
- 834 Posamentier, H., Allen, G., James, D.P. and Tesson, M., 1992,
835 Forced regressions in a sequence stratigraphic framework:
836 Concepts, examples, and exploration significance, *AAPG Bull.* **76**, 1687–1709.
837
- 838 Rabineau, M., Berne, S., Ledrezen, E., Lericolais, G., Marsset, T.
839 and Rotunno, M., 1998, 3D architecture of lowstand and
840 transgressive Quaternary sand bodies on the outer shelf of the
841 Gulf of Lion, France, *Mar. Petrol. Geol.* **15**, 439–452.
842
- 843 Ridente, D. and Trincardi, F., 2002, Eustatic and tectonic
844 control on deposition and lateral variability of Quaternary
845 regressive sequences in the Adriatic basin (Italy), *Mar. Geol.*
846 **184**(3–4), 273–293.
847
- 848 Simpkin, P.G. and Davis, A., 1993, For seismic profiling in very
849 shallow water, a novel receiver, *Sea Technol.* **34**, 21–28.
850
- 851 Stéphanian, A. and Levoy, F., 2003, Séquences d'évolution
852 morphodynamique des barres intertidales d'une plage
853 macrotidale: l'exemple d'Omaha beach (Normandie,
854 France): Morphodynamical evolution sequences of inter-
855 tidal bars on a macrotidal beach: case study of Omaha
856 beach (Normandy, France), *Oceanol. Acta* **26**(2), 167–177.
857
- 858 Suter, J.R., Berryhill, Jr. H.L. and Penland, S., 1987, Late
859 Quaternary sea-level fluctuations and depositional se-
860 quences, southwest Louisiana continental shelf, in Num-
861 medal, D., Pilkey, O.H. and Howard, J.D. (Eds.), *Sea-level
862 Fluctuation And Coastal Evolution*, pp. 199–219, SEPM
863 Spec. Publ vol. 41.
864
- 865 Tamura, T. and Masuda, F., 2004, Inner shelf to shoreface
866 depositional sequence in the Sendai coastal prism, Pacific
867 coast of northeastern Japan: spatial and temporal growth
868 patterns in relation to Holocene relative sea-level change, *J.
869 Asian Earth Sci.* **23**(4), 567–576.
870
- 871 Tesson, M., Gensous, B., Allen, G. and Ravenne, C., 1990, Late
872 Quaternary deltaic lowstand wedges on the Rhône conti-
873 nental shelf, France, *Mar. Geol.* **91**, 325–332.
874
- 875 Tesson, M., Allen, G.P. and Ravenne, C., 1993, Late Pleisto-
876 cene shelf-perched lowstand wedges on the Rhône conti-
877 nental shelf, in Posamentier, H.W., Summerhayes, C.P.,
878 Haq, B.U. and Allen, G.P. (Eds.), *Sequence Stratigraphy
879 and Facies Associations: International Association of Sedi-
880 mentologists*, pp. 183–196. Special Publication vol. 18.
881
- 882 Tesson, M. and Allen, G., 1995, Contrôle tectonique et eusta-
883 tique haute-fréquence de l'architecture et de la stratigraphie
884 de dépôts de plate-forme péricontinentale. Exemple du Golfe
885 du Lion (Méditerranée, France) et des dépôts quaternaires,
886 *C. R. Acad. Sci. Paris- série IIa* **320**, 39–46.
887
- 888 Tesson, M., Posamentier, H. and Gensous, B., 2000, Stratig-
889 graphic organization of the Late Pleistocene deposits of the
890 western part of the Golfe du Lion Shelf (Languedoc shelf),
891 Western Mediterranean Sea, using high resolution seismic
892 and core data, *AAPG Bull.* **84**, 119–150.
893
- 894 Thomas, M.A. and Anderson, J.B., 1994, Sea-level controls on
the facies architecture of the Trinity/Sabine incised-valley
system, Texas continental shelf, 1994, in Dalrymple, R.W.,
Boyd, R. and Zaitlin, B. (Eds.), *Incised-Valley Systems:
Origin and Sedimentary Sequences*, pp. 63–82, SEPM Spec.
Publ. vol. 5.
- 895 Van wagoner, J.C., Posamentir, H.W., Mitchum, Jr. R.M., Vail,
896 P.R., Sarg, J.F., Loutit, T.S. and Hardenbol, J., 1988, An
897 overview of the fundamentals of sequence stratigraphy and
898 key definitions, in Wilgus, C., Kendall, C., Posamentier, H.,
899 Ross, C. and Van Wagoner, J. (Eds.), *Sea-level Changes: An
900 Integrated Approach*, pp. 39–46, SEPM Spec. Publ vol. 42.
901